POTSDAM-INSTITUT FÜR
KLIMAFOLGENFORSCHUNG

Modeling the future resilience of the Greenland Ice Sheet

From the flow of ice to the interplay of feedbacks

Maria Zeitz

Publikationsbasierte Universitätsdissertation
zur Erlangung des akademischen Grades

doctor rerum naturalium
(Dr. rer. nat.)

in der Wissenschaftsdisziplin
Klimaphysik

eingereicht im Juni 2022 an der
Mathematisch Naturwissenschaftlichen Fakultät
der Universität Potsdam

Datum der Disputation: 17. Oktober 2022

Betreuer*innen

Prof. Dr. Ricarda Winkelmann
Potsdam Institut für Klimafolgenforschung
Universität Potsdam

Dr. Jonathan F. Donges
Potsdam Institut für Klimafolgenforschung
Stockholm Resilience Center

Gutachter*innen

Prof. Dr. Ricarda Winkelmann
Potsdam Institut für Klimafolgenforschung
Universität Potsdam

Dr. Jonathan F. Donges
Potsdam Institut für Klimafolgenforschung
Stockholm Resilience Center

Dr. Nanna B. Karlsson
Geological Survey of Denmark and Greenland

Published online on the
Publication Server of the University of Potsdam:
https://doi.org/10.25932/publishup-56883
https://nbn-resolving.org/urn:nbn:de:kobv:517-opus4-568839

Abstract

The Greenland Ice Sheet is the second-largest mass of ice on Earth. Being almost 2000 km long, more than 700 km wide, and more than 3 km thick at the summit, it holds enough ice to raise global sea levels by 7 m if melted completely. Despite its massive size, it is particularly vulnerable to anthropogenic climate change: temperatures over the Greenland Ice Sheet have increased by more than 2.7°C in the past 30 years, twice as much as the global mean temperature. Consequently, the ice sheet has been significantly losing mass since the 1980s and the rate of loss has increased sixfold since then. Moreover, it is one of the potential tipping elements of the Earth System, which might undergo irreversible change once a warming threshold is exceeded. This thesis aims at extending the understanding of the resilience of the Greenland Ice Sheet against global warming by analyzing processes and feedbacks relevant to its centennial to multi-millennial stability using ice sheet modeling.

One of these feedbacks, the *melt-elevation-feedback* is driven by the temperature rise with decreasing altitudes: As the ice sheet melts, its thickness and surface elevation decrease, exposing the ice surface to warmer air and thus increasing the melt rates even further. The *glacial isostatic adjustment* (GIA) can partly mitigate this melt-elevation feedback as the bedrock lifts in response to an ice load decrease, forming the negative GIA feedback. In my thesis, I show that the interaction between these two competing feedbacks can lead to qualitatively different dynamical responses of the Greenland Ice Sheet to warming – from permanent loss to incomplete recovery, depending on the feedback parameters. My research shows that the interaction of those feedbacks can initiate self-sustained oscillations of the ice volume while the climate forcing remains constant.

Furthermore, the increased surface melt changes the optical properties of the snow or ice surface, e.g. by lowering their albedo, which in turn enhances melt rates – a process known as the *melt-albedo feedback*. Process-based ice sheet models often neglect this melt-albedo feedback. To close this gap, I implemented a simplified version of the diurnal Energy Balance Model, a computationally efficient approach that can capture the first-order effects of the melt-albedo

feedback, into the Parallel Ice Sheet Model (PISM). Using the coupled model, I show in warming experiments that the melt-albedo feedback almost doubles the ice loss until the year 2300 under the low greenhouse gas emission scenario RCP2.6, compared to simulations where the melt-albedo feedback is neglected, and adds up to 58% additional ice loss under the high emission scenario RCP8.5. Moreover, I find that the melt-albedo feedback dominates the ice loss until 2300, compared to the melt-elevation feedback.

Another process that could influence the resilience of the Greenland Ice Sheet is the warming induced softening of the ice and the resulting increase in flow. In my thesis, I show with PISM how the uncertainty in *Glen's flow law* impacts the simulated response to warming. In a flow line setup at fixed climatic mass balance, the uncertainty in flow parameters leads to a range of ice loss comparable to the range caused by different warming levels.

While I focus on fundamental processes, feedbacks, and their interactions in the first three projects of my thesis, I also explore the impact of specific climate scenarios on the sea level rise contribution of the Greenland Ice Sheet. To increase the carbon budget flexibility, some warming scenarios – while still staying within the limits of the Paris Agreement – include a temporal overshoot of global warming. I show that an overshoot by 0.4°C increases the short-term and long-term ice loss from Greenland by several centimeters. The long-term increase is driven by the warming at high latitudes, which persists even when global warming is reversed. This leads to a substantial long-term commitment of the sea level rise contribution from the Greenland Ice Sheet.

Overall, in my thesis I show that the melt-albedo feedback is most relevant for the ice loss of the Greenland Ice Sheet on centennial timescales. In contrast, the melt-elevation feedback and its interplay with the GIA feedback become increasingly relevant on millennial timescales. All of these influence the resilience of the Greenland Ice Sheet against global warming, in the near future and on the long term.

Zusammenfassung

Das grönländische Eisschild ist die zweitgrößte Eismasse der Erde. Es fasst genug Eis, um den globalen Meeresspiegel um 7 m anzuheben, wenn er vollständig schmilzt. Trotz seiner Größe ist es durch den vom Menschen verursachten Klimawandel immens gefährdet: Die Temperaturen über Grönland sind in den letzten 30 Jahren um mehr als 2,7°C gestiegen, doppelt so stark wie im globalen Mittel. Daher verliert das Eisschild seit den 1980er Jahren an Masse und die Verlustrate hat sich seitdem versechsfacht. Zudem ist das grönländische Eisschild ein Kippelement des Erdsystems, es könnte sich unwiederbringlich verändern, wenn die globale Erwärmung einen Schwellwert überschreiten sollte. Ziel dieser Arbeit ist es, das Verständnis für die Resilienz des grönländischen Eisschildes zu erweitern, indem relevante Rückkopplungen und Prozesse analysiert werden.

Eine dieser Rückkopplungen, die positive Schmelz-Höhen-Rückkopplung wird durch den Temperaturanstieg bei abnehmender Höhe angetrieben: Wenn der Eisschild schmilzt, nehmen seine Dicke und die Oberflächenhöhe ab, wodurch die Eisoberfläche wärmerer Luft ausgesetzt wird und die Schmelzraten noch weiter ansteigen. Die glaziale isostatische Anpassung (GIA) kann die Schmelz-Höhen-Rückkopplung teilweise abschwächen, da sich der Erdmantel als Reaktion auf die abnehmende Eislast hebt und so die negative GIA-Rückkopplung bildet. Ich zeige, dass die Interaktion zwischen diesen beiden konkurrierenden Rückkopplungen zu qualitativ unterschiedlichem dynamischen Verhalten des grönländischen Eisschildes bei Erwärmung führen kann - von permanentem Verlust bis hin zu unvollständiger Erholung. Das Zusammenspiel dieser Rückkopplungen kann zudem Oszillationen des Eisvolumens in einem konstanten Klima auslösen.

Die verstärkte Oberflächenschmelze ändert die optischen Eigenschaften von Schnee und Eis und verringert deren Albedo, was wiederum die Schmelzraten erhöht – die sogenannte Schmelz-Albedo Rückkopplung. Da viele Eisschildmodelle diese vernachlässigen, habe ich eine vereinfachte Version des tageszeitlichen Energiebilanzmodells, welches die Effekte der Schmelz-Albedo-Rückkopplung erster Ordnung erfassen kann, in das Eisschildmodell PISM implementiert. Mithilfe des gekoppelten Modells zeige ich, dass die Schmelz-Albedo-Rückkopplung

den Eisverlust bis zum Jahr 2300 im moderaten Klimaszenario RCP2.6 fast verdoppelt und im RCP8.5-Szenario, welches von starken Emissionen ausgeht, bis zu 58% zusätzlichen Eisverlust verursacht, im Vergleich zu Simulationen in denen die Schmelz-Albedo-Rückkopplung vernachlässigt wird. Bis zum Jahr 2300 trägt die Schmelz-Albedo-Rückkopplung mehr zum Eisverlust bei als die Schmelz-Höhen-Rückkopplung.

Ein weiterer Prozess, der die Widerstandsfähigkeit des grönländischen Eisschilds beeinflussen könnte, ist die Erweichung des Eises bei steigenden Temperaturen, sowie die daraus resultierende Zunahme des Eisflusses. In meiner Dissertation zeige ich, wie sich die parametrische Unsicherheit in dem Flussgesetz auf die Ergebnisse von PISM Simulationen bei Erwärmung auswirkt. In einem idealisierten, zweidimensionalem Experiment mit fester klimatischer Massenbilanz führt die Unsicherheit in den Strömungsparametern zu einer Bandbreite des Eisverlustes, die mit der Bandbreite durch unterschiedliche Erwärmungen vergleichbar ist.

Neben den grundsätzlichen Prozessen und Rückkopplungen untersuchte ich auch die Auswirkungen konkreter Klimaszenarien auf den Eisverlust von Grönland. Um die Flexibilität des Kohlenstoffbudgets zu erhöhen sehen einige Erwärmungsszenarien eine temporäre Überschreitung der globalen Temperaturen über das Ziel von 1,5°C vor. Ich zeige, dass eine solche Temperaturerhöhung den kurz- und langfristigen Eisverlust von Grönland um mehrere Zentimeter erhöht. Der langfristige Meeresspiegelanstieg ist auf die anhaltende Temperaturerhöhung in hohen Breitengraden zurückzuführen. Solche Prozesse führen zu einem langfristigen und bereits festgelegtem Meeresspiegelanstieg, selbst wenn die Temperaturen nicht weiter steigen.

Insgesamt zeige ich in meiner Arbeit, dass die Schmelz-Albedo-Rückkopplung für den Eisverlust des grönländischen Eisschilds in den nächsten Jahrhunderten am wichtigsten ist. Im Gegensatz dazu werden die Schmelz-Höhen-Rückkopplung und ihr Zusammenspiel mit der GIA-Rückkopplung auf längeren Zeiträumen immer relevanter.

Acknowledgments

I want to thank my *Doktormutter* (first PhD advisor) Ricarda Winkelmann, who has always believed in me. Her positive support was crucial for my journey during the past years and allowed me to learn about science, but also way beyond. Ricarda always made time for discussing with me when I needed it, but also gave me space when i needed that.

I also want to thanks Jonathan Donges, my second supervisor for his support and his commitment to my PhD project, and who has provided so much helpful feedback, in particular, but not only, for this thesis.

Moreover I thank Ronja Reese, who inspired me to join the ice dynamics group at the Potsdam Institute for Climate Impact Research in the first place. Her friendship and scientific advise have helped me through the inevitable rough patches and have made my work scientifically better and much more enjoyable! Thank you!

Further, I want to thank everyone (else) from the ice dynamics group: Johanna Beckmann, Tanja Schlemm, Julius Garbe, Ann Kristin Klose, Moritz Kreutzer, Torsten Albrecht, Jan Haacker, Simon Schöll, Johannes Feldmann, Matthias Mengel, Lena Nicola, Helen Werner and Xylar Asay-Davis. You have made coming to the office a pleasure and I cannot emphasize enough, how valuable the positive and supportive atmosphere, which we created, is. In particular, I appreciated the group outings to the alps and to the Berlin-Brandenburg lakes, the helpfulness, be it through mutually reviewing our work, discussing PISM details, the pandemic-driven zoom sprints, or the general kindness. My special thanks go also to Ronja, Johanna, Jan and Torsten, who have been fantastic to collaborate with!

In addition, I want to thank the DominoES group, Jobst Heitzig, Marc Wiedermann, Nico Wunderling, Keith Smith, Christina Eder and Alexia Katsanidou. It was a pleasure participating in the group meetings and in the workshops, as it really broadened my horizon and allowed me to learn a lot outside of my field. The same is true for the community of the Future Lab, many thanks particularly to Sina Loriani for the for the good collaboration.

Many thanks to Uta Krebs-Kanzow and Anders Levermann, not only for your close scientific collaboration, where you brought in new ideas, reignited the inspiration, and provided valuable feedback and the opportunity to learn. In addition, coming from different angles, you have provided mentorship and advice beyond the scientific question at hand.

I would have not been able to pursue this research, if it had not been for the work of countless people who are developing the software and the languages I use. In particular I want to thank the PISM developers Constantine Khroulev, Andy Aschwanden, Ed Bueler, and many others, who have created, co-developed, or maintained the Parallel Ice Sheet Model PISM. The open-science approach and your generosity with advice laid out the foundation, on which my specific research builds.

Many thanks also to Regine Hock for organizing the international glacier summer school in McCarthy, which has inspired me in so many ways, and also to all the lecturers, the people of the Wrangell Mountain Center, who have been hosting us, and the other participants, creating a lovely and inspired atmosphere. I am also more than grateful to Andy and Constantine for hosting me over one summer at UAF and allowing me to learn from them and the entire UAF glaciers group.

In general, PIK has been a great and inspiring environment to work at, where I have learned a lot about climate science, outreach, policy relevant research and developed friendships. Thanks to all of my PIK friends like Benni, Feli, Jess, Efi, Giorgia, Kilian, just to name a few... And most importantly many, many thanks to the people who take care of stuff, e.g. short-notice business trips, or financial questions, or simply the organization of a PhD program. Many thanks to Gitta Krukenberg and Christine von Bloh in particular.

My deepest thanks go also to the important people in my life outside of academia, most importantly my partner Conrad, who has been at my side throughout this long journey (and longer) and whose love, care, and support were always present. He and my dear friends, my housemates, my family have been crucial for grounding me, contributing to my happiness and the quality of my life.

Contents

1 Introduction

The Greenland Ice Sheet is a sensitive part of the Earth system, over past glacial cycles it has experienced large fluctuation in its ice volume. The aim of this thesis is to help understanding the resilience of the Greenland Ice Sheet facing current and future anthropogenic global warming. The following chapter provides an introduction to anthropogenic climate change and the observed impacts onto the Greenland Ice Sheet. Then it summarizes current sea level rise projections and briefly introduces the concepts of tipping and resilience. Three important feedback mechanisms, which govern the dynamics of the Greenland Ice Sheets and are at the center of this thesis, are introduces. Finally, I summarize modeling approaches for some of the main processes contributing to the mass balance of the Greenland Ice Sheet.

1.1 The Greenland Ice Sheet in a warming world

1.1.1 Warming

Anthropogenic climate change and its impacts onto the Earth system are observed around the world. During the last decade (2010-2019), the global mean temperature has increased by 1.09°C, with 1.59°C over land and 0.88°C over the ocean, compared to the preindustrial temperatures averaged over 1850–1900 (Masson-Delmotte et al. 2021).

Projections of possible future warming in the 21st century are computed based on representative concentration pathways (RCP) and shared socioeconomic pathways (SSP) describing different levels of greenhouse gas emissions and other radiative forcings that might occur in the future. While the RCP scenarios focus on greenhouse gases and radiative forcing alone, they do not include any socioeconomic narratives. The SSP scenarios, in contrast, look at five different ways the world might evolve in future, with or without additional climate policy. Depending on the scenario of future carbon emissions, we face between 1.4°C and more than 5°C of warming until the end of the century (Masson-Delmotte et al. 2021). In 2015, UN leaders agreed at the COP 21 in Paris to limit global

warming to well below 2°C above preindustrial and on the long term to 1.5°C, which is an important threshold to be able to preserve most climate tipping elements in their current stable state (Armstrong McKay et al. 2021; Lenton, H. Held, et al. 2008; Lenton, Rockström, et al. 2019; Schellnhuber et al. 2016). However, climate policy that is currently in place would lead to 2.7°C warming until the end of the century (Climate Analytics and NewClimate 2021). This amount of warming might be sufficient to trigger the irreversible loss of the Greenland Ice Sheet (Robinson et al. 2012).

1.1.2 Observations of changes on the Greenland Ice Sheet

The Greenland Ice Sheet holds enough water for 7.4 m of global sea level rise (Morlighem et al. 2017). It is subject to climate change and contributes to sea level rise with increasing global warming (Hanna, Pattyn, et al. 2020; T. Slater et al. 2021). Due to the Arctic Amplification, temperature increase in the central Arctic is more than double the global average (Masson-Delmotte et al. 2021; Pörtner et al. 2019). The currently observed warming over Greenland amounts to 2.7°C over the summit (Pörtner et al. 2019) and locally exceeds 10°C along the west Greenland coast in winter (Hanna, Mernild, et al. 2012). The runoff rates respond in a nonlinear way to warming (Trusel et al. 2018). Until today, in a 1.1°C warmer world, sea level has risen by 20 cm since the year 1901 (Masson-Delmotte et al. 2021), affecting societies and coastal populations world wide. Approximately 1.3 cm of this sea level rise can be attributed to ice loss from the Greenland Ice Sheet, of which 34% are due to decreases in the climatic mass balance and 66% are due to increased discharge into the ocean (IMBIE Team 2020; Mouginot, Rignot, Bjørk, et al. 2019). The main outlet glaciers of the Greenland Ice Sheet have been retreating in the past years and discharge increased by 14% between the periods from 1985–1999 and 2007–2018 (King, Howat, Candela, et al. 2020). These changes, over the period from 1972-2018, are shown in Figure 1.1, taken from Mouginot, Rignot, Bjørk, et al. (2019). Velocity changes in response to warming and frontal retreat are complex and depend on the effectiveness of subglacial drainage networks, meltwater availability and the position of the terminus (Moon, Joughin, B. Smith, et al. 2012; Moon, Joughin, Ben Smith, et al. 2014). Moreover, several extreme melt years have been observed over the Greenland Ice Sheet, e.g. the years 2010, 2012 and 2019, with meltwater observed on more than 98% of the surface in 2012 (Nghiem et al. 2012; Tedesco and Fettweis 2020; Tedesco, Fettweis, et al. 2011). The lowered reflectivity due to the melted

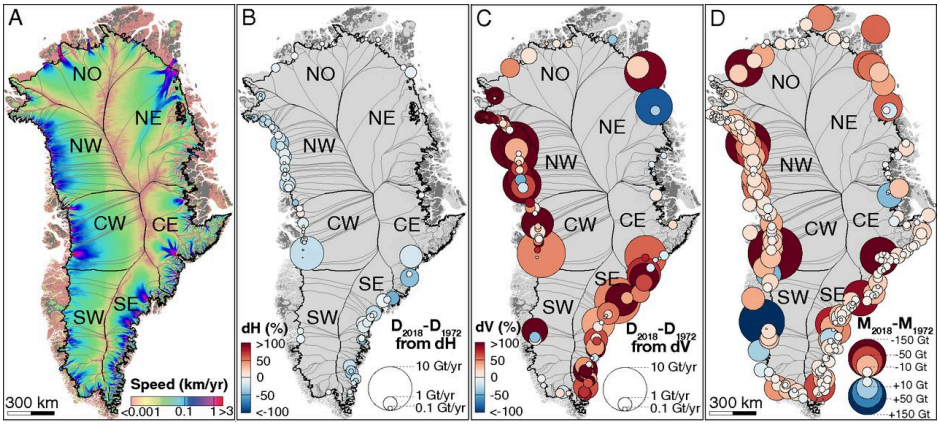

Figure 1.1: Changes in the Greenland Ice Sheet, figure taken from Mouginot, Rignot, Bjørk, et al. (2019). (A) Catchment basins and ice speeds taken from Mouginot, Rignot, Scheuchl, et al. (2017). The changes depicted are for 1972–2018, (B) percentage of thickness change. (C) Percentage of acceleration in ice flux from each basin, and (D) cumulative loss per basin.

snow can increase surface melt. In addition, dust and algae are accumulating on the south-western margin of the Greenland Ice Sheet, further darkening the surface of the ice (Cook et al. 2020; McCutcheon et al. 2021; Ryan, Hubbard, et al. 2018; Stibal et al. 2017; Tedstone, Bamber, et al. 2017; Williamson et al. 2020).

1.1.3 Current projections of sea level rise contribution of the Greenland Ice Sheet

Current sea level rise projections expect between 0.5 and 1 m of global mean sea level rise in the year 2100 (compared to 1900). The numbers depend on both, the greenhouse gas emission pathway and model uncertainty (Masson-Delmotte et al. 2021), but exclude still uncertain processes like the marine ice cliff instability. Until the year 2100, the Greenland Ice Sheet is projected to contribute between 1 and 10 cm (likely range) for a low emission scenario RCP2.6 and between 9 and 18 cm (likely range) for a high emission scenario RCP8.5 (Aschwanden, Fahnestock, Truffer, et al. 2019; Fürst et al. 2015; Goelzer et al. 2020; Masson-Delmotte et al. 2021). The dynamical response of outlet glaciers and their interaction with ocean warming might add up to 50% to Greenland's

ice loss (Beckmann et al. 2018). So far the actual trend in sea level rise follows the upper end of previous projections, both the contribution of the Greenland Ice Sheet and total sea level rise (T. Slater et al. 2021).

The IPCC usually gives sea level projections until 2100. However, sea level rise is a slow process and the full impacts of current climate change on future sea level might become only apparent after 2100. Aschwanden, Fahnestock, Truffer, et al. (2019) suggest that under an extended worst-case warming scenario (RCP8.5 with increasing temperatures until 2500) the Greenland Ice Sheet might indeed be lost by the end of this millennium.

1.1.4 Tipping behavior and resilience of the Greenland Ice Sheet

Following Lenton, H. Held, et al. (2008), the Greenland Ice Sheet can be classified as a *tipping element* of the climate system, as a small change in climate forcing can qualitatively and irreversibly alter the state of the ice sheet. The results from Robinson et al. (2012) and Anne M. Solgaard and Langen (2012) indicate the multistability of the Greenland Ice Sheet, and in addition Robinson et al. (2012) suggest that the complete loss of the Greenland Ice Sheet is irreversible above a threshold global warming of 1.6°C (likely range: 0.8°C – 3.2°C), while a stable state close to the present day can be maintained with lower warming. This threshold behavior is supported by several conceptual analyses (Levermann and Winkelmann 2016; Weertman 1961). Boers and Rypdal (2021) suggest, via a statistical analysis of the melt rate timeseries since 1850, that early warning signals might already be observed in the western part of the Greenland Ice Sheet, indicating that the ice is, at least regionally, potentially close to a tipping point. In contrast, coupled ice-atmosphere simulations find that a single tipping threshold cannot be identified in Greenland Ice Sheet due to the strong negative feedbacks arising from ice-atmosphere interactions (Gregory et al. 2020). Nevertheless, ice loss could be irreversible if a critical ice volume is lost: once shrinking below a volume of 4 m sea level equivalent, the Greenland Ice Sheet does not fully recover (Gregory et al. 2020).

In view of these observations and projections, the important question is how resilient the Greenland Ice Sheet is to the perturbation of anthropogenic global warming. Before discussing this question in detail, the term 'resilience' needs to be introduced. It describes the capacity of a system to adapt to or to recover from perturbations. Resilience is a well established term in psychology and ecology, and has been increasingly applied to Earth system science (Tamberg

et al. 2022). In that context, the term resilience can be used to describe the ability to maintain desirable (from a human perspective) states of the Earth System in the face of anthropogenic disturbance (Rockström et al. 2009) or for a system to maintain a safe distance to critical thresholds (Folke et al. 2010). The concept of resilience suggests that multiple stable states exist and one of them is more desirable than the other, and can resist perturbations and shocks to some extent. Folke et al. (2010) define 'resilience' as *"The capacity of a system to absorb disturbance and reorganize while undergoing change so as to still retain essentially the same function, structure and feedbacks, and therefore identity, that is, the capacity to change in order to maintain the same identity"*. This is different from the stability domain, which is simply the basin of attraction (the region in the phase space from which every trajectory approaches the attractor, also called basin of stability). Therefore the concept of resilience is broader than just the absence of tipping or irreversibility.

In approaching the resilience of the Greenland Ice Sheet specifically, it is useful to start with a list of four question, defined by Tamberg et al. (2022) and inspired the specific resilience after Folke et al. (2010): 1) Resilience of what? What is the system? 2) Resilience regarding what? What is the feature or the property of the system, that needs to be sustained? 3) Resilience against what? What is the adverse influence or the perturbation? 4) Resilience how? What are the response options? In the context of this thesis, I will focus on the Greenland Ice Sheet as the system in question 1). The answer to question 2) "Resilience regarding what?" is ambiguous and could mean different properties of the system as:

1. the Greenland Ice Sheet volume
2. an adaptable rate of sea level rise, and therefore the Greenland Ice Sheet contribution
3. the albedo of the ice sheet
4. frontal position of outlet glaciers
5. capacity of the firn to retain and refreeze meltwater
6. Greenland as biotope
7. Greenland as living space for human societies

This is by no means a comprehensive list of answers, yet some of the items, in particular Item 6 and Item 7, are well beyond the scope of this thesis. The possible answers to questions 3) "Resilience against what (perturbation)?" could read:

(i) increase / change of the global mean temperature
(ii) change of atmospheric patterns, i.e. Greenland blocking, and the associated increase in extreme melt events
(iii) accumulation of algae, dust and other impurities on the ice surface
(iv) oceanic conditions in fjords
(v) changes in sea level

Question 4) "Resilience how?" can only be answered on a case by case basis, as the response options depend on what property needs to be sustained (question 2) against which perturbation (question 3).

With this lists in mind, we can later study how our understanding of the specific resilience of the Greenland Ice Sheet evolves if we take certain ice-dynamical processes or feedbacks into account.

1.1.5 The Greenland Ice Sheet in the context of the Earth System

Fyke et al. (2018) outline the possible interactions between the ice sheets and the larger Earth system and list systematically how exactly the Earth system impacts the ice sheet and how, in turn, the ice sheet impacts the Earth system, deducing possible feedbacks. The Greenland Ice Sheet is affected by the Earth system at its boundaries, e.g. through climate and atmospheric patterns, such as Greenland Blocking or North Atlantic Oscillation (Bevis et al. 2019), and the ocean conditions (Straneo and Heimbach 2013). In turn it impacts the larger Earth system via its topography and its albedo, which help damming cold air and induce katabatic winds.

A total absence of the ice sheet would lead to significantly higher temperatures due to the lapse rate and albedo, and to a significantly different distribution of precipitation patterns, however there is no clear evidence on how exactly the absence of the Greenland Ice Sheet would affect large scale atmospheric patterns, like the jet stream. The increased melt in Greenland and associated albedo changes do not only lead to further melt by absorbing more radiation energy, but also affect atmospheric temperatures directly (Hall 2004). If the Greenland Ice Sheet would disappear completely, the resulting increase in planetary surface albedo alone would trigger 0.13°C of global warming on top of 1.5°C, the temperature target of the Paris agreement (Wunderling, Willeit, et al. 2020).

The freshwater input into the North Atlantic via surface runoff or iceberg calving contributes to the deep water formation and is relevant to the Atlantic Meridional Overturning Circulation (AMOC) (Gaucherel and Moron 2016; Kriegler et al. 2009) Increased freshwater input from Greenland Ice Sheet might destabilize the current state of the AMOC, thus, the resilience of the Greenland Ice Sheet is linked to the resilience of the AMOC. A weakening or a shutdown of the AMOC would changes oceanic conditions in Antarctica, possibly leading to increased melt as heat accumulated in the Southern ocean (Kriegler et al. 2009) but also reduces the amount of warm waters reaching the Greenland Ice Sheet, thereby driving a local cooling (Hu et al. 2013), which can mitigate the heat accumulation in the Arctic and increase its resilience. Decrease of the strength of the AMOC is already observable at present day (Caesar et al. 2018). A more direct effect between the Greenland and the Antarctic Ice Sheet is the interaction through rising sea levels, destabilizing the ice shelves in Antarctica and thus leading to additional sea level rise (Kriegler et al. 2009). Both long-reach interactions link the resilience of the Antarctic Ice Sheet to the Greenland Ice Sheet.

Finally the ice sheet also impacts the lithosphere, on the one hand by isostacy, the viscoelastic response of the elastic lithosphere and the viscous Earth mantle and on the other hand by erosion of the underlying bedrock. Local sea level is impacted by the self-gravitation of the ice sheet, thus it can decrease if the ice sheet is losing mass. As a consequences the local sea level in locations far away from the Greenland Ice Sheet would rise, thus creating a long-reach interaction between the Greenland and the Antarctic Ice Sheet.

Several possible feedbacks between the Greenland Ice Sheet and the Earth system follow from these interaction pathways: besides the positive melt-elevation feedback the orographic precipitation constitutes a negative feedback between the climate and the topography of the Greenland Ice Sheet. The reduced elevation of the Greenland Ice Sheet allows more moisture to be advected to the interior of the ice sheet, thereby increasing the climatic mass balance. Increased precipitation and feedbacks between the topography and precipitation patterns might increase the resilience of the Greenland Ice Sheet to global warming (Gregory et al. 2020) and therefore need to be understood and included in more models (see also Le Clec'h et al. 2019; Vizcaíno et al. 2015).

The Greenland Ice Sheet is not the only tipping element of the Earth system; Lenton, H. Held, et al. (2008) identified nine policy relevant tipping elements, namely the Arctic summer sea sce, the West Antarctic ice sheet, the Atlantic

meridional overturning circulation, the El Niño–Southern Oscillation, the Indian summer monsoon, the West African monsoon, the Boreal forest and the Amazon rainforest. A first assessment concluded that of three of these are at risk for being tipped within the Paris agreement, namely the two ice sheets and the Arctic summer sea ice (Schellnhuber et al. 2016). An updated assessment attributes an even higher risk within the Paris agreement and more so under current policies (Armstrong McKay et al. 2021). The interaction of different tipping points might reduce their critical temperatures for tipping even further (Martin et al. 2021; Wunderling, Gelbrecht, et al. 2020) and tipping cascades might be preferentially initiated by the loss of the Greenland Ice Sheet (Wunderling, Donges, et al. 2021). These findings suggest, that the resilience of the Earth system against anthropogenic global warming depends on the resilience of the Greenland Ice Sheet.

Finally, there is also an interaction between Greenland and the social sphere. On the one hand human actions directly impact the fate of the Greenland Ice Sheet through anthropogenic climate change. On the other hand the resulting sea level rise impacts human societies and threatens cultural heritage (Levermann, P. U. Clark, et al. 2013; Masson-Delmotte et al. 2021; Pörtner et al. 2019). Recent research efforts concentrate on closing the loop between the Earth System and the Social system, focusing for example on how sea level rise anticipation might shift people toward stronger climate action (Donges, Heitzig, et al. 2020; Donges, Lucht, et al. 2021; Donges, Winkelmann, et al. 2017; Müller-Hansen et al. 2017; E. K. Smith et al. 2022).

1.2 Feedbacks

In this section, I will present the most important feedbacks governing the dynamics of the Greenland Ice Sheet. I will not explain the mechanisms driving marine feedbacks, like the Marine Ice Sheet Instability (MISI) (see e.g. Schoof 2007; Weertman 1974 for further information) or the Marine Ice Cliff Instability (MICI) (see e.g. DeConto and Pollard 2016; Edwards et al. 2019; Pörtner et al. 2019 for further information). Those feedbacks are relevant for marine ice sheets with large ice shelves, like the Antarctic Ice Sheet, but are of less importance for the Greenland Ice Sheet.

For the Greenland Ice Sheet, an important and well known feedback is the **melt-elevation feedback**. It is driven by atmospheric temperatures: the air

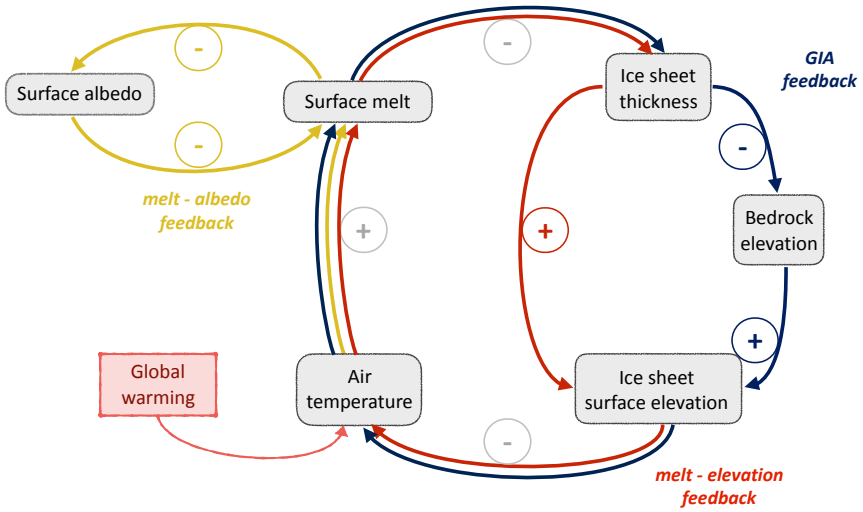

Figure 1.2: Schematic representation of the three important feedbacks for the Greenland Ice Sheet studied in this thesis. The plus and minus signs on the arrows represent positive and negative correlation between the two variables connected by that arrow. **Melt-albedo feedback (positive)** (yellow): Air temperatures over Greenland increase with global warming, which leads to more melt (positive correlation). Increased melt decreases the ice surface albedo (negative correlation), allowing the ice to absorb more radiative energy. This in turn increases the melt rate (negative correlation). **Melt-elevation feedback (positive)** (red): Increased air temperatures lead to more melt (positive correlation). Increased melt decreases the ice thickness (negative correlation), and this in turn decreases the ice surface latitude (positive correlation). Due to the temperature lapse rate, a lowered surface elevation leads to warmer air temperatures (negative correlation). **GIA feedback (negative)** (blue): Increased air temperatures lead to more melt (positive correlation), which reduces the ice thickness (negative correlation). In consequence the load onto the viscous solid Earth decreases, allowing for a bedrock uplift (negative correlation). This in turn increases the ice surface elevation (positive correlation). At this point the GIA feedback feeds into the melt-elevation feedback, namely a decrease in air-temperature due to the increase in surface elevation (negative correlation) and therefore a decrease in surface melt (positive correlation). Note that the melt-albedo feedback is on a fast timescale and is reset annually due to winter snow. The melt-elevation feedback is on an intermediate timescale, as topographical changes are typically on a time-scale of several years. The GIA-feedback is on a multi-centennial to multi-millennial timescale, due to the high viscosity of the bedrock.

at higher elevation is usually colder than the air at lower elevations, typically the vertical temperature change is as high as $5 - 7°C/km$. This is called the atmospheric temperature lapse rate. Note that temperature inversion, where cold air sinks down while higher elevations remain warmer may occur in low altitudes of the Greenland Ice Sheet, however, this is rather a local and seasonal effect (Reeh 1991). The positive (self-reinforcing) melt elevation feedback is driven by the atmospheric lapse rate: The local surface air temperature increase (e.g. due to global warming), leads to increased melt rates. As a consequence to higher melt rates the ice thickness decreases. Assuming a static bedrock, the surface height of the ice sheet decreases as the thickness is reduced. Due to the atmospheric temperature lapse rate this decrease in surface height, in turn, exposes the ice surface to even warmer air temperatures, which trigger higher melt rates. As the ice surface elevation decreases further due to high melt rates, the positive (reinforcing initial changes) feedback loop is closed. A schematic of the melt-elevation feedback is given in Figure 1.2.

Studies of the melt-elevation feedback on an idealized ice-sheet suggest that this feedback is sufficient to induce a tipping behavior, leading to irreversible ice loss if temperatures exceed a threshold, even in the absence of further forcing (Levermann and Winkelmann 2016). Boers and Rypdal (2021) have already found through the analysis of melt rate time series first early warning signals in the west Greenland Ice Sheet, suggesting that these parts of the ice sheet might already be in the process of tipping, mainly driven by the melt-elevation feedback.

Another important feedback associated with melt is expressed through the albedo, a measure for the ability to reflect solar radiation, of the ice sheet: the **melt-albedo feedback**. It is driven by the increased absorption of solar radiation: darker surfaces absorb more radiation energy than lighter surfaces and therefore experience stronger melt under otherwise similar conditions. The melt, in turn, tends to reduce the albedo of the surface. Fresh snow for instance has the highest albedo, but melt changes the optical properties of the snow cover, leading to reduced albedos (Stroeve 2001). Once the snow cover has melted completely, firn or bare ice which have an even lower albedo are exposed. The positive feedback is thus driven by the melt, which lowers albedo, which in turn promotes melt. A schematic of the melt-albedo feedback is given in Figure 1.2. Box, Wehrlé, et al. (2022) quantify the impact of the melt-albedo feedback in the 2021 melt event of the Greenland Ice Sheet and find that it locally adds

up to 51% of additional melt rates where the bare is exposed. This feedback is periodically interrupted though fresh snowfall in the winter (Gardner and Sharp 2010; Noël, van de Berg, van Meijgaard, et al. 2015). Note that the albedo might decrease below the bare ice value through e.g. the formation of deep melt ponds, accumulation of algae and dust or the opening crevasses (Box 2013; Box, Fettweis, et al. 2012; Box, van As, et al. 2017; Cook et al. 2020; Ryan, L. C. Smith, et al. 2019; Tedstone, Bamber, et al. 2017; Tedstone, Cook, et al. 2020; Williamson et al. 2020), however the details of these processes are difficult to model and therefore they are mostly not represented in ice melt models.

The interaction of the ice with the solid Earth drives the **GIA feedback**. Local changes in ice load induce a solid Earth response, also known as glacial isostatic adjustment (GIA). In particular, ice losses reduce the load onto the solid ground and lead to bedrock uplift, increases in ice mass lead to subsidence of the bedrock. The response of the bedrock partially counteracts changes of ice surface elevation due to changing ice thickness, it thus acts as a stabilizing negative feedback and mitigates the positive melt-elevation feedback.

As the asthenosphere is approximately three times more dense than ice, Archimedes' principle allows us to estimate the bedrock response after a change in ice load to be approximately 1/3 of the ice thickness change in equilibrium. This response happens on both, very long and short timescales. As detailed in Section 1.3.3 the elastic lithosphere responds on short timescales to contemporary changes in the ice load, in contrast the viscous mantle responds on timescales between centuries and many tens of millennia, depending on the local viscosity. The negative (dampening initial changes) GIA feedback can partly counteract the melt elevation feedback in Greenland and thus mitigate ice thinning – as the bedrock responds to changes in ice load a decrease in ice thickness does not translate directly to a decrease in ice surface altitude, weakening the link between ice thickness and climatic mass balance. A schematic of the GIA feedback is given in Figure 1.2.

In the scope of this thesis I focus on the three feedbacks described above, namely the melt-elevation, the melt-albedo and the GIA feedback. There are, however, feedbacks and interactions between the ice and the regional climate system, which need a detailed description of not only the ice but also the dynamics of the surrounding circulation system. As Gregory et al. (2020) found, these feedbacks, especially the change in precipitation patterns, might play an important role in stabilizing the Greenland Ice Sheet.

Feedbacks are also found in interactions between the ice sheet and the ocean, either through the effect on the supraglacial meltwater plume, which in turn affects the melt rates at the tidewater glacier front (Carroll et al. 2016; Fyke et al. 2018) or through the glacier front retreating to deeper areas, being exposed to warmer waters over a larger area (Rignot et al. 2010). However, under strong warming scenarios the Greenland Ice Sheet is expected to retreat inland, thus the ice-ocean feedbacks might be of limited relevance for the overall stability of the Greenland Ice Sheet.

1.3 Modeling ice-sheet dynamics

Process-based numerical modeling of ice sheets in a warming world is crucial to estimating future sea level rise and understanding their resilience to global changes. The main processes covered in ice sheet models, which are most relevant to the present state of the ice sheet, are summarized in the following section and in Figure 1.3.

The mass balance of continental ice sheets, such as the Greenland Ice Sheet, is governed by multiple processes: basal melt, ice flow and discharge into the ocean, melt at the ice-ocean interface, and the climatic mass balance. Currently the mass loss of the Greenland Ice Sheet is at 148 Gt/yrear (IMBIE Team 2020). The climatic mass balance contributes 76 Gt/year and the dynamical ice losses are usually assumed to be the difference between total mass loss and the climatic mass balance contribution (IMBIE Team 2020). However, basal melt amounts to 21.4 Gt/year and is increasing further with ongoing global warming Karlsson et al. 2021.

Changes in the regional climate, for example in air temperature, cloud conditions, or precipitation, directly affect melt and accumulation rates and thereby the climatic mass balance. Currently, approximately 57% of the mass loss rate is caused by changes in the climatic mass balance and the rest is driven by changes in the dynamic discharge of ice into the ocean (IMBIE Team 2020). This share has already increased in comparison to the past 46 years (Mouginot, Rignot, Bjørk, et al. 2019) and is expected to increase further under global warming, as the Greenland Ice Sheet retreats from the coast and increased melt becomes the most dominant process of ice loss (Aschwanden, Fahnestock, Truffer, et al. 2019). The flow of ice transports the ice masses from the accumulation zone inland, where the climatic mass balance is positive, to the margins, where the

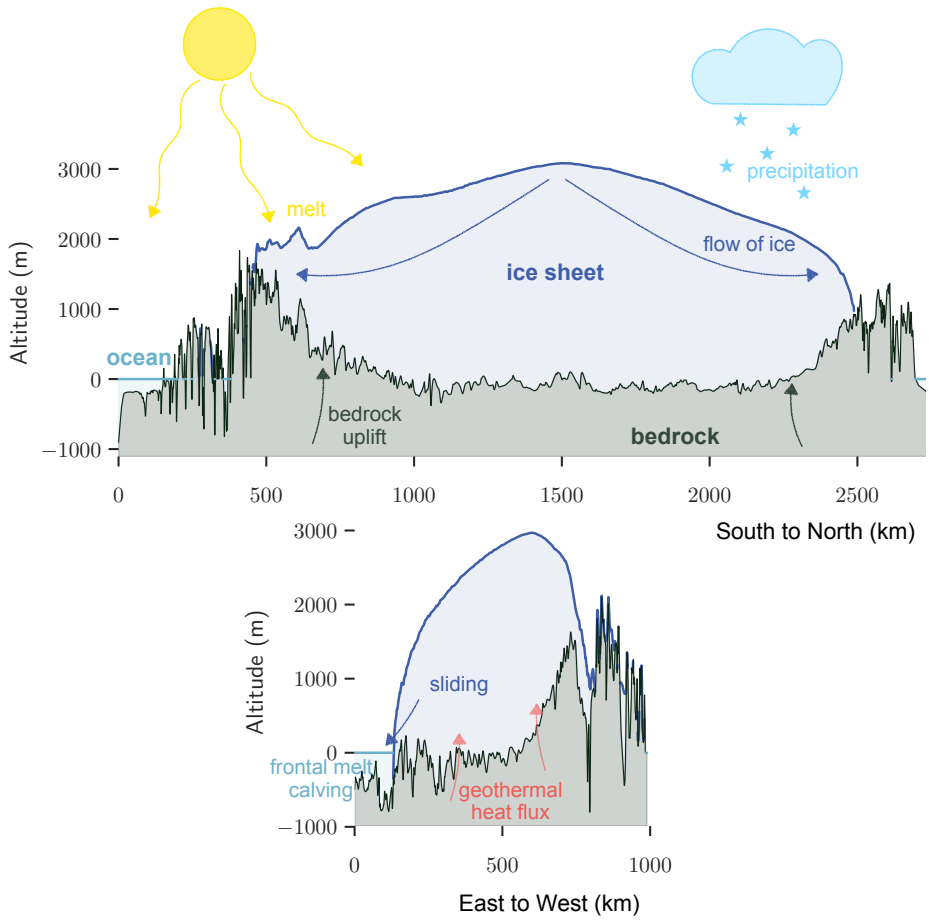

Figure 1.3: Two cross sections of the Greenland Ice Sheet and the underlying bedrock, from South to North and from East to West with a schematic of several important processes related to the mass balance of the Greenland Ice Sheet. Relevant processes are precipitation and melt for the climatic mass balance, the ice-ocean interaction, and the flow and sliding of ice. The bedrock responds to a decrease in ice load with a bedrock uplift. Topography data from BedMachine v3 (Morlighem et al. 2017). Please note that the x-axis is shown in km while the y-axis is shown in m and therefore greatly exaggerated. In reality the ice sheet is much less high than wide, justifying the shallow ice and the shallow shelf approximation used by many ice sheet models (see text).

ice is either directly discharged into the ocean or melts while being on land. An isostatic adjustment of the solid Earth is expected if the ice load is changing. While this alone has no direct effect on the mass balance of the ice sheet, it can have indirect effects by changing the surface altitude and thereby affecting the local climatic mass balance.

Numerical ice sheet models can help us to improve our understanding of these processes and compute the evolution of the ice sheet under particular boundary conditions. Aschwanden, Fahnestock, and Truffer (2016) for instance, have shown that the ice sheet model PISM can capture complex ice flow though the outlet glaciers of the Greenland Ice Sheet, provided the resolution is sufficiently high. These models help to project future sea level rise in different climate scenarios, as presented, for instance, in the IPCC reports (Masson-Delmotte et al. 2021; Pörtner et al. 2019).

Process based ice sheet models aim to describe the internal physics of the ice body, including the stresses and strains and the thermodynamics, all affecting the flow of ice. In addition to the internal physics of ice, the ice sheet models require boundary conditions at the bottom of the ice, the ice-ocean and the ice-atmosphere interfaces, for both, mass fluxes and temperatures or heat fluxes. An overview of the different processes is found in Figure 1.3.

In the following, I will give more detailed introductions to the model components crucial for my PhD projects, concerning in particular the flow of ice, the melting at the ice-atmosphere interface and the interaction of ice and solid Earth.

1.3.1 Modeling the flow of ice

In process-based ice sheet models, the ice is commonly treated like a viscous fluid and it's evolution is modeled using the equations of continuum dynamics, e.g. mass continuity and conservation of momentum. Together with constitutive equations describing the material laws, and the appropriate approximations, e.g. homogeneity and isotropy, the large scale dynamics of ice sheets can be described. In particular, the full *Navier-Stokes Equation* is simplified to the *Stokes Equation* (Greve and Blatter 2009) by neglecting the acceleration- and the Coriolis-term. In addition to the hydrostatic approximation, the thermomechanically coupled Parallel Ice Sheet Model (PISM) uses the shallow ice approximation (SIA) and the shallow shelf approximation (SSA) in order to efficiently calculate ice

velocities (Bueler and Brown 2009; Greve and Blatter 2009; the PISM authors 2018; Winkelmann et al. 2011).

In addition to the balance equation for mass, momentum and internal energy, and the appropriate approximations, constitutive equations are needed in order to close the under-determined system of equations. Before we look at the most widely used constitutive equation for polycrystalline ice, *Glen's flow law*, it is important to understand the creep behavior of ice. The response of ice to stress, e.g. simple shear stress, is characterized by three consecutive creep regimes. The initial response is an elastic deformation of the ice, which is typically neglected in ice sheet models. This initial response is followed by the primary creep, where the deformation rate decreases continuously, even when the stress is held constant. This behavior is explained by the random orientation of individual, anistropic ice crystals: their increasing geometric incompatibilities decrease the deformation rate of the ice. Then, in the secondary creep, the deformation rate reaches a minimum and remains constant, the ice acts as a isotropic medium. This secondary creep regime allows to easily establish a clear relation between stress and strain rate, as the strain rate is constant in time. At high temperatures or high stresses, the ice grains themselves are affected, undergoing a so-called dynamic recrystallization, orienting themselves favorably to the deformation. This leads to increasing deformation rates in the third creep regime, the so called tertiary creep (Cuffey and Paterson 2010; Greve and Blatter 2009).

The unique (for a given stress, a given temperature and a given ice probe with its microstructure) relationship between stress and strain rate in the secondary creep is used to establish a material law, the flow law, which can close the equation system. It is implicitly assumed that the ice is of homogeneous density and isotropic.

The flow law reads

$$\dot{\epsilon}_{ij} = A\tau_{\text{eff}}^{n-1}\tau_{ij}, \tag{1.1}$$

with the tensor components of the strain rate tensor $\dot{\epsilon}_{ij}$, the deviatoric stress tensor τ_{ij}, the effective stress τ_{eff}, which corresponds to the second invariant of the stress tensor (Cuffey and Paterson 2010; Greve and Blatter 2009) and the flow parameters for softness A and flow exponent n.

The flow exponent n is usually assumed to be constant throughout the ice sheet, $n = 3$ is the most widely used value, meaning the flow of ice is highly non-linear. The softness A is typically described as an Arrhenius function of (pressure

adjusted) temperature, describing the softening with increasing temperature:

$$A(T) = A_0 \cdot \exp\left(-\frac{Q}{RT'}\right) \tag{1.2}$$

with the factor A_0, the activation energy Q, the universal gas constant R and the temperature difference to the pressure melting point T'. In order to account for the increased temperature dependence of the ice softness at high temperatures (typically above -10°C) the Arrhenius function uses a different activation energy Q (and a different factor A_0) for ice above and below the threshold temperature, here termed warm and cold ice (Cuffey and Paterson 2010; Greve and Blatter 2009).

While ice sheet modeling studies mostly use a specific set of parameters for the flow parameters n, Q and A_0 in fact major uncertainties remain with respect to these parameters and are discussed in Section 3.1.

While the flow law as shown in Equation (1.1) is widely used by the ice sheet modeling community, other, more complex, flow laws exits and are adopted into ice sheet models. For example it has been argued, that for glaciers and ice sheets both, grain boundary sliding (GBS) and dislocation creep are relevant processes. Grain boundary sliding is dependent on grain size and associated with a lower flow exponent, dislocation creep is independent of grain size and associated with a higher flow exponent. A composite flow law including both processes can then be used (Goldsby and Kohlstedt 2001; Kuiper et al. 2020; Montagnat and Duval 2000; Saruya et al. 2019). However, covering these flow laws in depth is beyond the scope of this thesis and we will use the flow law as shown in Equation (1.1).

In the shallow ice approximation (SIA), only the bed-parallel shear stress is considered for driving the flow of ice. The *driving stress* τ_d is described as

$$\tau_d = -\rho g H \nabla h \tag{1.3}$$

with the ice density ρ, the gravity g, the ice thickness H and the gradient in x and y direction of the surface elevation h. Together with the flow law, as shown in Equation (1.1) the ice velocity in shallow shelf approximation $\mathbf{v}_{\mathrm{SIA}}$ reads as

$$\mathbf{v}_{\mathrm{SIA}}(z) = -2(\rho g)^n |\nabla h|^{n-1} \left[\int_b^z E_{\mathrm{SIA}} A(T')(h-\xi)^n \mathrm{d}\xi\right] \nabla h, \tag{1.4}$$

with the the vertical coordinate z, the altitude of the bedrock b, and the enhance-

ment factor E_{SIA}, which is used to account for the non-isotropic nature of glacial ice in tertiary creep (the PISM authors 2018; Winkelmann et al. 2011).

The shallow shelf approximation (SSA) is typically used for ice shelves or sliding ice streams, in conditions where the basal drag is very low and the ice slides. While the stress regime is different from the SIA regime, the flow law enters here as well. Models like PISM allow to use different flow exponents n and different enhancement factors for SSA and SIA velocities which can be a way to represent anisotropy and other unresolved effects (Ma et al. 2010).

1.3.2 Modeling surface melt

In contrast to the flow law described above, which is critical for calculating the internal deformation of ice, surface melt is part of the climatic mass balance and thus an important boundary condition in ice sheet modeling efforts. The climatic mass balance describes the mass fluxes at the ice-atmosphere interface, which is what a stand-alone ice sheet model like PISM needs as boundary condition, together with the temperature of the ice surface. See also the schematics in Figure 1.3.

The climatic mass balance of an ice sheet is a combination of several processes: accumulation contributes positively to the climatic mass balance while sublimation and melt contribute negatively. The meltwater penetrating the snow and firn pack can partly refreeze and, thus, refreezing is contributing positively to climatic mass balance, while the remaining meltwater is counted as runoff of the ice sheet.

A wide range of (melt) models is available to provide that boundary condition: from process-based snowpack models coupled to regional climate models, explicitly computing the regional climate and energy fluxes in the snow and at the ice surface (Fettweis, Box, et al. 2017; Fettweis, Franco, et al. 2013; Krapp et al. 2017; Langen et al. 2015; Niwano et al. 2018; Noël, van de Berg, van Meijgaard, et al. 2015), to simpler parameterizations like the positive-degree-day (PDD) or other temperature index models (e.g. Reeh 1991). The interaction between the ice and the atmosphere is characterized by various feedbacks, e.g. the melt–elevation feedback or the melt-albedo feedback (Box, Fettweis, et al. 2012; Tedstone, Bamber, et al. 2017). A similar feedback can be found with algae living on the ice, which also change local albedo and therefore enhance melt (Cook et al. 2020; Di Mauro et al. 2020; McCutcheon et al. 2021; Tedstone, Cook, et al. 2020; Williamson et al. 2020). However, the interactions with the biosphere

are beyond the scope of this work. These feedbacks can be captured by interactively coupling a regional climate models with an ice sheet model to compute all relevant interactions between ice, snow and atmosphere (Le Clec'h et al. 2019). For simulations over centuries to millennia, where explicitly resolving all processes would come at a considerable computational cost, a simpler approach is needed. In such cases, the surface mass balance is typically calculated from near-surface air temperatures with temperature index methods, e.g. the positive degree day (PDD) model (Aschwanden, Fahnestock, Truffer, et al. 2019; Rückamp et al. 2019; Wilton et al. 2017). The PDD model (Reeh 1991) needs only monthly mean air-temperature and information about snow cover to compute melt from the number of positive degree days PDD, which reads as

$$\mathrm{PDD} = \frac{1}{\sigma\sqrt{2\pi}} \int_{t_0}^{t_0+\Delta t} \mathrm{d}t \int_0^{\infty} \mathrm{d}T\, T \exp\left(-\frac{(T - T_{\mathrm{ac}}(t))^2}{2\sigma^2}\right). \tag{1.5}$$

Here t_0 is the beginning and Δt the length of the time interval over which the melt is computed, T_{ac} is the monthly mean temperature in an annual cycle, and σ is the standard deviation of the temperature from the annual cycle. The melt of snow or ice is then computed by multiplying a degree day factor f_s or f_i to the number of positive degree days. The melt factor is larger for ice than for snow, implicitly accounting for the fact that ice has a lower albedo, absorbs more radiation and therefore melts stronger at the same temperature. For the PDD approach, the full climatic mass balance is usually computed by assuming a fixed refreezing rate and a fixed yearly precipitation cycle, which is given as input. At present day, the PDD model compares well with the results of regional climate models such as RACMO or MAR (Fettweis, Box, et al. 2017; Fettweis, Hofer, et al. 2020; Noël, van de Berg, van Wessem, et al. 2018). This is not surprising, because PDD models are often calibrated using these regional models.

However, the PDD approach cannot explicitly account for changes in solar radiation over the course of a year. Several more or less simple models are available to correct for that issue, e.g. the extention of the PDD model to include insolation by Hock (1999), the insolation–temperature–melt equation used by van den Berg et al. (2008) and Robinson et al. (2010), or the Surface Energy and Mass balance model of Intermediate Complexity (SEMIC) from Krapp et al. (2017). In my PhD project I chose to implement a simplified version of the diurnal energy balance model *dEBM-simple* (Krebs-Kanzow, Gierz, and Lohmann 2018; Krebs-Kanzow, Gierz, Rodehacke, et al. 2021) into the Parallel Ice Sheet Model

PISM. *dEBM-simple* includes solar radiation induced melting and an implicit diurnal scheme to account for changing day lengths, but is simple enough to require as few inputs as the PDD model. The melt equation in dEBM-simple reads

$$M = \frac{\Delta t_\Phi}{\Delta t \rho_w L_m}\left(\tau_\mathrm{A}(1-\alpha_s)\bar{S}_\Phi + c_1 T_\mathrm{eff} + c_2\right), \tag{1.6}$$

with fresh water density ρ_w, latent heat of fusion L_m, the short wave downward radiation averaged over the daily melt period (when the sun is above the angle Φ) $\bar{S}_\Phi$, and the surface albedo α_s. Here, the first term of the equation describes insolation driven melt, which depends on the albedo and the amount of short wave radiation reaching the ice surface, the second term describes the directly temperature driven melt, and the third term is a constant offset related to the longwave upward radiation. The time period of a day, when the sun is above the elevation angle Φ is denoted by Δt_Φ. The length of a day is Δt and the fractional time that the sun is above the elevation angle Φ is given by:

$$\frac{\Delta t_\Phi}{\Delta t} = \frac{h_\Phi}{\pi} = \frac{1}{\pi}\frac{\sin\Phi - \sin\varphi\sin\delta}{\cos\varphi\cos\delta} \tag{1.7}$$

with h_Φ being the hour angle when the sun has an elevation angle of at least Φ, δ being the solar declination angle and φ the latitude.

1.3.3 Modeling the solid-Earth response

Solid Earth responds to changes in ice load, as depicted by gray arrows in Figure 1.3, and typically this response is thought to happen on a long timescale (i.e. the uplift due to the last deglaciation is still measurable). Similarly to models computing the climatic mass balance, which range from process-based full representations of energy and mass balance to simpler approximations of the most relevant processes, a broad range of models describing the interactions between ice sheets and solid Earth exist. Many solid Earth models explicitly solve the sea-level equation, taking into account the spherical shape of the Earth, gravitational and rotational effects and possibly even lateral variations of the solid Earth structure, see e.g. (De Boer et al. 2014; Fleming and Lambeck 2004; Gomez, Latychev, et al. 2018; Gomez, Pollard, et al. 2013; Gomez, Weber, et al. 2020; Haeger et al. 2019; Khan et al. 2016; Lambeck et al. 2014; Martinec 2000;

Simpson et al. 2009; Tosi et al. 2005; Whitehouse 2018; Whitehouse, Gomez, et al. 2019; Whitehouse, Latychev, et al. 2006). While there is ongoing work to couple ice sheet models to fully process based solid Earth models, many ice sheet focused studies use simpler models to represent the response of the solid Earth, for example elastic lithosphere relaxing asthenosphere (ELRA) type models. The elastic lithosphere is often modeled as a plate with flexural rigidity, reacting instantly to changes in ice load. In contrast the relaxing asthenosphere is often modeled as a delayed adjustment with a constant slow relaxation time of the solid Earth (Le Meur and Huybrechts 1996; Zweck and Huybrechts 2005).

The Lingle-Clark model, which is used in this thesis, generalizes the ELRA type model with a viscous half-space and solves the resulting equations explicitly in time (Bueler, Lingle, et al. 2007; Lingle and J. A. Clark 1985). The resulting partial differential equation for vertical displacement u of the bedrock can be described by

$$2\eta|\nabla|\frac{\partial u}{\partial t} + \rho_r g u + D\nabla^4 u = \sigma_{zz}, \tag{1.8}$$

with the viscosity of the upper mantle η, its density ρ_r, the flexural rigidity of the lithosphere D, the gravitational acceleration of the Earth g, and σ_{zz}, the ice load force per unit area (Bueler, Lingle, et al. 2007). The relaxation time of the solid Earth then depends on the spatial wavelength of the perturbation in ice load. However, it assumes a fixed structure of the solid Earth, not taking any lateral variations of the mantle viscosities or the thickness of the lithosphere into account.

1.4 Scope and contents of the thesis

In my thesis, I focus on modeling the Greenland Ice Sheet in a warming world. In particular, I explore how different feedbacks affect our understanding of the relevant mass balance processes. In addition, I study the uncertainties arising from uncertainties in the flow law or in melt modeling. Figure 1.4 gives an overview of the manuscripts related to this thesis.

The results of this thesis are based on numerical simulations with the ice sheet model PISM, but the modeling choices and experimental details used for each sub-project differ. An idealized flowline experiment was chosen in order to study how ice flow responds to changes in uncertain parameters of the flow law, as it

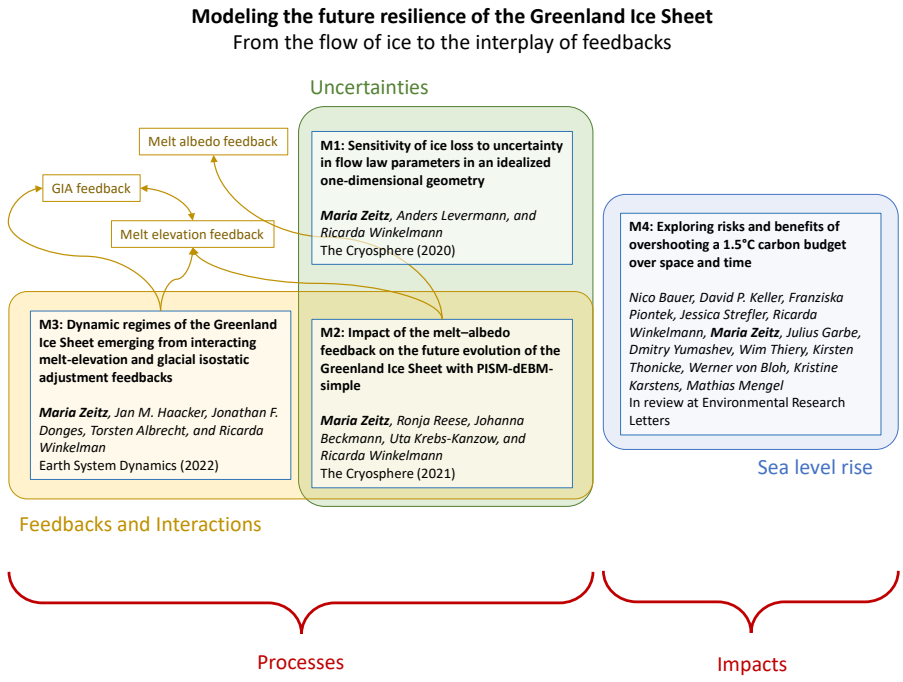

Figure 1.4: Overview over the sub-projects of this thesis. The two main topics of my thesis are the analysis of process uncertainties, as e.g. the impact of the parametric uncertainties in Glen's flow law (Manuscript 1) or in the melt model dEBM-simple (Manuscript 2), and the analysis of feedbacks, as in Manuscript 2 and 3. While those sub-projects are mainly focused on advancing our understanding of fundamental processes, I also study the impacts of particular anthropogenic global warming scenarios onto the sea level contribution of the Greenland Ice Sheet (Manuscripts 4). All parts of my thesis are tied together by the common question of how anthropogenic global warming affects the Greenland Ice Sheet.

allows to disentangle the flow driven ice losses from other impacts, such as melt or the impacts of geometry (Manuscript 1). For the second sub-project, studying the impact of the melt-albedo feedback on Greenland ice loss in future warming scenarios, I implemented a new sub-module in PISM and developed simple parameterizations for the ice surface albedo and the atmospheric transmissivity. In addition, I performed simulations of the Greenland Ice Sheet in a realistic warming scenario, focusing on the impact of albedo on melt (Manuscript 2). To study the long-term dynamic regimes of the Greenland Ice Sheet, I simulated the ice dynamics under idealized warming scenarios with a particular focus on the melt-elevation feedback and the glacial isostatic adjustment (GIA) feedback (Manuscript 3). Moreover, I explored the sea-level contribution from the Greenland Ice Sheet under policy-relevant scenarios – the flexibility of the carbon budget on the one hand (Manuscript 4).

Within the next section, the publications that constitute my dissertation are outlined with the original publications given in Chapter 2. In Chapter 3, I provide a synthesis of the results. This is followed by a final discussion in Chapter 4.

1.5 Overview of manuscripts

This thesis comprises three-peer reviewed scientific articles as first author and one additional manuscript as co-author, which is currently under review. Each article is a stand-alone contribution with an introduction, results, methods and conclusions as well as references. I here give an overview of the individual articles and the author contributions. A more detailed summary together with the original manuscript can be found for each article in Chapter 2. Supplementary material to the articles can be found in the Appendix A.

Manuscript 1 (published): Sensitivity of ice loss to uncertainty in flow law parameters in an idealized one-dimensional geometry

Maria Zeitz, Anders Levermann, and Ricarda Winkelmann

In this paper, the impact of the flow law parameters on ice loss under warming is explored in a idealized flow-line model. The idealization allows to disentangle the impacts of the flow parameters from other influences like bed topography or climate. Maria Zeitz designed the research and the appropriate experimental

procedure with the help of Anders Levermann and Ricarda Winkelmann. Maria Zeitz conducted the literature research in order to estimate the uncertainty range for the flow law parameters. She conducted the simulations and analyzed and visualized the data. Maria Zeitz created all figures supporting the manuscript. She wrote the manuscript with support of the co-authors.
Published in The Cryosphere (2020), doi:10.5194/tc-14-3537-2020
https://tc.copernicus.org/articles/14/3537/2020/

Manuscript 2 (published): Impact of the melt–albedo feedback on the future evolution of the Greenland Ice Sheet with PISM-dEBM-simple

Maria Zeitz, Ronja Reese, Johanna Beckmann, Uta Krebs-Kanzow, and Ricarda Winkelmann

The impact of the melt-elevation feedback on ice loss of the Greenland ice sheet is studied with warming simulations. To this end Maria Zeitz adapted and implemented the diurnal Energy Balance Model (dEBM), originally developed by Uta Krebs-Kanzow, in the Parallel Ice Sheet Model (PISM). She developed parameterizations and simplifications, which make PISM-dEBM-simple usable with only temperature fields as input. Maria Zeitz conducted the PISM simulations and analyzed and visualized the data. She created all figures in the manuscript. Maria Zeitz and Ronja Reese designed the experiments and wrote the manuscript, with support from all authors.
Published in The Cryosphere (2021), doi:10.5194/tc-15-5739-2021
https://tc.copernicus.org/articles/15/5739/2021/

Manuscript 3 (published): Dynamic regimes of the Greenland Ice Sheet emerging from interacting melt-elevation and glacial isostatic adjustment feedbacks

Maria Zeitz, Jan M. Haacker, Jonathan F. Donges, Torsten Albrecht, and Ricarda Winkelmann

The interaction between the positive (enhancing) melt-elevation feedback and the negative (mitigating) glacial isostatic uplift feedback allows for diverse dynamic regimes of the Greenland Ice Sheet like recovery, self-sustained oscillations and irreversible loss. Together with Ricarda Winkelmann, Maria Zeitz

supervised the Master thesis of Jan Haacker, who performed and analyzed the first experiments. She then expanded on the experiments by including variations in the temperature lapse rate, allowing to interpret the results with the concept of two competing feedbacks. All figures in the manuscript were created by Maria Zeitz. She wrote the manuscript with contributions from all co-authors.
Published in Earth System Dynamics (2022), doi:10.5194/esd-13-1077-2022
https://esd.copernicus.org/articles/13/1077/2022/

Manuscript 4 (in review): Exploring risks and benefits of overshooting a 1.5°C carbon budget over space and time

Nico Bauer, David P. Keller, Franziska Piontek, Jessica Strefler, Ricarda Winkelmann, Maria Zeitz, Julius Garbe, Dmitry Yumashev, Wim Thiery, Kirsten Thonicke, Werner von Bloh, Kristine Karstens, Mathias Mengel.

Temperature targets as specified in the Paris Agreement limit global net cumulative emissions to very tight carbon budgets. The possibility to overshoot the budget and offset near-term excess carbon emissions by future net-negative emissions is considered economically attractive because it can ease near-term mitigation pressure. Potential side effects of carbon removal deployment is discussed extensively, the additional climate risks and the impacts and damages have attracted less attention so far. Here we couple various models for an integrative analysis of the climatic, environmental and socio-economic consequences of temporarily overshooting a carbon budget consistent with the 1.5°C temperature target. Maria Zeitz contributed the PISM simulations of the sea-level contribution of the Greenland Ice Sheet under both climate scenarios. She created, together with Julius Garbe, the figure showing the sea level contributions from the two large ice sheets and has contributed to writing the sea level rise related parts of the manuscript.
In review at Environmental Research Letters

2 Original Manuscripts

Manuscript 1 (published): The impact of the uncertainty in flow law to an idealized flow-line setup

Here, we use the uncertainty in flow law parameters from an in-depth literature research (see Figure 3.1) in order to asses how the parametric uncertainty of *Glen's flow law* translates into uncertainty of ice flow. In order to disentangle the effect of the flow parameters from other possible influences, we use an idealized flow-line setup of a two-dimensional ice sheet sitting on a flat bed subject to surface warming, while keeping the accumulation rate fixed. Indeed, the variation of the flow exponent n and the activation energies Q_w and Q_c leads to a significant acceleration of flow-driven ice loss due to warming. In the first century, the ice loss varies by a factor of two over the whole parameter range compatible with published values. This impact, however, decreases over time and once the ice sheet has reached equilibrium under the new surface temperature (after several millennia), the ice volume varies only by approx. 10%. The absolute uncertainty increases with increasing temperature forcing, and the uncertainty ranges for flow-driven ice losses at different temperatures overlap.

While these results do not translate directly onto the uncertainty of flow driven ice losses of the Greenland or Antarctic Ice Sheet, they nevertheless point to overlooked uncertainties in ice sheet modeling.

Published in The Cryosphere (2020), doi:10.5194/tc-14-3537-2020
https://tc.copernicus.org/articles/14/3537/2020/

The Cryosphere, 14, 3537–3550, 2020
https://doi.org/10.5194/tc-14-3537-2020

The Cryosphere Open Access EGU

Sensitivity of ice loss to uncertainty in flow law parameters in an idealized one-dimensional geometry

Maria Zeitz[1,2], **Anders Levermann**[1,2,3], **and Ricarda Winkelmann**[1,2]

[1]Potsdam Institute for Climate Impact Research (PIK), Member of the Leibniz Association,
P.O. Box 60 12 03, 14412 Potsdam, Germany
[2]Institute of Physics and Astronomy, University of Potsdam, Karl-Liebknecht-Str. 24–25, 14476 Potsdam, Germany
[3]LDEO, Columbia University, New York, USA

Correspondence: Maria Zeitz (maria.zeitz@pik-potsdam.de) and Ricarda Winkelmann
(ricarda.winkelmann@pik-potsdam.de)

Received: 20 March 2020 – Discussion started: 7 April 2020
Revised: 26 August 2020 – Accepted: 9 September 2020 – Published: 27 October 2020

Abstract. Acceleration of the flow of ice drives mass losses in both the Antarctic and the Greenland Ice Sheet. The projections of possible future sea-level rise rely on numerical ice-sheet models, which solve the physics of ice flow, melt, and calving. While major advancements have been made by the ice-sheet modeling community in addressing several of the related uncertainties, the flow law, which is at the center of most process-based ice-sheet models, is not in the focus of the current scientific debate. However, recent studies show that the flow law parameters are highly uncertain and might be different from the widely accepted standard values. Here, we use an idealized flow-line setup to investigate how these uncertainties in the flow law translate into uncertainties in flow-driven mass loss. In order to disentangle the effect of future warming on the ice flow from other effects, we perform a suite of experiments with the Parallel Ice Sheet Model (PISM), deliberately excluding changes in the surface mass balance. We find that changes in the flow parameters within the observed range can lead up to a doubling of the flow-driven mass loss within the first centuries of warming, compared to standard parameters. The spread of ice loss due to the uncertainty in flow parameters is on the same order of magnitude as the increase in mass loss due to surface warming. While this study focuses on an idealized flow-line geometry, it is likely that this uncertainty carries over to realistic three-dimensional simulations of Greenland and Antarctica.

1 Introduction

Current and future sea-level rise is one of the most iconic impacts of a warming climate and affects shorelines worldwide (Hinkel et al., 2014; Strauss et al., 2015). The contribution of the large ice sheets in Greenland and Antarctica to sea-level rise sums up to $13.7 + 14.0$ mm over the last 4 decades (Mouginot et al., 2019; Rignot et al., 2019). It has been accelerating in recent years and is expected to further increase with sustained warming (Levermann et al., 2014, 2020; Mengel et al., 2016; Seroussi et al., 2020; Goelzer et al., 2020; Aschwanden et al., 2019; Bamber et al., 2019). Although some convergence can be observed in the projections of the median contribution of ice loss from Antarctica and Greenland, large uncertainties remain, and coastal protection cannot rely on the median estimate since there is a 50 % likelihood that it will be exceeded. Rather, an estimate of the upper uncertainty range is crucial. The most recent IPCC Special Report on the Ocean and Cryosphere in a Changing Climate provides projections of sea-level rise for the year 2100 of 0.43 m (0.29–0.59 m) and 0.84 m (0.61–1.10 m) for RCP2.6 and RCP8.5 scenarios, respectively (IPCC, 2020). Other studies find slightly different (Goelzer et al., 2011, 2016; Huybrechts et al., 2011) and partly wider ranges (Levermann et al., 2020). Such projections are typically performed with process-based ice-sheet models which represent the physics in the interior and the processes at the boundaries of the ice sheet.

Published by Copernicus Publications on behalf of the European Geosciences Union.

In contrast to these processes at the boundaries of the ice sheet, many rheological parameters of the ice are typically not represented as an uncertainty in sea-level projections. The theoretical basis of ice flow, as implemented in ice-sheet models, has been studied in the lab and by field observations for more than half a century and is perceived as well established (Glen, 1958; Paterson and Budd, 1982; Budd and Jacka, 1989; Greve and Blatter, 2009; Cuffey and Paterson, 2010; Schulson and Duval, 2009; Duval et al., 2010). *Glen's flow law*, which relates stress and strain rate in a power law, is most widely used in ice-flow models. It is described in more detail in Sect. 2.1. Some alternatives to the mathematical form of the flow law have been proposed: multi-term power laws like the *Goldsby–Kohlstedt* law or similar (Peltier et al., 2000; Pettit and Waddington, 2003; Ma et al., 2010; Quiquet et al., 2018) and anisotropic flow laws (Ma et al., 2010; Gagliardini et al., 2013) might be better suited to describe ice flow over a wide range of stress regimes. However, they have not been picked up by the ice-modeling community widely, possibly because this would require introducing another set of parameters which are not very well constrained.

Of all flow parameters, the enhancement factor is varied most routinely and its influence on ice dynamics is well understood (Quiquet et al., 2018; Ritz et al., 1997; Aschwanden et al., 2016). However, recent developments suggest that the other parameters of the flow law are also less certain than typically acknowledged in modeling approaches: A review of the original literature on experiments and field observations shows a large spread in the flow exponent n (which describes the nonlinear response in deformation rate to the given/applied stress), which can be between 2 and 4. New experimental approaches suggest a flow exponent larger than $n = 3$, which has been the most accepted value so far (Qi et al., 2017). Further, via an analysis of the thickness, surface slope, and velocities of the Greenland Ice Sheet from remote-sensing data, Bons et al. (2018) relate the driving stress to the ice velocities in regions where sliding is negligible, and can thus infer a flow exponent $n = 4$ under more realistic conditions. The activation energies Q in the Arrhenius law (which describe the dependence of the deformation rate on temperature) can also vary by a factor of 2 (Glen, 1955; Nye, 1953; Mellor and Testa, 1969; Barnes et al., 1971; Weertman, 1973; Paterson, 1977; Goldsby and Kohlstedt, 2001; Treverrow et al., 2012; Qi et al., 2017)

Here we assess the implications of this uncertainty in simulations with the thermomechanically coupled Parallel Ice Sheet Model (PISM authors, 2018; Bueler and Brown, 2009; Winkelmann et al., 2011), showing that variations in flow parameters have an important influence on flow-driven ice loss in an idealized flow-line scenario.

This paper is structured as follows: in Sect. 2 we recapitulate the theoretical background of ice-flow physics and describe the simulation methods used. The results of the equilibrium and warming experiments in a flow-line setup with different flow parameters are presented in Sect. 3. Section 4 discusses the results and the limitations of the experimental approach, draws conclusions, and suggests possible implications of these results.

2 Methods

2.1 Theoretical background of ice-flow physics

The flow of ice cannot be described by the equations of fluid dynamics alone but needs to be complemented by a material-dependent constitutive equation which relates the internal forces (stress) to the deformation rate (strain rate). Numerous laboratory experiments and field measurements show that the ice deformation rate responds to stress in a nonlinear way. Under the assumptions of isotropy, incompressibility, and uni-axial stress, this observation is reflected in Glen's flow law, which gives the constitutive equation for ice,

$$\dot{\epsilon} = A\tau^n, \tag{1}$$

where $\dot{\epsilon}$ is the strain rate, τ the dominant shear stress, n the flow exponent, and A the softness of ice (Glen, 1958).

Both the flow exponent and the softness are important parameters which determine the flow of ice. Usually, the exponent n is assumed to be constant through space and time. At present, there is no comprehensive understanding of all the physical processes determining the softness A. It may depend on water content, impurities, grain size, anisotropy, and temperature of the ice, among other things. Within the scope of ice-sheet modeling, A is typically expressed as a function of temperature alone:

$$A = A_0 \exp\left(-\frac{Q}{RT'}\right), \tag{2}$$

where A_0 is a constant factor, Q is an activation energy, R is the universal gas constant, and T' is the temperature relative to the pressure melting point (Greve and Blatter, 2009; Cuffey and Paterson, 2010).

Due to pre-melt processes, the softness responds more strongly to warming at temperatures close to the pressure melting point, which is often described by a piecewise adaption of the activation energy Q (Barnes et al., 1971; Paterson, 1991), with a larger value of Q at temperatures $T' > -10\,^\circ\mathrm{C}$. When using these piecewise defined values for Q for warm and for cold ice in the functional form of the flow law, the respective factors A_0 ensure that the function is continuous at $T' = -10\,^\circ\mathrm{C}$. A_0 is therefore dependent on the values of the flow exponent n and both values of Q for cold and for warm ice.

The scalar form of Glen's flow law (Eq. 1) is only valid for uni-axial stress, acting in only one direction. For a complete picture the stress is described as a tensor of order 2. The generalized flow law reads

$$\dot{\epsilon}_{jk} = A(T')\tau_e^{n-1}\tau_{jk}, \tag{3}$$

where $\dot{\epsilon}_{jk}$ are the components of the strain rate tensor and τ_{jk} are the components of the stress deviator, and τ_e is the effective stress, which is closely related to the second invariant of the deviatoric stress tensor:

$$\tau_e^2 = \frac{1}{2}\left[\tau_{xx}^2 + \tau_{yy}^2 + \tau_{zz}^2\right] + \tau_{xy}^2 + \tau_{xz}^2 + \tau_{yz}^2. \quad (4)$$

Each component of the strain rate tensor depends on all the components of the deviatoric stress tensor through the effective stress τ_e.

Glen's flow law (Eq. 3) and the softness parametrization (Eq. 2) are at the center of most numerical ice-sheet and glacier models, independent of the other approximations they might use (PISM authors, 2018; Winkelmann et al., 2011; Greve, 1997; Pattyn, 2017; Larour et al., 2012; de Boer et al., 2013; Fürst et al., 2011; Lipscomb et al., 2019).

2.2 Ice-flow model PISM

The simulations in this study were performed with the Parallel Ice Sheet Model (PISM) release v1.1. PISM uses shallow approximations for the discretized physical equations: the shallow-ice approximation (SIA) (Hutter, 1983) and the shallow-shelf approximation (SSA) (Weis et al., 1999) are solved in parallel within the entire simulation domain. The shallow-ice approximation is typically dominant in regions with high bottom friction, such that the vertical shear stress dominates over horizontal shear stress and longitudinal stress. The shallow-shelf approximation is typically dominant for ice shelves, with zero traction at the base of the ice, and for the fast-flow regime in ice streams (Winkelmann et al., 2011). PISM assumes a non-sliding SIA flow and uses the results of the SSA approximations for fast-flowing and sliding ice. In PISM, the flow law enters both the SIA and the SSA part of the velocities, as detailed in Winkelmann et al. (2011). It is possible to choose different flow exponents n for the SSA and the SIA, but the softness is the same for both approximations.

The simulations performed here use mostly the SIA mode: the geometry of a two-dimensional ice sheet sitting on a flat bed and the SIA mode serve to study the effects of changes in flow parameters on internal deformation and to separate those effects from others, such as changes in sliding. Including the shallow-shelf approximation reproduces and even enhances the effect of changes in the activation energies Q (see Sect. 3.5).

2.3 Uncertainty in flow exponent and activation energies

The flow exponent n and the activation energies for warm and for cold ice, Q_w and Q_c, determine the deformation of the ice as a response to stress or temperature. A recent review (Zeitz et al., 2020; see also literature in the Introduction above) reveals a broad range of potential flow parameters n, Q_w, and Q_c. In line with these findings, in this study the activation energy Q_c is varied between 42 and 85 kJ mol^{-1} (a typical reference value is $Q_c = 60$ kJ mol^{-1}). The activation energy for warm ice Q_w is varied between 120 and 200 kJ mol^{-1} (a reference value is $Q_w = 139$ kJ mol^{-1}). For the flow exponent n, values as low as 1 have been reported, but since many experiments and observations confirm a nonlinear flow of ice, n is varied between 2 and 4, with a reference value of $n = 3$. The reference values above correspond to the default values in many ice-sheet models (PISM authors, 2018; Greve, 1997; Pattyn, 2017; Larour et al., 2012; de Boer et al., 2013; Fürst et al., 2011; Lipscomb et al., 2019).

2.4 Adaption of the flow factor A_0

The flow factor A_0 in the flow law must be adapted to fulfill the following conditions: first, the continuity of the piecewise defined softness $A(T')$ must be ensured for all combinations of Q_w, Q_c, and n. Secondly, a reference deformation rate $\dot{\epsilon}$ at the reference magnitude of the driving stress τ_0 and a reference temperature T'_0 (PISM authors, 2018) should be maintained regardless of the parameters. This is because the coefficient and the power are non-trivially linked when a power law is fitted to experimental data. These conditions give

$$A_{0,\mathrm{old}} \cdot \exp\left(-\frac{Q_{\mathrm{old}}}{RT'_0}\right) \cdot \tau_0^{n_{\mathrm{old}}} = A_{0,\mathrm{new}} \cdot \exp\left(-\frac{Q_{\mathrm{new}}}{RT'_0}\right) \cdot \tau_0^{n_{\mathrm{new}}}, \quad (5)$$

$$A_{0,\mathrm{new}} = A_{0,\mathrm{old}} \cdot \exp\left(-\frac{Q_{\mathrm{old}} - Q_{\mathrm{new}}}{RT'_0}\right) \cdot \tau_0^{n_{\mathrm{old}} - n_{\mathrm{new}}}. \quad (6)$$

If the reference temperature is $T'_0 < -10\,^\circ$C, the values for cold ice $A_{0,c}$ and Q_c are used in the equation above, or else $A_{0,w}$ and Q_w are used. The corresponding $A_{0,\mathrm{new}}$ for cold and warm ice is calculated from the continuity condition at $T' = -10\,^\circ$C. For $T'_0 < -10\,^\circ$C, for example, it follows that

$$A_{0,\mathrm{c,new}} = A_{0,\mathrm{c,old}} \cdot \exp\left(-\frac{Q_{\mathrm{c,old}} - Q_{\mathrm{c,new}}}{RT'_0}\right) \cdot \tau_0^{n_{\mathrm{old}} - n_{\mathrm{new}}}, \quad (7)$$

$$A_{0,\mathrm{w,new}} = A_{0,\mathrm{c,new}} \cdot \exp\left(-\frac{(Q_{\mathrm{c,new}} - Q_{\mathrm{w,new}})}{R \cdot 263.15\,\mathrm{K}}\right). \quad (8)$$

Here we choose $\tau_0 = 80$ kPa as a typical stress magnitude in a glacier and $T'_0 = -20\,^\circ$C. Choosing another τ_0 on the same order of magnitude has only little effect on the differences in dynamic ice loss. Choosing another T'_0 on the other hand influences how the softness changes with the activation energy Q; see Fig. S1 in the Supplement. With T'_0 closer to the melting temperature, the difference in softness at the pressure melting point decreases and thus the ice loss is less sensitive to changes in the activation energy Q.

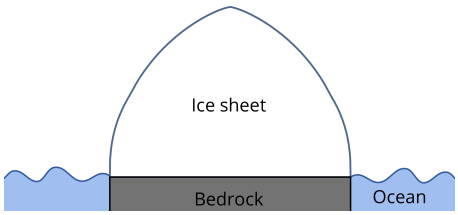

Figure 1. Sketch of the flow-line setup. The ice is sitting on a flat bed; the fixed calving front does not allow ice shelves. The accumulation rate is constant throughout the simulation domain, and the temperature is altitude dependent.

2.5 Experimental design

The study is performed in a flow-line setup, similar to Pattyn et al. (2012), where the computational domain has an extent of 1000 km in the x direction and 3 km in the y direction (with a periodic boundary condition). The spatial horizontal resolution is 1 km. The ice rests on a flat bed of length $L = 900$ km with a fixed calving front at the edge of the bed, such that no ice shelves can form (Fig. 1). In contrast to Pattyn et al. (2012), the temperature and the enthalpy of the ice sheet are allowed to evolve freely.

The model is initialized with a spatially constant ice thickness and is run into equilibrium for different combinations of flow parameters Q_c, Q_w, and n. The ice surface temperature is altitude dependent, $T_s = -6\,^\circ\mathrm{C\,km^{-1}} \cdot z - 2\,^\circ\mathrm{C}$, where z is the surface elevation in kilometers. The accumulation rate is constant in space and time for each simulation. A constant geothermal heat flux of $42\,\mathrm{mW\,m^{-2}}$ is prescribed. In the warming experiments, for each ensemble member an instantaneous temperature increase of $\Delta T \in [1, 2, 3, 4, 5, 6]\,^\circ\mathrm{C}$ is applied to the ice surface for a duration of 15 000 years (until a new equilibrium is reached), while the climatic mass balance remains unchanged. That means the temperature increase can lead to an acceleration of ice flow but is prohibited from inducing additional melt. This idealized forcing allows us to disentangle the effect of warming on the ice flow from climatic drivers of ice loss.

The thickness profile of the equilibrium state is similar to the *Vialov profile* (see e.g. Cuffey and Paterson, 2010; Greve and Blatter, 2009). However, in contrast to the isothermal Vialov profile, here the temperature of the ice is allowed to evolve freely, leading to a non-uniform softness of the ice (PISM authors, 2018). The extent in the x direction is given by the geometry of the setup, a flat bed with a calving boundary condition at the margin, and the height and shape of the ice sheet depend on the flow parameters n, Q_w, and Q_c and the accumulation rate a.

3 Results

3.1 Effect of activation energies in model simulations compared to analytical solution

In order to gain a deeper understanding of the influences of Q_c and Q_w on the equilibrium shape of ice sheets, we here compare the simulated results to analytical considerations based on the Vialov profile.

At a fixed accumulation rate of $a = 0.5\,\mathrm{m\,yr^{-1}}$, each flow parameter combination leads to an equilibrium state with a thickness profile similar to the Vialov profile but differences in maximal thickness and volume (Fig. 2a). Overall, high activation energies increase ice-flow velocities and reduce the ice-sheet volume. The activation energy for warm ice, Q_w, affects the volume and the velocities more strongly than the activation energy for cold ice, Q_c. A high Q_w leads to softer ice close to the pressure melting point (Fig. S1) and at the base of the ice sheet, which leads to higher velocities and a lower equilibrium volume of the ice sheet, while a low Q_w leads to stiffer ice close to the pressure melting point and at the base of the ice sheet, and in consequence the velocities decrease and the volume increases (Fig. 2b and c). For a fixed Q_w, the volume appears to decrease linearly with increasing Q_c and the velocity appears to increase linearly with increasing Q_c.

The maximal thickness of an isothermal ice sheet can be estimated with the Vialov profile:

$$h_m = 2^{n/(2n+2)} L^{1/2} \left(\frac{(n+2)a}{2A(T')(\rho g)^n} \right), \tag{9}$$

with the Glen exponent n, the ice-sheet extent $2L$, the pressure-adjusted temperature T', the gravity g, and the ice density ρ (Greve and Blatter, 2009). The Vialov thickness of a temperate ice sheet (isothermal at the pressure melting point), where the softness is evaluated at the pressure melting point depending on the activation energies Q_c and Q_w (see Eq. 2), gives a lower bound to the thickness, given the same geometry and flow parameters. The simulated maximal thickness is larger than the lower bound for all parameter combinations (Fig. 3a, lower bound indicated by a grey line), and the ratio between the maximal thickness h_m from the PISM simulation to the lower bound from the Vialov profile depends on both Q_w and Q_c. The ratio increases with higher Q_w and decreases with higher Q_c (Fig. 3b). The ice-sheet thickness of the polythermal ice sheet, as simulated with PISM, matches well the Vialov thickness calculated with Eq. (9) if an effective temperature $T'_{\mathrm{eff}} < 0\,^\circ\mathrm{C}$ is assumed. The effective temperature T'_{eff} that matches simulations best varies for different Q_w. For $Q_w = 120\,\mathrm{kJ\,mol^{-1}}$, an effective temperature of $T'_{\mathrm{eff}} = -5\,^\circ\mathrm{C}$ matches well the equilibrium thickness of the polythermal ice sheets. For $Q_w = 200\,\mathrm{kJ\,mol^{-1}}$, an effective temperature of $T'_{\mathrm{eff}} = -3.3\,^\circ\mathrm{C}$ matches well the equilibrium thickness of the polythermal ice sheets. These differences can be partly explained by the

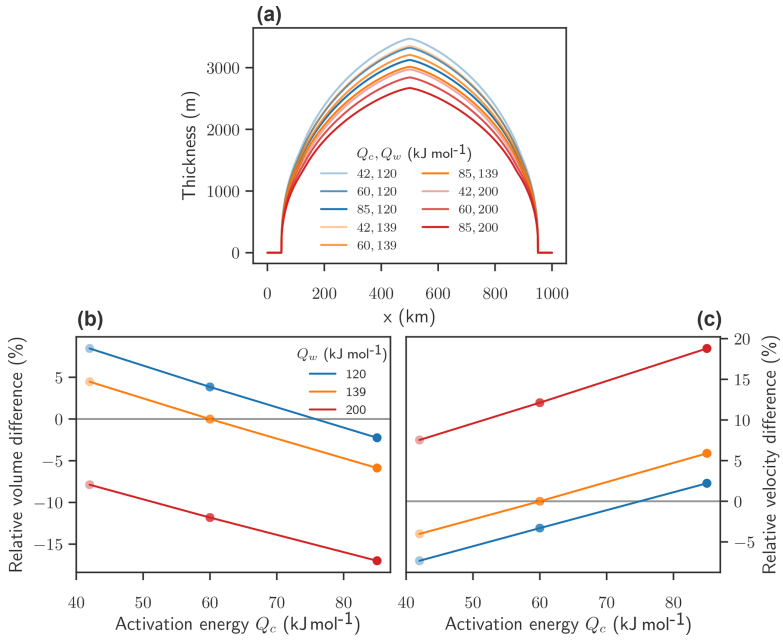

Figure 2. Effect of activation energies on equilibrium volume and velocities with fixed accumulation rate $a = 0.5\,\mathrm{m\,yr^{-1}}$ and flow exponent $n = 3$. Thickness profiles of equilibrium states for different combinations of activation energies Q_w and Q_c **(a)**. Relative difference of average equilibrium volumes **(b)** and velocities **(c)** compared to the reference state with standard parameters for parameter combinations of Q_w and Q_c. Q_c is shown on the x axis, and Q_w is given through the color of the markers (blue: $Q_\mathrm{w} = 120\,\mathrm{kJ\,mol^{-1}}$; orange: $Q_\mathrm{w} = 139\,\mathrm{kJ\,mol^{-1}}$; red: $Q_\mathrm{w} = 200\,\mathrm{kJ\,mol^{-1}}$).

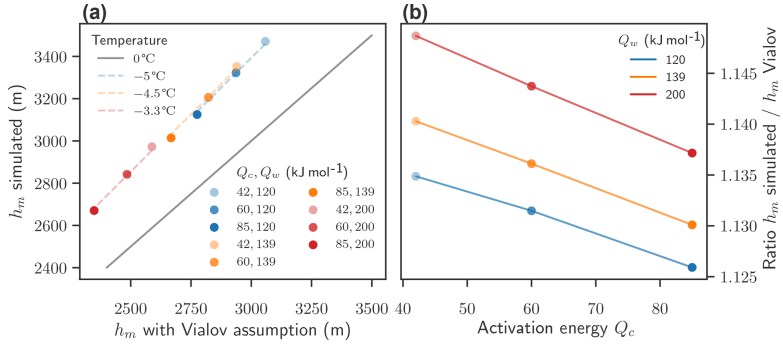

Figure 3. Comparison of simulated equilibrium thickness with analytical results. **(a)** Dots: maximal thickness h_m of the simulated polythermal ice sheet versus the analytical solution for the maximal thickness h_m of a temperate Vialov profile with the same flow parameters and accumulation rate. Colors indicate the flow–parameter combination. The grey line indicates identity. Short dashed lines indicate the analytical h_m with a temperature lower than the pressure melting point versus h_m at the pressure melting point with the same flow parameters and accumulation rate. The temperature, which fits the simulated results best, is indicated in the legend. **(b)** Ratio of the simulated h_m to the analytic h_m (assuming a temperate ice sheet) versus Q_c for different parameter combinations of Q_c and Q_w. The value of Q_w is indicated by the color.

altitude-dependent surface temperature: the maximal thickness of the ice sheets varies by approximately 800 m, which leads to a difference in ice surface temperature of approximately 4.8 °C between the thickest and the thinnest ice and thus influences the temperature within the ice sheet.

The relative difference of average velocities $d_v = (\overline{v} - \overline{v}_0)/\overline{v}_0$ spans from $d_v = -7\,\%$ (with a corresponding relative difference in ice-sheet volume of $d_{vol} = +10\,\%$) for the lowest combination of activation energies to $d_v = +18\,\%$ with a difference in volume of $d_{vol} = -15\,\%$ for the highest combination of values for Q_c and Q_w (Fig. 2b).

3.2 Ice-sheet initial states

In order to keep the initial ice volume largely fixed (with variations of less than 1 %) in the warming experiments, we adapt the accumulation rate for each parameter combination of Q_c and Q_w.

Since simulations with high activation energies Q_w have a smaller equilibrium volume at the same accumulation rate than simulations with standard activation energies, the accumulation rate a is increased to maintain an equilibrium volume close to the reference value. Simulations with low activation energies Q_c have a higher volume at the same accumulation rate, so the accumulation rate a is decreased. In the case of an isothermal ice sheet the maximal thickness and the volume can be computed analytically as shown above in Eq. (9). In our model simulations, however, the temperature distribution within the ice can evolve freely; thus the softness is not uniform and an analytical solution cannot be found.

In order to find the right adaptation for the accumulation rates, we start from the ice profile from the isothermal approximation as a first guess and run the model into equilibrium. If the relative difference between the new equilibrium volume and the standard equilibrium volume exceeds 1 %, we further change the accumulation rate and repeat the equilibrium simulation, always starting from the same initial state. The final equilibrium states found via this iterative approach differ by a maximum of 0.8 % in ice volume (Fig. S2), and the difference in maximal thickness is less than 100 m (Fig. 4a and b).

For the combination of high activation energies Q_w and Q_c, the relative differences $d_x = (x - x_0)/x_0$ of both adapted accumulation rates a and mean surface velocities v increase by more than 300 % (Fig. 4c and d), and for the combination of low activation energies Q_c and Q_w both adapted accumulation rates a and surface velocities v are approximately 50 % lower compared to the case with standard parameters. Both the accumulation rate and the velocities change in the same way since they balance each other in equilibrium. A change in accumulation rates controls the vertical velocity profile and thus influences the thermodynamics in the ice, which leads to differences in the temperatures of the ice sheet (pressure-adjusted temperature distributions shown in Fig. S4a). The change in temperature is most prominent at the top of the ice sheet, where higher accumulation rates (associated with high activation energies) lead to lower temperatures and vice versa. Thus the temperature change introduced from increased accumulation counteracts the effect of increased softness. In order to estimate how changed temperature on the one hand and changed flow parameters on the other hand impact the resulting ice softness, either one was kept fixed. The effect of the temperature changes on the ice softness is negligible, compared to parameter changes (see Fig. S4b, c, and d).

The maximal thickness of the polythermal simulated ice sheet is approximately 13–16 % larger than the lower bound estimated with a temperate ice sheet (Fig. 5a and b) with the same flow parameters and accumulation rates. Similar to the case with fixed accumulation rates, the simulated thickness matches the Vialov thickness well if an effective temperature $T'_{eff} < 0\,°C$ is assumed. The effective temperature that matches simulations best varies for different Q_w, from $-5\,°C$ for $Q_w = 120\,kJ\,mol^{-1}$ to $-3.6\,°C$ for $Q_w = 200\,kJ\,mol^{-1}$. This difference cannot be sufficiently explained by variations in surface temperature due to the difference in ice-sheet thickness. Rather the higher effective temperatures are linked to increased flow velocities of the ice, which in turn might lead to strain heating. In simulations with a high Q_w the simulated thickness has a higher discrepancy to the estimated lower bound (assuming a temperate ice sheet) than simulations with a low Q_w. In contrast to the case with fixed accumulation rate (Fig. 3) the ratio between the estimated and the simulated thickness depends only very little on Q_c.

3.3 Flow-driven ice loss under warming

Disentangling the purely flow-driven ice losses from the influences of melting, different initial temperature profiles, and variations in sliding requires several conditions:

1. The initial volume is fixed, which here is attained through adjustment of the accumulation rate for the different flow parameter combinations as explained in Sect. 3.2.

2. The surface mass balance is fixed – i.e., we do not allow for additional melt – and the accumulation rate does not change with warming.

3. Sliding is effectively inhibited (which is here ensured by applying an SIA-only condition).

The effect of the temperature increase is limited to warming at the ice surface, which can propagate into the interior of the ice sheet through diffusion and advection. Warming makes the ice softer and thus accelerates the flow and ice discharge. Since temperature diffusion in an ice sheet is a very slow process, we apply the temperature anomaly for a total duration of 15 000 years. The total mass balance is evaluated and compared to the standard parameter simulation after 100, 1000, and 10 000 years of warming. A new equilibrium state is reached after 10 000 years for all parameter combinations (see longer time series in Fig. S3).

In the experiments, the ice sheet loses mass for all warming levels and all parameter combinations. However, the

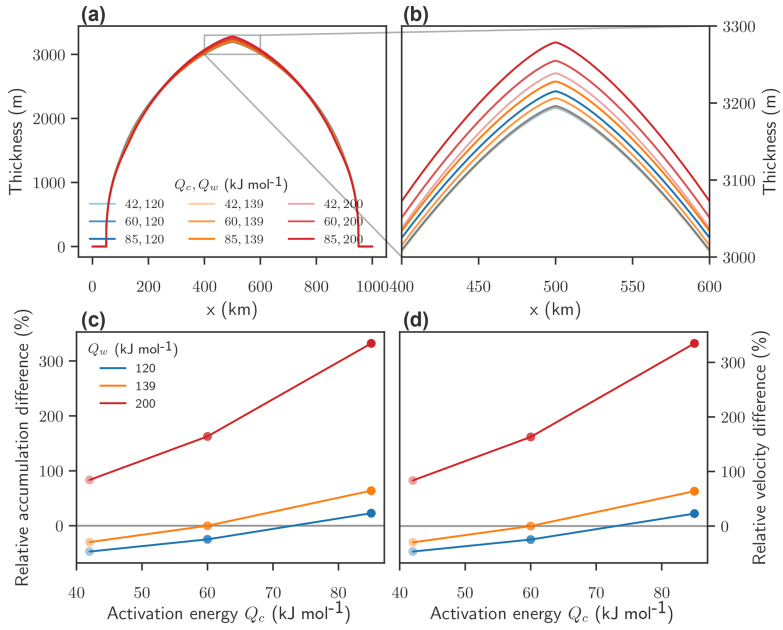

Figure 4. Effect of flow parameters on equilibrium state without warming with adapted accumulation rates and flow exponent $n = 3$. **(a)** Thickness profile of equilibrium states for parameter combinations of Q_w and Q_c, with a zoom on the ice divide **(b)**. Relative difference of accumulation rates **(c)** needed to keep the ice-sheet volume in equilibrium close to the reference simulations with standard flow parameters and relative difference in average surface velocities **(d)** versus Q_c. The value of Q_w is given by the color.

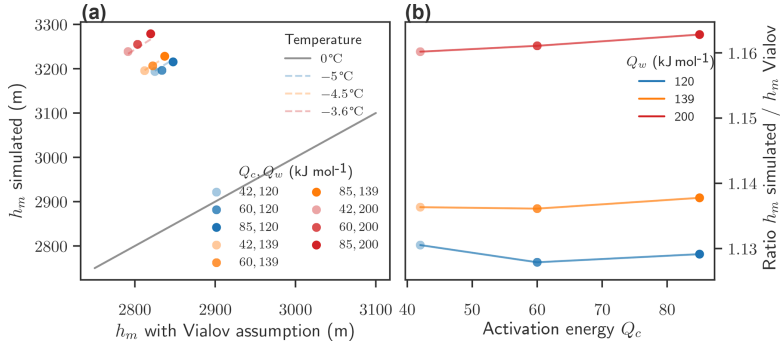

Figure 5. Comparison of simulated equilibrium thickness with analytical results. **(a)** Dots: maximal thickness h_m of the simulated polythermal ice sheet versus the analytical solution for the maximal thickness h_m of a temperate Vialov profile with the same flow parameters and accumulation rate. Colors indicate the parameter combination. The grey line indicates identity. Short dashed lines indicate the analytical h_m with a temperature lower than the pressure melting point versus h_m at the pressure melting point with the same flow parameters and accumulation rate. The temperature which fits the simulated results best is indicated in the legend. **(b)** Ratio of the simulated h_m to the analytic h_m (assuming a temperate ice sheet) versus Q_c for different parameter combinations of Q_c and Q_w. The value of Q_w is indicated by the color.

amount and rate of the ice loss are dependent on the flow parameters. Figure 6 shows the ice-sheet response to a warming of 2 °C. For a fixed flow exponent of $n = 3$ the fastest ice loss is observed for the flow parameter combination of $Q_c = 85\,\mathrm{kJ\,mol^{-1}}$ and $Q_w = 200\,\mathrm{kJ\,mol^{-1}}$, and the slowest ice loss for $Q_c = 42\,\mathrm{kJ\,mol^{-1}}$ and $Q_w = 120\,\mathrm{kJ\,mol^{-1}}$. Simulations with $Q_w = 200\,\mathrm{kJ\,mol^{-1}}$ reach a new, temperature-

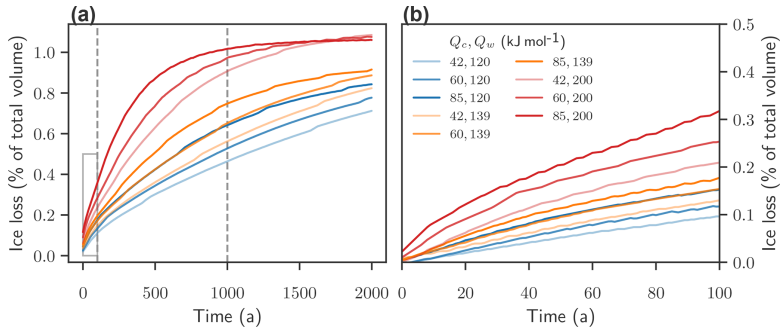

Figure 6. Time series for flow-driven ice discharge under 2 °C warming: **(a)** time evolution of ice loss with different activation energies Q_c and Q_w and the flow exponent $n = 3$, subject to a temperature anomaly forcing of $\Delta T = 2$ °C. **(b)** Zoom on the first 100 years.

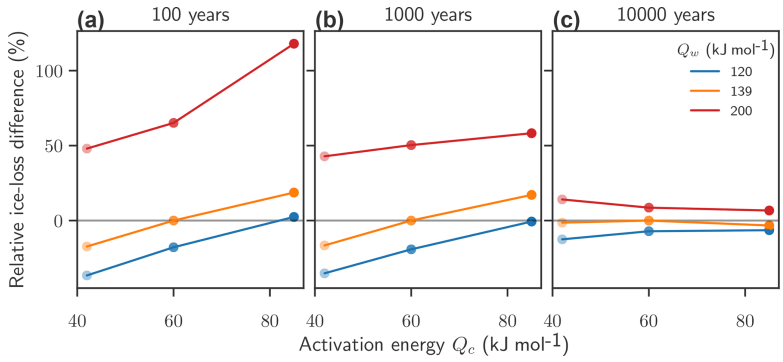

Figure 7. Effect of activation energy on flow-driven ice discharge under 2 °C warming: relative difference of flow-driven ice loss after 100 **(a)**, 1000 **(b)**, and 10 000 **(c)** years versus Q_c. The value of Q_w is given by the color. The simulations have reached a new equilibrium after 10 000 years.

adapted equilibrium after only 2000 years, while simulations with lower Q_w continue to lose mass.

The sensitivity to variations in flow parameters is measured via the relative differences for flow-driven ice loss $d_m = (\Delta m - \Delta m_0)/\Delta m_0$, where the reference Δm_0 is always given by the simulation with standard parameters under the same temperature increase (Fig. 7). While the long-term response to warming, after 10 000 years, is not very sensitive to the particular choice of flow parameters, the rate of flow-driven ice loss is. The largest relative differences in ice loss is found in the first century after the temperature increase (Fig. 7a), indicating that high Q_w speeds up the flow-driven ice loss. Under 2 °C of warming, ice loss after 100 years is enhanced more than 2-fold (i.e., increased by up to 118 %) in simulations with $Q_w = 200\,\mathrm{kJ\,mol^{-1}}$, while low Q_w reduces the relative ice loss by up to 37 %.

The effect of the flow parameters on flow-driven ice loss upon warming is robust for different temperature increases. Ice losses and the spread in flow-driven ice loss both increase for higher warming levels (see Fig. 8). For a warming of $\Delta T = 1$ °C the idealized ice sheet loses 0.09 % after 100 years and 0.35 % of ice after 1000 years for standard parameters. For a warming of $\Delta T = 6$ °C the ice sheet loses 0.46 % after 100 years and 1.89 % of ice after 1000 years for standard parameters (solid red line). For comparison, the Greenland Ice Sheet lost approximately 0.18 % of its mass in the period between 1972 and 2018 (Mouginot et al., 2019), which includes all processes: increase in flow, melting, and sliding.

The effect of flow parameter changes on the purely flow-driven ice loss after 100 years is on the same order of magnitude as the effect of surface warming by several degrees. In particular the uncertainty ranges of ice loss for warming of 2 °C and warming of 6 °C overlap (Fig. 8b) when solely considering the ice loss driven by changes in flow and excluding surface mass balance changes.

3.4 Influence of the flow exponent *n*

Variations in the flow exponent n do not change the qualitative effect of variations in activation energies Q on the ice

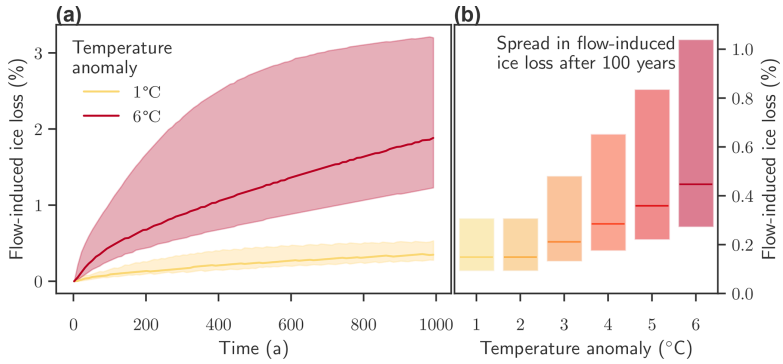

Figure 8. Effect of temperature forcing and activation energy on flow-driven ice. **(a)** Time evolution of ice loss under warming of 1 °C and 6 °C. For warming of $\Delta T = 1\,^{\circ}\mathrm{C}$ the conceptual ice sheet loses 0.35 % of ice after 1000 years for standard parameters (solid yellow line). Variations in the activation energies Q lead to variations in ice loss on the same order of magnitude (shaded area). For a warming of $\Delta T = 6\,^{\circ}\mathrm{C}$ the conceptual ice sheet loses 1.89 % of ice after 1000 years for standard parameters (solid red line). The variations in ice loss due to different parameters for the activation energy Q (shaded area) are strongly asymmetrical and, in particular during the first 300 years, high compared to the total amount of ice loss. **(b)** Uncertainty in flow-induced ice loss after 100 years of simulation time over all combinations of Q_w and Q_c, and temperature anomalies ΔT. The flow exponent $n = 3$ is kept fixed for all simulations.

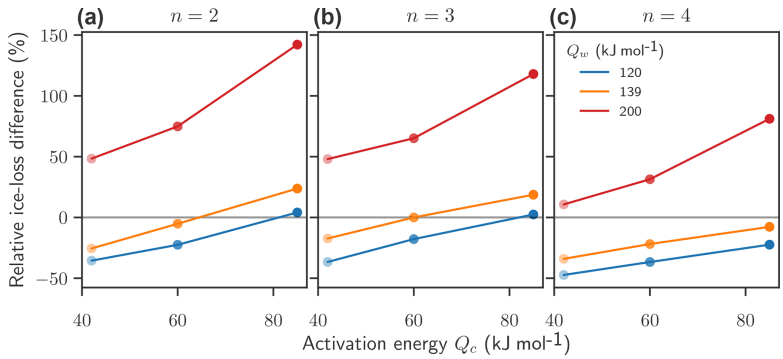

Figure 9. Effect of the flow exponent and activation energies on flow-driven ice loss after 100 years under 2 °C of warming: relative difference in flow-driven ice discharge for $n = 2$ **(a)**, $n = 3$ **(b)**, and $n = 4$ **(c)** for different combinations of the flow exponent n and activation energies Q_c and Q_w. The reference is always a simulation performed with standard parameters $n = 3$, $Q_\mathrm{c} = 60\,\mathrm{kJ\,mol^{-1}}$, and $Q_\mathrm{w} = 139\,\mathrm{kJ\,mol^{-1}}$.

loss. After 100 years for a temperature anomaly of $\Delta T = 2\,^{\circ}\mathrm{C}$ a higher n seems to mitigate the effect of the activation energy on differences in ice loss, while a lower n seems to enhance this effect (Fig. 9). However, the effect of variations in activation energy on the average surface velocity is almost independent of the choice of the flow exponent n (Fig. 10).

The influence of the activation energies Q_c and Q_w on ice flow is similar even with different flow exponents n. This is robust for different warming scenarios from +1 to +6 °C. A higher flow exponent n, which leads to a more pronounced nonlinearity in ice flow, does not enhance but reduces variations in dynamic ice loss. Compared to the nonlinear stress dependency τ^n in the flow law, the temperature-dependent softness $A(T') = A_0 \cdot \exp(-Q/RT')$ becomes less important with increasing flow exponent n.

3.5 Robustness of results to changes in accumulation and sliding

The overall effect of uncertainties in the activation energies Q remains robust, even if an additional driver of ice loss is taken into account. In a simulation where in addition to warming of 2 °C we also reduce the accumulation rate by 50 %, the ice losses remain dependent on the flow parameters Q_c and Q_w (Fig. 11; lines indicate results without a change in accumulation rate, analogous to Fig. 7, and squares indicate results with an additional 50 % decrease in accumulation rate). After 100 years of forcing, the relative spread of ice

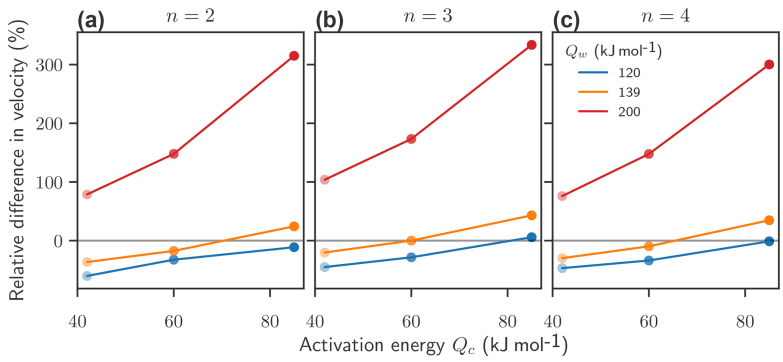

Figure 10. Effect of the flow exponent and activation energies on mean velocity change after 100 years under 2 °C of warming: relative difference in average surface velocity f or $n = 2$ **(a)**, $n = 3$ **(b)**, and $n = 4$ **(c)** for different combinations of the flow exponent n and activation energies Q_c and Q_w. The reference is always a simulation performed with standard parameters $n = 3$, $Q_c = 60\,\mathrm{kJ\,mol^{-1}}$, and $Q_w = 139\,\mathrm{kJ\,mol^{-1}}$. Variations in the flow exponent n do not significantly influence the relative difference of mean velocities after 100 years.

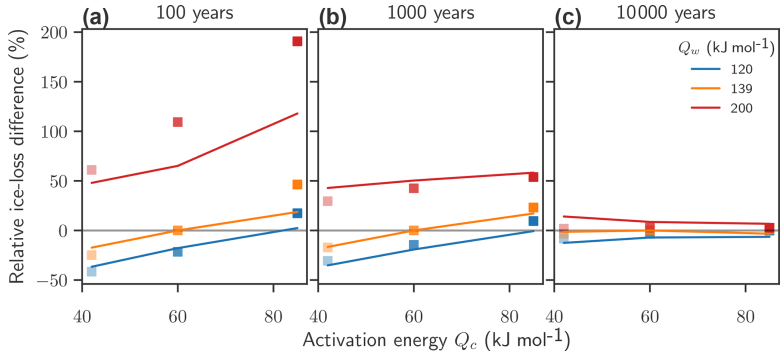

Figure 11. Effect of the flow exponent and activation energies on flow-driven ice loss under 2 °C of ice warming in combination with a 50 % reduction in accumulation rates: relative difference in flow-driven ice discharge after 100 **(a)**, 1000 **(b)**, and 10 000 **(c)** years. The ice sheet has reached a new equilibrium after 10 000 years. Relative difference for 2 °C warming with an additional reduction of the accumulation rate of 50 % (squares) is compared to the results without changes in the accumulation rate (lines; also see Fig. 7).

loss is slightly larger if accumulation changes are included. In particular, for $Q_w = 200\,\mathrm{kJ\,mol^{-1}}$ the relative increase of mass loss mounts from 118 to 190 %. On longer timescales, the spread in ice loss is reduced (after 10 000 years of forcing, when the ice sheet has reached a new equilibrium, the relative spread is below ±10 %).

When sliding is taken into account via the shallow-shelf approximation for sliding ice (see PISM authors, 2018) the uncertainty in flow parameters leads to relative changes in ice loss from −30 to +470 % after 100 years, which is a considerably larger spread than without sliding. The relative differences decrease with time but remain ranger than without sliding. After 1000 years the ensemble member with low activation energies have lost 40 % less ice than the standard parametrization, and high activation energies almost double the ice loss (+90 %). After 10 000 years, when the ice sheets have reached a new equilibrium, the relative differences still range from −16 to +40 % (see Fig. 12).

4 Discussion and conclusion

In this study we present a first attempt to disentangle and quantify the effect of uncertainties in the flow law parameters, in particular the activation energies Q and the flow exponent n, on ice dynamics.

The effect of ice rheology in ice-sheet models has been addressed in several studies with different experimental setups and different time frames. In particular the effect of the enhancement factors, which are often used to approximate the change in ice flow due to anisotropy, has been explored (Ritz et al., 1997; Ma et al., 2010; Humbert et al., 2005; Quiquet et al., 2018). In addition, the effect of the initial conditions

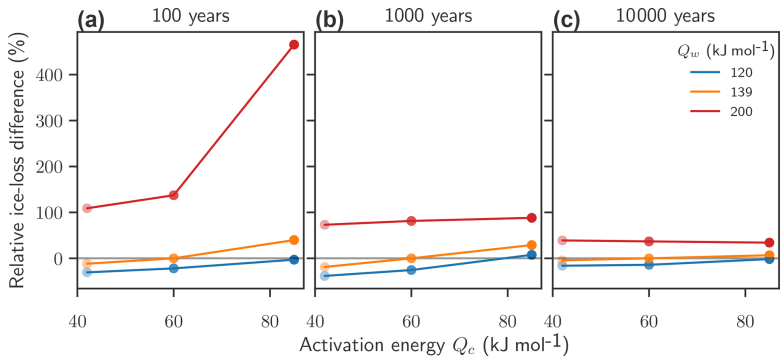

Figure 12. Effect of activation energy on flow-driven ice discharge under 2 °C warming, including sliding: relative difference of flow- and sliding-driven ice loss after 100 **(a)**, 1000 **(b)**, and 10 000 **(c)** years. The simulations have reached a new equilibrium after 10 000 years.

(Seroussi et al., 2013; Nias et al., 2016; Humbert et al., 2005) and the effect of the mathematical form of the flow law itself (Quiquet et al., 2018; Peltier et al., 2000; Pettit and Waddington, 2003) have been studied. These studies have been crucial for the understanding of different enhancement factors in the shallow-ice and the shallow-shelf approximation (Ma et al., 2010), for the reconciliation of the aspect ratios of the Greenland Ice Sheet and the Laurentide Ice Sheet during the Last Glacial Maximum (Peltier et al., 2000) and the ice flow in Antarctica and the Greenland Ice Sheet (Ritz et al., 1997; Seroussi et al., 2013; Quiquet et al., 2018; Nias et al., 2016; Humbert et al., 2005).

However, the approach presented in this paper is different in two important respects: firstly, the systematic study of not only the flow exponent n but also the activation energies Q has not been performed so far. Secondly, the idealized experimental setup, as presented in this study, allows us to disentangle the effects of the flow itself from other drivers and other sources of uncertainty. Several conditions need to hold to this end: the ice sheet is sitting on a flat bed and its maximal extent is determined by a calving front at the borders of the bed; thus no ice–ocean interactions or impacts of the bed geography influence the ice flow. Sliding is generally inhibited (the ice dynamics are described by the shallow-ice approximation, with zero basal velocity); no changes in sliding velocity influence the ice flow. The accumulation rate is fixed and independent of the temperature change, so that the ice loss is only driven by changes in flow and not by melting. These idealizations allow a clear understanding of the impact of the flow exponent and the activation energies on ice flow. In addition, they allow us to compare the simulations of the polythermal ice sheet to the analytically solvable limit of an isothermal ice sheet by using the Vialov approximation.

In this setup the largest effect of the uncertainties in the flow parameters is observed in the first century after warming, while the effect of the uncertainties on ice loss becomes less important as the ice approaches a new equilibrium. Uncertainties in the activation energies alone account for up to a doubling in ice loss during the first 100 years of warming and are on the same order of magnitude as the effects of increased temperature forcing, under fixed surface mass balance. This effect remains robust, even if changes in the surface mass balance are taken into account. Reducing the surface mass balance by 50 %, which is comparable to the changes in total surface mass balance of the Greenland Ice Sheet from 1972 to 2012 (Mouginot et al., 2019), increases the effect of the flow parameters on a timescale of 100 years and remains comparable on a timescale of 1000 years. Only as the ice sheet approaches its new equilibrium does the effect of the flow parameters become negligible. Allowing for not only flow but sliding while keeping all other conditions equal increases the effect of flow parameters substantially, leading to up to a 5-fold increase in ice loss after 100 years compared with standard parameters.

Acknowledging the uncertainty in flow parameters might slightly shift the interpretation of previous studies. For instance, the effect of the initial thermal regime, as studied by Seroussi et al. (2013), could be enhanced if the activation energies were higher than assumed, by making the ice softness more sensitive to changes in temperature. The crossover stress in the multi-term flow law presented by Pettit and Waddington (2003), at which the linear and the cubic term are of the same importance, is highly sensitive to the values of the activation energies. The positive feedback through shear heating, as studied for example by Minchew et al. (2018), could also be enhanced if activation energies were higher than usually assumed. The uncertainty in the flow law parameters may further provoke a re-evaluation of other parameters, for instance concerning melting and basal conditions. In particular, the thorough analysis by Bons et al. (2018) of observational data on the Greenland Ice Sheet supports a flow exponent of $n = 4$, not the standard value of $n = 3$, which is in line with recent laboratory experiments which also find $n > 3$ (Qi et al., 2017). Assuming a higher

flow exponent $n = 4$ has shown to significantly reduce the previously assumed area where sliding is possible (Bons et al., 2018; MacGregor et al., 2016). Moreover, both the flow exponent n and the activation energies Q feed into the grounding line flux formula (Schoof, 2007). In several ice-sheet models, this formula is used to determine the position and the flux over the grounding line in transient simulations (Reese et al., 2018). A change in the flow parameters n and Q thus has implications for the advance and retreat of grounding lines in simulations of the Antarctic Ice Sheet and possibly the onset of the marine ice-sheet instability, a particularly relevant process for the long-term stability of the Antarctic Ice Sheet. On the Greenland Ice Sheet increased ice flow might drive ice masses into ablation regions, where the ice melts. A possible effect of uncertainty in flow parameters on this particular feedback remains to be explored. Aschwanden et al. (2019) have found that uncertainty in ice dynamics plays a major role for mass loss uncertainty during the first 100 years of warming. While their study attributes the uncertainty mostly to large uncertainties in basal motion and only to a lesser extent to the flow via the enhancement factor, the uncertainties of the flow law and of the basal motion are not independent, as suggested for instance by Bons et al. (2018).

While the conclusions from the idealized experiments presented here cannot be transferred directly to assessing uncertainty in sea-level-rise projections, they are an important first step which helps to inform choices about parameter variations in more realistic simulations of continental-scale ice sheets.

Code and data availability. Data and code are available from the authors upon request.

Supplement. The supplement related to this article is available online at: https://doi.org/10.5194/tc-14-3537-2020-supplement.

Author contributions. RW and AL conceived the study. MZ, AL, and RW designed the research and contributed to the analysis. MZ carried out the literature review and the analysis. MZ, RW, and AL wrote the manuscript.

Competing interests. The authors declare that they have no conflict of interest.

Acknowledgements. Maria Zeitz and Ricarda Winkelman are supported by the Leibniz Association (project DOMINOES). Ricarda Winkelman is grateful for support by the Deutsche Forschungsgemeinschaft (DFG) and by the PalMod project (FKZ: 01LP1925D), supported by the German Federal Ministry of Education and Research (BMBF) as a Research for Sustainable Development (FONA). This research was further supported by the European Union's Horizon 2020 research and innovation program under grant agreement no. 820575 (TiPACCs). Development of PISM is supported by NASA grant NNX17AG65G and NSF grants PLR-1603799 and PLR-1644277. The authors gratefully acknowledge the European Regional Development Fund (ERDF), the German Federal Ministry of Education and Research, and the Land Brandenburg for supporting this project by providing resources on the high-performance computer system at the Potsdam Institute for Climate Impact Research. We thank Hilmar Gudmundsson, David Prior, and Thomas Kleiner for insightful discussions.

We would also like to thank the anonymous reviewers for their helpful comments on the manuscript and the editor, Alexander Robinson, for handling the review process and his helpful suggestions.

Financial support. This research has been supported by the Leibniz Association, Deutsche Forschungsgemeinschaft (DFG) (grant nos. WI4556/3-1, WI4556/5-1), NASA (grant no. NNX17AG65G), and the NSF (grant nos. PLR-1603799 and PLR-1644277).

Review statement. This paper was edited by Alexander Robinson and reviewed by two anonymous referees.

References

Aschwanden, A., Fahnestock, M. A., and Truffer, M.: Complex Greenland outlet glacier flow captured, Nat. Commun., 7, 10524, https://doi.org/10.1038/ncomms10524, 2016.

Aschwanden, A., Fahnestock, M. A., Truffer, M., Brinkerhoff, D. J., Hock, R., Khroulev, C., Mottram, R., and Khan, S. A.: Contribution of the Greenland Ice Sheet to sea level over the next millennium, Sci. Adv., 5, eaav9396, https://doi.org/10.1126/sciadv.aav9396, 2019.

Bamber, J. L., Oppenheimer, M., Kopp, R. E., Aspinall, W. P., and Cooke, R. M.: Ice sheet contributions to future sea-level rise from structured expert judgment, P. Natl. Acad. Sci. USA, 116, 11195–11200, https://doi.org/10.1073/pnas.1817205116,2019.

Barnes, P., Tabor, D., and Walker, J. C. F.: The friction and creep of polycrystalline ice, P. Roy. Soc. A-Math. Phy., 324, 127–155, 1971.

Bons, P. D., Kleiner, T., Llorens, M.-G., Prior, D. J., Sachau, T., Weikusat, I., and Jansen, D.: Greenland Ice Sheet: Higher Nonlinearity of Ice Flow Significantly Reduces Estimated Basal Motion, Geophys. Res. Lett., 45, 6542–6548, https://doi.org/10.1029/2018GL078356, 2018.

Budd, W. F. and Jacka, T. H.: A review of ice rheology for ice sheet modelling, Cold Reg. Sci. Technol., 16, 107–144, 1989.

Bueler, E. and Brown, J.: Shallow shelf approximation as a "sliding law" in a thermomechanically coupled ice sheet model, J. Geophys. Res.-Sol. Ea., 114, F03008, https://doi.org/10.1029/2008JF001179, 2009.

Cuffey, K. M. and Paterson, W. S. B.: The Physics of glaciers, Geoforum, 2, 90–91, https://doi.org/10.1016/0016-7185(71)90086-8, 2010.

de Boer, B., van de Wal, R. S. W., Lourens, L. J., Bintanja, R., and Reerink, T. J.: A continuous simulation of global ice volume over

the past 1 million years with 3-D ice-sheet models, Clim. Dynam., 41, 1365–1384, https://doi.org/10.1007/s00382-012-1562-2, 2013.

Duval, P., Montagnat, M., Grennerat, F., Weiss, J., Meyssonnier, J., and Philip, A.: Creep and plasticity of glacier ice: a material science perspective, J. Glaciol., 56, 1059–1068, https://doi.org/10.3189/002214311796406185, 2010.

Fürst, J. J., Rybak, O., Goelzer, H., De Smedt, B., de Groen, P., and Huybrechts, P.: Improved convergence and stability properties in a three-dimensional higher-order ice sheet model, Geosci. Model Dev., 4, 1133–1149, https://doi.org/10.5194/gmd-4-1133-2011, 2011.

Gagliardini, O., Zwinger, T., Gillet-Chaulet, F., Durand, G., Favier, L., de Fleurian, B., Greve, R., Malinen, M., Martín, C., Råback, P., Ruokolainen, J., Sacchettini, M., Schäfer, M., Seddik, H., and Thies, J.: Capabilities and performance of Elmer/Ice, a new-generation ice sheet model, Geosci. Model Dev., 6, 1299–1318, https://doi.org/10.5194/gmd-6-1299-2013, 2013.

Glen, J. W.: The Creep of Polycrystalline Ice, P. Roy. Soc. A-Math. Phy., 228, 519–538, https://doi.org/10.1098/rspa.1955.0066, 1955.

Glen, J. W.: The mechanical properties of ice I. The plastic properties of ice, Adv. Phys., 7, 254–265, https://doi.org/10.1080/00018735800101257, 1958.

Goelzer, H., Huybrechts, P., Loutre, M.-F., Goosse, H., Fichefet, T., and Mouchet, A.: Impact of Greenland and Antarctic ice sheet interactions on climate sensitivity, Clim. dynam., 37, 1005–1018, 2011.

Goelzer, H., Huybrechts, P., Loutre, M.-F., and Fichefet, T.: Last Interglacial climate and sea-level evolution from a coupled ice sheet–climate model, Clim. Past, 12, 2195–2213, https://doi.org/10.5194/cp-12-2195-2016, 2016.

Goelzer, H., Nowicki, S., Payne, A., Larour, E., Seroussi, H., Lipscomb, W. H., Gregory, J., Abe-Ouchi, A., Shepherd, A., Simon, E., Agosta, C., Alexander, P., Aschwanden, A., Barthel, A., Calov, R., Chambers, C., Choi, Y., Cuzzone, J., Dumas, C., Edwards, T., Felikson, D., Fettweis, X., Golledge, N. R., Greve, R., Humbert, A., Huybrechts, P., Le clec'h, S., Lee, V., Leguy, G., Little, C., Lowry, D. P., Morlighem, M., Nias, I., Quiquet, A., Rückamp, M., Schlegel, N.-J., Slater, D. A., Smith, R. S., Straneo, F., Tarasov, L., van de Wal, R., and van den Broeke, M.: The future sea-level contribution of the Greenland ice sheet: a multi-model ensemble study of ISMIP6, The Cryosphere, 14, 3071–3096, https://doi.org/10.5194/tc-14-3071-2020, 2020.

Goldsby, D. L. and Kohlstedt, D. L.: Superplastic deformation of ice: Experimental observations, J. Geophys. Res., 106, 11017–11030, https://doi.org/10.1029/2000JB900336, 2001.

Greve, R.: Application of a Polythermal Three-Dimensional Ice Sheet Model to the Greenland Ice Sheet: Response to Steady-State and Transient Climate Scenarios, J. Climate, 10, 901–918, https://doi.org/10.1175/1520-0442(1997)010<0901:AOAPTD>2.0.CO;2, 1997.

Greve, R. and Blatter, H.: Dynamics of Ice Sheets and Glaciers, Advances in Geophysical and Environmental Mechanics and Mathematics, Springer Berlin Heidelberg, Berlin, Heidelberg, https://doi.org/10.1007/978-3-642-03415-2, 2009.

Hinkel, J., Lincke, D., Vafeidis, A. T., Perrette, M., Nicholls, R. J., Tol, R. S., Marzeion, B., Fettweis, X., Ionescu, C., and Levermann, A.: Coastal flood damage and adaptation costs under 21st century sea-level rise, P. Natl. Acad. Sci. USA, 111, 3292–3297, 2014.

Humbert, A., Greve, R., and Hutter, K.: Parameter sensitivity studies for the ice flow of the Ross Ice Shelf, Antarctica, J. Geophys. Res.-Ea. Surf., 110, 1–13, https://doi.org/10.1029/2004JF000170, 2005.

Hutter, K.: Theoretical glaciology material science of ice and the mechanics of glaciers and ice sheets, Springer, 1983.

Huybrechts, P., Goelzer, H., Janssens, I., Driesschaert, E., Fichefet, T., Goosse, H., and Loutre, M.-F.: Response of the Greenland and Antarctic ice sheets to multi-millennial greenhouse warming in the Earth system model of intermediate complexity LOVECLIM, Surv. Geophys., 32, 397–416, 2011.

IPCC: IPCC Special Report on the Ocean and Cryosphere in a Changing Climate, in press, 2020.

Larour, E. Y., Seroussi, H., Morlighem, M., and Rignot, E.: Continental scale, high order, high spatial resolution, ice sheet modeling using the Ice Sheet System Model (ISSM), J. Geophys. Res.-Ea. Surf., 117, F01022, https://doi.org/10.1029/2011JF002140, 2012.

Levermann, A., Winkelmann, R., Nowicki, S., Fastook, J. L., Frieler, K., Greve, R., Hellmer, H. H., Martin, M. A., Meinshausen, M., Mengel, M., Payne, A. J., Pollard, D., Sato, T., Timmermann, R., Wang, W. L., and Bindschadler, R. A.: Projecting Antarctic ice discharge using response functions from SeaRISE ice-sheet models, Earth Syst. Dynam., 5, 271–293, https://doi.org/10.5194/esd-5-271-2014, 2014.

Levermann, A., Winkelmann, R., Albrecht, T., Goelzer, H., Golledge, N. R., Greve, R., Huybrechts, P., Jordan, J., Leguy, G., Martin, D., Morlighem, M., Pattyn, F., Pollard, D., Quiquet, A., Rodehacke, C., Seroussi, H., Sutter, J., Zhang, T., Van Breedam, J., Calov, R., DeConto, R., Dumas, C., Garbe, J., Gudmundsson, G. H., Hoffman, M. J., Humbert, A., Kleiner, T., Lipscomb, W. H., Meinshausen, M., Ng, E., Nowicki, S. M. J., Perego, M., Price, S. F., Saito, F., Schlegel, N.-J., Sun, S., and van de Wal, R. S. W.: Projecting Antarctica's contribution to future sea level rise from basal ice shelf melt using linear response functions of 16 ice sheet models (LARMIP-2), Earth Syst. Dynam., 11, 35–76, https://doi.org/10.5194/esd-11-35-2020, 2020.

Lipscomb, W. H., Price, S. F., Hoffman, M. J., Leguy, G. R., Bennett, A. R., Bradley, S. L., Evans, K. J., Fyke, J. G., Kennedy, J. H., Perego, M., Ranken, D. M., Sacks, W. J., Salinger, A. G., Vargo, L. J., and Worley, P. H.: Description and evaluation of the Community Ice Sheet Model (CISM) v2.1, Geosci. Model Dev., 12, 387–424, https://doi.org/10.5194/gmd-12-387-2019, 2019.

Ma, Y., Gagliardini, O., Ritz, C., Gillet-Chaulet, F., Durand, G., and Montagnat, M.: Enhancement factors for grounded ice and ice-shelf both inferred from an anisotropic ice flow model, J. Glaciol., 56, 805–812, https://doi.org/10.3189/002214310794457209, 2010.

MacGregor, J. A., Colgan, W. T., Fahnestock, M. A., Morlighem, M., Catania, G. A., Paden, J. D., and Gogineni, S. P.: Holocene deceleration of the Greenland Ice Sheet, Science, 351, 590–593, https://doi.org/10.1126/science.aab1702, 2016.

Mellor, M. and Testa, R.: Effect of temperature on the creep of ice, J. Glaciol., 8, 131–145, 1969.

Mengel, M., Levermann, A., Frieler, K., Robinson, A., Marzeion, B., and Winkelmann, R.: Future sea level rise constrained by observations and long-term commitment, P. Natl. Acad. Sci. USA,

113, 2597–2602, https://doi.org/10.1073/pnas.1500515113, 2016.

Minchew, B. M., Meyer, C. R., Robel, A. A., Gudmundsson, G. H., and Simons, M.: Processes controlling the downstream evolution of ice rheology in glacier shear margins: case study on Rutford Ice Stream , West Antarctica, Geophys. Res. Lett., 64, 583–594, https://doi.org/10.1017/jog.2018.47, 2018.

Mouginot, J., Rignot, E., Bjørk, A. A., van den Broeke, M., Millan, R., Morlighem, M., Noël, B., Scheuchl, B., Wood, M., and Morlighem, M.: Forty-six years of Greenland Ice Sheet mass balance from 1972 to 2018, P. Natl. Acad. Sci. USA, 116, 9239–9244, https://doi.org/10.1073/pnas.1904242116, 2019.

Nias, I. J., Cornford, S. L., and Payne, A. J.: Contrasting the Modelled sensitivity of the Amundsen Sea Embayment ice streams, J. Glaciol., 62, 552–562, https://doi.org/10.1017/jog.2016.40, 2016.

Nye, J. F.: The Flow Law of Ice from Measurements in Glacier Tunnels, Laboratory Experiments and the Jungfraufirn Borehole Experiment, P. Roy. Soc. A-Math. Phy., 219, 477–489, https://doi.org/10.1098/rspa.1953.0161, 1953.

Paterson, W. S. B.: Secondary and Tertiary Creep of Glacier Ice as Measured by Borehole Closure Rates, Rev. Geophys., 15, 47–55, https://doi.org/10.1029/RG015i001p00047, 1977.

Paterson, W. S. B.: Why ice-age ice is sometimes "soft", Cold Reg. Sci. Technol., 20, 75–98, https://doi.org/10.1016/0165-232X(91)90058-O, 1991.

Paterson, W. S. B. and Budd, W. F.: Flow parameters for ice sheet modeling, Cold Reg. Sci. Technol., 6, 175–177, https://doi.org/10.1016/0165-232X(82)90010-6, 1982.

Pattyn, F.: Sea-level response to melting of Antarctic ice shelves on multi-centennial timescales with the fast Elementary Thermomechanical Ice Sheet model (f.ETISh v1.0), The Cryosphere, 11, 1851–1878, https://doi.org/10.5194/tc-11-1851-2017, 2017.

Pattyn, F., Schoof, C., Perichon, L., Hindmarsh, R. C. A., Bueler, E., de Fleurian, B., Durand, G., Gagliardini, O., Gladstone, R., Goldberg, D., Gudmundsson, G. H., Huybrechts, P., Lee, V., Nick, F. M., Payne, A. J., Pollard, D., Rybak, O., Saito, F., and Vieli, A.: Results of the Marine Ice Sheet Model Intercomparison Project, MISMIP, The Cryosphere, 6, 573–588, https://doi.org/10.5194/tc-6-573-2012, 2012.

Peltier, R., Goldsby, D. L., Kohlstedt, D. L., and Tarasov, L.: Ice-age ice-sheet rheology: Constraints from the Last Glacial Maximum form of the Laurentide ice sheet, Ann. Glaciol., 30, 163–176, https://doi.org/10.3189/172756400781820859, 2000.

Pettit, E. C. and Waddington, E. D.: Ice flow at low deviatoric stress, J. Glaciol., 49, 359–369, https://doi.org/10.3189/172756503781830584, 2003.

PISM authors: PISM, a Parallel Ice Sheet Model, available at: http://www.pism-docs.org (last access: 20 October 2020), 2018.

Qi, C., Goldsby, D. L., and Prior, D. J.: The down-stress transition from cluster to cone fabrics in experimentally deformed ice, Earth and Planet. Sc. Lett., 471, 136–147, https://doi.org/10.1016/j.epsl.2017.05.008, 2017.

Quiquet, A., Dumas, C., Ritz, C., Peyaud, V., and Roche, D. M.: The GRISLI ice sheet model (version 2.0): calibration and validation for multi-millennial changes of the Antarctic ice sheet, Geosci. Model Dev., 11, 5003–5025, https://doi.org/10.5194/gmd-11-5003-2018, 2018.

Reese, R., Winkelmann, R., and Gudmundsson, G. H.: Grounding-line flux formula applied as a flux condition in numerical simulations fails for buttressed Antarctic ice streams, The Cryosphere, 12, 3229–3242, https://doi.org/10.5194/tc-12-3229-2018, 2018.

Rignot, E., Mouginot, J., Scheuchl, B., van den Broeke, M., van Wessem, M. J., and Morlighem, M.: Four decades of Antarctic Ice Sheet mass balance from 1979–2017, P. Natl. Acad. Sci. USA, 116, 1095–1103, https://doi.org/10.1073/pnas.1812883116, 2019.

Ritz, C., Fabre, A., and Letréguilly, A.: Sensitivity of a Greenland ice sheet model to ice flow and ablation parameters: Consequences for the evolution through the last climatic cycle, Clim. Dynam., 13, 11–24, https://doi.org/10.1007/s003820050149, 1997.

Schoof, C.: Ice sheet grounding line dynamics: Steady states, stability, and hysteresis, J. Geophys. Res.-Earth Surf., 112, 1–19, https://doi.org/10.1029/2006JF000664, 2007.

Schulson, E. M. and Duval, P.: Creep and fracture of ice, Cambridge University Press, 2009.

Seroussi, H., Morlighem, M., Rignot, E., Khazendar, A., Larour, E., and Mouginot, J.: Dependence of century-scale projections of the Greenland ice sheet on its thermal regime, J. Glaciol., 59, 1024–1034, https://doi.org/10.3189/2013JoG13J054, 2013.

Seroussi, H., Nowicki, S., Payne, A. J., Goelzer, H., Lipscomb, W. H., Abe-Ouchi, A., Agosta, C., Albrecht, T., Asay-Davis, X., Barthel, A., Calov, R., Cullather, R., Dumas, C., Galton-Fenzi, B. K., Gladstone, R., Golledge, N. R., Gregory, J. M., Greve, R., Hattermann, T., Hoffman, M. J., Humbert, A., Huybrechts, P., Jourdain, N. C., Kleiner, T., Larour, E., Leguy, G. R., Lowry, D. P., Little, C. M., Morlighem, M., Pattyn, F., Pelle, T., Price, S. F., Quiquet, A., Reese, R., Schlegel, N.-J., Shepherd, A., Simon, E., Smith, R. S., Straneo, F., Sun, S., Trusel, L. D., Van Breedam, J., van de Wal, R. S. W., Winkelmann, R., Zhao, C., Zhang, T., and Zwinger, T.: ISMIP6 Antarctica: a multi-model ensemble of the Antarctic ice sheet evolution over the 21st century, The Cryosphere, 14, 3033–3070, https://doi.org/10.5194/tc-14-3033-2020, 2020.

Strauss, B. H., Kulp, S., and Levermann, A.: Carbon choices determine US cities committed to futures below sea level, P. Natl. Acad. Sci. USA, 112, 13508–13513, 2015.

Treverrow, A., Budd, W. F., Jacka, T. H., and Warner, R. C.: The tertiary creep of polycrystalline ice: experimental evidence for stress-dependent levels of strain-rate enhancement, J. Glaciol., 58, 301–314, https://doi.org/10.3189/2012JoG11J149, 2012.

Weertman, J.: Creep of ice, in: Physics and Chemistry of Ice, edited by: Whalley, E., Jones, S. J., and Gold, L., 320–337, Royal Society of Canada, Ottawa, 1973.

Weis, M., Greve, R., and Hutter, K.: Theory of shallow ice shelves, Continuum Mech. Therm., 11, 15–50, https://doi.org/10.1007/s001610050102, 1999.

Winkelmann, R., Martin, M. A., Haseloff, M., Albrecht, T., Bueler, E., Khroulev, C., and Levermann, A.: The Potsdam Parallel Ice Sheet Model (PISM-PIK) – Part 1: Model description, The Cryosphere, 5, 715–726, https://doi.org/10.5194/tc-5-715-2011, 2011.

Zeitz, M., Winkelmann, R., and Levermann, A.: How flawed is Greenland's flow law?, submitted, 2020.

Manuscript 2 (published): Impact of the melt–albedo feedback on the future evolution of the Greenland Ice Sheet with PISM-dEBM-simple

In this manuscript, we focus on modeling the surface melt of the Greenland Ice Sheet. For this study, the diurnal Energy Balance Model, expanded by simple parameterizations of the albedo to melt relation and the transmissivity of the atmosphere, was implemented in the Parallel Ice Sheet Model (PISM). The surface melt model dEBM-simple needs only monthly means of near-surface air temperature as input and is therefore simple to use, even in a stand alone ice sheet model. In contrast to similarly simple melt models, dEBM-simple captures the main impacts of insolation and albedo changes. Here, we use PISM-dEBM-simple for an estimate of the impact of melt-albedo feedback in future warming scenarios over the Greenland Ice Sheet. We therefore probe three different scenarios: 1) No melt-albedo feedback: the albedo remains constant at its monthly averaged values from the 1990s. This scenario serves as a lower limit in this study. 2) No melt-albedo feedback and darkening: summer albedo decreases to the bare ice value during all summer months. In this study this scenario represents the upper limit. 3) Melt-albedo feedback: albedo has a piece wise linear dependence to melt. The relative contribution of the melt-albedo feedback is greater for moderate warming scenarios, while the absolute contribution is more pronounced for high warming scenarios. The effect of artificial summer darkening (scenario 2) is much more important in the moderate warming scenario while the ice losses due to the melt-albedo feedback alone are already close to the upper limit in the strong warming scenario. We also find that on the timescale until the year 2300 the melt-albedo feedback is more important than the melt-elevation feedback. Finally, we explore the parametric uncertainty of the dEBM-simple model.

Published in The Cryosphere (2021), doi:10.5194/tc-15-5739-2021
https://tc.copernicus.org/articles/15/5739/2021/

The Cryosphere, 15, 5739–5764, 2021
https://doi.org/10.5194/tc-15-5739-2021

The Cryosphere Open Access EGU

Impact of the melt–albedo feedback on the future evolution of the Greenland Ice Sheet with PISM-dEBM-simple

Maria Zeitz[1,2], **Ronja Reese**[1], **Johanna Beckmann**[1], **Uta Krebs-Kanzow**[3], **and Ricarda Winkelmann**[1,2]

[1]Potsdam Institute for Climate Impact Research (PIK), Member of the Leibniz Association,
P.O. Box 60 12 03, 14412 Potsdam, Germany
[2]Institute of Physics and Astronomy, University of Potsdam, Karl-Liebknecht-Str. 24–25, 14476 Potsdam, Germany
[3]Alfred Wegener Institute Helmholtz Centre for Polar and Marine Research, Bremerhaven, Germany

Correspondence: Maria Zeitz (maria.zeitz@pik-potsdam.de) and Ricarda Winkelmann
(ricarda.winkelmann@pik-potsdam.de)

Received: 12 March 2021 – Discussion started: 24 March 2021
Revised: 3 November 2021 – Accepted: 8 November 2021 – Published: 20 December 2021

Abstract. Surface melting of the Greenland Ice Sheet contributes a large amount to current and future sea level rise. Increased surface melt may lower the reflectivity of the ice sheet surface and thereby increase melt rates: the so-called melt–albedo feedback describes this self-sustaining increase in surface melting. In order to test the effect of the melt–albedo feedback in a prognostic ice sheet model, we implement dEBM-simple, a simplified version of the diurnal Energy Balance Model dEBM, in the Parallel Ice Sheet Model (PISM).

The implementation includes a simple representation of the melt–albedo feedback and can thereby replace the positive-degree-day melt scheme. Using PISM-dEBM-simple, we find that this feedback increases ice loss through surface warming by 60 % until 2300 for the high-emission scenario RCP8.5 when compared to a scenario in which the albedo remains constant at its present-day values. With an increase of 90 % compared to a fixed-albedo scenario, the effect is more pronounced for lower surface warming under RCP2.6. Furthermore, assuming an immediate darkening of the ice surface over all summer months, we estimate an upper bound for this effect to be 70 % in the RCP8.5 scenario and a more than 4-fold increase under RCP2.6. With dEBM-simple implemented in PISM, we find that the melt–albedo feedback is an essential contributor to mass loss in dynamic simulations of the Greenland Ice Sheet under future warming.

1 Introduction

The Greenland Ice Sheet is currently one of the main contributors to sea level rise (Frederikse et al., 2020). Roughly 35 % of the observed mass loss during the last 40 years is attributed to changes in surface mass balance, and 65 % of the mass loss is due to an increase in discharge fluxes (Mouginot et al., 2019). Overall, the contribution of changes in surface mass balance is expected to increase with ongoing warming (Shepherd et al., 2020).

Observations show that the surface of the Greenland Ice Sheet has been darkening over the last decades (He et al., 2013; Tedesco et al., 2016), and projections show that it is likely to darken further with increasing warming (Tedesco et al., 2016). Changes in albedo are driven by melt, the retreat of the snow line, black carbon, dust, and algae growth (Cook et al., 2020; Williamson et al., 2020; Box et al., 2012, 2017; Box, 2013; Tedstone et al., 2017, 2020; Ryan et al., 2019). In particular, the dark zone in the southwest of the Greenland Ice Sheet is subject to increased darkening, where ice albedo values reach values as low as 0.27 due to surface water and impurities at the surface (for comparison, clean ice typically has an albedo between 0.45 and 0.55) (Ryan et al., 2019). As darker surfaces absorb more radiation than brighter surfaces, the effect of darkening due to increased melt could trigger a positive feedback mechanism: surface darkening increases melting, which in turn can lead to further darkening (Stroeve, 2001). In addition to the darkening through melt, studies suggest a positive feedback mechanism between mi-

crobes, minerals, and melting, where algae-induced melting releases ice-bound dust, which in turn increases glacier algal blooms, leading to more melt (Di Mauro et al., 2020; McCutcheon et al., 2021). The melt–albedo feedback is usually interrupted by winter snow accumulation and snow events in summer (Gardner and Sharp, 2010; Noël et al., 2015). In light of recent extreme melting events as in 2010 (Tedesco et al., 2011), 2012 (Nghiem et al., 2012), or 2019 (Tedesco and Fettweis, 2020), when large parts of the surface area were at melting point and therefore darker than usual, it is important to model the response of the ice sheet to such large-scale changes in albedo.

To assess the influence of the atmosphere on the surface mass balance of ice sheets, a range of models are available and typically used: from process-based snowpack models coupled to regional climate models, which explicitly compute the regional climate and energy fluxes in the snow and at the ice surface (Fettweis et al., 2013, 2017; Noël et al., 2015; Langen et al., 2015; Niwano et al., 2018; Krapp et al., 2017), to simpler parameterizations like the positive-degree-day (PDD) models (e.g. Reeh, 1991). Regional climate models, for example, can be coupled with an ice sheet model to compute interactions of the ice and the atmosphere while explicitly resolving all relevant feedbacks (Le clec'h et al., 2019). Since this is computationally expensive, often a simpler approach is required in order to run simulations over centuries to millennia or large ensembles of simulations. In such cases, the surface mass balance is typically calculated from near-surface air temperatures with a positive-degree-day approach (Wilton et al., 2017; Aschwanden et al., 2019; Rückamp et al., 2019), which is computationally much less expensive but lacks the direct contribution of shortwave radiation and albedo to melting. The insolation–temperature–melt equation used by van den Berg et al. (2008) and Robinson et al. (2010) uses explicit albedo and insolation on long timescales. The Surface Energy and Mass balance model of Intermediate Complexity (SEMIC) uses the explicit energy balance and albedo parametrization and an implicit diurnal cycle for the temperature (Krapp et al., 2017) and is therefore capable to predict present and future melt.

The recent development of the diurnal energy balance model (dEBM) presented by Krebs-Kanzow et al. (2021) (with a simpler version introduced in Krebs-Kanzow et al., 2018) is computationally efficient, works well for the Greenland Ice Sheet, and can represent melt contributions from changes in albedo as well as seasonal and latitudinal variations in the diurnal cycle. In the Greenland Surface Mass Balance Model Intercomparison Project (Goelzer et al., 2020), the dEBM shows a good correlation with observations and is among the models which compare the closest with observed integrated mass losses from 2003–2012 (Fettweis et al., 2020). Thus it fills the gap between a process-based snowpack model coupled to a regional climate model and a simple and efficient temperature-index approach such as PDD.

We here expand the surface module of the Parallel Ice Sheet Model (PISM) (The PISM authors, 2018; Winkelmann et al., 2011; Bueler and Brown, 2009) by the simple version of the diurnal energy balance model (dEBM-simple), which includes melt driven by changes in albedo based on Krebs-Kanzow et al. (2018), in order to explore their effects on the future ice evolution. Beyond the work of Krebs-Kanzow et al. (2018), we additionally introduce parameterizations of albedo and atmospheric transmissivity to make it possible to run the model in stand-alone, prognostic mode (see Sect. 2). In particular the nonlinear albedo–melt relation (see Sect. 2.3.2) serves as an approximation to the melt–albedo feedback and allows us to estimate its importance. First, we compare the model against regional climate model simulations from the Regional Atmosphere Model (Modèle Atmosphérique Régional, MAR; Fettweis et al., 2013, 2017) and find a good fit (Sect. 3). In order to explore the minimal and maximal contribution of the melt–albedo feedback to future mass losses, we test the effect of albedo changes on future mass loss under RCP2.6 and RCP8.5 warming (Sect. 4). Here we distinguish between simulations which do not allow for changes in albedo, simulations with adaptive albedo, and darkening simulations, where the surface of the whole ice sheet is at the bare-ice value. While the latter experiments are inspired by the large-scale melt events (see Sect. 4.3), the dark zone in Greenland serves as motivation to explore the influence of the ice albedo value (see Sect. 4.4 and Appendix B). We compare dEBM-simple with PDD and find a better performance for the historic period (Appendix D). A detailed comparison of dEBM and PDD can be found in Krebs-Kanzow et al. (2018, 2021). The results considering future warming are discussed in Sect. 5.

2 Methods

We first present the Parallel Ice Sheet Model (PISM) and then describe the diurnal energy balance model as introduced in Krebs-Kanzow et al. (2018) and its implementation in PISM. To be able to run the model in stand-alone, prognostic mode, we introduce parameterizations of the surface albedo and transmissivity in Sect. 2.3.2 and 2.3.1 (see Appendix A for more detail). In the last two subsections, we describe the spin-up of PISM for the Greenland Ice Sheet and the experiments conducted in the next sections.

2.1 Ice sheet model PISM

PISM is a thermomechanically coupled ice sheet model which uses a superposition of the shallow-ice approximation (SIA) for slow-flowing ice, and the shallow-shelf approximation (SSA) for fast-flowing ice streams and ice shelves (Bueler and Brown, 2009; Winkelmann et al., 2011; The PISM authors, 2018). PISM was shown to be capable of reproducing the complex flow patterns evident in Greenland's

outlet glaciers at high resolution of less than 1 km (Aschwanden et al., 2016).

The SSA basal sliding velocities are related to basal shear stress via a power law with a Mohr–Coulomb criterion that relates the yield stress to parameterized till material properties and the effective pressure of the overlaying ice on the saturated till (Bueler and Pelt, 2015). We use a non-conserving simple hydrology model that connects the till water content to the basal melt rate (Bueler and van Pelt, 2015). The internal deformation of the ice is described by Glen's flow law with the flow exponent $n = 3$ for both SIA and SSA flow and with the enhancement factors $E_{\mathrm{SSA}} = 1$ and $E_{\mathrm{SIA}} = 1.5$ for SSA and SIA flow respectively.

Using PISM, we first create an initial configuration of the Greenland Ice Sheet under present-day climate conditions, using a climatology averaged over 1971–1990. Then we run a suite of experiments to validate dEBM-simple for present day as well as to test the role of insolation and temperature melting in future warming scenarios.

In this paper we concentrate on the changes in the surface mass balance, which are modelled using the newly implemented dEBM-simple. The atmospheric conditions, namely the monthly 2D temperature and precipitation fields, are read in as input fields. The precipitation fields remain fixed, and the share of snowfall and rain is determined from the local near-surface air temperature, with rain at temperatures above 2 °C and snow at temperatures below 0 °C. We neglect effects from changing ocean temperatures; thus the sub-shelf melting is constant in space and time at 0.05193 m/yr, the default PISM value. Also, calving is not modelled explicitly but induced by a fixed calving front at its present-day location based on Morlighem et al. (2017). Thus changes in mass losses from ice–ocean interaction are not considered here. Isostatic adjustment of the bedrock is not considered here. All experiments were run on a 4.5 km horizontal grid with a constant vertical resolution of 16 m. While this resolution is too low to reproduce the details of the outlet glacier flow, it still preserves the general flow pattern. Moreover the focus of the paper on climatic mass balance justifies this choice.

2.2 Adapted diurnal energy balance model dEBM-simple

For the implementation of dEBM-simple, we follow the parametrization as laid out by Krebs-Kanzow et al. (2018). The melt equation reads

$$M = \frac{\Delta t_\Phi}{\Delta t \rho_{\mathrm{w}} L_{\mathrm{m}}} \left(\tau_{\mathrm{A}} (1 - \alpha_{\mathrm{s}}) \overline{S}_\Phi + c_1 T_{\mathrm{eff}} + c_2 \right), \tag{1}$$

with fresh water density ρ_{w}, latent heat of fusion L_{m}, and the surface albedo α_{s}. dEBM-simple is based on the assumption that melting occurs only during daytime, when the sun is above an elevation angle Φ, which is estimated to be constant in space and time $\Phi = 17.5°$; see Krebs-Kanzow et al. (2018). The time period of a day when the sun is above the elevation angle Φ is denoted by Δt_Φ. The length of a day is Δt, and the fractional time that the sun is above the elevation angle Φ is given by

$$\frac{\Delta t_\Phi}{\Delta t} = \frac{h_\Phi}{\pi} = \frac{1}{\pi} \frac{\sin \Phi - \sin \varphi \sin \delta}{\cos \varphi \cos \delta}, \tag{2}$$

with h_Φ being the hour angle when the sun has an elevation angle of at least Φ, δ being the solar declination angle, and φ being the latitude. The incoming radiation over the time Δt_Φ, obtained from the insolation at the top of the atmosphere (TOA), $\overline{S}_\Phi$, and the parameterized transmissivity τ_{A} (see Eq. 6), drives the insolation melt described in the first term of Eq. (1).

The temperature-dependent melting described in the second term of Eq. (1) is not simply a function of the air temperature directly as in, for example, Pellicciotti et al. (2005) and van den Berg et al. (2008), but a function of the cumulative temperature exceeding the melting point in a given month T_{eff} as in Krebs-Kanzow et al. (2018, 2021).

$$T_{\mathrm{eff}}(\overline{T}, \sigma) = \frac{1}{\sigma \sqrt{2\pi}} \int_0^\infty dT\, T \exp\left(-\frac{(T - \overline{T})^2}{2\sigma^2} \right) \tag{3}$$

Here, T is the fluctuating daily temperature, $\overline{T}$ is the monthly average temperature, which is used as an input, and σ is the standard deviation of the temperature. The melting point is at 0 °C.

The parameters describing the effective temperature influence on melting c_1 and the melt intercept c_2 are estimated from MAR v3.11 simulations (Fettweis et al., 2017); see Sect. 3. The values used here are given in Table A2.

Refreezing is assumed to be constant, with 60 % of snow melt refreezing independent of temperature or melt. Meltwater from ice melt does not refreeze but immediately runs off.

2.3 Implementation of dEBM-simple in PISM

The diurnal energy balance model is implemented in PISM as a climatic mass balance module. It takes the local near-surface air temperature and the precipitation as an input and computes the local climatic mass balance. The shortwave downward radiation and the broadband albedo are not needed as inputs, as they are parameterized internally, with the possibility to use other orbital parameters than the present-day values. The melt module is evaluated at least weekly, independent of the adaptive time step used for the ice dynamics in PISM. The amount of melt is balanced with refreezing and snowfall before the surface mass balance is aggregated over the adaptive time steps in PISM. The aggregated values feed into the update of the ice geometry. The ice geometry is used as an input for the dEBM melt, as it feeds into the parametrization of the atmospheric transmissivity (see Eq. 6) and updates the local temperature when the atmospheric temperature lapse rate is considered. If a run is started without knowledge about melting in the previous time step, the

albedo is assumed to be at the fresh snow value everywhere on the ice sheet or can be read in from an input file. In line with Krebs-Kanzow et al. (2018), no melting is allowed below −6.5 °C even if the insolation alone would be sufficient to cause melting.

2.3.1 Parametrization of shortwave downward radiation

The shortwave downward radiation is computed from the top of the atmosphere (TOA) insolation and a linear model of the transmissivity of the atmosphere. Daily average TOA insolation $\overline{Q}^{\text{day}}$ is computed from

$$\overline{Q}^{\text{day}} = \frac{S_0}{\pi}\left(\frac{\overline{d}}{d}\right)^2 (h_0 \sin\varphi \sin\delta + \cos\varphi \cos\delta \sin h_0), \quad (4)$$

where $S_0 = 1367\,\text{W/m}^2$ is the annual mean of the total solar irradiance (solar constant), $\overline{d}$ is the annual mean distance of the earth to the sun, d is the current distance, φ is the latitude, δ is the declination angle, and h_0 is the hour angle of sunrise and sunset. The average TOA insolation during the daily melt period $\overline{S}_\Phi$ is given by

$$\overline{S}_\Phi = \frac{S_0}{\Delta t_\Phi \pi}\left(\frac{\overline{d}}{d}\right)^2 (h_\Phi \sin\varphi \sin\delta + \cos\varphi \cos\delta \sin h_\Phi). \quad (5)$$

Under present-day conditions the declination angle δ and the sun–earth distance d are approximated with trigonometric expansions depending on the day of the year; see Liou (2002, chap. 2.2.). This approximation is used as long as the user does not specifically demand paleo simulations.

To scale the insolation to the ice surface, we assume that the transmissivity of the atmosphere depends only on the local surface altitude in a linear way (similar to Robinson et al., 2010). The linear fit for the shortwave downward radiation from TOA insolation is obtained from a linear regression of MAR v3.11 data averaged over the years 1958 to 2019, considering only the summer months (June, July, and August) (see Appendix A2 and Fig. A3). The parametrization relies on the assumption that the mean transmissivity does not change in a changing climate. In particular the impact of cloud conditions and events like Greenland blocking, which might become more frequent in the future, is not captured with this approach. The transmissivity is given by

$$\tau_A = a + b \cdot z, \quad (6)$$

where a and b are parameters (here $a = 0.57$ and $b = 0.037\,\text{km}^{-1}$) and z is the surface altitude in kilometres. The approach to calculate shortwave downward radiation is further described in Appendix A2; in particular it is described how TOA conditions different than present-day conditions, e.g. during the Eemian, can be modelled.

2.3.2 Albedo parametrization

PISM-dEBM-simple allows us to read in the albedo field as an input. However, in order to keep the input requirements for a stand-alone version of the model minimal and to allow for a melt-dependent albedo, a simple albedo parametrization is implemented. Snow albedo in MAR is calculated using a snowpack model, explicitly based on snow grain size, cloud optical thickness, solar zenith angle, and impurity concentration in snow (van Dalum et al., 2020). In MAR, ice albedo is explicitly calculated as a function of ice density, time of the day, solar angle, spectrum of the solar radiation, etc. Here, in contrast, albedo is parameterized in an ad hoc way as a function of the melt in the last (weekly) time step. As the time step in the climatic mass balance module is typically smaller than the adaptive ice dynamics time step, and the temporal resolution of the 2 d air temperature input, this approach allows for several iterations of the melt-dependent albedo under otherwise identical conditions.

The corresponding parameters are fitted using MARv3.11 data (Fettweis, 2021). The advantage of this approach is that it requires no further information in PISM (e.g. a fully resolved firn layer) but still captures melt processes driven by changes in albedo or insolation. In this approach, the albedo decreases linearly with increasing melt from the maximal value $\alpha_{\max} = 0.81$ (close to the fresh-snow albedo) for regions with no melting to $\alpha_{\min} = 0.47$ (close to the bare-ice albedo). The albedo cannot drop below the value of $\alpha_{\min}$.

$$\alpha_s = \max[\alpha_{\max} + \alpha_s \cdot M, \alpha_{\min}] \quad (7)$$

The slope $\alpha_s = -0.025\,\text{yr/m}$ is estimated from MAR data (see Appendix Fig. A1 and Sect. A1). We will later on test the sensitivity of the melting to the slope and the value of $\alpha_{\min}$. Lowering the value of $\alpha_{\min}$ may indicate the sensitivity to darker ice. While an explicit darkening of the ice, possibly with a different albedo-to-melt relation, is not captured in this framework, it can be easily expanded to incorporate darkening ice.

For comparison, the observed albedos are shown in Fig. A2.

2.4 Initial state

All simulations are started from a spun-up state and run with full ice dynamics (SIA and SSA as well as temperature evolution and a thermomechanical coupling). The procedure detailed in Aschwanden et al. (2019) is used for the spin-up: a temperature anomaly is applied over the last 125 kyr to the climatological mean (1971 to 1990 monthly averages) of the 2D temperature field of MAR v3.9 in order to obtain a realistic temperature distribution within the ice while the topography is allowed to evolve. During the spin-up the more conventional positive-degree-day model is used to compute changes in climatic mass balance. In the simulations, surface temperatures are scaled with changes in surface elevation (at-

mospheric temperature lapse rate of −6 K/km) to include the melt–elevation feedback in the simulations.

Initial ice geometry and bedrock topography are taken from BedMachine V3 (Morlighem et al., 2017). Basal heat flux is obtained from Maule (2005). The yearly cycle of precipitation is kept fixed but during the spin-up the precipitation fields are scaled: for each degree of warming we apply 7.3 % precipitation increase for each degree of surface warming (Huybrechts, 2002). The root-mean-square error in thickness amounts to 237 m, overestimating the thickness values in the west and northwest (Morlighem et al., 2017). The velocity anomalies of the initial state show a root-mean-square error of 145 m/yr compared to observed data (Rignot and Mouginot, 2012). The northeast Greenland Ice Stream and several other fast-flowing outlet glaciers are underestimated in the surface velocities. See Fig. S1 in the Supplement for anomaly maps.

2.5 Validation experiments

To calibrate the model parameters and test the parameterizations, we perform diagnostic experiments with PISM-dEBM-simple over the period between 1958 and 2019. In order to disentangle the surface module from indirect effects of ice dynamics, e.g. dynamic thinning and thus a temperature increase through the temperature lapse rate, changes in the ice topography are suppressed in these diagnostic experiments. Monthly MAR v3.11 near-surface air temperature and precipitation fields from 1958 to 2019 are used as atmosphere input while the albedo, the transmissivity, and the melt rate are computed as shown above.

In order to explore the sensitivity to insolation, Eemian insolation values are used in an analogous experiment where only the orbital parameters, which determine the top of the atmosphere insolation, are changed. The temperature and precipitation inputs remain the same as described above. Precipitation and albedo are calculated using the respective parameterizations.

2.6 Warming and darkening experiments over the next centuries

Here, we describe the series of experiments which are performed to assess the impact of the melt–albedo feedback onto the mass losses of the Greenland Ice Sheet. All experiments start from the same initial state, described in Sect. 2.4 and run over the period from 2000 to 2300. In contrast to the previously described experiments in Sect. 2.5, the ice topography is now allowed to change, and the results are expressed in terms of cumulated mass losses since 2000 in metres of sea level equivalent (m s.l.e.). Melt rates are calculated by PISM-dEBM-simple using periodic monthly temperature fields given by the climatological mean over the period 1971 to 1990 from the regional climate model MAR v3.11. MAR was forced with ERA reanalysis data (ERA-40 from 1958–1978 and ERA-5 after) (Kittel et al., 2021; Fettweis et al., 2021). In the warming experiments, scalar temperature anomalies are applied uniformly over the entire ice sheet. The temperature anomalies are obtained from averaging the output of the IPSL-CM5A-LR model (Dufresne et al., 2013), which is one of four CMIP5 models extended until 2300, over the simulation domain containing the Greenland Ice Sheet and computing the anomaly relative to the 1971–1990 period over the same domain.

In addition to forced temperature changes, the local near-surface air temperature adapts to topography changes of the ice sheet with a lapse rate of −6 K/km, thus taking the melt–elevation feedback into account. Note that in all experiments changes in albedo do not feed back onto the atmosphere; in particular albedo changes do not affect near-surface air temperatures.

The experiments can be summarized into seven groups. The α_{1990} experiments use an interannually constant yearly albedo cycle and therefore suppress the adaptation of albedo to increased melt rates under warming. They are used to estimate future ice loss without the melt–albedo feedback and serve as a reference. The std experiments include the melt–albedo feedback through the standard parametrization for albedo. The α_{dark} experiments represent an extreme scenario, assuming that the whole ice surface will be snow free or covered with meltwater during the months June, July, and August in each year. This is not a realistic scenario but rather an upper limit to the possible impact of albedo changes on ice loss. The α_{ls}, α_{hs}, and α_{min} experiments explore the uncertainty from the albedo parametrization. Doubling the slope to −0.05 yr/m leads to a steeper decrease in albedo with increasing melt rates, which is closer to the conditions in August (see Appendix Fig. A1). Assuming that in the future the melting period over the Greenland Ice Sheet is longer and therefore the conditions we observe in August might be more characteristic over the melting period justifies the exploration of the impact of an increased sensitivity in the α_{hs} experiments. However, in this approach the minimal albedo for bare ice remains at 0.47 and is therefore reached with melt rates of 7 m/yr (instead of 14 m/yr in the standard parametrization). Halving the slope to −0.013 yr/m explores the lower boundary of albedo–melt sensitivity (see Fig. A1) in the α_{ls} experiments. In the α_{min} experiments, we test the influence of a reduced minimum albedo, as observed today in the dark zone of the Greenland Ice Sheet. The T_{noLR} experiments neglect the atmospheric temperature lapse rate. Thus the local temperature is independent of the ice sheet topography, and the representation of the melt–elevation feedback is interrupted.

An overview of all experiments is given in Table 1.

3 Validation for the Greenland Ice Sheet

In this section, we validate the dEBM-simple melt for present-day conditions and show as an example melt rates

Table 1. Overview of the experiments performed in this study.

Experiment group	Name	Temperature forcing	Albedo	Lapse rate
α_{1990}	Ctrlα_{1990}	None	Fixed yearly cycle	−6 K/km
	RCP2.6α_{1990}	RCP2.6	Fixed yearly cycle	−6 K/km
	RCP8.5α_{1990}	RCP8.5	Fixed yearly cycle	−6 K/km
std	Ctrl	None	std parameterized	−6 K/km
	RCP2.6	RCP2.6	std parameterized	−6 K/km
	RCP8.5	RCP8.5	std parameterized	−6 K/km
α_{dark}	Ctrlα_{dark}	None	Bare-ice value	−6 K/km
	RCP2.6α_{dark}	RCP2.6	Bare-ice value	−6 K/km
	RCP8.5α_{dark}	RCP8.5	Bare-ice value	−6 K/km
α_{ls}	Ctrlα_{ls}	None	Parameterized, low slope	−6 K/km
	RCP2.6α_{ls}	RCP2.6	Parameterized, low slope	−6 K/km
	RCP8.5α_{ls}	RCP8.5	Parameterized, low slope	−6 K/km
α_{hs}	Ctrlα_{hs}	None	Parameterized, high slope	−6 K/km
	RCP2.6α_{hs}	RCP2.6	Parameterized, high slope	−6 K/km
	RCP8.5α_{hs}	RCP8.5	Parameterized, high slope	−6 K/km
α_{min}x	Ctrlα_{min}x	None	Parameterized, changed ice albedo	−6 K/km
	RCP2.6α_{min}x	RCP2.6	Parameterized, changed ice albedo	−6 K/km
	RCP8.5α_{min}x	RCP8.5	Parameterized, changed ice albedo	−6 K/km
T_{noLR}	CtrlT_{noLR}	None	std parameterized	none
	RCP2.6T_{noLR}	RCP2.6	std parameterized	none
	RCP8.5T_{noLR}	RCP8.5	std parameterized	none

with Eemian insolation. The experiments are performed as described in Sect. 2.5.

3.1 Present-day melt rates

Here, we compare the melt modelled with PISM-dEBM-simple over the historic period with melt modelled by MARv3.11 (see Fig. 1). The setup is described in Sect. 2.5. Note that here the evolution of the ice sheet topography is suppressed; that is the melt rates are calculated over a fixed geometry corresponding to present day.

Due to the parametrization of the albedo and the transmissivity (and thus the shortwave downward radiation) detailed in Sect. 2.3 and in Table A2, the parameters of the dEBM-simple model are adjusted from Krebs-Kanzow et al. (2018). The chosen dEBM-simple parameters c_1 and c_2 (see Table A2) minimize the product of spatial and temporal root-mean-square error in the melt rate over the whole period from 1958 to 2019 while using the parameterizations for albedo and shortwave downward radiation. The temporal root-mean-square error is computed from a comparison of total yearly melt (see Fig. 1), and the spatial root-mean-square error is computed from a comparison of the 2D fields of summer (JJA) melt rates averaged over the whole period (see Fig. 2), both with respect to MAR data. Both of the root-

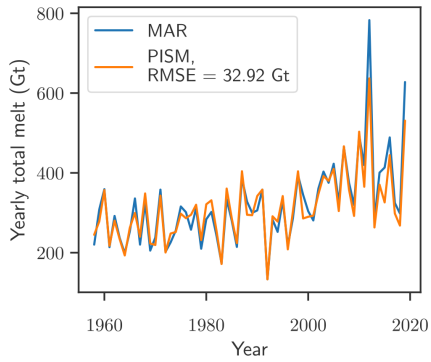

Figure 1. Comparison of annual total melt of the Greenland Ice Sheet as calculated with MAR v3.11 and PISM-dEBM-simple. The diagnostic simulation with PISM-dEBM-simple (orange line) is performed using monthly MAR 2D temperature fields as forcing. The albedo α_s is parameterized with the local melt rate m as $\alpha_s = 0.82 - 0.025\,\mathrm{yr/m} \cdot m$, and the shortwave downward radiation is approximated by the top-of-the-atmosphere radiation and the transmissivity τ_A parameterized with surface altitude z as $\tau_A = 0.037\,\mathrm{km}^{-1} \cdot z + 0.57$. The root-mean-square difference between the PISM-dEBM-simple simulation and total melt as given by MAR (blue line) is 32.92 Gt.

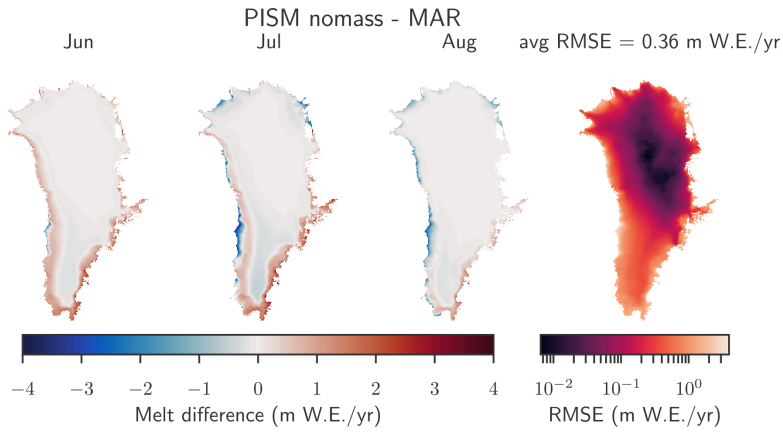

Figure 2. Local differences between the monthly averaged June, July, and August melt rates as diagnosed with PISM-dEBM-simple compared to MAR. The PISM simulation uses monthly 2D temperature fields from MAR as forcing and parameterizes albedo and shortwave downward radiation as detailed in Sect. 2.3.1 and 2.3.2. Positive numbers mean that PISM overestimates the melt, and negative numbers mean that PISM underestimates the melt. The local root-mean-square error averaged over June, July, and August from 1958–2019 is shown in the right plot. The spatial average of the RMSE is 0.36 m/yr.

mean-square errors are minimized by the dEBM-simple parameters c_1 and c_2 given in Table A2.

Yearly total melt computed with PISM-dEBM-simple follows the MAR data closely (see Fig. 1). That extreme melt years such as 2012 and 2019 are underestimated can be explained by the parametrization of shortwave downward radiation, which neglects temporal variability in the cloud cover, one of the drivers of recent mass loss in Greenland (Hanna et al., 2014; Hofer et al., 2017). We also test dEBM-simple with shortwave downward radiation and albedo from MAR directly. Figure A4 shows that in this case the extreme melt in 2019 is better captured, while melting in 2012 is still underestimated.

As Fig. 2 shows, melt is generally overestimated in June, at the beginning of the melt season, and underestimated as the melt season progresses. In July dEBM-simple underestimates melt mostly at the western margin, where ablation is highest. In August, toward the end of the melt season, melt is systematically underestimated by the dEBM-simple module, in particular in the regions where the darkest albedo values are observed. The systematic underestimation could be caused by taking a constant minimal value for the ice albedo and not allowing for processes which would lead to a natural darkening of the surface, i.e. algae growths, supra-glacial lakes, or ageing of snow or exposed ice. On the other hand, many of those processes, in particular bio–albedo feedbacks or dust deposition, are not yet represented in the MAR model either and thus should not induce a systematic bias when comparing to MAR data.

The melt Eq. (1) can be used to attribute the melt rates of the present day to temperature- or insolation-driven melt in a first-order approximation. To this end we compare both

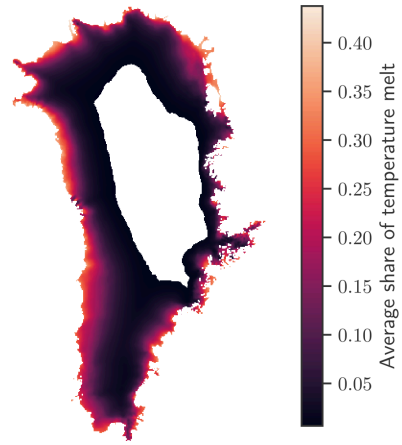

Figure 3. Share of temperature-induced melt. The fraction of temperature-induced melt, defined as $M_t/(M_t + M_i)$, is diagnosed with PISM-dEBM-simple and averaged over the months June, July, and August over the whole simulation period from 1958–2019. The white part in the centre illustrates areas of the Greenland Ice Sheet where the average melt is zero at present.

contributions to the total melt rate, with the temperature-driven melt $M_t = \frac{\Delta t_\Phi}{\Delta t \rho_w L_m} c_1 T_{eff}$ and the insolation-driven melt $M_i = \frac{\Delta t_\Phi}{\Delta t \rho_w L_m} \tau_\alpha (1-\alpha_s) \overline{S}_\Phi$. The share is then defined by $M_t/(M_t+M_i) = (c_1 T_{eff})/(c_1 T_{eff} + \tau_\alpha (1-\alpha_s)\overline{S}_\Phi)$ over the regions which experience melt. Under present-day conditions, this approach indicates that the melt over the whole ice sheet is mainly driven by the insolation (see Fig. 3). Even at the

margins, where monthly mean temperatures and the fraction of temperature-driven melt are highest, the fraction does not exceed one-half. In particular over the high and cold regions of the ice sheet, the melt seems to be entirely driven by the insolation, with an indirect effect of the temperature only allowing melt if monthly mean air temperatures are above −6.5 °C.

The model is able to capture melt patterns of the Greenland Ice Sheet over the historic period between 1958–2019 with a root-mean-square error of 32.92 Gt for the yearly total melt and an average root-mean-square error of 0.36 m w.e./yr for the local summer melt rates. A more thorough discussion on the performance and the sensitivity of the melt Eq. (1) (without the parametrization of albedo and transmissivity) and a comparison to the positive-degree-day model can also be found in Krebs-Kanzow et al. (2018). An overview of the performance of the full dEBM model compared with other state-of-the-art models can be found in Fettweis et al. (2020).

Overall, the skill of the PISM-dEBM-simple model under present-day conditions and using high-resolution forcing from MAR is similar to the skill of the full dEBM model (Krebs-Kanzow et al., 2021). Compared to MAR, dEBM revealed a RMSE of 27 Gt for the annual mean 1979–2016 climatic mass balance in an experiment which was forced with reanalysis data (Uta Krebs-Kanzow, personal communication, 2021). The dEBM full model accounts for changes in the atmospheric emissivity and transmissivity, both caused by changes in cloud cover. As the cloud cover was the main driver in the 2012 melt event, the full dEBM model is therefore better suited to reproduce this and similar melt events. Furthermore, dEBM computes the refreezing on the basis of the surface energy balance.

3.2 Sensitivity to Eemian solar radiation

The dEBM approach together with the approximations for albedo and transmissivity allows us to include changing orbital parameters for simulations on paleo timescales. Here we explore the melt response to Eemian (125 kyr before present) orbital parameters in order to test for the sensitivity to insolation values and compare with other results from the literature. Therefore we use the eccentricity $e = 0.0400$, the obliquity $\varepsilon = 23.79°$, and the longitude of the perihelion $\omega = 307.13°$. The insolation at the top of the atmosphere is then calculated as detailed in Sect. A1. We use the present-day topography for the diagnosis of melt rates and keep the surface air temperature fields unchanged from the previous experiment (MAR v3.11 in the period of 1958–2019).

The increase in solar radiation leads to increased melt, as seen in Fig. 4. The inter-annual variability in yearly total melt is very close to the present-day variability computed with MAR, mainly driven by inter-annual temperature changes. Averaged over the whole time period (1958–2019), the yearly total melt increases by 98 Gt/yr, which corresponds to a relative increase of 31 %. This is in line with findings of Van De Berg et al. (2011), who find that Eemian insolation alone leads to a 40 Gt/yr increase in runoff compared to present day and a 113 Gt/yr increase in runoff when compared to preindustrial values.

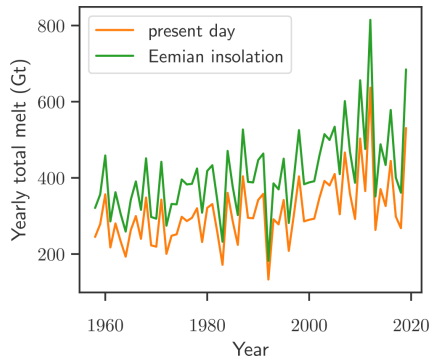

Figure 4. Comparison of Eemian vs. present-day insolation in dEBM-simple. Yearly total melt of the Greenland Ice Sheet as diagnosed with PISM-dEBM-simple under present-day insolation (orange) and Eemian insolation (green). The diagnostic simulations with PISM were performed using monthly MAR 2D temperature fields as forcing and the parameterizations for shortwave downward radiation and albedo mentioned in the text.

4 Influence of the melt–albedo feedback on Greenland's ice loss under future warming

Here, we analyse how changes in albedo may impact the melt rates and the ice loss of the Greenland Ice Sheet under the greenhouse gas emission scenarios RCP2.6 and RCP8.5. In particular we focus on the melt–albedo feedback, and on the additional ice loss driven by changes in albedo. The experiments are motivated and described in detail in Sect. 2.6. The volume of the ice sheet and the mass losses until the years 2100 and 2300 due to the respective warming scenarios are summarized in Table 2.

4.1 Ice loss under warming without the melt–albedo feedback

The α_{1990} experiments use fixed monthly albedo fields and thereby interrupt the melt–albedo feedback. Those experiments illustrate a lower bound of ice losses due to warming in this model setup. Note that the lower bound of projected future ice loss under global warming likely differs due to the coarse resolution and the lack of ice–ocean interaction in this study. As described in Sect. 2.6, the monthly albedo in the α_{1990} experiments is fixed to an average yearly cycle given by the pre-1990 values in MARv.3.11. Consequently the insolation-related melt, as given by the first term of Eq. (1), remains constant or even decreases due to decreasing

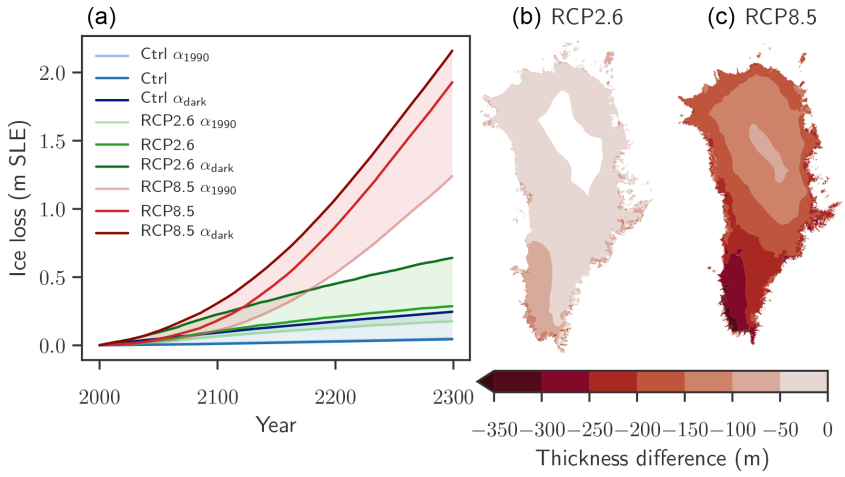

Figure 5. Influence of the melt–albedo feedback on Greenland's ice loss under future warming. The scenarios consist of a control experiment (blue) and temperature forcing with RCP2.6 (green) and RCP8.5 (red). **(a)** Ctrl, RCP2.6, and RCP8.5: ice losses between 2000 and 2300 modelled with PISM-dEBM-simple using the standard parameters and the respective temperature forcing. α_{1990}: ice losses for the respective temperature forcing with monthly albedo fixed to the average pre-1990 values, thereby interrupting the melt–albedo feedback. α_{dark}: ice losses with the respective temperature forcing with summer albedos (June, July, August) set to the bare-ice value over the whole ice sheet. This yields an upper limit of ice loss driven by albedo changes. The shading is to illustrate the range between the lower and upper limits. Ice loss is given in metres of sea level equivalent. A value of 1 m s.l.e. corresponds to approx. 361 800 Gt of ice. Panels **(b)** and **(c)** show the ice thickness difference between the lower bound experiments α_{1990} and the standard experiments for RCP2.6 **(b)** and RCP8.5 **(c)** in the year 2300.

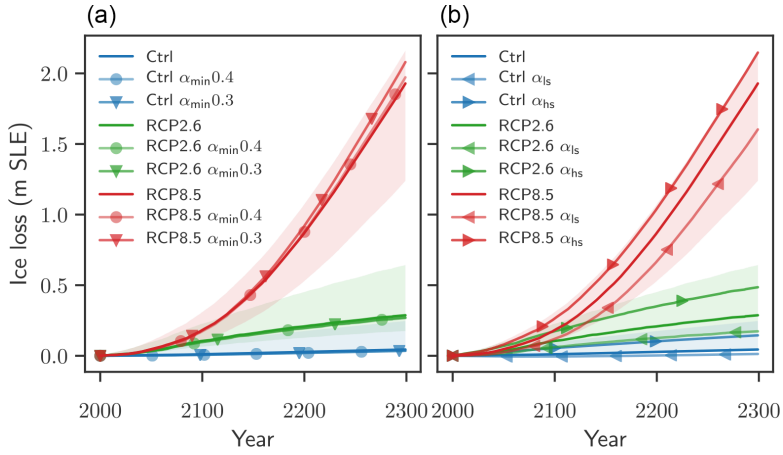

Figure 6. Uncertainty of albedo-change-driven ice loss. Ice losses of the Greenland Ice Sheet under the Ctrl, RCP2.6, and RCP8.5 scenarios, exploring the effect of different albedo sensitivities, as described in detail in Sect. 2.3.2 and Fig. A1. Shaded regions correspond to the range between the lower and upper bounds for ice loss, as shown in Fig. 5. **(a)** Ice losses with variations in the minimal value for albedo. Lower α_{min} corresponds to darker bare ice. **(b)** Ice losses with variation in the slope of the albedo parametrization. α_{ls} experiments use a lower slope (half of the standard value); thus the sensitivity of albedo to melt is reduced. α_{hs} experiments use a higher slope (double the standard value), thus increasing the sensitivity of albedo to melt. Ice loss is given in metres of sea level equivalent. A value of 1 m s.l.e. corresponds to approx. 361 800 Gt of ice.

Table 2. Sea-level-relevant volume (in metres of sea level rise equivalent) and mass loss (in centimetres of sea level rise equivalent). All values are relative to the respective control simulation. Only α_{dark} simulations are given in absolute values, since the Ctrl α_{dark} is an extreme scenario which does not qualify as a control experiment.

Experiments	Volume (m s.l.e.)		ΔVolume (cm s.l.e.)	
	2100	2300	2100	2300
Ctrl α_{1990}	7.59	7.55	–	–
Ctrl	7.59	7.55	–	–
Ctrl α_{dark}	7.51	7.35	8.3	20.1
Ctrl α_{ls}	7.60	7.59	–	–
Ctrl α_{hs}	7.54	7.45	–	–
Ctrl $\alpha_{\text{min}}0.4$	7.59	7.56	–	–
Ctrl $\alpha_{\text{min}}0.3$	7.59	7.56	–	–
RCP2.6 α_{1990}	7.53	7.42	5.2	12.6
RCP2.6	7.49	7.31	9.4	24.3
RCP2.6 α_{dark}	7.37	6.96	21.4	59.7
RCP2.6 α_{ls}	7.54	7.43	6.7	16.0
RCP2.6 α_{hs}	7.42	7.11	11.9	34.1
RCP2.6 $\alpha_{\text{min}}0.4$	7.50	7.33	9.0	23.3
RCP2.6 $\alpha_{\text{min}}0.3$	7.50	7.33	9.2	23.5
RCP8.5 α_{1990}	7.49	6.36	9.3	119.0
RCP8.5	7.42	5.67	16.8	188.4
RCP8.5 α_{dark}	7.29	5.44	29.3	211.5
RCP8.5 α_{ls}	7.48	6.00	12.2	159.0
RCP8.5 α_{hs}	7.34	5.45	20.5	200.2
RCP8.5 $\alpha_{\text{min}}0.4$	7.43	5.63	16.4	193.7
RCP8.5 $\alpha_{\text{min}}0.3$	7.42	5.52	17.0	204.4

transmissivity of the atmosphere, and only the temperature-dependent term increases due to the warming.

In this scenario, the Ctrl α_{1990} experiment remains constant in volume, while the RCP2.6 α_{1990} shows 5.2 cm ice loss until 2100 and 12.6 cm until 2300. In the RCP8.5 α_{1990} experiment the ice loss amounts to 9.8 cm until 2100 and to 119 cm until 2300 (see Fig. 5). The mass loss until 2100 is in line with the estimate of 9 ± 5 cm in the community-wide ISMIP6 projections (Goelzer et al., 2020). Note that in contrast to ISMIP6, the ocean-driven melting remains constant, even under increased temperatures, and there is no glacier retreat due to ice–ocean interactions. However, the mitigating effect of precipitation increase in a warmer climate is also missing.

4.2 Increased ice loss through the melt–albedo feedback

In the following we present the results for the std experiments with PISM-dEBM-simple, taking into account the melt–albedo feedback through the melt-dependent albedo parameterizations as described in Sect. 2. In the control simulation Ctrl, without temperature forcing or artificial darkening, the ice sheet is stable in volume on the timescale of 300 years.

In the RCP2.6 simulations, the moderate increase in temperatures leads to an approximately linear decline in ice volume with an ice loss of 9.4 cm until 2100 and 24.3 cm until 2300 in comparison to the year 2000. This is an increase in ice loss of +82 % in 2100 and +93 % in 2300 in comparison to the α_{1990} simulation without melt–albedo feedback; see Fig. 5 and Table 2. The RCP8.5 simulations show a strong and non-linear decline in ice volume, with ice loss of 16.8 cm in 2100 and 1.88 m in 2300. This corresponds to a relative increase of +80 % and +58 % respectively due to the melt–albedo feedback. The relative contribution of the melt–albedo feedback to ice loss keeps increasing with time for the RCP2.6 experiment, while it becomes less important with time for the RCP8.5 experiment, as the whole ice sheet approaches the minimal albedo value α_{min}. However, in absolute terms the melt–albedo feedback still contributes almost 70 cm s.l.e. mass loss in the RCP8.5 experiment until the year 2300.

We compare these values with the influence of the melt–elevation feedback (T_{noLR}; see Fig. C1). This feedback is weaker; it increases the ice loss by 18 % and 13 % in the RCP2.6 and RCP8.5 simulations respectively.

The melt–albedo feedback is particularly important in the south of Greenland, where the insolation averaged over the daily melt period $\overline{S}_{\Phi}$ (see Eq. 1) is highest. Until the year 2300 it initiates up to 100 m of additional thinning in the southwest for the RCP2.6 scenario compared to RCP2.6 α_{1990} (Fig. 5b). In the RCP8.5 experiment, the melt–albedo feedback is impacting the thinning over the whole ice sheet (Fig. 5c). However, the most important contribution remains in the southwest of Greenland, with an additional 300 m of thinning compared to RCP8.5 α_{1990}.

4.3 An upper limit for ice loss through extreme surface darkening

As a next step, the upper limit of the melt–albedo feedback is explored via prescribing summer albedos equal to the bare-ice albedo over the whole ice sheet in each year (see details in Sect. 2.6). First, the effect of such a surface darkening is explored without any temperature forcing in the Ctrl α_{dark} scenario. In this experiment approximately linear mass loss is observed, with a rate of 8 mm s.l.e. per decade (see Fig. 5a), and induces ice loss of 8.3 cm until 2100 and 20.1 cm until 2300. The condition that the local monthly mean air temperature needs to be higher than −6.5 °C to allow melt, prevents further melting in the ice sheet's interior. Topographic changes together with the temperature–lapse rate feedback increase the melt area slowly, but do not have a major impact over the 300 years. Note that this extreme darkening Ctrl α_{dark} scenario alone induces more ice loss than the RPC2.6 α_{1990} scenario (see Fig. 5 and Table 2).

The RCP2.6 α_{dark} experiment combines the extreme summer darkening with the RCP2.6 temperature anomaly, thereby increasing ice loss from the RCP2.6 α_{1990} experiment by more than a factor of 4 in comparison to the α_{1990} experiments (Fig. 5 and Table 2). This corresponds to a more than 4-fold increase in ice loss. The darkening together with the moderate temperature increase induces an expansion of the melt zone and thus strong melt in areas that are not affected in the Ctrl or RCP2.6 experiments. The ice volume evolution in the RCP2.6 experiment is closer to the lower than to the upper bound of the melt–albedo feedback.

In the RCP8.5 α_{dark} experiment the summer darkening leads to an increase in ice loss of 214 % in 2100 and 77 % in 2300 in comparison to the no-feedback RCP8.5 α_{1990} experiment (see Fig. 5 and Table 2). The strong shock of albedo darkening is particularly relevant when overall temperature increases are still low. In contrast to the RCP2.6 α_{dark} experiment, where the additional mass losses increase with time, here the relative impact of extreme summer darkening decreases on long timescales. As the warming progresses, the temperature becomes a more important driver to melt.

Reducing the frequency of darkening in the RCP2.6 α_{dark} and RCP8.5 α_{dark} experiments to darkening events every 2 or every 5 years instead of every year reduces the difference in mass loss between the RCP α_{dark} and the RCP experiments (see Appendix Fig. B1). When the darkening happens every 2 years, the additional ice loss decreases to approximately half of the ice loss due to darkening every year. Similarly, a darkening event every 5 years leads to only 20 % of the additional ice loss due to the darkening in each year. The effect is approximately linear in event frequency. This might help to estimate additional albedo-driven ice loss in extreme years such as 2012, if projections for the frequency of such extreme events are available.

Reducing the length of the dark period from the whole summer (i.e. June, July, and August) to only 1 month reveals that the month of June is most sensitive to additional darkening, inducing more than half of the additional ice loss between the RCP8.5 and the RCP8.5 α_{dark} experiments (see Appendix Fig. B1). The increased sensitivity to darkening in June could be due to the fact that the Northern Hemisphere receives the most insolation during the month of June. Moreover, in the beginning of the melt season the albedo has not yet decreased due to the melt processes, so an artificial darkening has the strongest effect, compared to the following summer months.

4.4 Exploring uncertainty in albedo-change-driven ice loss

The standard parameters for the albedo parametrization used in the RCP2.5 and the RCP8.5 experiments provide the best fit to the MARv3.11 data over the historic period. However, the range for possible contributions of the melt–albedo feedback is large; therefore we test how changes in the albedo parametrization affect the ice loss driven by albedo changes. The albedo parametrization can affect the strength of the melt–albedo in two ways: first by changing α_{min}, the lowest albedo possible, and second by changing the sensitivity of albedo to melt via the slope in Eq. (7). To ensure that the subsequent mass changes are not primarily due to model drift, they are corrected by a Ctrl experiment without warming but with otherwise identical parameters.

A decreased value of α_{min} does not affect regions where melt rates are below 14 m/yr. Consequently, strong melt rates are necessary to observe its impacts: in the RCP8.5 α_{min} simulations with $\alpha_{\mathrm{min}} = 0.4$ the lowered α_{min} value causes an additional 5.3 cm of ice loss in 2300 (compared to RCP8.5), and the RCP8.5 α_{min} simulations with $\alpha_{\mathrm{min}} = 0.3$, it causes an additional 16 cm until 2300 (Fig. 6a).

In contrast to the α_{min} experiments, changing the slope in the albedo parametrization in Eq. (7) affects the sensitivity of the albedo to melt already at low melt rates. In the Ctrl α_{hs} experiment, the ice sheet loses 10 cm s.l.e. until 2300 from the increase in the albedo sensitivity alone, twice as much as with standard parameters. The increased melt sensitivity, although at the upper end of the uncertainty of the parameters presented in Sect. 2.5, might not be optimal in representing historical melt when the other parameters remain unchanged. We thus test the mass losses of the warming scenarios with respect to the Ctrl α_{hs} experiment, in order to explore the interplay of an increased melt–albedo feedback and warming.

The additional effect of the increased sensitivity on ice volume evolution depends on the warming scenario. The RCP2.6 α_{hs} experiment with moderate warming is affected by a more sensitive albedo parametrization, with up to 40 % increases in ice loss until 2300 with respect to the RCP2.6 experiment (see Fig. 6). In contrast, the additional mass loss in RCP8.5 α_{hs} is lower with +6 % in 2300 compared to the RCP8.5 scenario. This can be explained by the fact that the high melt rates in the RCP8.5 scenario quickly induce the minimal albedo over the whole ice sheet and thereby interrupt the feedback. Once the minimal albedo is reached, further increase in melt rates does not affect the albedo any more; thus the melt is not affected by the stronger feedback any more.

If the sensitivity of albedo to melt is reduced, the ice sheet in the Ctrl α_{ls} experiment shows slight mass gains (4 cm over 300 years). The lower sensitivity mitigates mass losses from both the RCP2.6 α_{ls} and RCP8.5 α_{ls} experiments, with 8.3 and 29.4 cm less mass loss until 2300 respectively. However, even with the reduced melt–albedo feedback the ice loss increases by approximately one-third when compared to the α_{1990} experiment without albedo–melt feedback.

5 Discussion

We have presented an implementation of a simple version of the diurnal energy balance model (dEBM-simple) as a mod-

ule in the Parallel Ice Sheet Model (PISM). Using this model we evaluate how changes in albedo impact future mass loss of the Greenland Ice Sheet under the RCP2.6 and RCP8.5 warming scenarios.

5.1 Implementation and validation

In dEBM, the surface melt is calculated as a function of near-surface air temperature and shortwave downward radiation. A first version of the dEBM was tested and validated in Krebs-Kanzow et al. (2018), and a full version was presented in Krebs-Kanzow et al. (2021). dEBM-simple adapts the approach taken in Krebs-Kanzow et al. (2018) and adds additional modules to calculate the albedo as a function of melt and the shortwave downward radiation. Therefore, the only inputs needed to compute the melt rate are two-dimensional near-surface temperature fields including the yearly cycle and a precipitation field in order to close the climatic mass balance. This approach makes the model as input-friendly as a temperature-index model such as the widely used positive-degree-day model, but with the advantage of capturing the melt–albedo feedback. The dEBM-simple surface mass balance module can be used with PISM in a stand-alone setting to simulate past and future ice sheet evolution, requiring only a temperature field, a precipitation field, and the time series of the temperature anomaly as inputs. As PISM is an open-source project, the module can easily be expanded or implemented in other stand-alone ice sheet models.

Being a simple model, dEBM-simple does not fully resolve the spatial pattern and temporal evolution of melt over the Greenland Ice Sheet; the melt rates are slightly overestimated towards the beginning of the melt season (June) and underestimated towards the end of the melt season (August) and at the margins of the ice sheet. This is possibly related to the albedo parametrization, which underestimates the albedo in June and overestimates the albedo in August, not capturing important processes like exposure of firn or ice, or darkening of the ice via algae or meltwater. However, the total yearly melt rates match those of MAR over the period 1958–2019 well and on this timescale the skill of the model is comparable to the dEBM (Krebs-Kanzow et al., 2021). The exceptions of the extreme melt in the years 2012 and 2019, where dEBM-simple clearly underestimates melt rates, are related to changes in cloud cover or blocking events (Delhasse et al., 2021; Hanna et al., 2014; Hofer et al., 2017), which are not captured by the parametrization of the transmissivity of the atmosphere.

Increased insolation values like during the Eemian increase the melt on average by 97 Gt/yr under otherwise identical conditions. This is in line with the findings of Van De Berg et al. (2011). While this is only an approximation with several strong assumptions (e.g. the present-day topography of the ice sheet is preserved and we did not apply changes in the temperature), it illustrates the possibility of extending this model to paleo timescales with relatively low effort.

The implemented parametrization for albedo is based on a phenomenological relation of albedo to the melt rate. It is a coarse representation of the effects that are important for the snow albedo, such as the grain size, surface water and melt ponds, impurities (e.g. black carbon or algae), or any dependence on the spectral angle or the cloudiness condition of the sky. The possible darkening of ice is considered only indirectly in this approach. In particular, lowering the minimal allowed albedo to values which are typical for either dirty ice or supraglacial melt ponds could allow us to include an approximation of albedo changes of the bare ice itself. Moreover, the parametrization neglects the impact of the snow cover thickness, which might mitigate melt-driven reduction in albedo after a winter with heavy precipitation (Box et al., 2012). As the parameters of the albedo scheme are fitted against monthly averages of the MAR albedo, processes which happen on a sub-monthly timescale are not well captured. The ageing or renewal of snow, associated with the frequency of snowfall events, is not directly represented in the monthly averaged MAR data used to fit the parameterization. Neither is the influence of shading, wind exposure, or rain spells. These could induce additional variability associated with the albedo–melt relations.

Similarly, the parametrization introduced for the shortwave downward radiation does not take into account temporal or spatial patterns. The inter-annual variability of the cloudiness over Greenland and blocking events can therefore not be represented with this approach.

However, the introduced parameterizations do not introduce a systematic bias or a large additional error in comparison to a purely diagnostic mode of dEBM-simple, where instead of parameterized albedo and shortwave downward radiation the 2D fields of MAR output are used to calculate the melt rates (see Fig. A4), while all other parameters are kept constant.

In this paper we optimize the dEBM parameters c_1 and c_2 independently from the parameters for the albedo and the transmissivity. All parameters are based on MAR v3.11 data. While this procedure gives an overall good fit, as seen in Sect. 2.5, it is not necessarily the optimal solution in combination. However, this procedure keeps the parameters independent from the forcing. One could, based on the application, choose to change the parameterizations independently from the dEBM parameters and thereby study the influence on the ice loss, as we have shown in Sect. 4.4.

In comparison to the widely used positive-degree-day model, PISM-dEBM-simple performs slightly better for both measures: the monthly averaged spatial melt and the integrated yearly melt (see Appendix D).

5.2 Sensitivity of the Greenland Ice Sheet to warming and surface darkening

In this paper we use the PISM-dEBM-simple model in order to assess the influence of albedo changes and surface

warming on the Greenland Ice Sheet. The simple surface mass balance model allows a first estimate of the influence of the melt–albedo feedback on the future evolution of the Greenland Ice Sheet in two temperature scenarios: moderate-warming RCP2.6, a scenario compatible with the Paris Agreement, and high-warming RCP8.5, a worst-case scenario. Experiments with a fixed yearly cycle of the albedo suppress the melt–albedo feedback and thus serve as a lower bound to future ice loss. In contrast, the extreme scenario in the α_{dark} experiments with the surface albedo lowered to the bare-ice value over the whole ice sheet for the months June, July, and August serves as an upper bound for future melt through the melt–albedo feedback. The experiments with adaptive albedo serve as a more realistic estimate of future mass losses.

This experimental design allows us to attribute ice loss to the melt–albedo feedback. Overall we find that the melt–albedo feedback has a strong influence on melt under future warming. For example in the RCP2.6 scenario, the ice loss almost doubles through the albedo feedback (compare RCP2.6 with RCP2.6 α_{1990}). Moreover, the relative amount of ice loss driven by changes in albedo keeps increasing over time. In contrast, the share of melt, driven by albedo changes, is lower in the high-temperature RCP8.5 scenario and decreases as the temperature increases, indicating that temperature is a more important driver under these conditions. Note, however, that the absolute increase in mass loss through the feedback is higher for RCP8.5 than for RCP2.6. We also find that extreme darkening alone, without any temperature anomaly, can initiate mass losses comparable to the RCP2.6 scenario.

Moreover, the interaction between the extreme darkening and warming initiates additional ice loss. In particular, the RCP2.6 α_{dark} scenario loses 23 % more mass until 2300 than the sum of RCP2.6 and the Ctrl α_{dark} simulations, suggesting that other feedbacks, such as the melt–elevation feedback, enhance the mass loss of the RCP2.6 α_{dark} scenario.

An ensemble analysis over the ice loss in the RCP8.5 scenario reveals how sensitive the model is towards variations in the dEBM-simple albedo and transmissivity parameters (see Appendix E). All of the simulated ice loss remains within the bounds given by the α_{1990} and α_{dark} experiments. Variations in the intercept of the atmospheric transmissivity have the greatest impact on ice loss, where higher values for the intercept shift the albedo- and insolation-dependent melt to higher values. Other parameters which seem to influence ice loss are the dEBM parameter c_1, which governs the relation to temperature, and the slope of the albedo parametrization. Here, higher absolute values favour higher ice loss. On the other hand, the dEBM-simple parameter c_2 and the slope of the transmissivity parametrization do not seem to have a strong effect on overall ice loss in a high-temperature scenario.

In this setup the melt–elevation feedback has a smaller impact on ice loss than the melt–albedo feedback: experiments which neglect the melt–elevation feedback (here parameterized through the atmospheric temperature lapse rate of -6 K/km) lose 18 % less mass in the RCP2.6 T_{noLR} scenario and 13 % less in the RCP8.5 T_{noLR} scenario until 2300 (see Fig. C1). This is in line with previous studies (Le clec'h et al., 2019) and suggests that the melt–elevation feedback, although weaker than the melt–albedo feedback, should not be neglected on the timescale of several centuries.

In comparing the ice loss with PISM-dEBM-simple in the RCP8.5 scenario to ice loss computed with PISM-PDD, we find that the positive-degree-day method increases losses by 12 % until 2100 and by 47 % by 2300 (see Appendix D). The losses for the RCP2.6 scenario do not differ significantly between PDD and dEBM-simple. The increase in ice loss for PDD can be explained by a higher temperature sensitivity of the PDD method: once all snow has melted, the sensitivity to positive-degree days (which is the time integral of Eq. 3) is given by the degree day factor for ice $f_{\mathrm{i}} = 8\,\mathrm{mm/(K\,d)}$. In contrast, with the parameters used in this paper, dEBM-simple scales to T_{eff} only with $\approx 4.37\,\mathrm{mm/K\,d}$ (plugging in the constants in Eq. (1) and assuming $\Delta t_\Phi/\Delta t = 0.6$, which is at the upper end of possible values). Thus, once the albedo effect saturates, PDD predicts higher melt rates with increasing temperatures. Moreover, due to the melt–elevation feedback, local temperatures rise even faster with increasing melt, leading to a stronger divergence between the dEBM-simple and the PDD ice loss.

In this study, we assume simplified representations of both the melt–elevation and the melt–albedo feedbacks. However, certain effects such as the feedbacks between the topography of the ice sheet and the atmospheric conditions which affect the surface mass balance cannot be expressed in the atmospheric temperature lapse rate alone. Similarly, the albedo is affected not only by melt, but also by the sky conditions, snow events, and impurities. While PISM-dEBM-simple is computationally efficient and represents the ice dynamics well, it cannot compete with an explicit process-based snowpack model as used by the regional climate models MAR or RACMO (Le clec'h et al., 2019; Kuipers Munneke et al., 2011) or represent the effect of summer snowfall on albedo (Noël et al., 2015). Moreover, here the melt–albedo feedback is represented by a relation linear at low melt rates and obtained from a MAR simulation over the historic period 1958–2019. This relation might not apply under future warming. Therefore we test uncertainties related to the albedo parametrization, with the resulting mass losses lying in the range between the lower bound, i.e. the no-feedback scenario, and the upper bound, i.e. the extreme-darkening scenario. Further analysis of the influence of the melt–albedo feedback with models that fully resolve the firn layer would be helpful to analyse processes that are neglected or simplified in this paper.

In observations, long-lasting albedo changes are already found as a consequence of heat waves which initiate strong surface melt (Nghiem et al., 2012; Tedesco and Fettweis, 2020). While the regions with the most rapid darkening in

Greenland are located in the ablation zones, ice-sheet-wide melt events trigger albedo changes over the whole ice sheet (Tedesco et al., 2016). Studies suggest that heat waves in the Arctic may become more frequent with future warming (Dobricic et al., 2020), with still unknown consequences to ice sheet melt and albedo. Currently, there are no explicit albedo projections that take all processes and feedbacks like the distribution of surface meltwater, algae growths, dust deposition, and dust meltout into account. While PISM-dEBM-simple does not explicitly model all these processes, it adds a tool to explore albedo change scenarios and their influence on the future evolution of the ice sheet in a numerically efficient way, which takes the ice dynamics into account.

6 Conclusions

The module dEBM-simple is implemented in the open-source Parallel Ice Sheet Model (PISM) and captures albedo- and insolation-dependent melt as well as temperature-driven melt in stand-alone ice sheet simulations. Due to its simplicity, it can be used to perform large-scale ensemble studies or long-term simulations over centuries to millennia. The source code is fully accessible and documented, as we want to encourage improvements and implementation in ice sheet other models. This includes the adaption to other ice sheets than the Greenland Ice Sheet.

Using PISM-dEBM-simple we find that the melt–albedo feedback can lead to an additional 12 cm of sea level equivalent of mass loss in RCP2.6 and an additional 70 cm in RCP8.5 in the projected mass loss until the year 2300 with PISM. While our experiments rely on a simple parametrization of albedo with surface melt, they show that future albedo changes can make an important contribution to Greenland's future mass loss.

Appendix A: Parameterizations for stand-alone ice sheet models

A1 Parametrization of albedo as a function of melt

Albedo is complicated to parametrize correctly, because of its dependence on a number of factors: the snow or firn albedo depends on grain size, impurities, surface water, refrozen ice, compaction, sky conditions, and spectral angle while the ice albedo depends on impurities, surface water, sky conditions, and spectral angle. Here we aim for a very simple phenomenological parametrization of albedo, which is good enough to be valid on large spatial scales and on long timescales. Only the broadband albedo is parameterized here, assuming that the average cloudiness of the sky does not change over long timescales. Further, it is assumed that grain size and surface water can be summarized in a single dependence of the albedo on the melt rate.

In the MAR v3.11 dataset, a negative correlation of albedo with melt is found (see Fig. A1). The average relation over the months June, July, and August in the period of 1958–2019 can be best described by the linear relation $\alpha = -0.025\,\mathrm{yr/m} \cdot m + 0.82$, indicated by the dashed orange lines in Fig. A1. The intersection with the y axis is interpreted as average snow albedo. At very high melt rates the albedo is less sensitive to additional increases with melt, which might be caused when the snow cover disappeared and bare ice is exposed. In this parametrization we introduce a lower limit to the albedo such that it can not be lower than 0.47 (approximately the value for bare ice Gardner and Sharp, 2010; Bøggild et al., 2010). This value is lower than the MAR value for bare ice, but in line with MODIS and RACMO at the ice margin, where impurities can accumulate (Noël et al., 2018; van Dalum et al., 2020; Stroeve et al., 2013). There is a large variance in how sensitively albedo is related to melt, which is due to both spatial and temporal (intra-annual as well as inter-annual) variability. However, a clear long-term trend of how the albedo depends on surface melt could not be established. In July, the albedo is on average less sensitive to melt, with an average slope of -0.021 yr/m. In June the monthly fit is identical to the whole summer, and in August the albedo decreases on average more strongly with melt, corresponding to a slope of -0.034 yr/m. In addition, in August there is a broad distribution of albedo values at zero melt, ranging from approximately 0.57 to the fresh snow value, which underlines that the correct albedo depends not only on the current condition but also on the melt during the past months. In order to estimate the sensitivity of future ice evolution to the exact parameters of the albedo parametrization, we vary the slope of the albedo over a broad range, by taking the double or half slope found with the linear regression, here indicated with the grey lines.

We tested other albedo parameterizations, which are successfully used in other models (e.g. Krebs-Kanzow et al., 2021; Krapp et al., 2017; Robinson et al., 2010).

We found that it is also better suited than a parametrization with the snow thickness, successfully used by many models as well (Krapp et al., 2017). The parametrization with snow thickness did lead to too low of albedo values and thus too high of melting in northwest Greenland, where precipitation is generally low. In our implementation, we found that the continuous relation of albedo to melt performed better to predict melt. Our approach comes with the caveat that the snow thickness is not considered for the calculation of the albedo, although observations suggest that increased winter snow can mitigate summer melt due to the higher albedo of the snow (Box et al., 2012; Riihelä et al., 2019).

The spatial distribution of summer albedos is shown in Fig. A2.

A2 Parametrization of shortwave downward radiation

Shortwave downward radiation that reaches the ice sheet's surface depends on the incoming radiation at the top of the atmosphere, the solar zenith angle, the surface altitude, and the cloud cover. In order to get the most correct estimate of shortwave downward radiation at the ice sheet's surface, it would be ideal to know the monthly average cloud cover. Since here we aim for a parametrization, which makes the model as simple as a temperature index model concerning the inputs needed, we instead parametrize the transmissivity of the atmosphere with the assumption that the average cloud cover does not change, either during the summer months or on longer timescales. Following Robinson et al. (2012), we assume that the transmissivity is solely a function of the surface altitude. In order to get a best estimate to this relation, the top of the atmosphere (TOA) radiation, which depends only on season and latitude, is compared to the MAR output for shortwave downward radiation. The daily average TOA radiation $\overline{Q}^{\text{day}}$ is described by Eq. (4). The local shortwave downward radiation SW would then be

$$\text{SW} = \overline{Q}^{\text{day}} \cdot \tau_\alpha.$$

A linear relation of the transmissivity to the surface altitude is given by

$$\tau_\alpha = a + b \cdot z,$$

with the surface elevation in metres z and the fit parameters a and b. The linear fit for the shortwave downward radiation from TOA insolation was obtained from a linear regression of MAR v3.11 data averaged over June, July, and August from 1958 to 2019 (see Fig. A3).

Because melting occurs predominantly over the summer months June, July, and August, we derive the average transmissivity of the atmosphere based on the transmissivity calculated in MAR in June, July, and August. The best fit over these 3 months simultaneously is obtained with $a = 0.57$ and $b = 0.037\,\text{km}^{-1}$, as indicated by the orange dashed line in Fig. A3. A seasonality can be observed: the transmissivity is on average higher in June ($a = 0.61$ and $b = 0.026\,\text{km}^{-1}$) than in July ($a = 0.57$ and $b = 0.040\,\text{km}^{-1}$) and August ($a = 0.053$ and $b = 0.046\,\text{km}^{-1}$).

For simulations under paleo-conditions, changes in orbital parameters affect the insolation at the top of the atmosphere, and the trigonometric expansion used under present-day conditions (see Sect. 2.3.1) does not hold. The declination angle is then described by $\sin\delta = \sin(\epsilon)\sin(\lambda)$ and the sun–earth distance

$$\left(\frac{\overline{d}}{d}\right)^2 = \frac{(1 + e\cos(\lambda - \omega))^2}{(1 - e^2)^2} \tag{A1}$$

with the oblique angle ϵ, the eccentricity e, the precession angle ω, and the true longitude of the earth λ. The orbital parameters e, ϵ, and ω are given in the input, while λ varies over the time of the year and is computed internally using an approximation of Berger (1978):

$$\lambda = \lambda_\text{m} + \left(2e - \frac{e^3}{4}\right)\sin(\lambda_\text{m} - \omega) + \frac{5}{4}e^2\sin(2(\lambda_\text{m} - \omega)) + \frac{13}{12}e^3\sin(3(\lambda_\text{m} - \omega)), \tag{A2}$$

with

$$\lambda_\text{m} = -2\left(\left(\frac{e}{2} + \frac{e^3}{8}\right)\left(1 + \sqrt{1 - e^2}\right)\sin(-\omega) - \frac{e^2}{4}\left(\frac{1}{2} + \sqrt{1 - e^2}\right)\sin(-2\omega) + \frac{e^3}{8}\left(\frac{1}{3} + \sqrt{1 - e^2}\right)\sin(-3\omega)\right) + \Delta\lambda$$

$$\Delta\lambda = 2\pi(\text{day} - 80)/\text{days per year}.$$

Here $\lambda = 0$ at the spring equinox. This approximation is used only for explicit paleo simulations.

Table A1. Variables used in dEBM-simple.

Name	Variable	Unit
z	Ice surface elevation	km
α_s	Albedo	
$\overline{T}$	Monthly average near-surface temperature	°C
T_{eff}	Cumulative temperature exceeding the melting point	°C
τ_α	Transmissivity of the atmosphere	
$\overline{S}_\Phi$	TOA insolation, averaged over Δt_Φ	W/m^2
SW	Shortwave downward radiation at the surface	W/m^2
M	Melt rate	kg/m^2/s^1
Δt_Φ	Time period with sun above elevation angle Φ	s
$\overline{Q}^{\text{day}}$	Daily average TOA insolation	W/m^2
ϵ, ω, e	Orbital parameters	°,°,

Table A2. Parameters used in dEBM-simple.

Name	Parameter	Value	Reference
ρ_w	Fresh water density	1000 kg/m^3	
L_m	Latent heat of fusion	3.34×10^5 J/kg	
c_1, c_2	dEBM parameters	29 W/m^2 K, −93 W/m^2	Optimized
S_0	Solar constant	1367 W/m^2	Liou (2002)
Φ	Minimal elevation angle for melt	17.7°	Krebs-Kanzow et al. (2018)
σ	Standard deviation of daily temperature	5 K	
a, b	Parameters for transmissivity	0.57, 0.0037 km^{-1}	Optimization
$\alpha_{\max}, \alpha_{\min}$	Maximal and minimal albedo values	0.82, 0.47	Optimization
α_{sl}	Slope in albedo parametrization	−0.025 yr/m	Optimization
γ	Atmospheric temperature lapse rate	−6 K/km	Typical value
$T_{\min}$	Temperature threshold for melt	−6.5°C	Krebs-Kanzow et al. (2018, 2021)

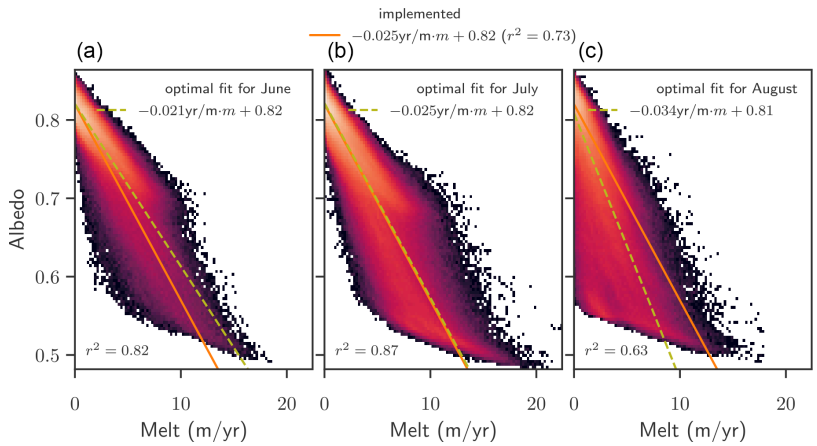

Figure A1. Fit for albedo parametrization. Histograms of albedo vs. melt in June **(a)**, July **(b)**, and August **(c)** over the period 1958–2019 in the MAR v3.11 dataset. Colours represent how often the combination of values is found in each grid cell on the ice sheet over the years. Note that the colour scale is logarithmic. Orange lines show the parametrization with parameters as used in PISM. Light green lines show the best linear fit for each month, with the parameters given in the legend.

A3 Validation of parametrization

In order to assess the validity of the parameterizations in PISM-dEBM-simple, the yearly melt with the fully parameterized model, as shown in Fig. 1, is compared to the yearly melt of a diagnostic analysis of dEBM-simple with otherwise fixed parameters. Instead of computing the albedo and the shortwave downward radiation internally, monthly fields of those variables from the MAR v3.11 date are given as input to compute the melt rates via Eq. (1) with the same parameters c_1 and c_2. While the diagnostic experiment performs better in the extreme melt years 2012 and particularly 2019, we find an increased mismatch, in particular in the 1970s, and a resulting larger root-mean-square error. This can be attributed to the fact that the parameters c_1 and c_2 were optimized for a low temporal and spatial RMSE with the parameterizations for albedo and transmissivity as described above. c_1 and c_2 differ from Krebs-Kanzow et al. (2018) and from an optimal value for the diagnostic melt rate.

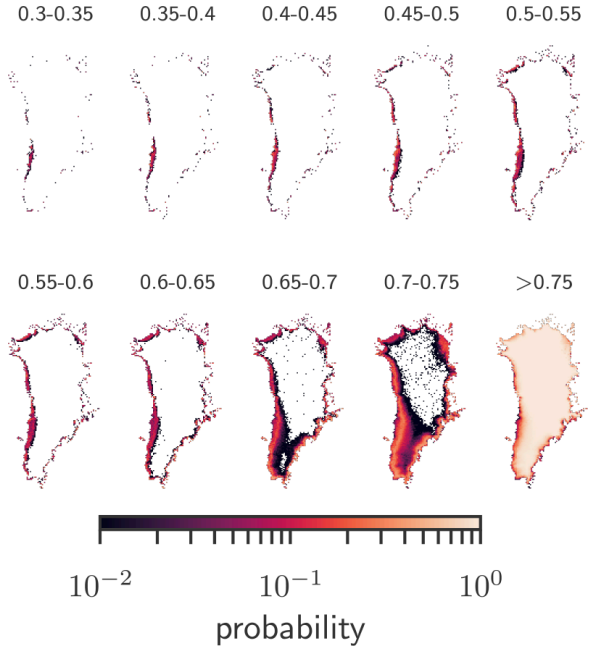

Figure A2. Observed albedo. Local probability to find an albedo value within the given bracket on any day in June, July, or August from 2000–2019. Data: MODIS Greenland albedo; see Box et al. (2017).

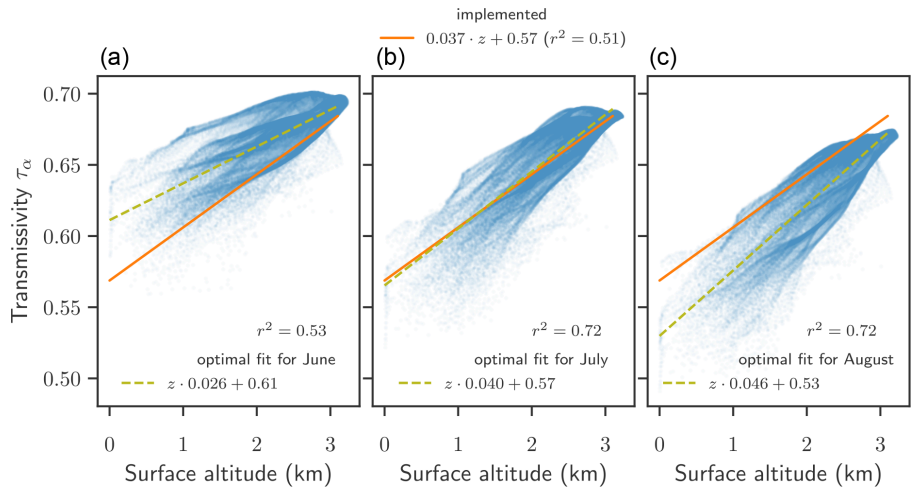

Figure A3. Fit for the parametrization of transmissivity. Shortwave downward radiation vs. surface altitude in June **(a)**, July **(b)**, and August **(c)** over the period 1958–2019 in the MAR v3.11 dataset. Each dot represents values in one cell of the ice sheet, averaged over a month. Orange lines show the parametrization with parameters as implemented, which is the best fit over the 3 months June, July, and August together. Light green lines show the best linear fit for each month, with the parameters given in the legend.

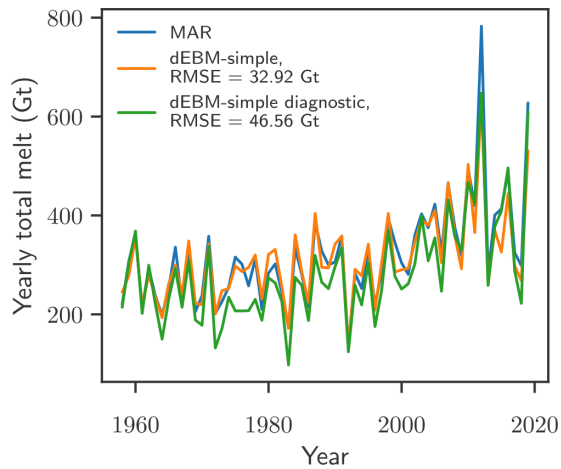

Figure A4. Yearly total melt of the Greenland Ice Sheet as calculated with MAR (blue), diagnosed with the fully parameterized PISM-dEBM-simple simulation (orange), which uses only the monthly 2D temperature fields as input, and diagnosed with a non-parameterized diagnostic dEBM-simple version, which takes the 2D temperature field, the shortwave downward radiation, and the albedo as inputs. The root-mean-square error for the individual time series is given in the legend.

Appendix B: Sensitivity to the darkening scenario

In order to test how the results are impacted by a shorter darkening period or even stronger albedo forcing, we study the upper-limit RCP8.5 α_{dark} scenario in greater detail.

Shortening the darkening period to only 1 month reduces, as expected, the impact of darkening. Moreover, it reveals which months are the most vulnerable to darkening. In particular, we observe that darkening in June leads to the highest mass losses (see dashed–dotted line in Fig. B1a). Darkening in June alone leads to 9.6 cm of additional mass loss in 2100 and to 14.8 cm of additional mass loss in 2300 compared to the warming RCP8.5 scenario without darkening. In contrast, darkening in only July or August has a less significant effect, with 4.3 and 1.4 cm of additional mass loss in 2100 and 7.5 and 5.4 cm in 2300. On the one hand this might be caused by the larger insolation and longer days during the month of June. In June average daily insolation at latitudes above 60° N is approximately 7 % larger than in July and 50 % larger than in August. Moreover, due to the high melt in the warming RCP8.5 scenario, albedo values are already low in July and August, even without darkening.

Using an albedo value which is lower than the value for bare ice leads to increased ice loss. An albedo value of 0.4 instead of 0.47 over the whole ice sheet increases ice loss by an additional 16 % or 4.6 cm by the year 2100 and by an additional 8 % or 17 cm by the year 2300 compared to the RCP8.5 α_{dark} scenario. An even lower albedo value of 0.3 increases ice loss by an additional 37 % or 11 cm by 2100 and by an additional 19 % or 41 cm by 2300 compared to the RCP8.5 α_{dark} scenario.

Reducing the frequency of dark summers to every 2 years leads to additional mass losses which are approximately half of the additional mass losses caused by the darkening in every year for both warming scenarios. A darkening frequency of every 5 years leads to additional mass losses of about 20 % of the additional mass loss with darkening in every year. This suggests that, at least on timescales of 300 years, the effects of more or less frequent darkening remain linear.

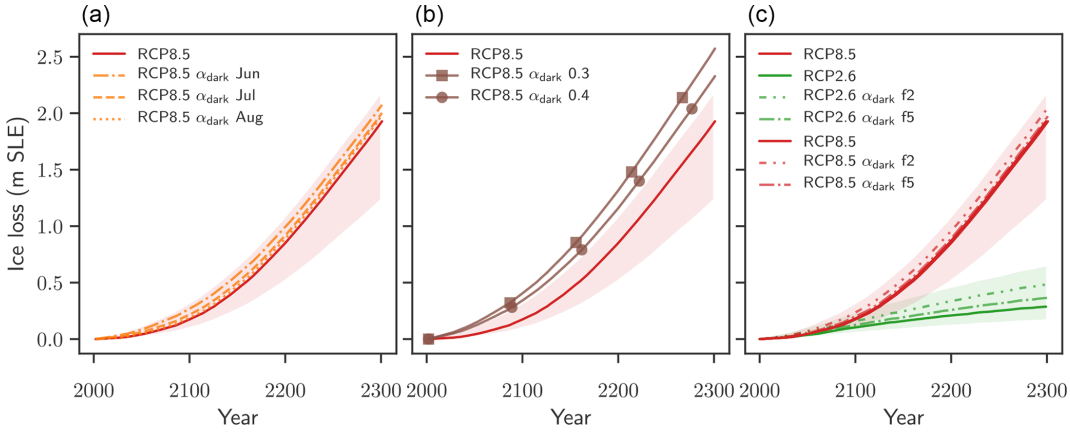

Figure B1. Sensitivity to the darkening scenario. Ice volume evolution for different implementations of the darkening scenario. The envelopes of minimal and maximal mass loss, given by the α_{1990} and α_{dark} experiments, and the RCP simulations with standard parameters are shown for reference. **(a)** Periods of extreme darkening in the α_{dark} scenario are shortened to 1 month (orange broken lines). **(b)** The albedo value for extreme summer darkening is lowered to 0.3 (brown line with square markers) or 0.4 (brown line with circle markers). **(c)** Reducing the frequency of extreme darkening summers to every 2 (f2) and every 5 years (f5). Ice loss is given in metres of sea level equivalent. A value of 1 m s.l.e. corresponds to approx. 361 800 Gt of ice.

Appendix C: Effect of the melt–elevation feedback

The melt–elevation feedback is generally represented in all experiments by adjusting surface temperatures with height changes by 6 K/km. The influence of the feedback on the simulations is tested by switching off this lapse-rate correction, with the resulting mass loss shown in Fig. C1.

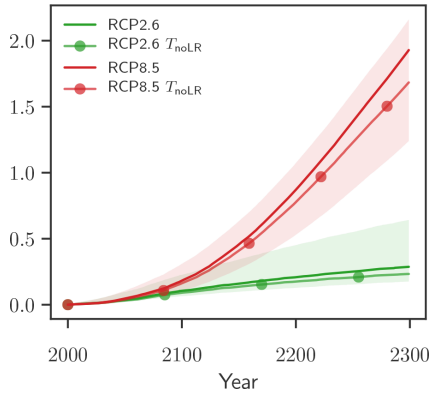

Figure C1. Impact of the melt–elevation feedback. PISM-dEBM-simple simulations of the Greenland Ice Sheet with RCP2.6 (green lines) and RCP8.5 (red lines) warming. Dark solid lines take the melt–elevation feedback through the atmospheric temperature lapse rate into account. Shaded lines with markers neglect the melt–elevation feedback and assume a zero atmospheric temperature lapse rate. Ice loss is given in metres of sea level equivalent. A value of 1 m s.l.e. corresponds to approx. 361800 Gt of ice.

Appendix D: Surface melt computed with the positive-degree-day method (PDD)

During the historic validation period, the simulation with the positive-degree-day method (PDD) for melt has a similar performance to PISM-dEBM-simple (see Fig. D1). The standard parameters were used for this simulation: the standard deviation of the temperature $\sigma = 5$ K, the melt factor for ice $f_i = 8$ (mm liquid water equivalent) / (pos degree day) and the melt factor for snow $f_s = 3$ (mm liquid water equivalent) / (pos degree day). However, the spatial distribution of melt anomalies shows a distinct north–south gradient, with an overestimate of melt in the north and an underestimate of melt in the south; see Fig. D2.

In the warming simulations, the simulations with PDD melting show increased melt compared to dEBM-simple in the high-temperature scenario (see Fig. D3).

In RCP2.6 the north–south bias in the melt rates compared with PISM-dEBM-simple persists. However, the positive and negative biases balance each other out and lead to mass losses very similar to those computed with PISM-dEBM-simple. In contrast, the melt rates in the RCP8.5 scenario are almost consistently higher with the PDD melt module; only in the southwest does PISM-dEBM-simple produce higher melt rates than PDD. We find an increase in ice loss of 12 % in the year 2100 and of 47 % in 2300, compared to the standard dEBM run. The difference between ice loss computed with dEBM and with PDD is not only due to different sensitivities to temperature increase.

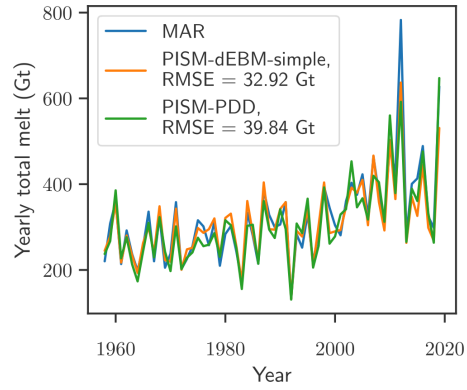

Figure D1. Comparison of annual total melt of the Greenland Ice Sheet as calculated with MAR v3.11 and PISM-PDD. The diagnostic simulation with PISM-PDD (green line) is performed using monthly MAR 2D temperature fields as forcing. The root-mean-square difference between the PISM-PDD simulation and total melt as given by MAR (blue line) is 39.84 Gt. Details on the PISM-dEBM-simple simulation are found in Fig. 1 and in Sect. 3.

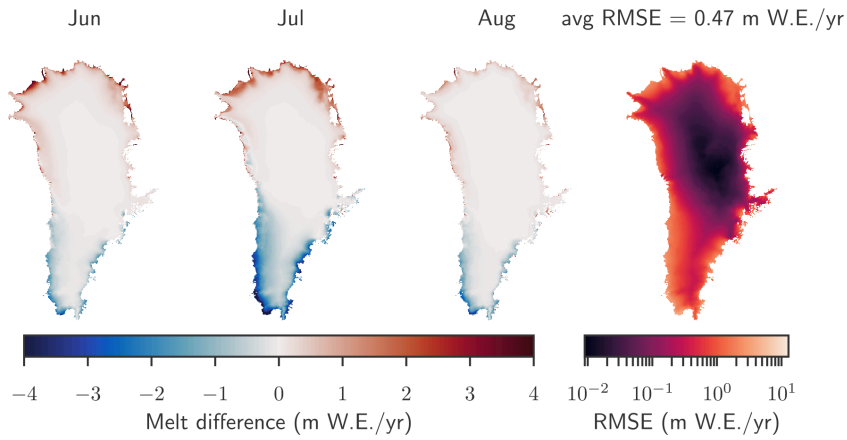

Figure D2. Local differences between the monthly averaged June, July, and August melt rates as diagnosed with PISM-PDD compared to MAR. The PISM simulation uses monthly 2D temperature fields from MAR as forcing. Positive numbers mean that PISM overestimates the melt, and negative numbers mean that PISM underestimates the melt. The local root-mean-square error averaged over June, July, and August from 1958–2019 is shown in the right plot. The spatial average of the RMSE is 0.47 m/yr.

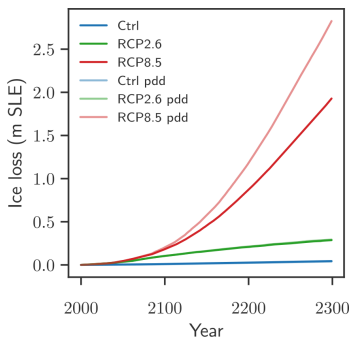

Figure D3. Comparison with the positive-degree-day model. PISM-dEBM-simple and PISM-PDD simulations of the Greenland Ice Sheet with RCP2.6 (green lines) and RCP8.5 (red lines) warming. Ice loss is given in metres of sea level equivalent. A value of 1 m s.l.e. corresponds to approx. 361800 Gt of ice.

Appendix E: Variability of RCP8.5 simulations

In addition to the RCP8.5 simulation with standard parameters, we tested how the variability of the parameters impacts the volume changes under an RCP8.5 forcing. Here, the experimental protocol is analogous to the protocol for standard parameters, described in the main paper in Sect. 2. However, instead of using only the standard set of parameters, the values for five parameters have been drawn randomly from a uniform distribution, creating an ensemble of 100 members. The varied parameters are summarized in Table E1.

The dEBM parameters c_1 and c_2 were derived by optimization of historic melt rates (see Sect. 3); therefore we do not have an estimate of a mean or a standard deviation. The range of parameters which were used for this ensemble were chosen such that for all parameters c_1 and c_2 the root-mean-squared error in the historic melt rates does not increase by more than 10% compared to the standard values. The parameters which describe the albedo and the transmissivity parameterizations were chosen such that the intra-annual variability is represented (see Appendix A).

The volume change of each ensemble member remains in the envelope given by the RCP8.5 α_{1990} simulations as a lower bound and the RCP8.5 α_{dark} as an upper bound (see Fig. E1a). The variability of the intercept of the transmissivity parametrization has the largest influence on the variability in ice loss after 300 years due to warming. The ice loss until 2300 also seems to be correlated (or anti-correlated) to the dEBM parameter c_1 and the slope of the albedo parametrization, while the dEBM parameter c_2 and the slope of the transmissivity parametrization seem to have only negligible influence on the ice loss due to warming (see Fig. E1b–f).

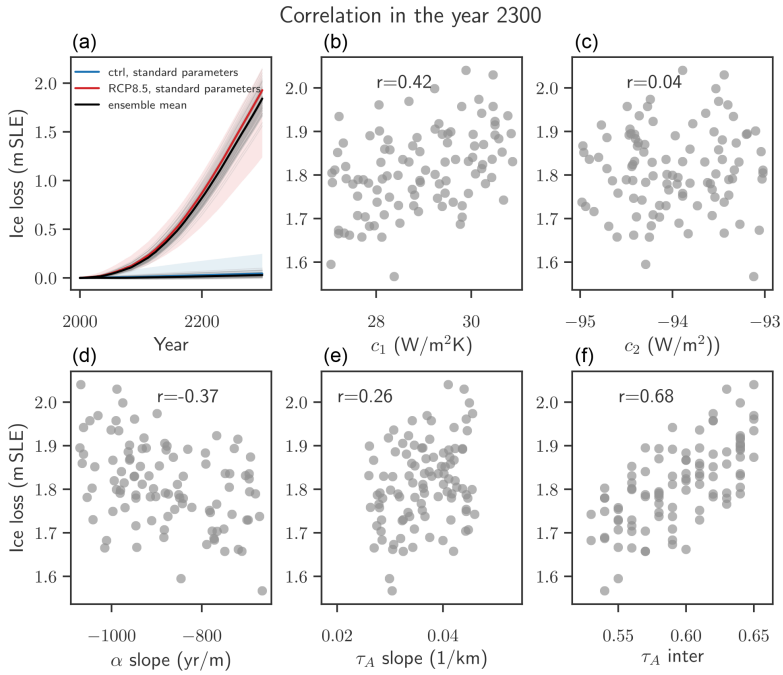

Figure E1. Impact of the parameter variability. **(a)** Time series of PISM-dEBM-simple simulations of the Greenland Ice Sheet with RCP8.5 warming and control simulations. The thick red and blue line are simulations with standard parameters, and the shading shows the upper and the lower bounds of the melt–albedo feedback, as shown in Fig. 5 and discussed in Sect. 4. The thin black lines are the ensemble simulations, with parameters drawn in randomly and shown in Table E1. Thick black lines show the ensemble average. Ice loss is given in metres of sea level equivalent. A value of 1 m s.l.e. corresponds to approx. 361 800 Gt of ice. **(b–f)** Ice loss until the year 2300 in m s.l.e. vs. each of the varied parameters. Note that here the ice loss is corrected by the respective control simulation, which uses the same set of parameters but has no temperature forcing. The Spearman correlation coefficient is given in each of the panels.

Table E1. Overview of the experiments performed in this study.

Name	Variable	Range
c_1	dEBM parameter	$[27, 31]$ W/m^2 K
c_2	dEBM parameter	$[-95, -93]$ W/m^2
α_{sl}	Slope in albedo parametrization	$[-0.034, 0.021]$ yr/m
$\tau_{\mathrm{A,sl}}$	Slope in transmissivity parametrization	$[0.026, 0.046]$ km^{-1}
$\tau_{\mathrm{A,in}}$	Intercept in transmissivity parametrization	$[0.53, 0.65]$

Code and data availability. The PISM source code including the dEBM-simple module is freely available through https://github.com/mariazeitz/pism/tree/pik/dEBM_dev (Zeitz, 2021). The code of the regional climate model MAR is available through https://mar.cnrs.fr/ (Drira, 2016). The CMIP5 datasets for the RCP2.6 and the RCP8.5 warming scenarios are available through https://esgf-node.llnl.gov/search/cmip5/ (Department of Energy, 2021).

Supplement. The supplement related to this article is available online at: https://doi.org/10.5194/tc-15-5739-2021-supplement.

Author contributions. MZ implemented the dEBM-simple module with the parameterizations for albedo and shortwave downward radiation and performed the analysis. RW conceived the study. JB contributed the initial state for PISM simulations. UKK developed the dEBM model, the basis for dEBM-simple, and provided support

with the setup. MZ and RR designed and wrote the manuscript with input and feedback from all co-authors.

Competing interests. The contact author has declared that neither they nor their co-authors have any competing interests.

Disclaimer. Publisher's note: Copernicus Publications remains neutral with regard to jurisdictional claims in published maps and institutional affiliations.

Acknowledgements. Maria Zeitz and Ricarda Winkelmann are supported by the Leibniz Association (project DOMINOES). Maria Zeitz and Ronja Reese are supported by the Deutsche Forschungsgemeinschaft (DFG) by grant WI4556/3-1. Ronja Reese was further supported through the TiPACCs project that receives funding from the European Union's Horizon 2020 Research and Innovation programme under grant agreement no. 820575. Johanna Beckmann is supported by the Deutsche Forschungsgemeinschaft through project 422877703. Ricarda Winkelmann is grateful for support by the Deutsche Forschungsgemeinschaft (DFG) through grants WI4556/3-1 and WI4556/5-1 and by the PalMod project (FKZ: 01LP1925D), supported by the German Federal Ministry of Education and Research (BMBF) as a Research for Sustainability initiative (FONA). Development of PISM is supported by NASA grant NNX17AG65G and NSF grants PLR-1603799 and PLR-1644277. The authors gratefully acknowledge the European Regional Development Fund (ERDF), the German Federal Ministry of Education and Research, and the federal state of Brandenburg for supporting this project by providing resources for the high-performance computer system at the Potsdam Institute for Climate Impact Research.

We would like to thank the reviewers Signe Hillerup Larsen and Mario Krapp for their helpful questions and comments and the editor Kerim Nisancioglu for handling the manuscript.

Financial support. This research has been supported by the Deutsche Forschungsgemeinschaft (grant no. 401011539) and the Leibniz-Gemeinschaft (DominoES grant).

Review statement. This paper was edited by Kerim Nisancioglu and reviewed by Mario Krapp and Signe Hillerup Larsen.

References

Aschwanden, A., Fahnestock, M. A., and Truffer, M.: Complex Greenland outlet glacier flow captured, Nat. Commun., 7, 10524, https://doi.org/10.1038/ncomms10524, 2016.

Aschwanden, A., Fahnestock, M. A., Truffer, M., Brinkerhoff, D. J., Hock, R., Khroulev, C., Mottram, R. H., and Khan, S. A.: Contribution of the Greenland Ice Sheet to sea level over the next millennium, Sci. Adv., 5, eaav9396, https://doi.org/10.1126/sciadv.aav9396, 2019.

Berger, A. L.: Long-Term Variations of Daily Insolation and Quaternary Climatic Changes, J. Atmos. Sci., 35, 2362–2367, 1978.

Bøggild, C. E., Brandt, R. E., Brown, K. J., and Warren, S. G.: The ablation zone in northeast greenland: Ice types, albedos and impurities, J. Glaciol., 56, 101–113, https://doi.org/10.3189/002214310791190776, 2010.

Box, J. E.: Greenland ice sheet mass balance reconstruction. Part II: Surface mass balance (1840–2010), J. Climate, 26, 6974–6989, https://doi.org/10.1175/JCLI-D-12-00518.1, 2013.

Box, J. E., Fettweis, X., Stroeve, J. C., Tedesco, M., Hall, D. K., and Steffen, K.: Greenland ice sheet albedo feedback: thermodynamics and atmospheric drivers, The Cryosphere, 6, 821–839, https://doi.org/10.5194/tc-6-821-2012, 2012.

Box, J. E., van As, D., Steffen, K., Fausto, R. S., Ahlstrøm, A. P., Citterio, M., and Andersen, S. B.: Greenland, Canadian and Icelandic land-ice albedo grids (2000–2016), Geol. Surv. Den. Greenl., 38, 53–56, 2017.

Bueler, E. and Brown, J.: Shallow shelf approximation as a "sliding law" in a thermomechanically coupled ice sheet model, J. Geophys. Res.-Sol. Ea., 114, 1–21, https://doi.org/10.1029/2008JF001179, 2009.

Bueler, E. and van Pelt, W.: Mass-conserving subglacial hydrology in the Parallel Ice Sheet Model version 0.6, Geosci. Model Dev., 8, 1613–1635, https://doi.org/10.5194/gmd-8-1613-2015, 2015.

Cook, J. M., Tedstone, A. J., Williamson, C., McCutcheon, J., Hodson, A. J., Dayal, A., Skiles, M., Hofer, S., Bryant, R., McAree, O., McGonigle, A., Ryan, J., Anesio, A. M., Irvine-Fynn, T. D. L., Hubbard, A., Hanna, E., Flanner, M., Mayanna, S., Benning, L. G., van As, D., Yallop, M., McQuaid, J. B., Gribbin, T., and Tranter, M.: Glacier algae accelerate melt rates on the south-western Greenland Ice Sheet, The Cryosphere, 14, 309–330, https://doi.org/10.5194/tc-14-309-2020, 2020.

Delhasse, A., Hanna, E., Kittel, C., and Fettweis, X.: Brief communication: CMIP6 does not suggest any atmospheric blocking increase in summer over Greenland by 2100, Int. J. Climatol., 41, 2589–2596, https://doi.org/10.1002/joc.6977, 2021.

Department of Energy: CMIP5 datasets for the RCP2.6 and the RCP8.5 warming scenarios, available at: https://esgf-node.llnl.gov/search/cmip5/, 3 December 2021.

Di Mauro, B., Garzonio, R., Baccolo, G., Franzetti, A., Pittino, F., Leoni, B., and Remias, D.: Glacier algae foster ice-albedo feedback in the European Alps, Sci. Rep., 10, 1–9, https://doi.org/10.1038/s41598-020-61762-0, 2020.

Dobricic, S., Russo, S., Pozzoli, L., Wilson, J., and Vignati, E.: Increasing occurrence of heat waves in the terrestrial Arctic, Environ. Res. Lett., 15, 024022, https://doi.org/10.1088/1748-9326/ab6398, 2020.

Drira, A: MAR Modèle Atmosphérique Régional, available at: https://mar.cnrs.fr/ (last access: 3 December 2021), 2016.

Dufresne, J.-L., Foujols, M.-A., Denvil, S., Caubel, A., Marti, O., Aumont, O., Balkanski, Y., Bekki, S., Bellenger, H., Benshila, R., Bony, S., Bopp, L., Braconnot, P., Brockmann, P., Cadule, P., Cheruy, F., Codron, F., Cozic, A., Cugnet, D., de Noblet, N., Duvel, J.-P., Ethé, C., Fairhead, L., Fichefet, T., Flavoni, S., Friedlingstein, P., Grandpeix, J.-Y., Guez, L., Guilyardi, E., Hauglustaine, D., Hourdin, F., Idelkadi, A., Ghattas, J., Joussaume, S., Kageyama, M., Krinner, G., Labetoulle, S., Lahellec, A., Lefebvre, M.-P., Lefevre, F., Levy, C., Li, Z. X., Lloyd, J., Lott, F., Madec, G., Mancip, M., Marchand, M., Masson, S.,

Meurdesoif, Y., Mignot, J., Musat, I., Parouty, S., Polcher, J., Rio, C., Schulz, M., Swingedouw, D., Szopa, S., Talandier, C., Terray, P., Viovy, N., and Vuichard, N.: Climate change projections using the IPSL-CM5 Earth System Model: from CMIP3 to CMIP5, Clim. Dynam., 40, 2123–2165, https://doi.org/10.1007/s00382-012-1636-1, 2013.

Fettweis, X.: MAR data, available at: ftp://ftp.climato.be/fettweis/MARv3.11/Greenland/ERA_1958-2019-10km/monthly_1km/, last access: 7 March 2021.

Fettweis, X., Franco, B., Tedesco, M., van Angelen, J. H., Lenaerts, J. T. M., van den Broeke, M. R., and Gallée, H.: Estimating the Greenland ice sheet surface mass balance contribution to future sea level rise using the regional atmospheric climate model MAR, The Cryosphere, 7, 469–489, https://doi.org/10.5194/tc-7-469-2013, 2013.

Fettweis, X., Box, J. E., Agosta, C., Amory, C., Kittel, C., Lang, C., van As, D., Machguth, H., and Gallée, H.: Reconstructions of the 1900–2015 Greenland ice sheet surface mass balance using the regional climate MAR model, The Cryosphere, 11, 1015–1033, https://doi.org/10.5194/tc-11-1015-2017, 2017.

Fettweis, X., Hofer, S., Krebs-Kanzow, U., Amory, C., Aoki, T., Berends, C. J., Born, A., Box, J. E., Delhasse, A., Fujita, K., Gierz, P., Goelzer, H., Hanna, E., Hashimoto, A., Huybrechts, P., Kapsch, M.-L., King, M. D., Kittel, C., Lang, C., Langen, P. L., Lenaerts, J. T. M., Liston, G. E., Lohmann, G., Mernild, S. H., Mikolajewicz, U., Modali, K., Mottram, R. H., Niwano, M., Noël, B., Ryan, J. C., Smith, A., Streffing, J., Tedesco, M., van de Berg, W. J., van den Broeke, M., van de Wal, R. S. W., van Kampenhout, L., Wilton, D., Wouters, B., Ziemen, F., and Zolles, T.: GrSMBMIP: intercomparison of the modelled 1980–2012 surface mass balance over the Greenland Ice Sheet, The Cryosphere, 14, 3935–3958, https://doi.org/10.5194/tc-14-3935-2020, 2020.

Fettweis, X., Hofer, S., Séférian, R., Amory, C., Delhasse, A., Doutreloup, S., Kittel, C., Lang, C., Van Bever, J., Veillon, F., and Irvine, P.: Brief communication: Reduction in the future Greenland ice sheet surface melt with the help of solar geoengineering, The Cryosphere, 15, 3013–3019, https://doi.org/10.5194/tc-15-3013-2021, 2021.

Frederikse, T., Landerer, F., Caron, L., Adhikari, S., Parkes, D., Humphrey, V. W., Dangendorf, S., Hogarth, P., Zanna, L., Cheng, L., and Wu, Y. H.: The causes of sea-level rise since 1900, Nature, 584, 393–397, https://doi.org/10.1038/s41586-020-2591-3, 2020.

Gardner, A. S. and Sharp, M. J.: A review of snow and ice albedo and the development of a new physically based broadband albedo parameterization, J. Geophys. Res.-Earth, 115, 1–15, https://doi.org/10.1029/2009JF001444, 2010.

Goelzer, H., Nowicki, S., Payne, A., Larour, E., Seroussi, H., Lipscomb, W. H., Gregory, J., Abe-Ouchi, A., Shepherd, A., Simon, E., Agosta, C., Alexander, P., Aschwanden, A., Barthel, A., Calov, R., Chambers, C., Choi, Y., Cuzzone, J., Dumas, C., Edwards, T., Felikson, D., Fettweis, X., Golledge, N. R., Greve, R., Humbert, A., Huybrechts, P., Le clec'h, S., Lee, V., Leguy, G., Little, C., Lowry, D. P., Morlighem, M., Nias, I., Quiquet, A., Rückamp, M., Schlegel, N.-J., Slater, D. A., Smith, R. S., Straneo, F., Tarasov, L., van de Wal, R., and van den Broeke, M.: The future sea-level contribution of the Greenland ice sheet: a multi-model ensemble study of ISMIP6, The Cryosphere, 14, 3071–3096, https://doi.org/10.5194/tc-14-3071-2020, 2020.

Hanna, E., Fettweis, X., Mernild, S. H., Cappelen, J., Ribergaard, M. H., Shuman, C. A., Steffen, K., Wood, L., and Mote, T. L.: Atmospheric and oceanic climate forcing of the exceptional Greenland ice sheet surface melt in summer 2012, Int. J. Climatol., 34, 1022–1037, https://doi.org/10.1002/joc.3743, 2014.

He, T., Liang, S., Yu, Y., Wang, D., Gao, F., and Liu, Q.: Greenland surface albedo changes in July 1981–2012 from satellite observations, Environ. Res. Lett., 8, 044043, https://doi.org/10.1088/1748-9326/8/4/044043, 2013.

Hofer, S., Tedstone, A. J., Fettweis, X., and Bamber, J. L.: Decreasing cloud cover drives the recent mass loss on the Greenland Ice Sheet, Sci. Adv., 3, e1700584, https://doi.org/10.1126/sciadv.1700584, 2017.

Huybrechts, P.: Sea-level changes at the LGM from ice-dynamic reconstructions of the Greenland and Antarctic ice sheets during the glacial cycles, Quaternary Sci. Rev., 21, 203–231, https://doi.org/10.1016/S0277-3791(01)00082-8, 2002.

Kittel, C., Amory, C., Agosta, C., Jourdain, N. C., Hofer, S., Delhasse, A., Doutreloup, S., Huot, P.-V., Lang, C., Fichefet, T., and Fettweis, X.: Diverging future surface mass balance between the Antarctic ice shelves and grounded ice sheet, The Cryosphere, 15, 1215–1236, https://doi.org/10.5194/tc-15-1215-2021, 2021.

Krapp, M., Robinson, A., and Ganopolski, A.: SEMIC: an efficient surface energy and mass balance model applied to the Greenland ice sheet, The Cryosphere, 11, 1519–1535, https://doi.org/10.5194/tc-11-1519-2017, 2017.

Krebs-Kanzow, U., Gierz, P., and Lohmann, G.: Brief communication: An ice surface melt scheme including the diurnal cycle of solar radiation, The Cryosphere, 12, 3923–3930, https://doi.org/10.5194/tc-12-3923-2018, 2018.

Krebs-Kanzow, U., Gierz, P., Rodehacke, C. B., Xu, S., Yang, H., and Lohmann, G.: The diurnal Energy Balance Model (dEBM): a convenient surface mass balance solution for ice sheets in Earth system modeling, The Cryosphere, 15, 2295–2313, https://doi.org/10.5194/tc-15-2295-2021, 2021.

Kuipers Munneke, P., Van Den Broeke, M. R., Lenaerts, J. T., Flanner, M. G., Gardner, A. S., and Van De Berg, W. J.: A new albedo parameterization for use in climate models over the Antarctic ice sheet, J. Geophys. Res.-Atmos., 116, 1–10, https://doi.org/10.1029/2010JD015113, 2011.

Langen, P. L., Mottram, R. H., Christensen, J. H., Boberg, F., Rodehacke, C. B., Stendel, M., van As, D., Ahlstrøm, A. P., Mortensen, J., Rysgaard, S., Petersen, D., Svendsen, K. H., Aðalgeirsdóttir, G., and Cappelen, J.: Quantifying Energy and Mass Fluxes Controlling Godthåbsfjord Freshwater Input in a 5-km Simulation (1991–2012), J. Climate, 28, 3694–3713, https://doi.org/10.1175/JCLI-D-14-00271.1, 2015.

Le clec'h, S., Charbit, S., Quiquet, A., Fettweis, X., Dumas, C., Kageyama, M., Wyard, C., and Ritz, C.: Assessment of the Greenland ice sheet–atmosphere feedbacks for the next century with a regional atmospheric model coupled to an ice sheet model, The Cryosphere, 13, 373–395, https://doi.org/10.5194/tc-13-373-2019, 2019.

Liou, K. N.: Solar Radiation at the Top of the Atmosphere, in: An Introduction to Atmospheric Radiation, 37–64, Elsevier, 2 edn., https://doi.org/10.1016/S0074-6142(02)80017-1, 2002.

Maule, C. F.: Heat Flux Anomalies in Antarctica Revealed by Satellite Magnetic Data, Science, 309, 464–467, https://doi.org/10.1126/science.1106888, 2005.

McCutcheon, J., Lutz, S., Williamson, C., Cook, J. M., Tedstone, A. J., Vanderstraeten, A., Wilson, S. A., Stockdale, A., Bonneville, S., Anesio, A. M., Yallop, M. L., McQuaid, J. B., Tranter, M., and Benning, L. G.: Mineral phosphorus drives glacier algal blooms on the Greenland Ice Sheet, Nat. Commun., 12, 570, https://doi.org/10.1038/s41467-020-20627-w, 2021.

Morlighem, M., Williams, C. N., Rignot, E., An, L., Arndt, J. E., Bamber, J. L., Catania, G., Chauché, N., Dowdeswell, J. A., Dorschel, B., Fenty, I. G., Hogan, K., Howat, I., Hubbard, A., Jakobsson, M., Jordan, T. M., Kjeldsen, K. K., Millan, R., Mayer, L., Mouginot, J., Noël, B. P. Y., O'Cofaigh, C., Palmer, S., Rysgaard, S., Seroussi, H., Siegert, M. J., Slabon, P., Straneo, F., Van Den Broeke, M. R., Weinrebe, W., Wood, M., and Zinglersen, K. B.: BedMachine v3: Complete Bed Topography and Ocean Bathymetry Mapping of Greenland From Multibeam Echo Sounding Combined With Mass Conservation, Geophys. Res. Lett., 44, 11051–11061, https://doi.org/10.1002/2017GL074954, 2017.

Mouginot, J., Rignot, E., Bjørk, A. A., Van Den Broeke, M. R., Millan, R., Morlighem, M., Noël, B. P. Y., Scheuchl, B., and Wood, M.: Forty-six years of Greenland Ice Sheet mass balance from 1972 to 2018, P. Natl. Acad. Sci. USA, 116, 201904242, https://doi.org/10.1073/pnas.1904242116, 2019.

Nghiem, S. V., Hall, D. K., Mote, T. L., Tedesco, M., Albert, M. R., Keegan, K., Shuman, C. A., DiGirolamo, N. E., and Neumann, G.: The extreme melt across the Greenland ice sheet in 2012, Geophys. Res. Lett., 39, 6–11, https://doi.org/10.1029/2012GL053611, 2012.

Niwano, M., Aoki, T., Hashimoto, A., Matoba, S., Yamaguchi, S., Tanikawa, T., Fujita, K., Tsushima, A., Iizuka, Y., Shimada, R., and Hori, M.: NHM–SMAP: spatially and temporally high-resolution nonhydrostatic atmospheric model coupled with detailed snow process model for Greenland Ice Sheet, The Cryosphere, 12, 635–655, https://doi.org/10.5194/tc-12-635-2018, 2018.

Noël, B., van de Berg, W. J., van Wessem, J. M., van Meijgaard, E., van As, D., Lenaerts, J. T. M., Lhermitte, S., Kuipers Munneke, P., Smeets, C. J. P. P., van Ulft, L. H., van de Wal, R. S. W., and van den Broeke, M. R.: Modelling the climate and surface mass balance of polar ice sheets using RACMO2 – Part 1: Greenland (1958–2016), The Cryosphere, 12, 811–831, https://doi.org/10.5194/tc-12-811-2018, 2018.

Noël, B., van de Berg, W. J., van Meijgaard, E., Kuipers Munneke, P., van de Wal, R. S. W., and van den Broeke, M. R.: Evaluation of the updated regional climate model RACMO2.3: summer snowfall impact on the Greenland Ice Sheet, The Cryosphere, 9, 1831–1844, https://doi.org/10.5194/tc-9-1831-2015, 2015.

Pellicciotti, F., Brock, B., Strasser, U., Burlando, P., Funk, M., and Corripio, J.: An enhanced temperature – index glacier melt model including the shortwave radiation balance: development and testing for Haut Glacier d' Arolla, Switzerland, J. Glaciol., 51, 573–587, https://doi.org/10.3189/172756505781829124, 2005.

Reeh, N.: Parameterization of melt rate and surface temperature on the Greenland ice sheet, Polarforschung, 59, 113–128, 1991.

Rignot, E. and Mouginot, J.: Ice flow in Greenland for the International Polar Year 2008-2009, Geophys. Res. Lett., 39, 1–7, https://doi.org/10.1029/2012GL051634, 2012.

Riihelä, A., King, M. D., and Anttila, K.: The surface albedo of the Greenland Ice Sheet between 1982 and 2015 from the CLARA-A2 dataset and its relationship to the ice sheet's surface mass balance, The Cryosphere, 13, 2597–2614, https://doi.org/10.5194/tc-13-2597-2019, 2019.

Robinson, A., Calov, R., and Ganopolski, A.: An efficient regional energy-moisture balance model for simulation of the Greenland Ice Sheet response to climate change, The Cryosphere, 4, 129–144, https://doi.org/10.5194/tc-4-129-2010, 2010.

Robinson, A., Calov, R., and Ganopolski, A.: Multistability and critical thresholds of the Greenland ice sheet, Nat. Clim. Change, 2, 429–432, https://doi.org/10.1038/nclimate1449, 2012.

Rückamp, M., Greve, R., and Humbert, A.: Comparative simulations of the evolution of the Greenland ice sheet under simplified Paris Agreement scenarios with the models SICOPOLIS and ISSM, Polar Science, 21, 14–25, https://doi.org/10.1016/j.polar.2018.12.003, 2019.

Ryan, J. C., Smith, L. C., van As, D., Cooley, S. W., Cooper, M. G., Pitcher, L. H., and Hubbard, A.: Greenland Ice Sheet surface melt amplified by snowline migration and bare ice exposure, Sci. Adv., 5, eaav3738, https://doi.org/10.1126/sciadv.aav3738, 2019.

Shepherd, A., Ivins, E. R., Rignot, E., Smith, B., Van Den Broeke, M. R., Velicogna, I., Whitehouse, P., Briggs, K. H., Joughin, I., Krinner, G., Nowicki, S. M. J., Payne, T., Scambos, T., Schlegel, N., A, G., Agosta, C., Ahlstrøm, A. P., Babonis, G., Barletta, V. R., Bjørk, A. A., Blazquez, A., Bonin, J., Colgan, W. T., Csatho, B., Cullather, R. I., Engdahl, M. E., Felikson, D., Fettweis, X., Forsberg, R., Hogg, A. E., Gallee, H., Gardner, A. S., Gilbert, L., Gourmelen, N., Groh, A., Gunter, B., Hanna, E., Harig, C., Helm, V., Horvath, A., Horwath, M., Khan, S. A., Kjeldsen, K. K., Konrad, H., Langen, P. L., Lecavalier, B., Loomis, B., Luthcke, S., McMillan, M., Melini, D., Mernild, S., Mohajerani, Y., Moore, P., Mottram, R., Mouginot, J., Moyano, G., Muir, A., Nagler, T., Nield, G., Nilsson, J., Noël, B. P. Y., Otosaka, I., Pattle, M. E., Peltier, W. R., Pie, N., Rietbroek, R., Rott, H., Sandberg Sørensen, L., Sasgen, I., Save, H., Scheuchl, B., Schrama, E., Schröder, L., Seo, K. W., Simonsen, S. B., Slater, T., Spada, G., Sutterley, T., Talpe, M., Tarasov, L., van de Berg, W. J., van der Wal, W., van Wessem, M., Vishwakarma, B. D., Wiese, D., Wilton, D., Wagner, T., Wouters, B., and Wuite, J.: Mass balance of the Greenland Ice Sheet from 1992 to 2018, Nature, 579, 233–239, https://doi.org/10.1038/s41586-019-1855-2, 2020.

Stroeve, J.: Assessment of Greenland albedo variability from the advanced very high resolution radiometer Polar Pathfinder data set, J. Geophys. Res.-Atmos., 106, 33989–34006, https://doi.org/10.1029/2001JD900072, 2001.

Stroeve, J. C., Box, J. E., Wang, Z., Schaaf, C., and Barrett, A.: Re-evaluation of MODIS MCD43 greenland albedo accuracy and trends, Remote Sens. Environ., 138, 199–214, https://doi.org/10.1016/j.rse.2013.07.023, 2013.

Tedesco, M. and Fettweis, X.: Unprecedented atmospheric conditions (1948–2019) drive the 2019 exceptional melting season over the Greenland ice sheet, The Cryosphere, 14, 1209–1223, https://doi.org/10.5194/tc-14-1209-2020, 2020.

Tedesco, M., Fettweis, X., Van Den Broeke, M. R., van de Wal, R. S. W., Smeets, C. J. P. P., van de Berg, W. J., Serreze, M. C., and Box, J. E.: The role of albedo and accumulation in the 2010 melting record in Greenland, Environ. Res. Lett., 6, 014005, https://doi.org/10.1088/1748-9326/6/1/014005, 2011.

Tedesco, M., Doherty, S., Fettweis, X., Alexander, P., Jeyaratnam, J., and Stroeve, J.: The darkening of the Greenland ice sheet: trends, drivers, and projections (1981–2100), The Cryosphere, 10, 477–496, https://doi.org/10.5194/tc-10-477-2016, 2016.

Tedstone, A. J., Bamber, J. L., Cook, J. M., Williamson, C. J., Fettweis, X., Hodson, A. J., and Tranter, M.: Dark ice dynamics of the south-west Greenland Ice Sheet, The Cryosphere, 11, 2491–2506, https://doi.org/10.5194/tc-11-2491-2017, 2017.

Tedstone, A. J., Cook, J. M., Williamson, C. J., Hofer, S., McCutcheon, J., Irvine-Fynn, T., Gribbin, T., and Tranter, M.: Algal growth and weathering crust state drive variability in western Greenland Ice Sheet ice albedo, The Cryosphere, 14, 521–538, https://doi.org/10.5194/tc-14-521-2020, 2020.

The PISM authors: PISM, a Parallel Ice Sheet Model, available at: http://www.pism-docs.org (last access: 3 December 2021), 2018.

van Dalum, C. T., van de Berg, W. J., Lhermitte, S., and van den Broeke, M. R.: Evaluation of a new snow albedo scheme for the Greenland ice sheet in the Regional Atmospheric Climate Model (RACMO2), The Cryosphere, 14, 3645–3662, https://doi.org/10.5194/tc-14-3645-2020, 2020.

Van De Berg, W. J., Van Den Broeke, M., Ettema, J., Van Meijgaard, E., and Kaspar, F.: Significant contribution of insolation to Eemian melting of the Greenland ice sheet, Nat. Geosci., 4, 679–683, https://doi.org/10.1038/ngeo1245, 2011.

van den Berg, J., van de Wal, R. S. W., and Oerlemans, H.: A mass balance model for the Eurasian Ice Sheet for the last 120,000 years, Global Planet. Change, 61, 194–208, https://doi.org/10.1016/j.gloplacha.2007.08.015, 2008.

Williamson, C. J., Cook, J. M., Tedstone, A., Yallop, M., McCutcheon, J., Poniecka, E., Campbell, D., Irvine-Fynn, T. D. L., McQuaid, J., Tranter, M., Perkins, R., and Anesio, A. M.: Algal photophysiology drives darkening and melt of the Greenland Ice Sheet, P. Natl. Acad. Sci USA, 117, 5694–5705, https://doi.org/10.1073/pnas.1918412117, 2020.

Wilton, D. J., Jowett, A., Hanna, E., Bigg, G. R., Van Den Broeke, M. R., Fettweis, X., and Huybrechts, P.: High resolution (1 km) positive degree-day modelling of Greenland ice sheet surface mass balance, 1870–2012 using reanalysis data, J. Glaciol., 63, 176–193, https://doi.org/10.1017/jog.2016.133, 2017.

Winkelmann, R., Martin, M. A., Haseloff, M., Albrecht, T., Bueler, E., Khroulev, C., and Levermann, A.: The Potsdam Parallel Ice Sheet Model (PISM-PIK) – Part 1: Model description, The Cryosphere, 5, 715–726, https://doi.org/10.5194/tc-5-715-2011, 2011.

Zeitz, M.: PISM dEBM dev, GitHub repository [code], available at: https://github.com/mariazeitz/pism/tree/pik/dEBM_dev, last access: 3 December 2021.

Manuscript 3 (published): Interaction of melt-elevation and bedrock uplift feedback leads to long term oscillations of Greenland Ice Sheet volume

The response of the Greenland Ice Sheet to global warming is modulated by feedbacks. Here, we focus on two specific feedbacks, one between the ice and the atmosphere – the positive melt-elevation feedback – and one between the ice and the solid Earth – the negative glacial isostatic adjustment (GIA) feedback. In this study, we explore how the interaction of both feedbacks shapes the response of the Greenland Ice Sheet to warming on long timescales of 500,000 years. We find that, depending on the amount of warming, the strength of the feedbacks and the associated timescales the Greenland Ice Sheet responds in qualitatively different ways. 1) It can either find a new equilibrium with an ice volume close to the initial state. 2) It can undergo initial ice loss and subsequent recovery to a new stable state with most of the ice volume preserved. 3) It can enter a state of self sustained oscillations, where ice loss and recovery alternate with a characteristic time of tens of millennia. Or 4) it can face irreversible ice loss and collapse. These results point to a possible mode of internal climate variability of the Earth system.

Published in Earth System Dynamics (2022), doi:10.5194/esd-13-1077-2022
https://esd.copernicus.org/articles/13/1077/2022/

Earth Syst. Dynam., 13, 1077–1096, 2022
https://doi.org/10.5194/esd-13-1077-2022

Earth System Dynamics
Open Access
EGU

Research article

Dynamic regimes of the Greenland Ice Sheet emerging from interacting melt–elevation and glacial isostatic adjustment feedbacks

Maria Zeitz[1,2], **Jan M. Haacker**[1,2,3], **Jonathan F. Donges**[1,4], **Torsten Albrecht**[1], **and Ricarda Winkelmann**[1,2]

[1]Earth System Analysis, Potsdam Institute for Climate Impact Research, Member of the Leibniz Association, Telegrafenberg A31, 14473 Potsdam, Germany
[2]Institute for Physics and Astronomy, University of Potsdam, Potsdam, Germany
[3]Delft University of Technology, Faculty of Civil Engineering and Geosciences, Department of Geoscience and Remote Sensing, Delft, the Netherlands
[4]Stockholm Resilience Centre, Stockholm University, Kräftriket 2B, 11419 Stockholm, Sweden

Correspondence: Maria Zeitz (maria.zeitz@pik-potsdam.de) and Ricarda Winkelmann (ricarda.winkelmann@pik-potsdam.de)

Received: 10 December 2021 – Discussion started: 17 December 2021
Revised: 18 June 2022 – Accepted: 28 June 2022 – Published: 22 July 2022

Abstract. The stability of the Greenland Ice Sheet under global warming is governed by a number of dynamic processes and interacting feedback mechanisms in the ice sheet, atmosphere and solid Earth. Here we study the long-term effects due to the interplay of the competing melt–elevation and glacial isostatic adjustment (GIA) feedbacks for different temperature step forcing experiments with a coupled ice-sheet and solid-Earth model. Our model results show that for warming levels above 2 °C, Greenland could become essentially ice-free within several millennia, mainly as a result of surface melting and acceleration of ice flow. These ice losses are mitigated, however, in some cases with strong GIA feedback even promoting an incomplete recovery of the Greenland ice volume. We further explore the full-factorial parameter space determining the relative strengths of the two feedbacks: our findings suggest distinct dynamic regimes of the Greenland Ice Sheets on the route to destabilization under global warming – from incomplete recovery, via quasi-periodic oscillations in ice volume to ice-sheet collapse. In the incomplete recovery regime, the initial ice loss due to warming is essentially reversed within 50 000 years, and the ice volume stabilizes at 61 %–93 % of the present-day volume. For certain combinations of temperature increase, atmospheric lapse rate and mantle viscosity, the interaction of the GIA feedback and the melt–elevation feedback leads to self-sustained, long-term oscillations in ice-sheet volume with oscillation periods between 74 000 and over 300 000 years and oscillation amplitudes between 15 %–70 % of present-day ice volume. This oscillatory regime reveals a possible mode of internal climatic variability in the Earth system on timescales on the order of 100 000 years that may be excited by or synchronized with orbital forcing or interact with glacial cycles and other slow modes of variability. Our findings are not meant as scenario-based near-term projections of ice losses but rather providing insight into of the feedback loops governing the "deep future" and, thus, long-term resilience of the Greenland Ice Sheet.

Published by Copernicus Publications on behalf of the European Geosciences Union.

1 Introduction

The Greenland Ice Sheet (GrIS) holds enough water to raise global sea levels by more than 7.4 m and is continuously losing mass at present, thereby contributing to global sea level rise (Morlighem et al., 2017; Frederikse et al., 2020). Current mass loss rates of 286 Gt yr^{-1} are observed, a 6-fold increase since the 1980s (Mouginot et al., 2019). While historically approximately 35 % can be attributed to a decrease in climatic mass balance and 65 % to an increase in ice discharge (Mouginot et al., 2019), the ratio has already shifted to approximately 50/50 (Mouginot et al., 2019; IMBIE Team, 2020). While it has been suggested that the Greenland Ice Sheet could become unstable beyond temperature anomalies of 1.6–3.2 °C due to the self-amplifying melt–elevation feedback (Levermann and Winkelmann, 2016), recent studies debate whether a tipping point might have already been crossed (Robinson et al., 2012; Boers and Rypdal, 2021). Understanding the feedback mechanisms and involved timescales at play in GrIS mass loss dynamics is necessary to understanding its stability under climatic changes.

Changing climatic conditions during the glacial cycles had a strong influence on the ice volume of the Greenland Ice Sheet. It varied from 3–7 m sea level equivalent (that is the volume above floatation, divided by the total ocean area) in the last interglacial (from 126 to 115 kyr BP) to 12 m during the last glacial maximum (19–20 kyr BP) (Vasskog et al., 2015), while the present-day volume of the GrIS is 7.42 m. Various processes and feedbacks in the ice sheet, atmosphere, ocean and solid Earth governing the ice dynamics, like ice–ocean interactions, the melt–elevation feedback and the snow–albedo feedback played an important role in past transitions from interglacial to glacial and vice versa (Denton et al., 2010; Willeit and Ganopolski, 2018; Pico et al., 2018). In this way, the GrIS has been a key component in the emergence of glacial cycles and their implications for overall Earth system stability, as can also be analyzed from a dynamical systems point of view (Crucifix, 2012). Simple models also allow to study the "deep future", i.e., the future on timescales beyond the ethical time horizon as defined by Lenton et al. (2019), for example, of the Greenland Ice Sheet and the Earth system and reveal that anthropogenic CO_2 emissions affect the climate evolution for up to 500 kyr and can postpone the next glaciation (Talento and Ganopolski, 2021).

The influence of the bedrock uplift onto the dynamics of the Greenland Ice Sheet has been studied with self-gravitating spherical viscoelastic solid-Earth models in glacial cycle simulations by Le Meur and Huybrechts (1998, 2001), for example. A study systematically varying the isostasy parameters was performed by Zweck and Huybrechts (2005) for the last glacial cycle. However, the interaction of the negative bedrock uplift feedback and the melt–elevation feedback, has, to our knowledge, not yet been explicitly and systematically studied in the context of the Greenland Ice Sheet (Pico et al., 2018). Here we aim to close this research gap by systematically exploring how the feedback between solid Earth, ice and climatic mass balance and their interactions affect the long-term response of the Greenland Ice Sheet.

Changes in ice load lead to glacial isostatic adjustment (GIA), a decrease in ice load initiates an uplift with characteristic timescales of hundreds to thousand of years (Barletta et al., 2018; Whitehouse et al., 2019). Currently observed post-glacial uplift rates in Greenland range between −5.6 and 18 mm yr^{-1} (Adhikari et al., 2021; Wahr et al., 2001; Dietrich et al., 2005; Schumacher et al., 2018; Khan et al., 2008). Some studies suggest that uplift rates are higher in the southeast, where the Iceland hot spot has possibly passed, which can be associated with locally low viscosities in the upper mantle (Khan et al., 2016).

The viscous bedrock response is generally assumed to be slow compared to ice losses, with characteristic response timescales of tens to hundreds of millennia. However, several studies suggest that the viscosity of the asthenosphere and the upper mantle varies spatially and could be locally lower than previously thought (e.g., in Iceland, Patagonia, the Antarctic peninsula, Alaska). This implies that the timescale of the viscous response to changes in ice load might be much shorter, e.g., close to tens or hundreds of years (Whitehouse et al., 2019). The elastic response component responds on an even faster timescale to changes in ice load; e.g., the 2012 extreme melt event caused a significant peak in GPS-measured uplift rates (Adhikari et al., 2017). A model of the solid Earth can help to interpret the GPS measurements in order to distinguish the elastic uplift caused by recent mass losses from the delayed viscous uplift caused by the retreat of ice since the last glacial maximum and deduce solid-Earth parameters like mantle viscosity and lithosphere thickness (Adhikari et al., 2021; Schumacher et al., 2018).

Efforts to model the solid-Earth response to changes in ice load range from local one-dimensional representations of the bedrock uplift to full three-dimensional models. The ELRA type of model represents the solid Earth as an elastic lithosphere and a relaxing asthenosphere and assigns a single time constant to the relaxation response (Le Meur and Huybrechts, 1996; Zweck and Huybrechts, 2005). These models are computationally efficient and are often coupled to ice-sheet models in long-term simulations (Robinson et al., 2012). The Lingle–Clark model expands the elastic plate lithosphere with a viscous half-space and solves the equations explicitly in time (Lingle and Clark, 1985; Bueler et al., 2007). The relaxation time of the solid Earth then depends on the spatial wavelength of the perturbation in ice load, as shown in Fig. A1. However, this model uses only one constant value for the mantle viscosity, and it does not include vertical or horizontal variations, nor does it solve the sea level equation including self-consistent water-load changes or the rotational state of the Earth (Farrell and Clark, 1976; Hagedoorn et al., 2007). Such a model can be expanded to

include more layers, e.g., the lower mantle, and take an additional model of the relaxation time spectrum into account; however, it becomes more difficult to constrain (Lau et al., 2016). One-dimensional solid-Earth models explicitly consider the spherical shape of the Earth instead of assuming a half-space (Tosi et al., 2005; Fleming and Lambeck, 2004; Simpson et al., 2009; Lambeck et al., 2014), but they do not represent lateral variations in solid-Earth parameters. Three-dimensional models, which not only resolve several layers of the vertical dimension, but also include additional variability in the horizontal direction, account for the ongoing discovery of lateral variations in mantle viscosity and lithosphere thickness (Khan et al., 2016; Whitehouse, 2018; Whitehouse et al., 2006, 2019; Haeger et al., 2019; Martinec, 2000). A laterally varying 3D model can change the estimate of projected global mean sea level rise due to an ice-sheet collapse in the West Antarctic by up to 10 % compared to a 1D model (Powell et al., 2021). Inferred values for mantle viscosities can span several orders of magnitude and therefore substantially impact the estimate of bedrock uplift rates as a response to present-day ice losses (Powell et al., 2020). So far the coupling efforts between 3D solid-Earth models and physical ice-sheet models have been focused mostly on the Antarctic Ice Sheet, exploring the feedback between solid Earth and ice sheets and its potential to dampen or inhibit unstable ice sheet retreat (Gomez et al., 2013; De Boer et al., 2014; Gomez et al., 2018, 2020). Self-gravitation effects affect the stability of the grounding line (Whitehouse et al., 2019; Pollard et al., 2017), and GIA models, which self-consistently solve the sea level equation, are crucial. Ongoing work focuses on the Northern Hemisphere, coupling for instance the Parallel Ice Sheet Model (PISM) to the solid-Earth model VILMA.

Similarly, modeling efforts of the climatic mass balance of the Greenland Ice Sheet range from computationally efficient temperature index models over energy balance models to sophisticated regional climate models, and an overview can be found in the model intercomparison effort by Fettweis et al. (2020).

The response of the solid Earth to ice loss can be part of a negative, meaning counteracting or dampening, feedback loop, called glacial isostatic adjustment (GIA) feedback, that can mitigate further ice loss. Studies focused on the GIA feedback in context of the Antarctic Ice Sheet and the Laurentide Ice Sheet suggest that the bedrock uplift can lead to a grounding line advance and therefore has a stabilizing effect on glaciers that are subjected to the marine ice sheet instability (MISI) (Whitehouse et al., 2019; Konrad et al., 2015; Kingslake et al., 2018; Bassis et al., 2017; Barletta et al., 2018). However, to our knowledge the GIA feedback has not yet been addressed in the context of the Greenland Ice Sheet, where, in comparison to the Antarctic Ice Sheet, marine-terminating glaciers contribute less to mass loss.

The feedback cycle we explore in this study is related to the self-amplifying melt–elevation feedback. The melt–elevation feedback establishes a connection between ice thickness and climatic mass balance: the lower the surface elevations the higher the typical temperatures and associated melt rates (see also Fig. 1, in particular the red arrows). An initial increase in melt thins the ice, bringing the ice surface to lower elevation. Subsequently the temperature increases and amplifies both melt rates and ice velocities and therefore leads to further ice loss and thinning. Once a critical thickness is reached, this feedback can lead to a destabilization of the ice sheet and irreversible ice loss (Levermann et al., 2013). (A similar feedback has also been known as the small ice cap instability, assuming constant accumulation rates above an elevation h_S and constant ablation rates below this elevation. Under these conditions a small ice cap can become unstable and expand, or similarly a large ice sheet can become unstable and collapse to nothing upon small changes in the parameters (Weertman, 1961).).

The instability of the melt–elevation feedback, as studied by Levermann and Winkelmann (2016), assumes a static bed, so that changes in ice thickness equal changes in ice surface altitude. GIA can mitigate this feedback: due to bedrock deformation, changes in ice thickness do not directly translate to changes in surface elevation. The loss of ice reduces the load on the bedrock and allows for a bedrock uplift, dampening the melt–elevation feedback (see blue arrows in Fig. 1). Due to the high viscosity of the mantle, the glacial isostatic adjustment can manifest on a slower timescale than the climatic changes that cause the ice losses in the first place.

From a static point of view a compensation of approximately one-third of ice thickness thinning due to GIA would be expected from Archimedes' principle, given that the ice density ($\rho_\mathrm{i} = 910\,\mathrm{kg\,m^{-3}}$) is approximately one-third of the asthenosphere density ($\rho_\mathrm{r} = 3300\,\mathrm{kg\,m^{-3}}$). In this study, we explore how the dynamic interaction of the feedbacks allows the GIA feedback not only to dampen but also to (periodically) overcompensate for the melt–elevation feedback. Here we focus on the long-term stability of the Greenland Ice Sheet and how it is affected by the positive melt–elevation feedback on the one hand and the negative GIA feedback on the other hand. We use simple representations of both the melt–elevation and the GIA feedbacks to study the interplay between them: the melt–elevation feedback is represented by an atmospheric temperature lapse rate which affects the melt rates. The GIA feedback is represented by the Lingle–Clark model, a generalization of the flat-Earth Elastic Lithosphere Relaxing Asthenosphere (ELRA) model (Bueler et al., 2007). The Lingle–Clark model accounts for non-local effects and different relaxation times depending on the spatial extent of the perturbation. We explore the parametric uncertainty range by varying the key parameters: asthenosphere viscosity for the bedrock uplift and the atmospheric lapse rate for the melt–elevation feedback.

We use the Parallel Ice Sheet Model (PISM) (Khroulev and the PISM authors, 2021; Bueler and Brown, 2009) coupled to the Lingle–Clark solid-Earth model (Bueler et al., 2007) in order to explore the interaction between the self-

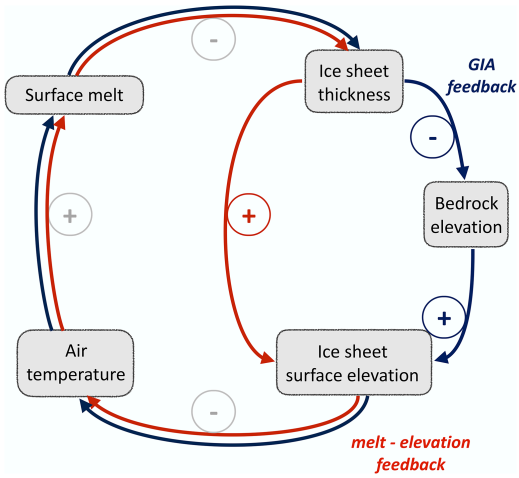

Figure 1. Interacting feedback loops for the proposed glacial isostatic adjustment feedback (GIA feedback). The red part indicates the melt–elevation feedback: higher air temperatures lead to decreasing climatic mass balance. This in turn leads to a decreasing ice thickness and in consequence to a decreasing ice surface elevation. If the surface elevation decreases, the air temperature rises due to the atmospheric lapse rate. This further decreases the climatic mass balance and leads to a positive (enhancing) feedback cycle. The timescale of this feedback cycle is driven by changes in the climate and is typically comparably fast. The blue part shows the counteracting mechanism of the ice load–bedrock uplift feedback. The decreasing ice thickness reduces the load on the bedrock, which leads to isostatic adjustment and therefore an uplift of the bedrock elevation. This mechanism partly counteracts the decrease in ice surface elevation and thus mitigates further increase in temperature. The timescale of this feedback loop depends on the rate of ice retreat and on the viscosity of the upper Earth mantle.

amplifying and the dampening feedbacks. The models and the experimental design are presented in Sect. 2. The warming experiments use an idealized temperature forcing and are analyzed in Sect. 3, followed by a discussion in Sect. 4.

2 Methods

2.1 Numerical modeling

2.1.1 Ice-sheet dynamics with the Parallel Ice Sheet Model (PISM)

The Parallel Ice Sheet Model, PISM, is a thermomechanically coupled finite difference ice-sheet model that combines the shallow-ice approximation (SIA) in regions of slow-flowing ice and the shallow-shelf approximation (SSA) of the Stokes flow stress balance in ice streams and ice shelves (Bueler and Brown, 2009; Winkelmann et al., 2011; The PISM authors, 2021a). The internal deformation of ice is described by Glen's flow law; here the flow exponents $n_{\mathrm{SSA}} = 3$ and $n_{\mathrm{SIA}} = 3$ are used. We use the enhancement factors $E_{\mathrm{SSA}} = 1$ and $E_{\mathrm{SIA}} = 1.5$ for the SSA and the SIA stress balance, respectively. Different enhancement factors of the shallow-ice and the shallow-shelf approximations of the stress balance can be used to reflect anisotropy of the ice, as shown by Ma et al. (2010). In their high-resolution simulations Aschwanden et al. (2016) used $E_{\mathrm{SSA}} = 1$ and $E_{\mathrm{SIA}} = 1.25$, as it provided good agreement with observed flow speeds.

The sliding is described by a pseudo-plastic power law, relating the basal stress $\boldsymbol{\tau}_{\mathrm{b}}$ to the yield stress τ_{c} as

$$\boldsymbol{\tau}_{\mathrm{b}} = -\tau_{\mathrm{c}} \frac{\boldsymbol{u}}{u_{\mathrm{threshold}}^{q} |\boldsymbol{u}|^{1-q}}, \tag{1}$$

with the sliding velocity $\boldsymbol{u}$, the sliding exponent $q = 0.6$ and the threshold velocity $u_{\mathrm{threshold}} = 100\,\mathrm{m\,yr^{-1}}$. The yield stress is determined from parameterized till material properties and the effective pressure of the saturated till via the Mohr–Coulomb criterion (Bueler and van Pelt, 2015):

$$\tau_{\mathrm{c}} = (\tan\phi) N_{\mathrm{till}}, \tag{2}$$

with the till friction angle ϕ linearly interpolated at the beginning of the run from the bedrock topography between $\phi_{\mathrm{min}} = 5^{\circ}$ and $\phi_{\mathrm{max}} = 40^{\circ}$ between bedrock elevations of -700 and 700 m. The effective pressure on the till N_{till} is determined from the ice overburden pressure and the till saturation as described in Bueler and van Pelt (2015).

2.1.2 Earth deformation model

While global GIA models with sea level coupling are available, to our knowledge no coupling efforts between ice dynamics and solid-Earth models have been undertaken for the Greenland Ice Sheet specifically. Here, the deformation of the bedrock in response to changing ice load is described with the Lingle–Clark (LC) model (Lingle and Clark, 1985; Bueler et al., 2007), incorporated as a solid-Earth module in PISM. In this model the response time of the bed topography depends on the wavelength of the load perturbation for a given asthenosphere viscosity (Bueler et al., 2007). The LC model uses two layers to model the solid Earth: the viscous mantle is approximated by a half-space of viscosity η and density ρ_{r}, complemented by an elastic layer of flexural rigidity D describing the lithosphere. The response of the elastic lithosphere happens instantaneously, while the response time of the viscous mantle lies between decades and tens of millennia, depending on both the viscosity of the mantle and the wavelength of the change in load. While the Lingle–Clark model does not consider local changes to viscosity or lithosphere thickness (Milne et al., 2018; Mordret, 2018; Khan et al., 2016) and approximates the Earth as a half-space, the relatively small spatial extent of the simulation region allows for such an approximation.

The resulting partial differential equation for vertical displacement u of the bedrock can be described by

$$2\eta|\nabla|\frac{\partial u}{\partial t} + \rho_r g u + D\nabla^4 u = \sigma_{zz}, \quad (3)$$

with g being the gravitational acceleration of the Earth and σ_{zz} the ice load force per unit area (Bueler et al., 2007).

Here the flexural rigidity D is assumed to be 5×10^{24} Nm, assuming a thickness of 88 km for the elastic plate lithosphere (Bueler et al., 2007). The mantle density ρ_r is approximated with 3300 kg m^{-3}.

Following Bueler et al. (2007), Eq. (14), we show how the spectrum of the relaxation time of the solid-Earth model depends on the wavelength of the ice load change and how this relationship changes for different mantle viscosities and lithosphere flexural rigidities in Fig. A1. In general high mantle viscosities shift the spectrum to higher relaxation times. The maximal relaxation time increases by more than 2 orders of magnitude, from approximately 100 years to approximately 50 000 years, while the thickness of the lithosphere has a weaker effect on the relaxation time spectrum.

2.1.3 Climatic mass balance and temperature forcing

The climatic mass balance in PISM is computed with the positive-degree-day (PDD) model from 2 m air temperature and precipitation given as inputs (Braithwaite, 1995). Here we use a yearly cycle of monthly averages from 1958 to 1967 of the outputs of the regional climate model RACMO v2.3 (Noël et al., 2019) in order to mimic preindustrial climate. The warming is implemented as a spatially uniform instantaneous shift in temperature. The temperature forcing itself has a yearly cycle, with the temperature shift in winter being twice as high as in summer. This corresponds to an average Arctic amplification of 150 % (see also Robinson et al., 2012).

The PDD method uses the spatially uniform standard deviation $\sigma = 4.23$ K, the melt factors for snow and for ice are $m_i = 8$ mm K^{-1} d^{-1} and $m_s = 3$ mm K^{-1} d^{-1} (PISM default), respectively. The melt–elevation feedback is approximated by an atmospheric temperature lapse rate Γ, so that local changes in the ice-sheet topography alter the temperature as

$$T_{ij} = T_{ij,\,\mathrm{input}} - \Gamma \cdot \Delta h_{ij}, \quad (4)$$

with T_{ij} being the effective temperature at grid cell i, j feeding into the PDD model. $T_{ij,\,\mathrm{input}}$ is the temperature at i, j given by the input, without any lapse rate correction, and Γ is a spatially constant air temperature lapse rate. $\Delta h_{i,\,j} = h_{t,\,ij} - h_{0,\,ij}$ is the local difference in surface elevation at i, j at time t, compared to a reference topography h_0. Here we use the initial state for h_0. The value of the lapse rate Γ, and thereby the strength of the melt–elevation feedback, is varied between 5 and 7 K km^{-1} in the experiments.

The yearly precipitation cycle remains fixed and does not scale with temperature; the local temperature affects how much of the precipitation is perceived as snow and therefore adds to the accumulation: at a temperature above 2 °C, all precipitation is perceived as rain, and below 0 °C all is perceived as snow, with a linear interpolation between the two states (the default in PISM). The climatic mass balance is adjusted via a flux correction in the regions which are ice-free in present day to keep them ice-free. How variations in these three assumptions affect the results is discussed in Sect. 4.3.

2.2 Experimental design

Here we use a spatial resolution in the x and y directions of 15 km in order to do many simulations over 0.5 million years. The spatial resolution in the z direction quadratically decreases from 36 m in the cell closest to the bedrock to 230 m in the top grid cell of the simulation box (at 4000 m above bedrock).

The temperature forcing is a spatially uniform step forcing, which is applied from $t = 0$ over the whole simulation time. Additional local temperature changes happen due to the atmospheric temperature lapse rate, as shown above. We explore different values for the atmospheric lapse rate in order to estimate the response of the system to changes in the strength of the melt–elevation feedback.

The ice–ocean interaction is modeled via PICO, with ocean temperatures and salinities taken from the World Ocean Atlas version 2 (Zweng et al., 2018; Locarnini et al., 2019) and remapped onto the simulation grid of 15 km horizontal resolution. PICO used one average value of temperature and salinity per extended drainage sector (for the extended sectors, the drainage sectors of Rignot and Mouginot (2012) are extended linearly into the ocean), even as the ice sheet advances or retreats. The averages are taken at bottom depth over the continental shelf. The warming signal at depth generally stabilizes at lower levels than the atmospheric or sea surface warming; here we assume that only 70 % of atmospheric warming reaches the ocean ground (see also Albrecht et al., 2020). However, only less than 0.2 % of the Greenland Ice Sheet area is made up of floating ice tongues, and the ocean forcing is not transferred to the ice fronts of grounded tidewater glaciers, so the ice–ocean interaction is not the main driver in this simulation setup.

Calving is modeled as a combination of eigencalving (Winkelmann et al., 2011; Levermann et al., 2012) and von Mises calving (Morlighem et al., 2016) with constant calving parameters. In addition a maximal floating ice thickness of 50 m is imposed.

2.2.1 Initial state

The initial state is in equilibrium for constant climate conditions. The misfits of the initial state compared to observed velocities (Joughin et al., 2018) and thicknesses (Morlighem

et al., 2017) and to modeled climatic mass balance (Noël et al., 2019) are shown in the Supplement in Figs. S1, S2 and S3. All simulations are run at a spatial horizontal resolution of 15 km. The basic dynamics of the melt–elevation feedback and the GIA feedback are well captured at this resolution, which allows effective exploration of the parameter space. However, a lot of features of the complex flow of outlet glaciers are not captured at this resolution.

2.2.2 Choice of model parameters

We chose to vary along three main parameters. On the one hand, we vary the strength of the melt–elevation feedback by varying the atmospheric temperature lapse rate Γ between 5 and 7 K km^{-1}. Many ice-sheet models use the free-air moist adiabatic lapse rate (MALR), which ranges between 6–7 K km^{-1} (Gardner et al., 2009) for high humidity, but is assumed to be higher in cold temperatures when the air is dry (Fausto et al., 2009). However, the mean slope lapse rates measured in Greenland and on other ice caps in the Arctic tend to be lower than the MALR and show seasonal variation (Fausto et al., 2009; Gardner et al., 2009; Steffen and Box, 2001; Hanna et al., 2005). By using spatially and temporally constant lapse rates between 5–7 K km^{-1} we try to cover a realistic range in lapse rates.

In addition, the response time and strength of the bedrock to changes in ice load is determined by the mantle viscosity η, varied between 1×10^{19} and 5×10^{21} Pa s. This range is larger than the values of the upper mantle viscosity given in the literature, which still range over more than 2 orders of magnitude over Greenland alone, usually around 1×10^{20} to 5×10^{21} Pa s, but local values from 1×10^{18} to 1×10^{23} Pa s cannot be ruled out (Tosi et al., 2005; Adhikari et al., 2021; Mordret, 2018; Khan et al., 2016; Wahr et al., 2001; Peltier and Drummong, 2008; Larour et al., 2019; Le Meur and Huybrechts, 1996, 1998; Milne et al., 2018; Fleming and Lambeck, 2004; Lecavalier et al., 2014; Lambeck et al., 2014; Lau et al., 2016). Ice retreat itself is affected by the temperature anomaly, here varied between 1.5 and 3.0 K global warming (note the Arctic amplification of 150 % leading to higher local temperature anomalies).

3 Results

Here, we analyze how the strengths of the melt–elevation feedback and the GIA feedback influence the long-term dynamics of the Greenland Ice Sheet in PISM simulations.

3.1 Temporal evolution of ice volume under temperature forcing depending on atmospheric lapse rate and mantle viscosity

The ice losses in simulations with applied warming are affected by both the amplifying melt–elevation feedback and the mitigating GIA feedback. The interaction of both feedbacks allows for a variety of dynamic regimes, depending on the amount of warming on the one hand and the parameters describing the feedback strength on the other hand.

At a given temperature anomaly (here $\Delta T = 2$ K) and a given mantle viscosity (here $\eta = 1 \times 10^{21}$ Pa s), both the rate and magnitude of the initial volume loss increase with increasing air temperature lapse rate, i.e., a stronger melt–elevation feedback (see Fig. 2a). With a lapse rate of $\Gamma = 5$ K km^{-1}, at the low end of the tested range, an incomplete recovery after an initial ice loss is observed, and the ice sheet loses approximately 1.5 m sea level equivalent in volume, before stabilizing at 6 m s.l.e. after approximately 50 kyr (1 m s.l.e. corresponds to approximately 361 800 Gt of ice). With an increasing lapse rate and thereby increasing strength of the melt–elevation feedback, the ice volume may still recover after a stronger initial loss. At sufficiently high lapse rates the recovered state is not stable on long timescales. A self-sustained oscillation of repeated ice losses and gains is observed for $\Gamma = 6$ K km^{-1} with an oscillation timescale of approximately 109 kyr. Increasing the lapse rate even further to $\Gamma = 7$ K km^{-1} does not allow the ice to recover at all; the ice volume is permanently lost.

Here, depending on the value of the lapse rate Γ, three qualitatively different response regimes are observed, (i) incomplete recovery, (ii) self-sustained quasi-periodic oscillation, and (iii) permanent ice loss.

In contrast a constant lapse rate of Γ =6 K km^{-1}, a warming of $\Delta T = 2$ K and varying mantle viscosities between $\eta = 1 \times 10^{19}$–5×10^{21} Pa s lead to self-sustained oscillations (ii) in the ice sheet volume independently of the value of the mantle viscosity (see Fig. 2b). The variations in mantle viscosity do not change the dynamic regime qualitatively; they do affect however the timescale and the amplitude of the observed oscillations. Large values for the mantle viscosity are associated with a smaller response timescale of the GIA and thereby allow for larger initial ice losses and large amplitudes of oscillation. The amplitude, here taken as the difference between the maximal and the minimal volume after an initial ice loss, increases from 1.2 to 5.5 m sea level equivalent by increasing the mantle viscosity from 1×10^{19} to 5×10^{21} Pa s. 1 m sea level equivalent corresponds to approximately 361 800 Gt of ice

The spatial configuration of the ice thickness, the bedrock topography and the equilibrium line, separating the accumulation from the ablation region, in response to warming is visualized for one example simulation in the oscillation regime (ii), with the parameters $\Delta T = 2$ K, $\eta = 1 \times 10^{21}$ Pa s and $\Gamma = 6$ K km^{-1}. We choose three points in time, representing the initial state, the state with minimal ice volume and the oscillation maximum, a recovered state which is unstable on long timescales (see Fig. 3). The time evolution of the volume is depicted by the thick green curve in Fig. 2. During the retreat phase, the mass loss of the ice is initiated from the north of the ice sheet. The area and volume

Table 1. Parameters used in experiments.

Name	Parameter	Value
ΔT	Temperature increase	$[1.5, 2, 3]$ K
Γ	Atmospheric temperature lapse rate	$[5, 5.5, 6, 6.5, 7]$ K km^{-1}
η	Mantle viscosity	$[1 \times 10^{19}, 1 \times 10^{20}, 1 \times 10^{21}, 5 \times 10^{21}]$ Pa s

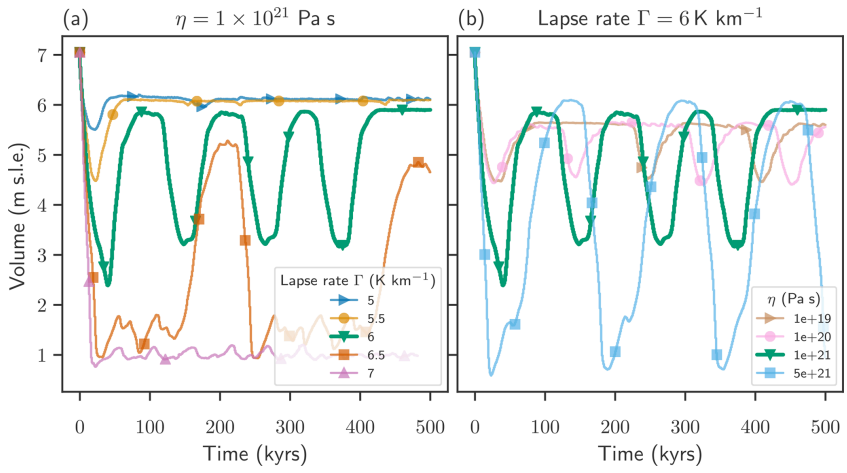

Figure 2. Temporal evolution of Greenland Ice Sheet volume at a temperature anomaly of $\Delta T = 2$ K. Depending on the atmospheric temperature lapse rate (between 5 and 7 K km^{-1}) **(a)** and on the mantle viscosity (between 1×10^{19} and 5×10^{21} Pa s) **(b)** distinct regimes of dynamic responses are observed, including incomplete recovery, quasi-periodic oscillations and permanent loss of ice volume.

of the ice sheet decrease and reach a minimal value after approximately 40 kyr, with a remaining ice dome over central Greenland and a second smaller ice patch over the southern tip of Greenland. This ice loss is accompanied by an uplift of the bedrock, which is most prominent in areas with complete ice loss. The maximal ice thickness decreases from 2940 to 2270 m in the minimal volume state, attained in the eastern region of the larger ice dome. The maximal bedrock uplift of 740 m is found in the northern region where the most ice is lost. The minimal state is also characterized by an increase in relative ablation area, 29 % compared to 24 % in the initial state. The maximal relative ablation area of 31 % is reached approximately 500 years before the minimum of the volume is reached. Eventually, the accumulation area expands and allows the ice sheet to regrow. However, the maximally recovered ice sheet differs from the initial state in area, thickness distribution, accumulation area and bedrock topography (see Fig. 3c and f). In particular the ice sheet extends much less to the north than in the initial state. The precipitation field is assumed to be constant in time; there is no feedback between the ice sheet topography and the precipitation pattern.

3.2 Competing positive melt–elevation and negative GIA feedbacks

Here we explore the competing feedbacks by varying the parameters, which determine the relative strengths of the involved feedbacks, simultaneously.

3.2.1 Dynamic regimes

To gain a better understanding of the dynamic regimes of the GrIS, we tested the long-term response of the ice-sheet volume to warming in the full-factorial parameter space $\Delta T, \Gamma$ and η with values given in Table 1. As stated above in Sect. 3.1 four qualitatively different response regimes can be distinguished: (i) incomplete recovery to a stable state after an initial ice loss, (ii) self-sustained quasi-periodic oscillations, and (iii) irreversible loss of a large portion of the ice or (iv) direct stabilization into a new equilibrium state which preserves 90 % or more of the initial ice volume. Note that only oscillations with a minimal amplitude of 0.5 m s.l.e. are included in the oscillating regime.

With increasing temperature anomalies ΔT, a larger portion of the parameter space experiences irreversible ice loss (iii) (Fig. 4). For a warming temperature of 3 K for example, irreversible ice loss is observed for lapse rates greater

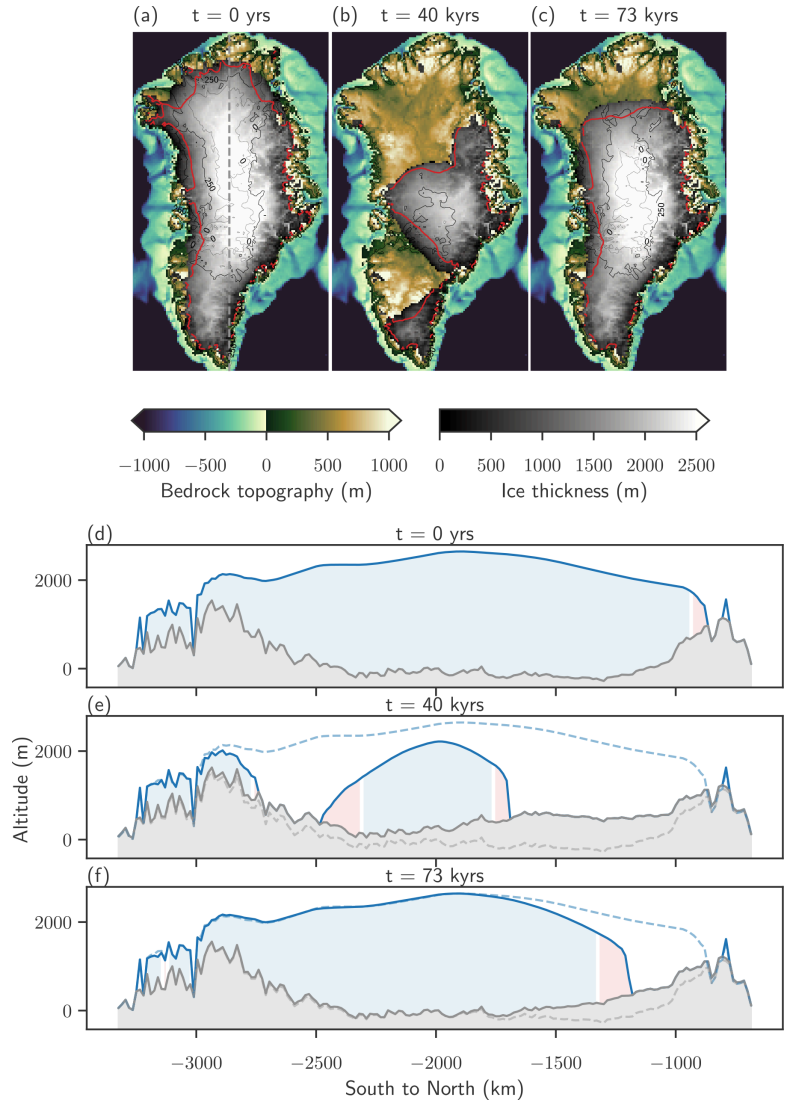

Figure 3. Spatial distribution of ice thickness at a temperature anomaly of $\Delta T = 2\,\mathrm{K}$ for the parameters $\eta = 1 \times 10^{21}\,\mathrm{Pa\,s}$ and $\Gamma = 6\,\mathrm{K\,km^{-1}}$. Maps and cross sections of the bedrock topography and ice thickness show the initial state at the start of the simulation **(a, d)**, the state with minimal volume after 40 kyr **(b, e)** and the recovered state after 73 kyr **(c, f)**. The red outline and the red shaded areas indicate the ablation regions. The dashed lines in **(e)** and **(f)** show the initial topography of the ice sheet.

than or equal to $6\,\mathrm{K\,km^{-1}}$ for all mantle viscosities and for $5.5\,\mathrm{K\,km^{-1}}$ for mantle viscosities lower than or equal to $1 \times 10^{20}\,\mathrm{Pa\,s}$.

Moreover, increasing temperature lapse rate promotes irreversible ice loss; for instance at $\Gamma = 7\,\mathrm{K\,km^{-1}}$, irreversible ice loss occurs for warming temperatures of 2 K or warmer, regardless of the choice for the mantle viscosity (see Fig. 4) and also for most simulations with $\Delta T = 1.5\,\mathrm{K}$.

Direct stabilization without going though a minimum (o) is only realized for the lowest temperature anomaly $\Delta T = 1.5\,\mathrm{K}$ and at the lowest lapse rate $\Gamma = 5\,\mathrm{K}$. While incomplete recovery or stabilization are the most prevalent regimes for low warming temperatures (1.5 K) in the tested parameter space, the oscillatory regime is realized most often at temperature anomalies of 2 K. High mantle viscosities promote oscillations of the ice sheet volume as they lead to a slower

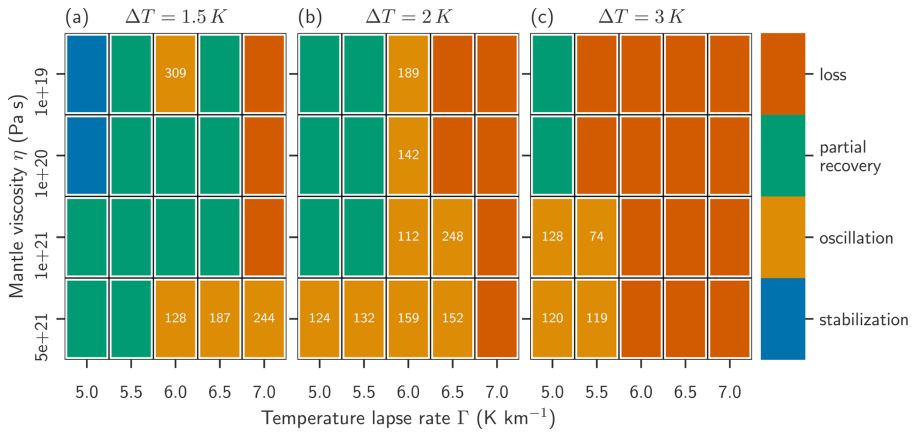

Figure 4. Blue indicates immediate stabilization to a stable state, which preserves more than 90 % of the initial ice sheet volume, without passing a minimum. Green indicates that the ice sheet volume recovers permanently after passing a minimum first. Gold indicates that the ice sheet volume does not recover permanently but shows self-sustained oscillations on a long timescale instead. Dark orange indicates a permanent loss of ice sheet volume. The numbers in the gold tiles show the approximate oscillation times.

response of the bedrock to changes in ice loss and thereby allow for a stronger retreat phase and thereby a faster initial ice loss with warming, as seen in Fig. 2. On the other hand, the more pronounced retreat initiates a strong bedrock response, which supports the recovery. However, the recovered state is not in equilibrium with the bedrock, and thereby a self-sustained oscillation can be triggered.

3.2.2 Timescales in the oscillation regime

The observed oscillations in ice sheet volume (regime iii) are not perfectly periodical; therefore the concepts of periodicity or frequency cannot be directly applied. This framing would require that the physical state of the ice sheet, regarding not only its volume but also spatially resolved variables like thickness distribution, velocity fields, the state of the solid Earth and the climate, return to exactly the same state after one oscillation period. Instead we here estimate the characteristic duration of the oscillation via a simple algorithm: first we identify the minimal and maximal volumes of the oscillation, and the center of both. As the oscillation is not symmetric, the time average of the volume would not be centered between the minimum and the maximum. In a next step we measure the time between two intersections of the time series with the central oscillation volume, which would correspond to a half oscillation, if those were perfectly symmetric and periodic. The average time between one intersection and the next one corresponds to the oscillation time. As only a few oscillation periods fit in to the simulation time of 500 kyr, a thorough statistical analysis can not be performed. Note that the uncertainty arising from choosing the central volume between the minimal and the maximal volumes, rather than a weighted average, is much less than the uncertainty due to the imperfect periodicity, as they amount to less than 1 % in most cases and to about 2.5 % in the worst case.

The oscillation times, as shown in Fig. 4, in this study vary between 79 kyr (for $\Delta T = 3\,\mathrm{K}$, $\eta = 1 \times 10^{21}\,\mathrm{Pa\,s}$ and $\Gamma = 5.5\,\mathrm{K\,km^{-1}}$) and 250 kyr (for $\Delta T = 2\,\mathrm{K}$, $\eta = 1 \times 10^{21}\,\mathrm{Pa\,s}$ and $\Gamma = 6.5\,\mathrm{K\,km^{-1}}$). An even longer oscillation time of 309 kyr is found for $\Delta T = 1.5\,\mathrm{K}$, $\eta = 1 \times 10^{19}\,\mathrm{Pa\,s}$ and $\Gamma = 6.0\,\mathrm{K\,km^{-1}}$, which is however strongly asymmetric: the ice sheet volume seems to recover and reach a permanently stable plateau, but after approximately 250 kyr a decline in ice-sheet volume is re-initiated. The oscillation times do not seem to show a clear dependence on the values for warming, lapse rate or mantle viscosity. Rather, it is governed by a more complex interplay of the dynamics: timescale and depth of the initial deglaciation, level of maximally recovered volume, and stability of the plateau between ice losses.

The analysis method described above allows us to distinguish between the average time for the lower half of the oscillation ("recovery time") and the upper half of the oscillation ("plateau time"). We find that generally the recovery time is shorter than the plateau time, 14 % in the case of $\Delta T = 1.5\,\mathrm{K}$, $\eta = 1 \times 10^{19}\,\mathrm{Pa\,s}$ and $\Gamma = 6.0\,\mathrm{K\,km^{-1}}$ (oscillation time 309 kyr). This ratio increases with temperature forcing ΔT, with the mantle viscosity η and most strongly with the lapse rate Γ up to 265 % for the parameter combination of $\Delta T = 2\,\mathrm{K}$, $\eta = 5 \times 10^{21}\,\mathrm{Pa\,s}$ and $\Gamma = 6.5\,\mathrm{K\,km^{-1}}$ (see Fig. 5). The smaller this ratio, the more stable the partially recovered state of the ice sheet.

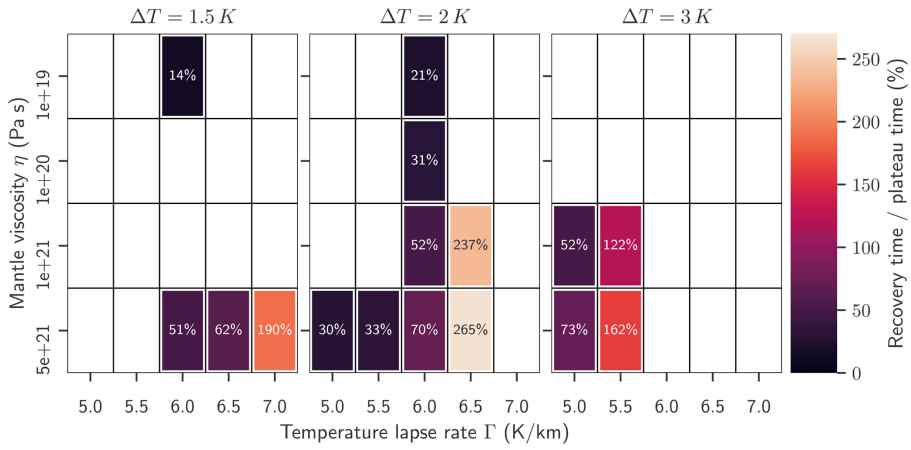

Figure 5. Ratio of recovery time vs. plateau time for three different warming temperatures, $\Delta T = 1.5$, 2 and 3 K. Measure for how long the lower half of the oscillation is compared to the upper half. A ratio of 100 % would signify a perfectly symmetric oscillation: the lower the number, the more time spent in a recovered regime (ice volume greater than the average of minimal and maximal oscillation volume), and the higher the number the more time spent at low ice volumes (ice volume less than the average of minimal and maximal oscillation volume).

3.2.3 Minimum and maximum ice volumes for incomplete recovery or oscillation regimes

The long-term response of the Greenland Ice Sheet volume to temperature anomalies can be characterized by the minimal and maximal long-term volumes, defined as the minimal and maximal volumes attained after passing an initial minimum. In the dynamic regimes of stabilization, incomplete recovery and permanent ice loss, the minimal and maximal long-term volumes are therefore almost identical. The absolute values of the minimal and maximal long-term volumes determine how much ice is lost, and the difference between them shows how large the amplitude of the oscillation is. The minimal and maximal long-term volumes are visualized in Fig. 6. Here, two values are shown for each parameter combination. The upper pixels represent the maximum long-term volume, while the lower pixel represents the minimum long-term volume. A comparison to the regime shown in Fig. 4 reveals that both volumes are high if the ice volume is stabilized directly or recovers, and both volumes are low if the ice is permanently lost. Oscillations are characterized by a significant difference between the minimal and maximal long-term volume. Generally, the absolute values for stabilized, oscillating or lost volume decrease with increasing warming. The amplitude of oscillations is highest for high mantle viscosities, since the slow response time associated with high mantle viscosities allows for more ice loss but also for a stronger recovery.

3.3 State space trajectories

Here we analyze the different dynamic regimes of the Greenland Ice Sheet via their trajectories through state space. The full state space of an ice sheet has a very high dimensionality, and even with the simplifications made by numerical modeling, the full state space remains inaccessible. Here we choose the projection of the state to three state variables: the temporal evolution of the average topography altitude of the glaciated areas on the one hand and the ablation or accumulation area of the ice sheet on the other hand. In both cases the variables are averaged over glaciated areas rather than over a fixed area (e.g., the initial ice sheet area), because this is where they affect the ice sheet. For instance the bedrock uplift in a region which has (permanently) lost its ice does not take part in the feedback as described in Fig. 1. The average topography altitude can change either via glacial isostatic adjustment while the ice sheet area is constant or by changing the ice sheet area at constant topography or a combination of those two processes. The ablation or accumulation area can either change though changes in the ice-sheet area at constant climatic mass balance or via changing the climatic mass balance but keeping the ice-sheet area constant (or a combination of those two processes).

We interpret the topography altitude as a measure of the GIA feedback and the accumulation and ablation area as a measure for the climatic processes.

We can distinguish three different "phase space trajectories" for the different regimes: incomplete recovery after an initial ice loss (i), oscillation (ii) and ice-sheet collapse (iii). All of the simulations shown here are at $\Delta T = 2$ K and with the mantle viscosity of $\eta = 1 \times 10^{21}$ Pa s.

For $\Gamma = 5\,\mathrm{K\,km^{-1}}$ (blue curves in Figs. 2a and 7), the ice sheet is in the incomplete recovery regime. Both the accumulation/ablation areas and the average topography diverge the least from the starting point compared to the other sim-

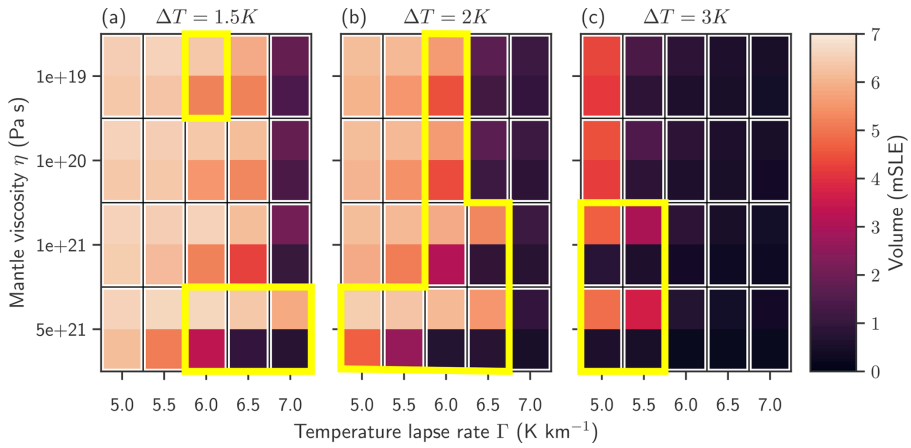

Figure 6. Minimal and maximal volumes after initial ice loss for three different warming temperatures, $\Delta T = 1.5$, 2 and 3 K. Two pixels represent the minimal (lower) and the maximal (upper) long-term volumes for each parameter combination. The minimal and maximal long-term volume is defined by the minimum or the maximum of the volume after passing the initial minimum. A significant difference between the minimal and the maximal volume indicates oscillation. The yellow outline highlights the parameter space of the oscillating regime.

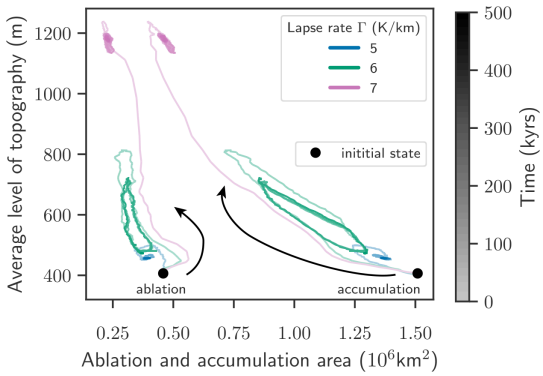

Figure 7. State space trajectories for different regimes for the three different lapse rates $\Gamma = [5, 6, 7]$ K km^{-1}. The curves represent the average height of the bedrock topography vs. the ablation and the accumulation area. Blue: lapse rate $\Gamma = 5$ K km^{-1}, incomplete recovery of the ice volume. Green: lapse rate $\Gamma = 6$ K km^{-1}, oscillation of the ice volume. Purple: lapse rate $\Gamma = 7$ K km^{-1}, irreversible loss of the ice volume. The color code corresponds to Fig. 2 a; that is the temperature forcing is $\Delta T = 2$ K and the mantle viscosity is $\eta = 1 \times 10^{21}$ Pa s. The color shading represents time, as indicated by the color bar on the right side. The average bedrock and the accumulation and ablation area of the initial state are represented by the black marker.

ulations. The trajectories for both accumulation and ablation area spiral quickly into a fixed point. The trajectory for the ablation area follows a counterclockwise spiral while the trajectory for the accumulation area follows a clockwise spiral. Here, changes in accumulation area seem to be more important than the changes in the ablation area and to drive the dynamics.

For $\Gamma = 6$ K km^{-1} (green curves in Figs. 2a and 7) the ice sheet is in the oscillation regime. The trajectories spiral into a closed loop rather than a fixed point, which is characteristic for limit cycles and non-linear oscillators. Again, the trajectory with the ablation area goes counterclockwise while the trajectory for the accumulation area goes clockwise. In absolute terms the accumulation area changes more drastically than the ablation area during one cycle, an indication that the change in accumulation area drives the ice loss. Even though these trajectories form closed loops, there is no perfect periodicity in the beginning, as the first loop of the trajectory is larger than the subsequent following ones.

The atmospheric lapse rate of $\Gamma = 7$ K km^{-1} (purple curves in Figs. 2a and 7) leads to irreversible ice-sheet collapse under these parameters. The trajectories again approach a fixed point. Both the accumulation and the ablation areas are smallest, compared to the other two lapse rate simulations, indicating that the total area of the ice sheet is also small. Again, the absolute change in accumulation area is more drastic than the change in ablation area, and the change in average level of bedrock topography is the highest. As indicated beforehand, this is related both to the bedrock uplift (most ice loss allows for the strongest uplift) and to the fact that the remaining ice retreats to high-altitude mountainous areas with a lot of precipitation and comparatively low temperatures.

4 Discussion

4.1 GIA feedback in different contexts

The impact of the GIA feedback on ice-sheet dynamics has been studied in different contexts. Marine-terminating glaciers and ice shelves are particularly sensitive to glacial isostatic rebound, as it can influence the position of the grounding line and how exposed the ice shelf or the glacier front is to warm ocean water (Larour et al., 2019; Whitehouse et al., 2019). Observational evidence pointing to an overshoot and readvance of the grounding line in the Ross Sea, Antarctica, can be explained by the viscous response of the solid Earth to changes in ice load within a confined range of mantle viscosities (Kingslake et al., 2018). Feldmann and Levermann (2017) showed that the complex interplay of timescales associated with the surge, buildup and stabilization feedbacks could explain Heinrich-like events.

4.2 GrIS ice volume oscillations

While oscillations of ice volume have already been discussed in the context of marine ice sheets (Antarctic Ice Sheet, Laurentide Ice Sheet) (Bassis et al., 2017), we here find that the interaction of the melt–elevation feedback and the GIA feedback can promote an oscillatory dynamic response in a mostly grounded ice sheet.

4.2.1 Analysis of oscillation times

The observed oscillation times vary widely over the range of tested parameters, between 74 and 309 kyr (see Fig. 4). However, the asymmetric shape of the oscillations and their irregularity makes it difficult to establish a straightforward dependence between the oscillation time itself and the parameters determining the dynamical response. When analyzing the asymmetry of the oscillations, however, a clear pattern emerges. The fraction of the time the GrIS spends during recovery in a low-volume or collapsed state compared to the time it spends in a high-volume plateau (here termed "recovery time" and "plateau time") depends strongly on the parameters (see Fig. 5). The recovery time fraction increases with increasing warming temperature ΔT, with increasing lapse rate Γ and with increasing mantle viscosity η. The fact that relatively more time is spent in a low-volume state seems to indicate a loss of stability of the Greenland Ice Sheet. This is particularly true for the warming temperature and the lapse rate, as they also promote the transition from the oscillatory regime to the collapse of the Greenland Ice Sheet. Although high mantle viscosities η promote the oscillatory regime, they also allow for higher ice loss rates and higher total amounts of ice loss, and therefore destabilize the ice sheet in our simulations.

4.2.2 GrIS ice volume oscillations in the context of the Earth system

The oscillation times, even if irregular, are of the same order of magnitude as the timescale of Earth's glaciation cycle, with a dominant period of 41 kyr before and a period of 100 kyr after the Mid-Pleistocene Transition 1.25–0.7 million years ago (Abe-Ouchi et al., 2013; Willeit et al., 2019). While the onset and the termination of glaciation are driven by changes in insolation, climate and Earth surface albedo (Ganopolski and Calov, 2011) our results offer a new perspective. The identified oscillatory regime reveals a possible mode of internal climatic variability in the Earth system on timescales on the order of 100 kyr that may be excited by or interact with orbital forcing, glacial cycles and other slow modes of variability (Ghil and Lucarini, 2020). As such, this oscillatory mode could be relevant in the long-term Earth system response (on the order of 100 kyr) to anthropogenic carbon emissions (Talento and Ganopolski, 2021).

Our findings suggest a sequence of dynamic regimes of the Greenland Ice Sheet on the route to destabilization under global warming, within a certain range of lapse rate coefficients: from recovery via quasi-periodic variations in ice volume to irreversible ice-sheet collapse. This transition might be similar to destabilization scenarios via oscillatory instabilities which have been revealed for other tipping elements in the climate system, such as the Atlantic Meridional Overturning Circulation (AMOC) (Alkhayuon et al., 2019). A relevant area of future research will be to develop a deeper understanding of such ice sheet destabilization routes via the concept of bifurcations (e.g., Hopf and fold bifurcations) in the context of dynamical systems. The interplay between an amplifying and a mitigating feedback contributes to our understanding of the long-term stability and the resilience of the Greenland Ice Sheet. Therefore we need to identify the most important underlying physical processes and the interactions of the feedbacks at play.

4.3 Robustness analysis

While large amplitude oscillations generated with a process-based ice-sheet model have not been reported in the peer-reviewed literature, small oscillations in the GrIS ice volume seem to appear in simulations with the CISM ice-sheet model coupled to an ELRA bedrock model (Petrini et al., 2021) under constant climate. Although the oscillatory regime is not studied explicitly by Petrini et al. (2021), its appearance indicates that this dynamic regime is unlikely to be an artifact of our particular experimental design.

In addition Oerlemans (1982) found unforced oscillations in a simple ice-sheet model, including simple representations of the melt–elevation feedback (depending on the latitude as well as on the altitude), the thermodynamics of the ice sheet including sliding and the bedrock uplift (using a constant relaxation time). They have found thermodynamics to be nec-

essary for the appearance of oscillations. Even though the amplitude and period found by Oerlemans (1982) are very sensitive to parameter choice, the free oscillations seem to be a robust feature of that model over a wide range of parameter values, confirming that the interaction of both feedbacks shown in Fig. 1 can indeed generate robust oscillation.

In order to make sure that the observed dynamical regimes discussed in the present study, in particular the oscillating regime, are not an artifact produced by specific modeling choices, we perform several robustness checks. In the following the impact of some assumptions made for the bedrock model and for the climatic mass balance is tested for one set of parameters ($\Gamma = 6\,\mathrm{K\,km^{-1}}$, $\Delta T = 2\,\mathrm{K}$, $\eta = 1 \times 10^{21}\,\mathrm{Pa\,s}$).

Changing the bedrock uplift model to the instantaneous point-wise isostasy model, defined as

$$b(t, x, y) = b(0, x, y) - \frac{\rho_\mathrm{i}}{\rho_\mathrm{r}} \left[H(t, x, y) - H(0, x, y) \right],$$

and leaving all other parameters and modeling choices fixed produces very similar oscillations to the reference run (see Fig. 8). Recovering an oscillating regime with instantaneous isostasy shows that the time lag between ice load change and full uplift is not the only driver of the oscillation. The change in bedrock model causes a decrease in amplitude, by shifting the minimal volume up, and an increase in oscillation time.

Including the precipitation scaling of 7.3 % per degree Celsius of global mean temperature change, in contrast to the fixed precipitation field, mitigates the ice losses and leads to higher minimal and maximal volumes and a decrease in oscillation amplitude and an increase in oscillation time.

In order to test the impact of the initial state, a different spin-up was performed in addition to the equilibrium spin-up, which was used for the standard runs. Here we use a spin-up similar to the "paleo-climate spin-up" in Aschwanden et al. (2013) over the last 125 kyr. However, the simulation of the past 125 kyr including bedrock deformation is performed twice, adding the anomaly of the bedrock topography at the end of the first run to the initial state of the second run. Therefore an initial state closer to present-day topography is obtained at the end of the second run, and the bedrock is in equilibrium with the ice topography. Using this paleo-climate spinup with explicit treatment of the bedrock still recovers the oscillatory regime for the first 300 kyr (see Fig. 8c). In contrast to the reference run, the amplitude of the oscillation decreases with time, and a stable plateau is observed in the past 150 kyr.

In the reference run we adapted the climatic mass balance in the areas which are ice-free under present day in order to keep them ice-free, such that the initial state would not grow beyond the area of the present-day ice sheet. The flux correction at the ice-free margins has only a minor effect on the oscillating regime (see Fig. 8). The oscillation amplitude is barely altered, the oscillation time is slightly shorter and the initial ice loss is less deep compared to the reference run. However, the volume of the unforced control run grows from 7.06 to 7.62 m.

The lithosphere thickness can be altered indirectly by changing the flexural rigidity of the lithosphere, which is proportional to the third power of the lithosphere thickness. Increasing the lithosphere thickness from 88 to 100 km increases the initial ice loss and the oscillation time; however the long-term amplitude of the oscillation and the minimal and maximal volumes remain almost unaffected. Decreasing the lithosphere thickness to 50 km reduces the initial ice loss and increases the maximal volume of the oscillation. An almost stable plateau of approximately 150 kyr appears after 350 kyr of simulation time, but a dip in the ice volume is observed at the end of the oscillation time, indicating that the plateau is not stable in the long term.

In the reference run all precipitation is perceived as snow if the local mean temperature is below 0 °C, and all precipitation is perceived as rain if the local mean temperature is above 2 °C, with a linear interpolation in between. Changing the critical temperatures to −1 and 3 °C allows a bigger window where both rain and snow are present. This change introduces a larger oscillation amplitude and reduces the oscillation time (see Fig. 8f).

The modeling choices will most likely also affect the distribution of the dynamical regimes in the parameter landscape as shown in Fig. 4, and changing more than one modeling choice at one would introduce stronger changes. For instance changing the spinup and flux correction (see Fig. 8c and d) at once shifts the regime from "oscillation" to "incomplete recovery". Recreating simulations for the full parameter space for each of the modeling choices and different combinations of those is, unfortunately, beyond the scope of this paper. However, we have shown that the oscillating regimes of the Greenland Ice Sheet under constant temperature forcing are robust against many modeling choices, including first tests with PISM interactively coupled to the global VIscoelastic Lithosphere and MAntle model (VILMA; see Klemann et al., 2008; Martinec et al., 2018) in forthcoming work and is therefore unlikely to be an artifact created by one particular simulation setup.

4.4 Limitations

This study is based on the results of the ice sheet model PISM coupled to simple models which capture the melt–elevation feedback, namely the positive-degree-day approach together with an atmospheric temperature lapse rate, and the GIA feedback, namely the Lingle–Clark model. The relative computational efficiency of those models allows us to conduct an ensemble of long-term simulations over 500 000 years exploring different parameter values characterizing the individual feedbacks and warming. This approach fits the conceptual research question of this study.

The Lingle–Clark approach assumes a flat Earth with two layers, one elastic and one viscous layer, in contrast to more

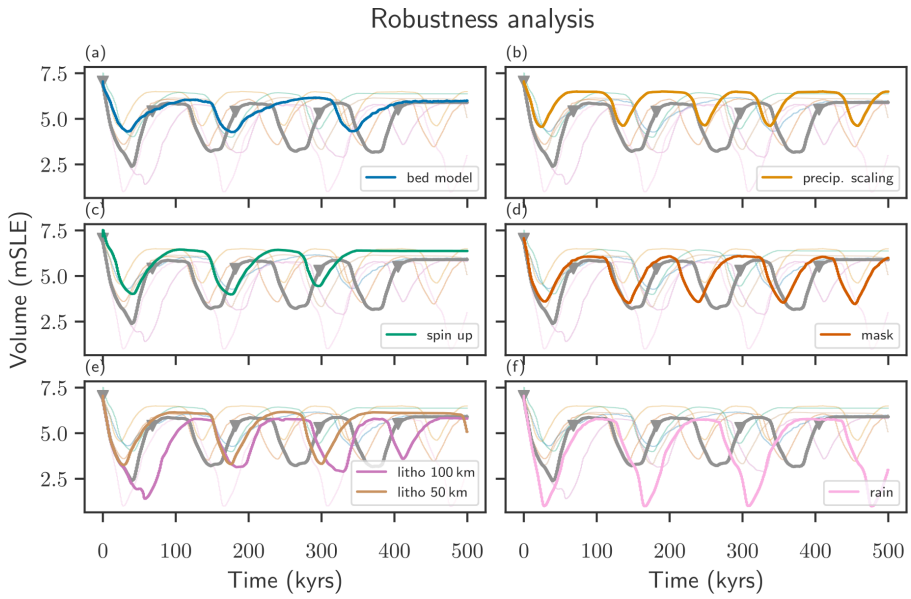

Figure 8. Robustness analysis for the simulation run with parameters $\Gamma = 6\,\mathrm{K\,km^{-1}}$, $\Delta T = 2\,\mathrm{K}$ and $\eta = 1 \times 10^{21}\,\mathrm{Pa\,s}$. The gray curve corresponds to the reference run, also shown in Figs. 2 and 3 and is shown in each panel for reference. The colored faint lines provide context. Each change in modeling choice is highlighted in its own panel. **(a)** Run with an instantaneous pointwise isostasy model. **(b)** Run which includes a 7.3 % precipitation increase per degree Celsius of global mean temperature increase. **(c)** Run which starts from a glacial spinup. **(d)** Run which omits the flux correction at the ice-free margin. **(e)** Runs with two different lithosphere thicknesses, 100 and 50 km. **(f)** Run which uses a different interpolation between rain and snow.

sophisticated solid-Earth models. It also assumes horizontally constant Earth structure and does not solve the self-consistent sea level equation. However, the relative importance of discharge and melt at the ice–ocean interface decreases with ongoing warming, as the tidewater glaciers retreat and the ice–ocean interface shrinks (Aschwanden et al., 2019). With ongoing coupling efforts between ice dynamics models and process-based solid-Earth models, this study is a first step in assessing the importance of the GIA feedback for the stability of the Greenland Ice Sheet.

While the design of the study was chosen in order to allow for long experiments and to cover parts of the parameter space (ΔT, Γ and η), it is also one of the main limitations of the study. The coarse resolution of the ice sheet model does not adequately resolve the flow patterns in outlet glaciers, therefore underestimating dynamical ice losses. Moreover, the parameters which govern the ice dynamics, although uncertain, were not varied (Zeitz et al., 2020).

The choice of the positive-degree-day (PDD) method in order to compute the climatic mass balance tends to underestimate the melt area for present climate, while at high temperatures PDD tends to overestimate melt. Moreover, the temperature anomaly is applied in a spatially and temporally constant way, and the precipitation pattern remains fixed, without any adaption to the temperature forcing. A more realistic approach would include the increase in precipitation with warmer air temperature and partially mitigate ice losses. However in this rather conceptual study we explore the stability landscape without taking the increase in precipitation into account, as it reduces the complexity of the system. We have shown in Sect. 4.3 that while the total ice losses are reduced when considering the increase in precipitation, the qualitative dynamics remains the same (oscillations). So far, scenario-based projections of future global warming are limited until the year 2300, with projections of the temperature evolution and changes in climatic mass balance over the Greenland Ice Sheet as results from regional climate models only available until the end of this century. The aim here, however, is not to present scenario-based projections of future ice losses but rather to study the distinct dynamical states in the "deep future" of the Greenland Ice Sheet in a fundamental way.

5 Conclusions

Here we present an analysis of the dynamic regimes in the deep future of the Greenland Ice Sheet. Depending on the amount of warming and the values of the parameters describing the strength of the melt–elevation feedback and the GIA

feedback, we find that four different dynamic regimes can be realized: (1) direct stabilization into a new equilibrium state which preserves 90 % or more of the initial ice volume, (2) incomplete recovery to a stable state after an initial ice loss, (3) self-sustained oscillations and (4) irreversible loss of a large portion of the ice. Our model configuration with parameterized melt–elevation feedback and a fast computation of the leading-order GIA effects allows for studying an ensemble of glacial timescale simulations and provides insight into how the interaction of feedbacks impacts the dynamics of the complex Earth system with implications for Earth system stability and resilience. Although it is not explicitly studied here, drastic changes in the ice volume of the Greenland Ice Sheet would have implications for the global Earth system via global sea level rise, changes in the planetary albedo, and changes in the atmospheric and oceanic circulation patterns such as the jet stream or the Atlantic Meridional Overturning Circulation (AMOC).

Appendix A: Relaxation times in the Lingle–Clark model

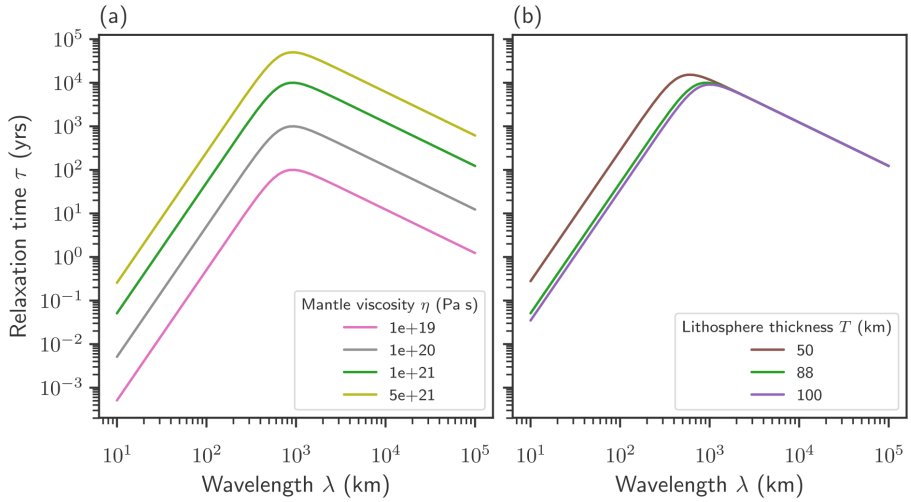

Figure A1. Spectrum of the relaxation time vs. wavelength of the load change for different mantle viscosities and lithosphere thicknesses, as shown in Bueler et al. (2007), Eq. (14).

Following Bueler et al. (2007), Eq. (14), the relaxation time of the Lingle–Clark model can be computed as a function of the load change wavelength λ from comparison to the ELRA model as

$$\tau(\lambda) = \frac{4\pi\eta|\lambda|^{-1}}{\rho_r g + 16\pi^4 D\lambda^{-4}}.$$

As the relaxation time is directly proportional to the mantle viscosity η, the maximal relaxation time increases by more than 2 orders of magnitude over the tested parameter range. The changes in lithosphere thickness induce fewer changes to the relaxation time spectrum. Wavelengths relevant for the deglaciation of the Greenland Ice Sheet are between several tens of kilometers (onset of retreat) and 500–1500 km (the spatial extent of the Greenland Ice Sheet).

Code availability. The PISM source code is freely available (https://github.com/pism/pism/tree/d4fe8ba520b71823bf73de20660db03f917974c7, The PISM authors, 2021b).

Data availability. The PISM output data and the analysis scripts used for creating the figures in this publications are available at https://doi.org/10.5281/zenodo.6827865 (Zeitz et al., 2022).

Supplement. The supplement related to this article is available online at: https://doi.org/10.5194/esd-13-1077-2022-supplement.

Author contributions. RW conceived this study. JMH prepared and analyzed the initial experiments during his master's project, advised by RW and MZ. MZ expanded the experiments, visualized the results and wrote the manuscript, with support from RW, JFD and TA. All authors interpreted and discussed the results. All the authors give their final approval of the article version to be published.

Competing interests. At least one of the (co-)authors is a member of the editorial board of *Earth System Dynamics*. The peer-review process was guided by an independent editor, and the authors also have no other competing interests to declare.

Disclaimer. Publisher's note: Copernicus Publications remains neutral with regard to jurisdictional claims in published maps and institutional affiliations.

Acknowledgements. We would like to thank the editor, Michel Crucifix, for handling our manuscript and Kristin Poinar and the one anonymous reviewer for their helpful comments on the initial version of the manuscript. Moreover, we would like to thank Michele Petrini, Anders Levermann and Fuyuki Saito for fruitful discussions.

Financial support. We received financial support from the European Research Council Advanced Grant project ERA (Earth Resilience in the Anthropocene, grant ERC-2016-ADG-743080) and the Leibniz Association (project DominoES). Maria Zeitz is supported by the Deutsche Forschungsgemeinschaft (DFG) by grant WI4556/3-1. Maria Zeitz received funding from the German Fulbright Commission for a PhD program. Ricarda Winkelmann and Torsten Albrecht acknowledge support from TiPACCs, PROTECT and PalMod. We received further funding from the European Regional Development Fund (ERDF), the German Federal Ministry of Education and Research (BMBF) and the German federal state of Brandenburg for supporting this project by providing resources on the high-performance computer system at the Potsdam Institute for Climate Impact Research. Development of PISM is supported by NASA grant NNX17AG65G and NSF grants PLR-1603799 and PLR-1644277.

The publication of this article was funded by the open-access fund of Leibniz Universität Hannover.

Review statement. This paper was edited by Michel Crucifix and reviewed by Kristin Poinar and one anonymous referee.

References

Abe-Ouchi, A., Saito, F., Kawamura, K., Raymo, M. E., Okuno, J., Takahashi, K., and Blatter, H.: Insolation-driven 100 000-year glacial cycles and hysteresis of ice-sheet volume, Nature, 500, 190–193, https://doi.org/10.1038/nature12374, 2013.

Adhikari, S., Ivins, E. R., and Larour, E. Y.: Mass transport waves amplified by intense Greenland melt and detected in solid Earth deformation, Geophys. Res. Lett., 44, 4965–4975, https://doi.org/10.1002/2017GL073478, 2017.

Adhikari, S., Milne, G. A., Caron, L., Khan, S. A., Kjeldsen, K. K., Nilsson, J., Larour, E. Y., and Ivins, E. R.: Decadal to Centennial Timescale Mantle Viscosity Inferred From Modern Crustal Uplift Rates in Greenland, Geophys. Res. Lett., 48, 1–11, https://doi.org/10.1029/2021gl094040, 2021.

Albrecht, T., Winkelmann, R., and Levermann, A.: Glacial-cycle simulations of the Antarctic Ice Sheet with the Parallel Ice Sheet Model (PISM) – Part 1: Boundary conditions and climatic forcing, The Cryosphere, 14, 599–632, https://doi.org/10.5194/tc-14-599-2020, 2020.

Alkhayuon, H., Ashwin, P., Jackson, L. C., Quinn, C., and Wood, R. A.: Basin bifurcations, oscillatory instability and rate-induced thresholds for Atlantic meridional overturning circulation in a global oceanic box model, P. R. Soc. A, 475, 20190051, https://doi.org/10.1098/rspa.2019.0051, 2019.

Aschwanden, A., Aðalgeirsdóttir, G., and Khroulev, C.: Hindcasting to measure ice sheet model sensitivity to initial states, The Cryosphere, 7, 1083–1093, https://doi.org/10.5194/tc-7-1083-2013, 2013.

Aschwanden, A., Fahnestock, M. A., and Truffer, M.: Complex Greenland outlet glacier flow captured, Nat. Commun., 7, 10524, https://doi.org/10.1038/ncomms10524, 2016.

Aschwanden, A., Fahnestock, M. A., Truffer, M., Brinkerhoff, D. J., Hock, R., Khroulev, C., Mottram, R. H., and Khan, S. A.: Contribution of the Greenland Ice Sheet to sea level over the next millennium, Sci. Adv., 5, eaav9396, https://doi.org/10.1126/sciadv.aav9396, 2019.

Barletta, V. R., Bevis, M., Smith, B. E., Wilson, T., Brown, A., Bordoni, A., Willis, M. J., Khan, S. A., Rovira-Navarro, M., Dalziel, I., Smalley, R., Kendrick, E., Konfal, S., Caccamise, D. J., Aster, R. C., Nyblade, A., and Wiens, D. A.: Observed rapid bedrock uplift in amundsen sea embayment promotes ice-sheet stability, Science, 360, 1335–1339, https://doi.org/10.1126/science.aao1447, 2018.

Bassis, J. N., Petersen, S. V., and Mac Cathles, L.: Heinrich events triggered by ocean forcing and modulated by isostatic adjustment, Nature, 542, 332–334, https://doi.org/10.1038/nature21069, 2017.

Boers, N. and Rypdal, M.: Critical slowing down suggests that the western Greenland Ice Sheet is close to

a tipping point, P. Natl. Acad. Sci. USA, 118, 1–7, https://doi.org/10.1073/pnas.2024192118, 2021.

Braithwaite, R. J.: Positive degree-day factors for ablation on the Greenland ice sheet studied by energy-balance modelling, J. Glaciol., 41, 153–160, https://doi.org/10.1017/S0022143000017846, 1995.

Bueler, E. and Brown, J.: Shallow shelf approximation as a "sliding law" in a thermomechanically coupled ice sheet model, J. Geophys. Res.-Sol. Ea., 114, 1–21, https://doi.org/10.1029/2008JF001179, 2009.

Bueler, E. and van Pelt, W.: Mass-conserving subglacial hydrology in the Parallel Ice Sheet Model version 0.6, Geosci. Model Dev., 8, 1613–1635, https://doi.org/10.5194/gmd-8-1613-2015, 2015.

Bueler, E., Lingle, C. S., and Brown, J.: Fast computation of a viscoelastic deformable Earth model for ice-sheet simulations, Ann. Glaciol., 46, 97–105, https://doi.org/10.3189/172756407782871567, 2007.

Crucifix, M.: Oscillators and relaxation phenomena in Pleistocene climate theory, Philos. T. R. Soc. A, 370, 1140–1165, https://doi.org/10.1098/rsta.2011.0315, 2012.

de Boer, B., Stocchi, P., and van de Wal, R. S. W.: A fully coupled 3-D ice-sheet–sea-level model: algorithm and applications, Geosci. Model Dev., 7, 2141–2156, https://doi.org/10.5194/gmd-7-2141-2014, 2014.

Denton, G. H., Anderson, R. F., Toggweiler, J. R., Edwards, R. L., Schaefer, J. M., and Putnam, A. E.: The Last Glacial Termination, Science, 328, 1652–1656, https://doi.org/10.1126/science.1184119, 2010.

Dietrich, R., Rülke, A., and Scheinert, M.: Present-day vertical crustal deformations in West Greenland from repeated GPS observations, Geophys. J. Int., 163, 865–874, https://doi.org/10.1111/j.1365-246X.2005.02766.x, 2005.

Farrell, W. E. and Clark, J. A.: On Postglacial Sea Level, Geophys. J. Int., 46, 647–667, https://doi.org/10.1111/j.1365-246X.1976.tb01252.x, 1976.

Fausto, R. S., Ahlstrøm, A. P., Van As, D., Bøggild, C. E., and Johnsen, S. J.: A new present-day temperature parameterization for Greenland, J. Glaciol., 55, 95–105, https://doi.org/10.3189/002214309788608985, 2009.

Feldmann, J. and Levermann, A.: From cyclic ice streaming to Heinrich-like events: the grow-and-surge instability in the Parallel Ice Sheet Model, The Cryosphere, 11, 1913–1932, https://doi.org/10.5194/tc-11-1913-2017, 2017.

Fettweis, X., Hofer, S., Krebs-Kanzow, U., Amory, C., Aoki, T., Berends, C. J., Born, A., Box, J. E., Delhasse, A., Fujita, K., Gierz, P., Goelzer, H., Hanna, E., Hashimoto, A., Huybrechts, P., Kapsch, M.-L., King, M. D., Kittel, C., Lang, C., Langen, P. L., Lenaerts, J. T. M., Liston, G. E., Lohmann, G., Mernild, S. H., Mikolajewicz, U., Modali, K., Mottram, R. H., Niwano, M., Noël, B., Ryan, J. C., Smith, A., Streffing, J., Tedesco, M., van de Berg, W. J., van den Broeke, M., van de Wal, R. S. W., van Kampenhout, L., Wilton, D., Wouters, B., Ziemen, F., and Zolles, T.: GrSMBMIP: intercomparison of the modelled 1980–2012 surface mass balance over the Greenland Ice Sheet, The Cryosphere, 14, 3935–3958, https://doi.org/10.5194/tc-14-3935-2020, 2020.

Fleming, K. and Lambeck, K.: Constraints on the Greenland Ice Sheet since the Last Glacial Maximum from sea-level observations and glacial-rebound models, Quaternary. Sci. Rev., 23, 1053–1077, https://doi.org/10.1016/j.quascirev.2003.11.001, 2004.

Frederikse, T., Landerer, F. W., Caron, L., Adhikari, S., Parkes, D., Humphrey, V. W., Dangendorf, S., Hogarth, P., Zanna, L., Cheng, L., and Wu, Y. H.: The causes of sea-level rise since 1900, Nature, 584, 393–397, https://doi.org/10.1038/s41586-020-2591-3, 2020.

Ganopolski, A. and Calov, R.: The role of orbital forcing, carbon dioxide and regolith in 100 kyr glacial cycles, Clim. Past, 7, 1415–1425, https://doi.org/10.5194/cp-7-1415-2011, 2011.

Gardner, A. S., Sharp, M. J., Koerner, R. M., Labine, C., Boon, S., Marshall, S. J., Burgess, D. O., and Lewis, D.: Near-surface temperature lapse rates over arctic glaciers and their implications for temperature downscaling, J. Climate, 22, 4281–4298, https://doi.org/10.1175/2009JCLI2845.1, 2009.

Ghil, M. and Lucarini, V.: The physics of climate variability and climate change, Rev. Mod. Phys., 92, 35002, https://doi.org/10.1103/RevModPhys.92.035002, 2020.

Gomez, N., Pollard, D., and Mitrovica, J. X.: A 3-D coupled ice sheet – sea level model applied to Antarctica through the last 40 ky, Earth Planet. Sci. Lett., 384, 88–99, https://doi.org/10.1016/j.epsl.2013.09.042, 2013.

Gomez, N., Latychev, K., and Pollard, D.: A coupled ice sheet-sea level model incorporating 3D earth structure: Variations in Antarctica during the Last Deglacial Retreat, J. Climate, 31, 4041–4054, https://doi.org/10.1175/JCLI-D-17-0352.1, 2018.

Gomez, N., Weber, M. E., Clark, P. U., Mitrovica, J. X., and Han, H. K.: Antarctic ice dynamics amplified by Northern Hemisphere sea-level forcing, Nature, 587, 600–604, https://doi.org/10.1038/s41586-020-2916-2, 2020.

Haeger, C., Kaban, M. K., Tesauro, M., Petrunin, A. G., and Mooney, W. D.: 3-D Density, Thermal, and Compositional Model of the Antarctic Lithosphere and Implications for Its Evolution, Geochem. Geophy. Geosy., 20, 688–707, https://doi.org/10.1029/2018GC008033, 2019.

Hagedoorn, J. M., Wolf, D., and Martinec, Z.: An estimate of global mean sea-level rise inferred from tide-gauge measurements using glacial-isostatic models consistent with the relative sea-level record, Pure Appl. Geophys., 164, 791–818, https://doi.org/10.1007/s00024-007-0186-7, 2007.

Hanna, E., Huybrechts, P., Janssens, I., Cappelen, J., Steffen, K., and Stenhens, A.: Runoff and mass balance of the Greenland ice sheet: 1958–2003, J. Geophys. Res.-Atmos., 110, 1–16, https://doi.org/10.1029/2004JD005641, 2005.

IMBIE Team: Mass balance of the Greenland Ice Sheet from 1992 to 2018, Nature, 579, 233–239, https://doi.org/10.1038/s41586-019-1855-2, 2020.

Joughin, I., Smith, B. E., and Howat, I.: Greenland Ice Mapping Project: ice flow velocity variation at sub-monthly to decadal timescales, The Cryosphere, 12, 2211–2227, https://doi.org/10.5194/tc-12-2211-2018, 2018.

Khan, S. A., Wahr, J., Leuliette, E., van Dam, T., Larson, K. M., and Francis, O.: Geodetic measurements of postglacial adjustments in Greenland, J. Geophys. Res.-Sol. Ea., 113, 1–16, https://doi.org/10.1029/2007JB004956, 2008.

Khan, S. A., Sasgen, I., Bevis, M., van Dam, T., Bamber, J. L., Wahr, J., Willis, M. J., Kjær, K. H., Wouters, B., Helm, V., Csatho, B., Fleming, K., Bjørk, A. A., Aschwanden, A., Knudsen, P., and Munneke, P. K.: Geodetic measurements reveal sim-

ilarities between post–Last Glacial Maximum and present-day mass loss from the Greenland ice sheet, Sci. Adv., 2, e1600931, https://doi.org/10.1126/sciadv.1600931, 2016.

Khroulev, C. and the PISM authors: PISM, a Parallel Ice Sheet Model v2.0: User's Manual, https://www.pism.io/docs/manual/ (last access: 11 July 2022), 2021.

Kingslake, J., Scherer, R. P., Albrecht, T., Coenen, J., Powell, R. D., Reese, R., Stansell, N. D., Tulaczyk, S., Wearing, M. G., and Whitehouse, P. L.: Extensive retreat and re-advance of the West Antarctic Ice Sheet during the Holocene, Nature, 558, 430–434, https://doi.org/10.1038/s41586-018-0208-x, 2018.

Klemann, V., Martinec, Z., and Ivins, E. R.: Glacial isostasy and plate motion, J. Geodyn., 46, 95–103, https://doi.org/10.1016/j.jog.2008.04.005 2008.

Konrad, H., Sasgen, I., Pollard, D., and Klemann, V.: Potential of the solid-Earth response for limiting long-term West Antarctic Ice Sheet retreat in a warming climate, Earth Planet. Sci. Lett., 432, 254–264, https://doi.org/10.1016/j.epsl.2015.10.008, 2015.

Lambeck, K., Rouby, H., Purcell, A., Sun, Y., and Sambridge, M.: Sea level and global ice volumes from the Last Glacial Maximum to the Holocene, P. Natl. Acad. Sci. USA, 111, 15296–15303, https://doi.org/10.1073/pnas.1411762111, 2014.

Larour, E. Y., Seroussi, H., Adhikari, S., Ivins, E. R., Caron, L., Morlighem, M., and Schlegel, N.: Slowdown in Antarctic mass loss from solid Earth and sea-level feedbacks, Science, 364, eaav7908, https://doi.org/10.1126/science.aav7908, 2019.

Lau, H. C., Mitrovica, J. X., Austermann, J., Crawford, O., Al-Attar, D., and Latychev, K.: Inferences of mantle viscosity based on ice age data sets: Radial structure, J. Geophys. Res.-Sol. Ea., 121, 6991–7012, https://doi.org/10.1002/2016JB013043, 2016.

Le Meur, E. and Huybrechts, P.: A comparison of different ways of dealing with isostasy: examples from modelling the Antarctic ice sheet during the last glacial cycle, Ann. Glaciol., 23, 309–317, https://doi.org/10.1017/S0260305500013586, 1996.

Le Meur, E. and Huybrechts, P.: Present-day uplift patterns over Greenland from a coupled ice-sheet/visco-elastic bedrock model, Geophys. Res. Lett., 25, 3951–3954, https://doi.org/10.1029/1998GL900052, 1998.

Le Meur, E. and Huybrechts, P.: A model computation of the temporal changes of surface gravity and geoidal signal induced by the evolving greenland ice sheet, Geophys. J. Int., 145, 835–849, https://doi.org/10.1046/j.1365-246X.2001.01442.x, 2001.

Lecavalier, B. S., Milne, G. A., Simpson, M. J., Wake, L. M., Huybrechts, P., Tarasov, L., Kjeldsen, K. K., Funder, S., Long, A. J., Woodroffe, S., Dyke, A. S., and Larsen, N. K.: A model of Greenland ice sheet deglaciation constrained by observations of relative sea level and ice extent, Quaternary Sci. Rev., 102, 54–84, https://doi.org/10.1016/j.quascirev.2014.07.018, 2014.

Lenton, T. M., Rockström, J., Gaffney, O., Rahmstorf, S., Richardson, K., Steffen, W., and Shellnhuber, H. J.: Climate tipping points – too risky to bet against, Nature, 575, 592–595, 2019.

Levermann, A. and Winkelmann, R.: A simple equation for the melt elevation feedback of ice sheets, The Cryosphere, 10, 1799–1807, https://doi.org/10.5194/tc-10-1799-2016, 2016.

Levermann, A., Albrecht, T., Winkelmann, R., Martin, M. A., Haseloff, M., and Joughin, I.: Kinematic first-order calving law implies potential for abrupt ice-shelf retreat, The Cryosphere, 6, 273–286, https://doi.org/10.5194/tc-6-273-2012, 2012.

Levermann, A., Clark, P. U., Marzeion, B., Milne, G. A., Pollard, D., Radic, V., and Robinson, A.: The multimillennial sea-level commitment of global warming, P. Natl. Acad. Sci. USA, 110, 13745–13750, https://doi.org/10.1073/pnas.1219414110, 2013.

Lingle, C. S. and Clark, J. A.: A numerical model of interactions between a marine ice sheet and the solid Earth: application to a West Antarctic ice stream., J. Geophys. Res., 90, 1100–1114, https://doi.org/10.1029/JC090iC01p01100, 1985.

Locarnini, R. A., Mishonov, A., Baranova, O., Boyer, T. P., Zweng, M., Garcia, H. E., Reagan, J., Seidov, D., Weathers, K. W., Paver, C., and Smolyar, I. V.: WORLD OCEAN ATLAS 2018 Volume 1: Temperature, Mishonov, A., Technical Editor, Tech. rep., 2019.

Ma, Y., Gagliardini, O., Ritz, C., Gillet-Chaulet, F., Durand, G., and Montagnat, M.: Enhancement factors for grounded ice and ice shelves inferred from an anisotropic ice-flow model, J. Glaciol., 56, 805–812, https://doi.org/10.3189/002214310794457209, 2010.

Martinec, Z.: Spectral-finite element approach to three-dimensional viscoelastic relaxation in a spherical earth, Geophys. J. Int., 142, 117–141, https://doi.org/10.1046/j.1365-246X.2000.00138.x, 2000.

Martinec, Z., Klemann, V., van der Wal, W., Riva, R. E., Spada, G., Sun, Y., Melini, D., Kachuck, S. B., Barletta, V., Simon, K., A, G., and James, T. S.: A benchmark study of numerical implementations of the sea level equation in GIA modelling, Geophys. J. Int., 215, 389–414, https://doi.org/10.1093/gji/ggy280, 2018.

Milne, G. A., Latychev, K., Schaeffer, A., Crowley, J. W., Lecavalier, B. S., and Audette, A.: The influence of lateral Earth structure on glacial isostatic adjustment in Greenland, Geophys. J. Int., 214, 1252–1266, https://doi.org/10.1093/GJI/GGY189, 2018.

Mordret, A.: Uncovering the Iceland Hot Spot Track Beneath Greenland, J. Geophys. Res.-Sol. Ea., 123, 4922–4941, https://doi.org/10.1029/2017JB015104, 2018.

Morlighem, M., Bondzio, J., Seroussi, H., Rignot, E., Larour, E. Y., Humbert, A., and Rebuffi, S.: Modeling of Store Gletscher's calving dynamics, West Greenland, in response to ocean thermal forcing, Geophys. Res. Lett., 43, 2659–2666, https://doi.org/10.1002/2016GL067695, 2016.

Morlighem, M., Williams, C. N., Rignot, E., An, L., Arndt, J. E., Bamber, J. L., Catania, G., Chauché, N., Dowdeswell, J. A., Dorschel, B., Fenty, I. G., Hogan, K., Howat, I. M., Hubbard, A., Jakobsson, M., Jordan, T. M., Kjeldsen, K. K., Millan, R., Mayer, L., Mouginot, J., Noël, B. P. Y., O'Cofaigh, C., Palmer, S., Rysgaard, S., Seroussi, H., Siegert, M. J., Slabon, P., Straneo, F., van den Broeke, M. R., Weinrebe, W., Wood, M., and Zinglersen, K. B.: BedMachine v3: Complete Bed Topography and Ocean Bathymetry Mapping of Greenland From Multibeam Echo Sounding Combined With Mass Conservation, Geophys. Res. Lett., 44, 11,051–11,061, https://doi.org/10.1002/2017GL074954, 2017.

Mouginot, J., Rignot, E., Bjørk, A. A., Van Den Broeke, M. R., Millan, R., Morlighem, M., Noël, B. P. Y., Scheuchl, B., and Wood, M.: Forty-six years of Greenland Ice Sheet mass balance from 1972 to 2018, P. Natl. Acad. Sci. USA, 116, 201904242, https://doi.org/10.1073/pnas.1904242116, 2019.

Noël, B. P. Y., van de Berg, W. J., Lhermitte, S., and van den Broeke, M. R.: Rapid ablation zone expansion

amplifies north Greenland mass loss, Sci. Adv., 5, 2–11, https://doi.org/10.1126/sciadv.aaw0123, 2019.

Oerlemans, J.: Glacial cycles and ice-sheet modelling, Climatic Change, 4, 353–374, https://doi.org/10.1007/BF02423468, 1982.

Peltier, W. R. and Drummong, R.: Rheological stratification of the lithosphere: A direct inference based upon the geodetically observed pattern of the glacial isostatic adjustment of the North American continent, Geophys. Res. Lett., 35, 1–5, https://doi.org/10.1029/2008GL034586, 2008.

Petrini, M., Vizcaino, M., Sellevold, R., Muntjewerf, L., Georgiou, S., Scherrenberg, M. D. W., Lipscomb, W., and Leguy, G.: Multi-millennial response of the Greenland Ice Sheet to anthropogenic warming, EGU General Assembly 2021, online, 19–30 April 2021, EGU21-12958, https://doi.org/10.5194/egusphere-egu21-12958, 2021.

Pico, T., Birch, L., Weisenberg, J., and Mitrovica, J. X.: Refining the Laurentide Ice Sheet at Marine Isotope Stage 3: A data-based approach combining glacial isostatic simulations with a dynamic ice model, Quaternary Sci. Rev., 195, 171–179, https://doi.org/10.1016/j.quascirev.2018.07.023, 2018.

Pollard, D., Gomez, N., and Deconto, R. M.: Variations of the Antarctic Ice Sheet in a Coupled Ice Sheet-Earth-Sea Level Model: Sensitivity to Viscoelastic Earth Properties, J. Geophys. Res.-Earth, 122, 2124–2138, https://doi.org/10.1002/2017JF004371, 2017.

Powell, E. M., Gomez, N., Hay, C., Latychev, K., and Mitrovica, J. X.: Viscous effects in the solid earth response to modern Antarctic ice mass flux: Implications for geodetic studies of WAIS stability in a warming world, J. Climate, 33, 443–459, https://doi.org/10.1175/JCLI-D-19-0479.1, 2020.

Powell, E. M., Pan, L., Hoggard, M. J., Latychev, K., Gomez, N., Austermann, J., and Mitrovica, J. X.: The impact of 3-D Earth structure on far-field sea level following interglacial West Antarctic Ice Sheet collapse, Quaternary Sci. Rev., 273, 107256, https://doi.org/10.1016/j.quascirev.2021.107256, 2021.

Rignot, E. and Mouginot, J.: Ice flow in Greenland for the International Polar Year 2008–2009, Geophys. Res. Lett., 39, 1–7, https://doi.org/10.1029/2012GL051634, 2012.

Robinson, A., Calov, R., and Ganopolski, A.: Multistability and critical thresholds of the Greenland ice sheet, Nat. Clim. Change, 2, 429–432, https://doi.org/10.1038/nclimate1449, 2012.

Schumacher, M., King, M. A., Rougier, J., Sha, Z., Khan, S. A., and Bamber, J. L.: A new global GPS data set for testing and improving modelled GIA uplift rates, Geophys. J. Int., 214, 2164–2176, https://doi.org/10.1093/gji/ggy235, 2018.

Simpson, M. J., Milne, G. A., Huybrechts, P., and Long, A. J.: Calibrating a glaciological model of the Greenland ice sheet from the Last Glacial Maximum to present-day using field observations of relative sea level and ice extent, Quaternary. Sci. Rev., 28, 1631–1657, https://doi.org/10.1016/j.quascirev.2009.03.004, 2009.

Steffen, K. and Box, J. E.: Surface climatology of the Greenland Ice Sheet: Greenland Climate Network 1995–1999, J. Geophys. Res.-Atmos., 106, 33951–33964, https://doi.org/10.1029/2001JD900161, 2001.

Talento, S. and Ganopolski, A.: Reduced-complexity model for the impact of anthropogenic CO_2 emissions on future glacial cycles, Earth Syst. Dynam., 12, 1275–1293, https://doi.org/10.5194/esd-12-1275-2021, 2021.

The PISM authors: PISM, a Parallel Ice Sheet Model, http://www.pism.io (last access: 11 July 2022), 2021a

The PISM authors: PISM, a Parallel Ice Sheet Model, https://github.com/pism/pism/tree/d4fe8ba520b71823bf73de20660db03f917974c7 (last access: 11 July 2022), GitHub repository [code], 8 April 2021b.

Tosi, N., Sabadini, R., Marotta, A. M., and Vermeersen, L. L.: Simultaneous inversion for the Earth's mantle viscosity and ice mass imbalance in Antarctica and Greenland, J. Geophys. Res.-Sol. Ea., 110, 1–14, https://doi.org/10.1029/2004JB003236, 2005.

Vasskog, K., Langebroek, P. M., Andrews, J. T., Nilsen, J. E. Ø., and Nesje, A.: The Greenland Ice Sheet during the last glacial cycle: Current ice loss and contribution to sea-level rise from a palaeoclimatic perspective, Earth-Sci. Rev., 150, 45–67, https://doi.org/10.1016/j.earscirev.2015.07.006, 2015.

Wahr, J., van Dam, T., Larson, K. M., and Francis, O.: Geodetic measurements in Greenland and their implications, J. Geophys. Res.-Sol. Ea., 106, 16567–16581, https://doi.org/10.1029/2001JB000211, 2001.

Weertman, J.: Stability of ice-age ice sheets, J. Geophys. Res., 66, 3783–3792, https://doi.org/10.1029/jz066i011p03783, 1961.

Whitehouse, P. L.: Glacial isostatic adjustment modelling: historical perspectives, recent advances, and future directions, Earth Surf. Dynam., 6, 401–429, https://doi.org/10.5194/esurf-6-401-2018, 2018.

Whitehouse, P. L., Latychev, K., Milne, G. A., Mitrovica, J. X., and Kendall, R.: Impact of 3-D Earth structure on Fennoscandian glacial isostatic adjustment: Implications for space-geodetic estimates of present-day crustal deformations, Geophys. Res. Lett., 33, 3–7, https://doi.org/10.1029/2006GL026568, 2006.

Whitehouse, P. L., Gomez, N., King, M. A., and Wiens, D. A.: Solid Earth change and the evolution of the Antarctic Ice Sheet, Nat. Commun., 10, 1–14, https://doi.org/10.1038/s41467-018-08068-y, 2019.

Willeit, M. and Ganopolski, A.: The importance of snow albedo for ice sheet evolution over the last glacial cycle, Clim. Past, 14, 697–707, https://doi.org/10.5194/cp-14-697-2018, 2018.

Willeit, M., Ganopolski, A., Calov, R., and Brovkin, V.: Mid-Pleistocene transition in glacial cycles explained by declining CO_2 and regolith removal, Sci. Adv., 5, 1–9, https://doi.org/10.1126/sciadv.aav7337, 2019.

Winkelmann, R., Martin, M. A., Haseloff, M., Albrecht, T., Bueler, E., Khroulev, C., and Levermann, A.: The Potsdam Parallel Ice Sheet Model (PISM-PIK) – Part 1: Model description, The Cryosphere, 5, 715–726, https://doi.org/10.5194/tc-5-715-2011, 2011.

Zeitz, M., Levermann, A., and Winkelmann, R.: Sensitivity of ice loss to uncertainty in flow law parameters in an idealized one-dimensional geometry, The Cryosphere, 14, 3537–3550, https://doi.org/10.5194/tc-14-3537-2020, 2020.

Zeitz, M., Haacker, J. M., Donges, J. F., Albrecht, T., and Winkelmann, R.: Dynamic regimes of the Greenland Ice Sheet emerging from interacting melt-elevation and glacial isostatic adjustment feedbacks – Dataset, Zenodo [data set], https://doi.org/10.5281/zenodo.6827865, 2022.

Zweck, C. and Huybrechts, P.: Modeling of the northern hemisphere ice sheets during the last glacial cycle and

glaciological sensitivity, J. Geophys. Res.-Atmos., 110, 1–24, https://doi.org/10.1029/2004JD005489, 2005.

Zweng, M. M., Reagan, J. R., Seidov, D., Boyer, T. P., Locarnini, R. A., Garcia, H. E., Mishonov, A. V., Baranova, O. K., Weathers, K. W., Paver, C. R., and Smolyar, I. V.: World Ocean Atlas 2018 Volume 2: Salinity, Mishonov, A., Technical Editor, Tech. Rep. September, 2018.

Manuscript 4 (in review): Risks and benefits of overshooting a 1.5°C carbon budget

This paper explores the carbon budget flexibility compatible with the goals defined in the Paris Agreement. Here, two scenarios are compared: One in which the temperatures remain within the bounds of the Paris Agreement during the whole 21st century, and one in which carbon removal technologies allow for an intermediate overshoot of both, the carbon budget and the temperatures, before reaching the same global mean temperature at the end of the century. The climatic, environmental and socio-economic consequences are explored using an analysis framework including integrated assessment models, an earth system model, the ice sheet model PISM, the vegetation model LPJmL and models to assess macroeconomic damages and risk exposures. The framework is a once-through information flow, that is feedbacks between the different modeling parts are not considered.

While the global mean air temperature is sufficiently reduced in the overshoot scenario, we find that the air temperatures in high latitudes and the heat content of the ocean are not as effectively reduced. This gap in temperatures drives the long-term increase of Greenland's sea level contribution.

In review at Environmental Research Letters

Exploring risks and benefits of overshooting a 1.5°C carbon budget over space and time

Nico Bauer[1,*], David P. Keller[2], Julius Garbe[1,3], Kristine Karstens[1], Franziska Piontek[1], Werner von Bloh[1], Wim Thiery[4], Maria Zeitz[1,3], Matthias Mengel[1], Jessica Strefler[1], Kirsten Thonicke[1], Ricarda Winkelmann[1,3]

(1) Potsdam Institute for Climate Impact Research (PIK), Member of the Leibniz Association, Potsdam, Germany
(2) GEOMAR Helmholtz Centre for Ocean Research, Kiel, Germany
(3) Institute of Physics and Astronomy, University of Potsdam, Potsdam, Germany
(4) Vrije Universiteit Brussel, Department of hydrology and hydraulic engineering, Brussels, Belgium

*corresponding author: nico.bauer@pik-potsdam.de, ++49 331 288 2540

Abstract

Temperature targets as specified in the Paris Agreement limit global net cumulative emissions to very tight carbon budgets. The possibility to overshoot the budget and offset near-term excess carbon emissions by net-negative emissions is considered economically attractive because it can ease near-term mitigation pressure. While potential side effects of carbon removal deployment are discussed extensively, the additional climate risks and the impacts and damages have attracted less attention so far. We link six models for an integrative analysis of the climatic, environmental and socio-economic consequences of temporarily overshooting a carbon budget consistent with the 1.5°C temperature target along the cause-effect chain from emissions and carbon removals to climate risks and impact. Global climatic indicators such as CO_2-concentration and mean temperature closely follow the carbon budget overshoot with mid-century peaks of 50ppmv and 0.35°C, respectively. Our findings highlight that investigating overshoot scenarios requires temporally and spatially differentiated analysis of climate, environmental and socioeconomic systems. We find persistent and spatially heterogeneous differences in the distribution of carbon across various pools, ocean heat content, sea level rise as well as economic damages. Moreover, we find that key impacts, including degradation of marine ecosystem, heat wave exposure and economic damages, are more severe in equatorial areas than in higher latitudes, although absolute temperature changes being stronger in higher latitudes. The detrimental effects of a 1.5°C warming and the additional effects due to overshoots are strongest in non-OECD countries. Constraining the overshoot inflates CO_2 prices, thus shifting carbon removal towards early afforestation while reducing the total cumulative deployment only slightly, while mitigation costs increase sharply in developing countries. Thus, scenarios with carbon budget overshoots can reverse global mean temperature increase but imply more persistent and geographically heterogeneous impacts. Overall, the decision about overshooting implies more severe trade-offs between mitigation and impacts in developing countries.

Introduction

The temperature targets of the Paris Agreement can be translated into carbon budgets (e.g. Meinshausen et al. 2009) as the global mean temperature (GMT) shows a short-term albeit permanent response to cumulative emissions (e.g., Matthews et al. 2009). Only for very large overshoot magnitudes and durations the symmetric temperature response to net positive and net-negative emission fluxes vanishes (e.g. Zickfeld et al. 2016, Jones et al. 2016). The focus on GMT inhibits quantification of temporal and spatial responses of systems and processes along the cause-effect chain from (i) emissions and removals through (ii) the climate system to (iii) impacts and damages. In this study we explore the differences between two scenarios that differ only in the overshoot of the carbon budget.

Integrated Assessment Models (IAMs) derived overshoot of up to 1000 GtCO2 above the carbon budget (Bauer et al. 2018, Riahi et al. 2021). The main argument in support of overshooting are the lower near-term mitigation costs. The positive economic effect is stronger the smaller the carbon budget (Kriegler et al. 2014, Bauer et al. 2018, Riahi et al. 2021). Riahi et al. (2021) identified potential positive effects on annual GDP of limiting the overshoot during the 2nd half of the 21st century. The overshoot magnitude also depends on the development of the climate policy ambition over time that can be measured by the carbon price path (Realmonte et al. 2019, Strefler et al. 2021a). Stronger near-term policy ambition result in deeper near-term emission reductions and larger deployment of carbon dioxide removal technologies (Strefler et al. 2021a, Riahi et al. 2021). This can aggravate environmental problems related to carbon removals such as bioenergy with carbon capture and storage (BECCS; Smith et al. 2015, Heck et al. 2018). A broader portfolio of carbon removal options tends to increase overshoots, but reduces overspecialization on a single option with spatially concentrated harmful effects (Strefler et al. 2021b).

Climate models are used to assess resulting additional climate risks. The overshoots are simulated by assuming: (i) single year removal pulses of 370 to nearly 2000 $GtCO_2$, (ii) emission-driven scenarios that lead to different cumulative CO2-emissions or (iii) concentration driven runs that also lead to differ by several thousand $GtCO_2$ of cumulative emission differences. Asymmetric and non-linear GMT changes to single year pulses of CO2-emissions or removals have been demonstrated if they are large or imposed on different equilibrium states (Zickfeld et al. 2021). Variations of CO_2-concentration overshoot scenarios identified additional climate risks due to inertia and path-dependency regarding carbon pools, ocean heat and sea-level rise (Boucher et al. 2012, McDougall 2013, Tokarska and Zickfeld 2015, Zickfeld et al. 2016). These studies are difficult to interpret because concentration

driven scenarios feature GMT differences up to 1.5°C (Boucher et al. 2012). Later studies extended the analysis to oceanic biogeochemistry (e.g. Mathesius et al. 2015, Hofmann et al. 2019).

The additional socioeconomic risks are under-researched. A recent study by Drouet et al. (2021) investigated overshoot scenarios with maximum GMT difference of 0.16°C, based on the MAGICC model. Differences of indicators representing heat and drought were “statistically indistinguishable” and showed no regional patterns. Also additional sea-level rise (SLR) would not exceed 2.3cm by 2200. Different to that, the overshoot causes no less than 4 trillion USD/yr by 2100 of GDP reduction, if the damage function relied on Burke et al. (2015).

Based on the existing literature it is difficult to assess overshoots because studies are mostly narrowly focused, use incoherent scenario assumptions and vary in their temporal and spatial focus. The present study addresses these shortcomings. First, we use a broad set of models to assess effects of carbon budget overshoot along the whole cause-effect chain considering, climatic and environmental issues. Second, we will not only consider emissions and removals, but also land-use change information derived with an IAM to drive ESMs. Third, we will investigate the temporal and geographical impacts of mitigation benefits and induced additional climate risks to better understand reversibility and trade-off relationships.

Integrated framework of models

For the evaluation of the overshoot flexibility we integrate a series of models from different disciplines into an analysis framework (Figure 1). The models are peer-reviewed and used by international assessment bodies, such as the Intergovernmental Panel on Climate Change (IPCC).

The framework works through the cause-effect chain, but information does not feedback between models. For example, climate impacts do not change the socioeconomic developments and policies that drive the emissions in REMIND-MAgPIE. The socio-economic assumptions are harmonized to the middle-of-the-road scenario of the Shared Socioeconomic Pathways (SSPs, Kriegler et al. 2017).

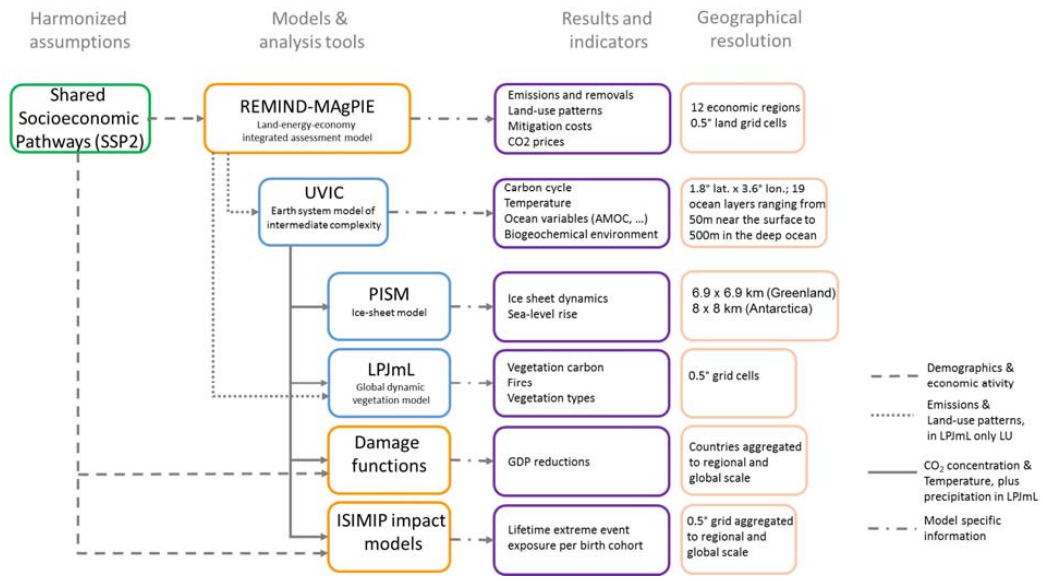

Figure 1: Overview on information flow of the integrated model framework. REMIND-MAgPIE: Bauer et al. (2020b), Strefler et al. (2021b); UVic 2.10 - Mengis et al., (2020); PISM - Winkelmann et al. (2011), Bueler and Brown (2009); LPJmL - Schaphoff et al. (2018); Macroeconomic damages - Burke et al. (2015), Schultes et al. (2021); Life-time extreme event exposure - Thiery et al (2021).

The REMIND-MAgPIE model computes the emission and land-use pathways with full and minimal overshoot flexibility. It derives scenarios for CO2 emissions and other climate forcers as well as land-use patterns consistent with deployment patterns of CDR technologies: bioenergy with carbon capture and storage, afforestation, direct air capture and storage (DACS) and enhanced weathering (Strefler et al. 2021b). The 1.5°C target at 66% no-exceedance likelihood is implemented by a global carbon budget with 600 $GtCO_2$ for the time horizon 2010-2100 (Rogelj et al. 2018, 2019). Emissions and removals are controlled by a globally uniform carbon price that starts in 2025 and grows at 5% per

year. All other GHG emissions are priced using CO_2-eq conversion factors based on Global Warming Potentials (GWP100).

The carbon budget is small and cannot be achieved in the model by completely avoiding a budget overshoot. Hence, we limit the over-shoot and name it minimal or low overshoot scenario. In this scenario net-negative emissions are not remunerated. In the full overshoot scenario all net-negative emissions are remunerated at the level of the carbon price. Thus, the duration and magnitude of the overshoot is derived endogenously given the socioeconomic conditions and the strength of the climate target. We also perform a sensitivity analysis that gradually reduces the overshoot by varying the remuneration factor.

The emission and land-use scenarios are used by the UVic model (Mengis et al., 2020) to simulate climatic and biogeochemical changes. The model provides insights into the dynamic changes of natural carbon pools (including the permafrost soils), atmospheric temperatures, precipitation, sea-ice, oceanic heat content and thermosteric expansion, ocean circulation as well as marine and terrestrial biogeochemistry. The model adequately simulates changes in historical temperature and carbon fluxes for the historical period 1850-2015 (Mengis et al., 2020). The model is also used to investigate parametric uncertainties (see SI).

The UVic model serves as the basis to evaluate a broad spectrum of changes in the climate system at the global level and is spatially resolved. For a more comprehensive assessment and integrated perspective we use the results of UVic and REMIND-MAgPIE to force a broader portfolio of models allowing us to evaluate impacts on more climate, environmental and socioeconomic systems (Figure 1).

The temperature and precipitation changes of UVic are used by the Parallel Ice Sheet Model (PISM, Winkelmann et al., 2011, Bueler and Brown, 2009, Garbe et al. 2020) to evaluate the impacts on the ice sheets of Greenland and Antarctica and resulting contributions to sea-level rise that is added to the ocean thermal expansion and glacier melting. PISM simulates mass changes due to snowing, melting and ice discharge (Calov and Greve, 2005, Zeitz et al. 2021, Reese et al., 2018). Additionally, the temperature changes as well as the ice sheet geometry changes caused by the melting lead to an increase in dynamic ice losses, further contributing to sea-level rise. The contribution of glaciers to sea-level rise is evaluated using a parsimonious emulator approach by Mengel et al. (2016) that parameterizes the results of 18 different climate models and separates the effect of anthropogenic warming from natural factors. The resulting sensitivity curves for SLR driven by glacier melting show the largest long-term equilibrium SLR for long-term global warming of up to 2°C. The SLR contribution from thermosteric expansion due to ocean heating is taken from the UVic runs.

The global terrestrial vegetation model LPJmL uses the global CO_2-concentration, temperature, precipitation, radiation and land-use patterns from REMIND-MAgPIE and UVic (Figure 1). All climate variables are used from the years 1901-1930 and randomly shuffled. It allows to evaluate the impacts on the vegetation and changes in the spatial distribution of biomes and potential degradation. Compared to UVic's terrestrial carbon cycle model LPJmL uses a finer spatial and temporal resolution, comprises more detailed processes, a broader set of vegetation types and an advanced representation of fire dynamics. We use LPJmL to detect hotspots of changes in terrestrial carbon pools and relate it to climatic or land-use changes.

Changes in economic activity are related to GMT changes (Burke et al. 2015). The relation is hump-shaped with a maximum at ~13°C. A change in one-year GMT shock implies change in the level of GDP with uncertain degree of permanence (Newell et al. 2020, Piontek et al. 2019). Thus, we formulate a decay function and vary the half-time in years after which half of the original annual GDP effect is still present (Schultes et al. 2021). In this study we assume permanence of five and 15 years along with the extreme values of zero and infinity for single year damage and fully permanent GDP reduction. The damages are calculated at country-level, using population-weighted mean country temperature based on the UVic simulations and GDP per capita (Dellink et al. 2017, KC and Lutz 2017).

Finally, we quantify the impacts on the exposure to extreme weather events over the lifetime of different age cohorts born between 1960 and 2020 (Thiery et al. 2021). The gridded population scenarios are mapped to the spatially explicit simulations of six extreme event categories (Lange et al. 2020): heatwaves, tropical cyclones, river floods, crop failures, wildfires and droughts. The results are summarized aggregating the frequency of extreme events over the remaining life-times per cohort. The cumulation over life-time provides a first indicator on potentially negative socioeconomic impacts, incl. more permanent consequences such as lower human capital formation due to reduced schooling.

Results

Overshoot, emissions, land-use change, carbon removals and costs

Net emissions would need to decrease immediately and quickly to minimize the carbon budget overshoot (Figure 2a). In the overshoot scenario global CO_2 emissions remain constant until 2030, which exceeds the range of 1.5°C-compatible scenarios considered by the sixth Assessment Report of the IPCC (AR6). The overshoot reaches 700GtCO_2 (see Figure 2b), while cumulative carbon removal are 900GtCO_2 with large contributions of BECCS and DACS. The full overshoot leads net-zero CO_2 emissions in 2065 and 27 GtCO_2/yr net negative emissions by 2100, which is 5 times the mass flow of today's oil extraction. In case with only minimum overshoot in 2030 net CO_2 emissions are reduced by 70% compared with 2020, which is comparable to the fastest reduction scenarios considered in AR6.

Limiting the overshoot (moving left-to-right along the x-axis in Figure 2(b) lowers carbon removals only slightly as removals are increasingly used to offset intratemporally rather than intertemporally (see also Johansson et al. (2020) and Strefler et al. (2021a). Further, afforestation on pasture and range lands becomes more important (see Figure 2c) particularly in non-OECD regions (Figure S1e) offering the near-term potential to achieve net zero carbon emissions as soon as 2040 (see Figure 2a).

Carbon prices vary substantially (in 2030 50-500US$/t$CO_2$) depending on the overshoot (Figure 2e). The reduction in GDP are substantially higher in non-OECD countries and also vary more strongly than in OECD countries (Figure 2d). The time profile indicates that limiting the overshoot leads to larger macroeconomic impact in non-OECD countries. During the second half of the 21st century the annual GDP reductions are lower without overshoot, but this difference is relatively small (see Figure S2). This asymmetric and regressive impact is due to differences in socioeconomic development and fossil fuel dependency (Bauer et al. 2020a).

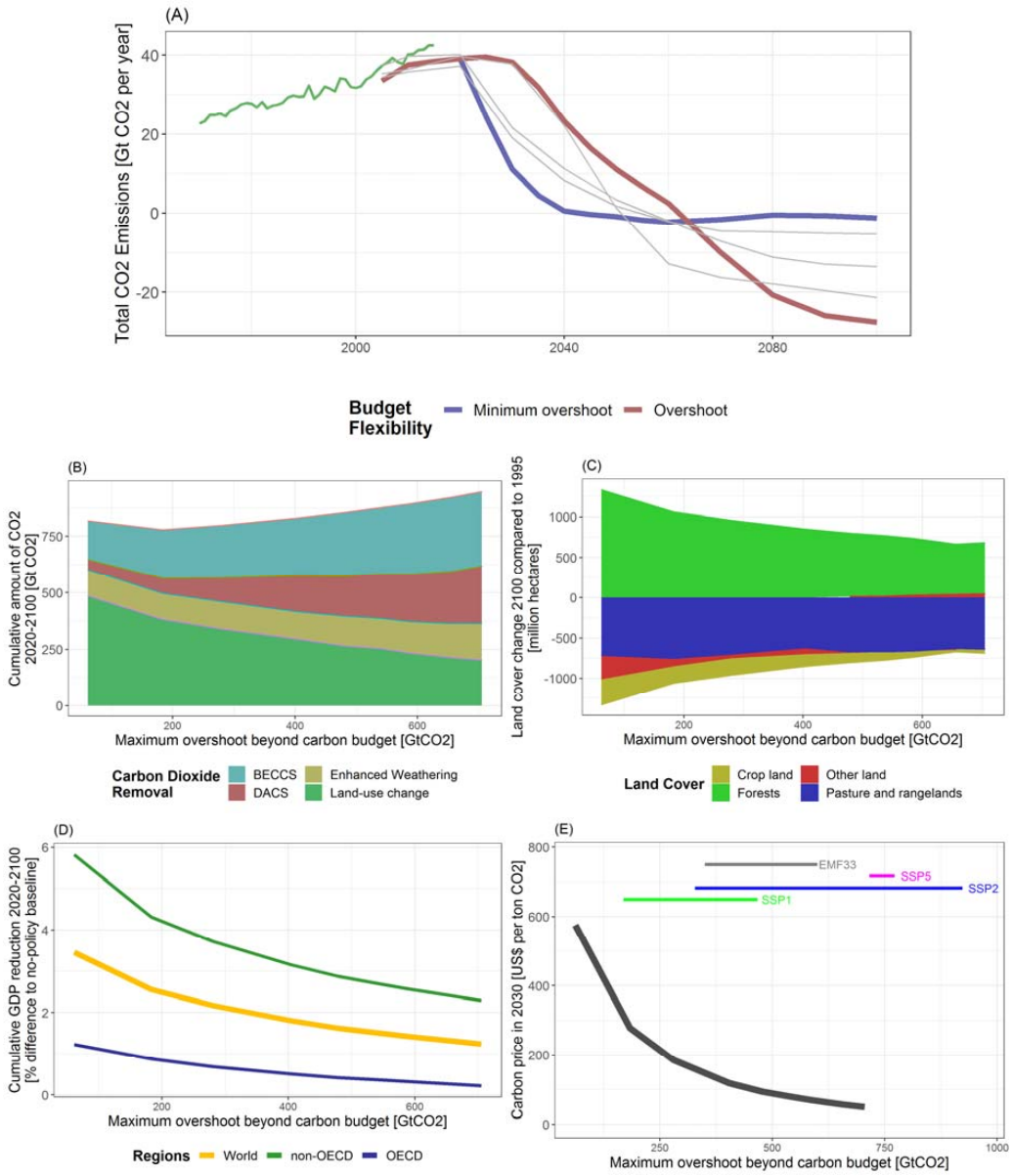

Figure 2: Overshoot flexibility and implications derived with REMIND-MAgPIE. Panel (A) shows global total net CO_2 emissions along with three illustrative scenarios of the IPCC SR15 (grey lines); the green line shows historical emissions according to CEDS. Note that the minimum overshoot scenario requires cumulative net negative emissions of 50 $GtCO_2$ to comply with the 600 $GtCO_2$ carbon budget. Panel (B) depicts the cumulative global carbon removals until 2100 against the global carbon budget overshoot on the x-axis. Panel (C) shows changes in land-cover until 2100 that are used in the UVic model. Panel (D) shows the cumulative global GDP reduction and in OECD and non-OECD countries. The numbers represent relative differences of net present values for the time horizon 2020-2100 assuming a discount rate of 5% per year. Panel (E) shows the carbon price in 2030 against the carbon budget overshoot and added the cross-model ranges of cumulative amounts of net-negative carbon emissions for three SSPs in case of the 1.9W/m² target.

Climate system and carbon cycle

The global CO_2 concentration in 2100 is slightly lower in the overshoot scenario (Figure 3a), whereas the GMT is narrowed to only 20% of the peak difference (Figure 4a). Thus, for these scenarios key global climate variables show temporary rather than persistent effects.

Terrestrial carbon reservoirs, including permafrost soil carbon respond within a decade, turning from sink to source after atmospheric CO_2 decreases (Figure 3b). Additional permafrost carbon losses ($20GtCO_2$) due to temperature feedbacks are irreversible (Figure 3d), but they are offset by a greening vegetation. However, the carbon loss from permafrost soils may be more responsive to the overshoot due termokarst dynamics from rapid warming (Pihl, et al., 2021). Overall, responses of the terrestrial carbon stocks are highly uncertain (Hewitt et al., 2016; Friedlingstein et al., 2014; Pihl et al., 2021; Melnikova et al., 2021). Specifically, in the overshoot the CO_2 fertilization effect weakens, while heterotroph respiration of previously accumulated carbon becomes dominant turning the vegetation system into a net-CO2 source. The relative magnitude of both effect is uncertain. The ocean also takes up more carbon in the overshoot scenario (Figure S3a) and turns from sink to source only in 2080 (Figure 3c). On balance the high CO_2 concentration leads to more carbon uptake by the vegetation and the oceans than the temperature feedback releases carbon from permafrost soils. The results are robust against variations of uncertain model parameters.

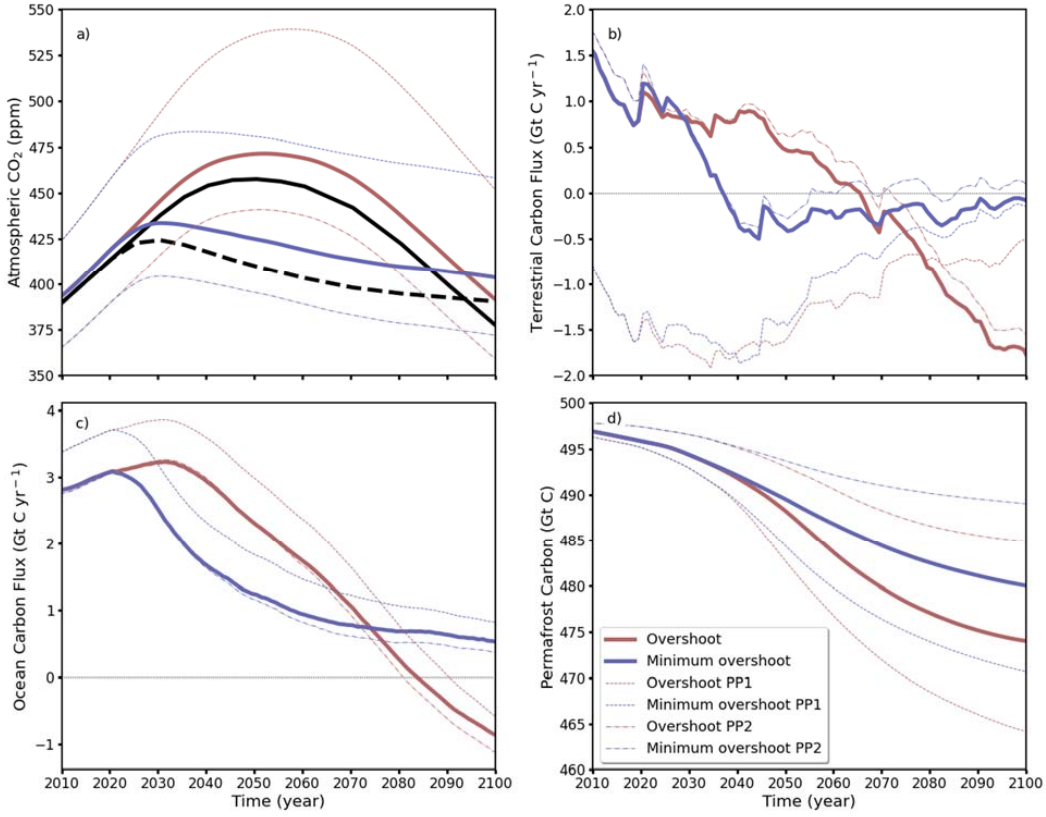

Figure 3: Comparison of UVic simulated global annual mean changes in (a) atmospheric CO_2, (b) terrestrial carbon fluxes (positive into the land), (c) the air-sea carbon flux (positive into the ocean), and (d) permafrost carbon. The black lines in (a) are the results from the MAGICC model. The dotted and dash-dotted lines are from perturbed parameter simulations that were chosen to investigate potential upper (dotted; PP1) and lower (dash-dotted; PP2) temperature responses to the forcing in these scenarios. Note: atmospheric CO_2 in both UVic scenarios (Fig. 3a) is slightly higher than in MAGICC, a behavioral bias that often occurs when Earth system models are forced with emissions (Hoffman et al., 2014). However, the biases are nearly equal in both scenarios (i.e., differences of the UVic and the MAGICC results are of a similar magnitude for both scenarios).

Climate systems show more persistent effects between both scenarios although GMT nearly fully converges by 2100. (Figure 4). The peak temperature difference between the scenarios occurs around 2065 reaching 0.35° C, upper end of the scenarios recently considered in AR6. This differences vanishes by 80% until 2100. Although GMT is nearly fully reversible by 2100 various climate systems, particularly oceans, show more persistent effects (Figure 4b-f).

The ocean heat content differs between scenarios (Figure 4b). While global annual mean sea surface temperature anomalies mostly follow atmospheric temperature change trends, deep ocean warming occurs more slowly and is driven by both mixing and diffusion as well as large-scale circulation (Figure S6). Most of the additional ocean heat storage in the overshoot scenario until 2100 occurs in the

upper ocean (above 2000m). However, warmer waters can be seen moving on circulatory pathways into the ocean interior, i.e., on the North Atlantic Deep Water, Antarctic Intermediate Water, and Antarctic Bottom Water pathways (Figure S6c). Consequently, deeper ocean layers (below the mixed layer depth, but mostly still in the upper 2000 m) show persistent temperature differences.

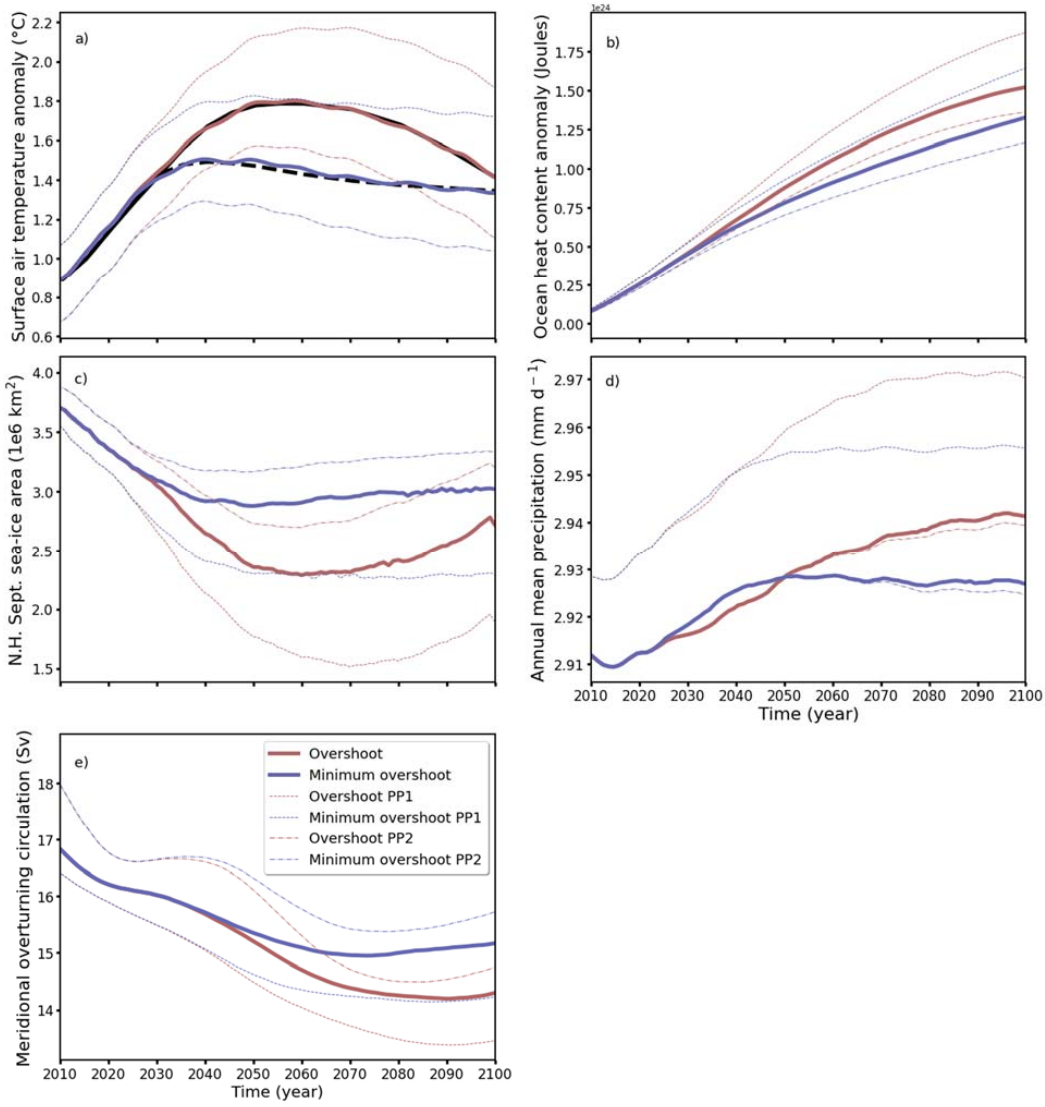

Figure 4. Comparison of UVic simulated global annual mean changes or anomalies in (a) near surface air temperature, (b) ocean heat content from 0 to 2000 m, (c) Northern hemisphere sea ice area, (d) precipitation, and (e meridional overturning circulation. The black lines in (a) are the results from the MAGICC model. The dotted and dash-dotted lines are from perturbed parameter simulations that were chosen to investigate potential upper (dotted; PP1) and lower (dash-dotted; PP2) temperature responses to the forcing in these scenarios.

Warming in both scenarios is largest at high latitudes due to polar amplification (up to 3.8 and 4.5° C above pre-industrial conditions at peak warming in the minimum overshoot and overshoot scenarios,

250 respectively; not shown). The largest temperature differences reach to 0.8°C for near surface air
251 temperature and ocean temperatures (Figure S4&S5a). Moreover, the differences vanish less towards
252 the poles than the GMT (> 0.1°C remain by 2100, Figure S5b). The latitudinal bias of the temperature
253 signal and the persistence of the heat retention have various knock-on effects.

254 The increasing temperatures lead to ocean sea-ice melting, weakening of meridional overturning, and
255 more precipitation (Fig. 4 c-e). The additional peak loss is about half a million additional square
256 kilometers. Sea-ice begins to recover from the overshoot, but at a slower rate than near-surface air
257 temperature and 40% of the peak difference remains in 2100. Furthermore, additional precipitation
258 doubles and is persistent throughout the century; the global anomaly is maximum 2% and mostly
259 related to oceans. Also, the weakening of the meridional overturning is twice as strong in case with
260 the overshoot, but this effect is more persistent and shows hardly any recovery until 2100 (Figure 4e).
261 Finally, warmer oceans contribute to stronger SLR, which is treated next.

262

Ice sheets and sea level rise

The scenario with minimal overshoot leads to long-lasting SLR driven by ice dynamics for both the Antarctica and Greenland ice-sheets as well as mountain glaciers and thermosteric expansion from warming oceans (Figure 5). In the minimal-overshoot scenario the sea level rises continuously by 39.7cm until 2100, which is comparable with the best-estimate 41cm assessed in AR6 WG1 for the 1.5°C scenario. The temperature overshoot leads to an additional SLR of 3.6cm or nearly 10% until 2100 that continues growing thereafter (Figure 5 b, d, f, h). The additional SLR exceeds the estimates of 0.4-2.3cm until 2200 by Drouet et al. (2021) substantially.

The major SLR driver until 2100 is thermosteric expansion with 19.4 cm in the low-overshoot scenario adding another 2.8cm at time of the peak difference in 2080. In both scenarios the ocean heat content increases until and beyond 2100 (Figure 4b) and, consequently drives the SLR, although the differences become smaller after 2080. Glaciers are expected to add 9.3cm, but the additional SLR from the overshoot only amounts to 0.75cm.

The Greenland and Antarctic ice-sheets are expected to contribute less to SLR until 2100. Surface melting of the Greenland ice-sheet is driven by air temperatures, which immediately reacts to differences in GMT. The Antarctic ice-sheet is more inert as the melting at the ocean-ice interface depends on increasing water temperatures, which respond with delay to air temperature changes. Antarctica could dominate the contributions to SLR, if the local temperature anomalies in Southern oceans turn out persistent and therefore increase the melting-rate in Antarctica (Figure 5b inlay) as small differences can drive long-term changes in ice mass (see Garbe et al. 2020). Overall the ice-sheets feature more mass loss from melting than mass gains from increasing snow accumulation (Medley and Thomas, 2019).

The dynamics of ice-sheets are highly uncertain. In recent analysis the near-term uncertainties regarding the Greenland ice-sheet have been highlighted suggesting a potential underestimation of future ice-sheet looses (Aschwanden et al. 2021). Also, impacts of SLR are difficult to assess. A recent study attributed nearly 15% of the total economic damage of hurricane Sandy in 2012 on the greater New York area to 9cm of regional SLR (Strauss et al. 2021). This highlights that small SLR changes can make a substantial difference. There are no studies that assess the differential impacts of small sea level differences like the one provided here that are in addition to larger future SLR.

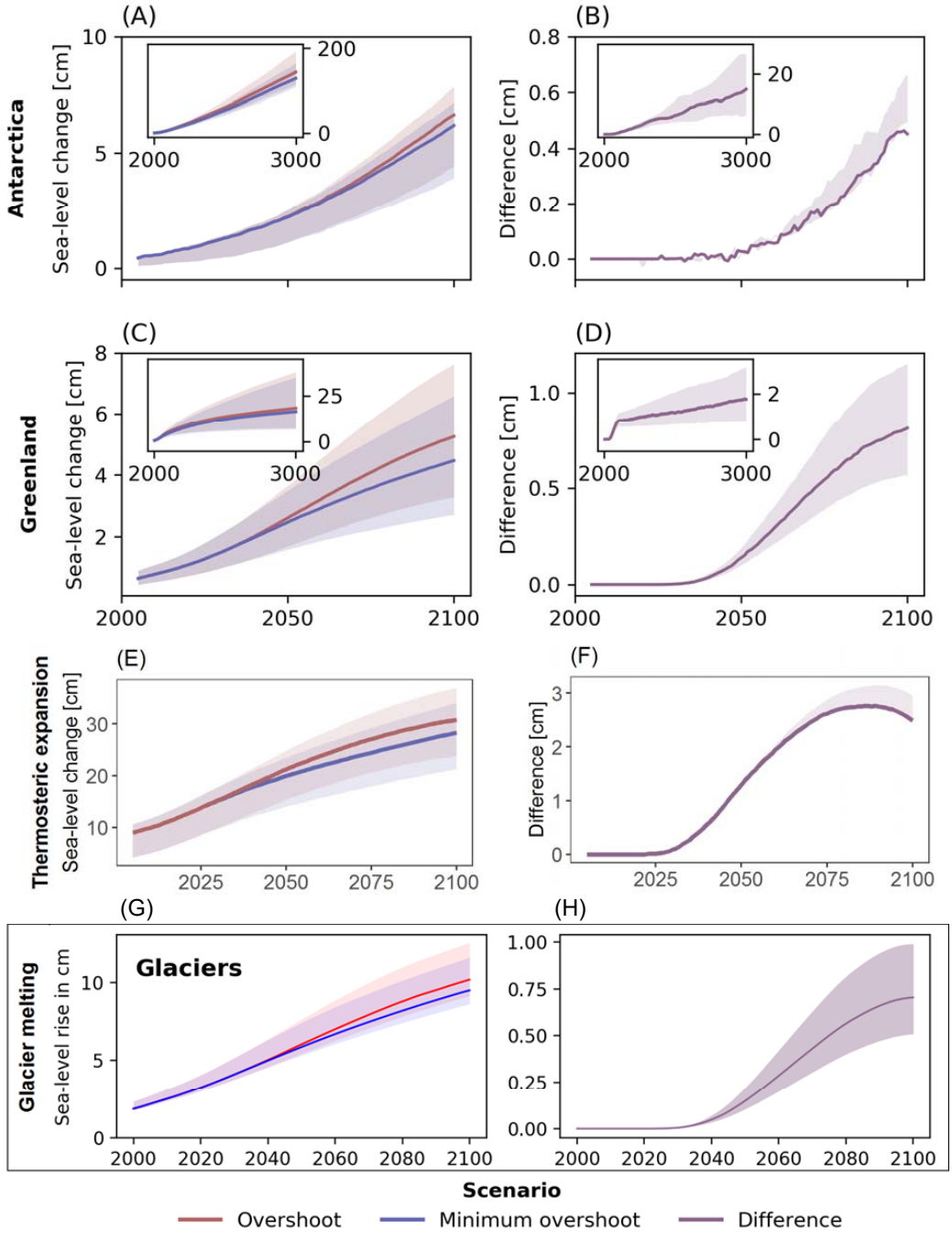

293
294
295
296

Figure 5: Impact of the overshoot on global sea-level rise. Contribution to sea level rise by ice-sheet mass loss in Antarctica until 2100 (inlay: until year 3000) (A) as well as effect of full overshoot from pairwise differences compared with minimal overshoot case (B). Absolute and additional contributions to SLR from Greenland ice sheet melting (c and d). Absolute and additional contributions to SLR due to thermosteric expansion (e and f), and panels (g and h) by the SLR emulator of Mengel et al. (2016). Results for panels (a-d) derived with PISM, panels (e and f) by UVic), panels (g and h) with a semi-empirical model. The shading denotes the uncertainty based on the Greenland melt sensitivity (as explained in detail in the appendix) and the temperature sensitivity of UViC for the

case of the Antarctic ice sheet. The shading in (g and h) denote the 5th and 95th percentile of the ensemble reflecting the parameter uncertainty in the semi-empirical glacier model. The insets of panels (a-d) are derived with the assumption that the geographical distributions of temperature and precipitation anomalies are kept constant at 2100 values.

Impact on marine and terrestrial ecosystems

Figure 6 shows the changes of coral calcification rates relative to pre-industrial levels derived with the UVic model. The calcification rates are lowered if water temperatures exceed the optimal level and pH value increases that indicates ocean acidification due to CO_2, which slows the growth and regeneration of coral reefs. The minimal overshoot scenario on the right-hand side shows calcification rates to drop by 40% in 2065 in the area North of Australia. In the full overshoot scenario the calcification rate decreases more severely by 50%. The differences between both scenarios vanish by 2100 as the differences of surface pH values and sea surface temperatures in the relevant areas fade out and thus establish similar environmental conditions allowing calcification rates also to converge (e.g., Albright et al. 2016). Nonetheless, in both scenarios calcification rates remain substantially below pre-industrial levels (20-40%).

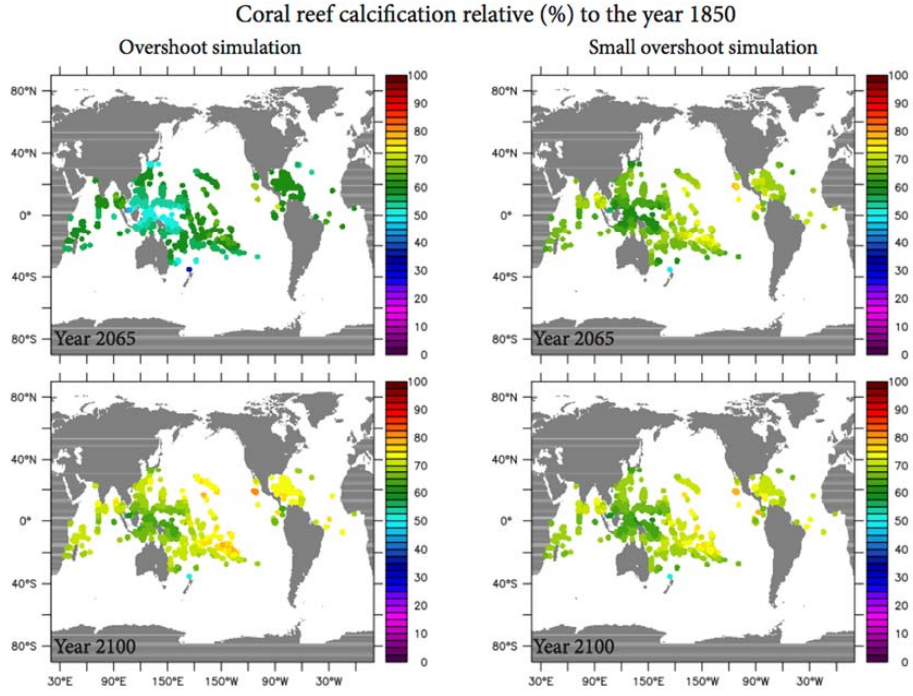

Figure 6: Impact on marine ecosystems measured by the coral calcification rate in % compared to pre-industrial levels. The top row shows results for 2065, whereas the bottom row shows results for 2100.

The calcification rate is calculated using simulated temperature and carbonate chemistry based on the Silverman equation, thereby serving as a proxy for the skeletal growth potential of hard corals. It does not represent the coral stock affected by marine heat waves that become more frequent and other stressors (Frölicher et al. 2018, Hughes et al. 2018). Moreover, thermal adaptation is an important, yet uncertain factor for coral reefs' ability to recover (Frieler et al. 2013, Sully et al. 2019). Projecting coral stock changes required more specific analysis with Earth System Models (for an earlier analysis see Frieler et al. 2013). Finally, coral reef degradation risks irreversible species losses (Tsiros et al., 2020).

(a) (b)

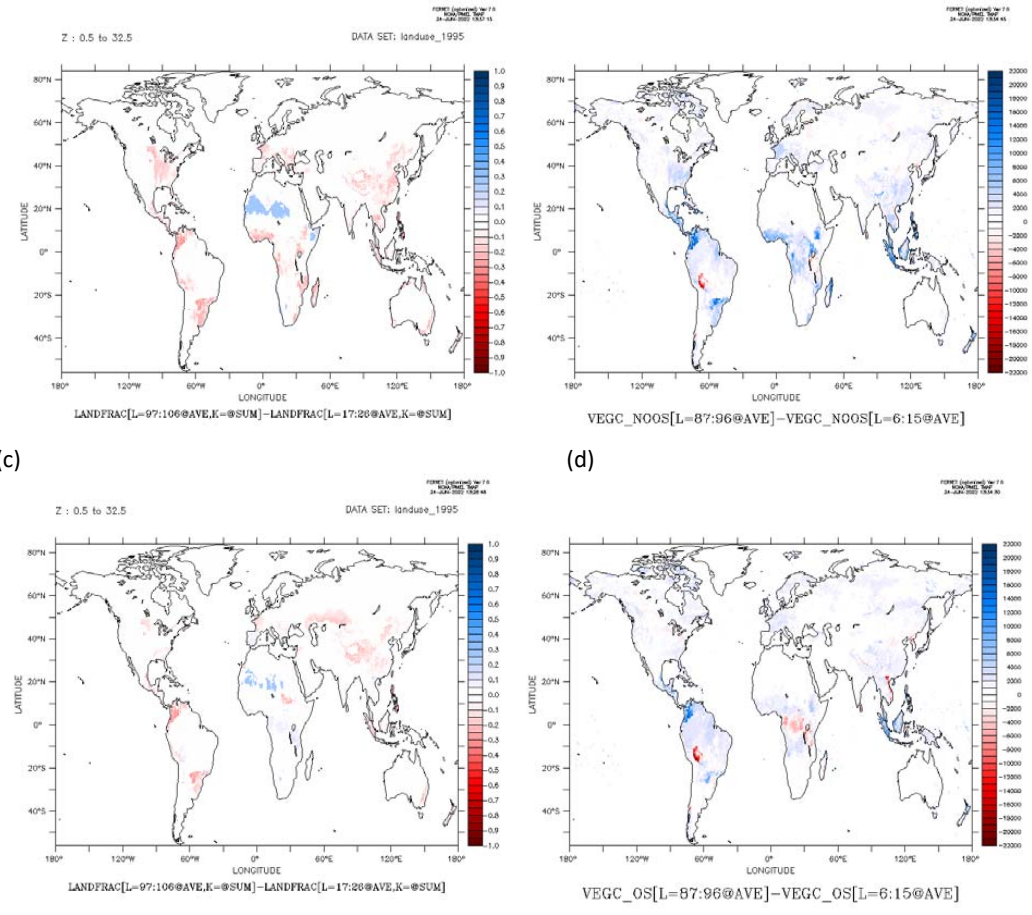

(c) (d)

Figure 7: Difference between overshoot and minimal overshoot scenario averaged from 2091-2100 for (a) land-use fraction and (b) total amount of carbon (biomass, litter and soil) in the biosphere (gC/m2). Increasing land-use diminishes carbon stored in biomass in, e.g. central Africa.

Terrestrial vegetation carbon stocks currently absorb 29% of anthropogenic CO_2 emissions (Friedlingstein et al., 2021). The analysis of the terrestrial ecosystems using LPJmL does not indicate

large-scale and abrupt degradation of vegetation carbon pools due to changes in climate conditions of temperature, CO_2-concentration and precipitation derived from UVic. Vegetation carbon pools (Figure 7b, d) are primarily driven by differences in land-use patterns of the two scenarios derived with the REMIND-MAgPIE model (Figure 7a, c). To validate this conclusion, LPJmL has been run with differences in climate variables but frozen land-use patterns 2005-2100, which does not show spatially concentrated differences. The results indicate that the main differences are explained by ubiquituous CO_2 fertilization. In both scenarios carbon losses are projected by 2100 in some regions, incl. North-America, Eurasia, and Northwest of Latin-America (Figure S8).

Large-scale and abrupt changes in terrestrial vegetation have been detected in a model ensemble only if global warming exceeds 2.5°C compared to pre-industrial levels (Drijfhout et al. 2015). The results suggest that a carbon budget overshoot does not imply additional risks to the integrity of vegetation carbon pools, whereas additional wide-area CO_2 fertilization increases vegetation carbon pools. Differences in land-use change related to afforestation and bioenergy production cause differences in vegetation carbon pools. The role of additional carbon injected into carbon cycle in the overshoot scenario increases the resilience of terrestrial vegetation systems, while it tends to harm maritime systems due to acidification along warming oceans.

Economic impacts and extreme event exposure

The impact of global warming on GDP as well as the differential effect caused by the additional overshoot strongly depend on the permanence parameter. OECD countries, as an aggregate, are expected to slightly benefit due to increasing GDP in both scenarios, whereas non-OECD countries are expected to experience substantial negative consequences for their economies that are even more sever in the scenario with full overshoot. The positive impact on the OECD is due to the hump-shaped quadratic function, where many regions in OECD countries at higher latitudes benefit from moderate temperature increases. Non-OECD countries already experience temperatures exceeding the optimal level and, therefore, additional warming as well as a temperature overshoot aggravate the negative effect on GDP (Figure 8b).

Under the minimal overshoot scenario the relative reduction of global GDP stabilizes (5-year permanence) or keeps on growing slightly (15-year permanence), whereas the difference peaks in the overshoot scenario in the second half of the 21st century and by 2100 a substantial gap still remains that depends on the assumed permanence. In case of 5-year permanence the global GDP reduction in the scenario without overshoot is expected to grow to 2% in 2060 stabilizing afterwards, while it peaks at 3.2% in case with full overshoot and converges slowly towards the no-overshoot case. For a 15-year persistence without overshoot the overall GDP effect more than doubles and the gap continues to

grow until 2100 despite temperature differences converging. Again, the effects in non-OECD countries are substantially stronger than the global average. Overall, the permanence parameter is crucial because it suggests to limit global warming to low levels and to avoid the temperature to overshoot.

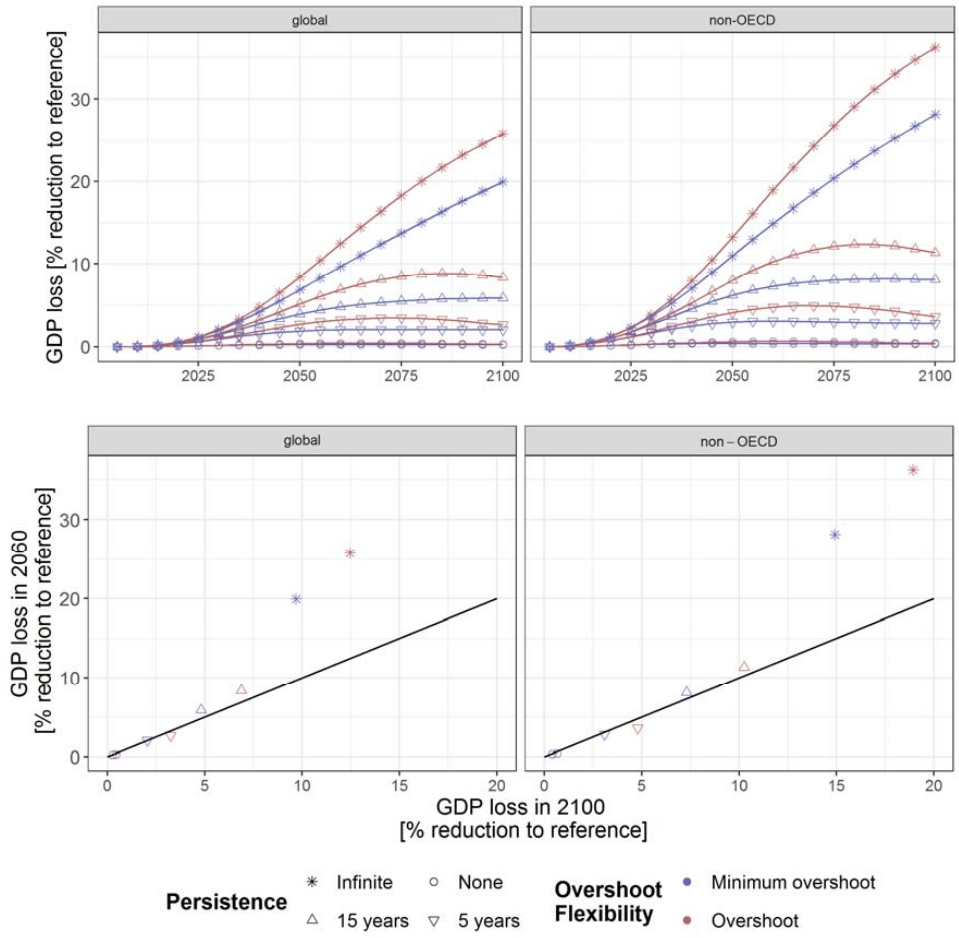

Figure 8: Macroeconomic damages as a percentage of GDP for the world and the aggregate of non-OECD countries differentiated by the overshoot flexibility and the assumption about persistence of damages." Infinite" and "none" represent the extreme values, whereas 5 and 15 year persistence are in the range of modelled and estimated values.

Assumptions about permanence parameter are highly uncertain. Burke et al. (2015) implicitly assumed infinite persistence. Econometric estimations found that tropical cyclone events have on average a persistent negative impact on GDP exceeding 15 years (Hsiang and Jina, 2014; Krichene et al., 2021). So far, econometric research has not uncovered the mechanisms that cause the permanent GDP reduction in the years following temperature anomalies. Theoretical and quantitative model research has shown that the alternative approaches of modeling economic damages matters because different macroeconomic transmission channels lead to broadly different transmission channels. An equivalent GDP reduction following a shock results in permanence between 3 and 40 years (Piontek et al., 2019).

Improved economic estimations are required to better understand the immediate economic impact as well as the longer-lasting macroeconomic adjustment processes.

Lifetime extreme event exposure is also sensitive to the carbon budget overshoot. Figure 9(a) depicts a substantial increase of total global land area affected by heat waves in the non-overshoot scenario and at maximum it is two thirds higher in the full overshoot scenario. Figure 9(b) shows the cumulative effect on people being born or having reached the age of 60 in 2020; while Figure 9(c) depicts the results for all cohorts in between. Under the no-overshoot scenario newborns in 2020 will be exposed five times more to heat waves during their lifetime than people aged 60 years in 2020. This value increase by 25% for newborns as a result of the carbon budget overshoot. The comparison of countries differentiated by income groups in Figure 9(d-g) shows that the additional heatwave exposure is already higher and increases more strongly in lower-middle income countries than in high-income countries. This pattern is pronounced for newborns and young people. In low-income countries the life expectancy is substantially lower and, therefore, the curve flattens out for people being relatively old today. As highlighted in Thiery et al. (2021) climate change is the dominant driver, while increasing life-expectancy is only a minor factor. Although temperature increases in tropical regions are smaller due to the polar amplification the increase of heat-wave frequency results from the already high exposure in these regions.

We find similar changes, albeit with less severe differences, for crops failures, droughts, river floods and tropical cyclones. The crops failure indicator shows reduced exposure in the full overshoot case, particularly in high income countries, due to the CO_2 fertilization effect. For wildfire exposure the uncertainty dominates. Higher income countries show a slight increase because they host a high share of boreal forests that are more sensitive than rain forests in tropical countries that typically enjoy lower incomes. Note: the modeling only includes wildfires caused by natural events, e.g. lightning, but not fires caused human activities.

Cumulative extreme event exposure over the lifespan of people provides a perspective on differences in their expected biographies. These differences can have potential knock-on effects on health, property and human capital formation (including schooling). Empirical research identified persistent effects of extreme events on socioeconomic variables in low-income countries (e.g., Groppo and Kraehnert, 2017).

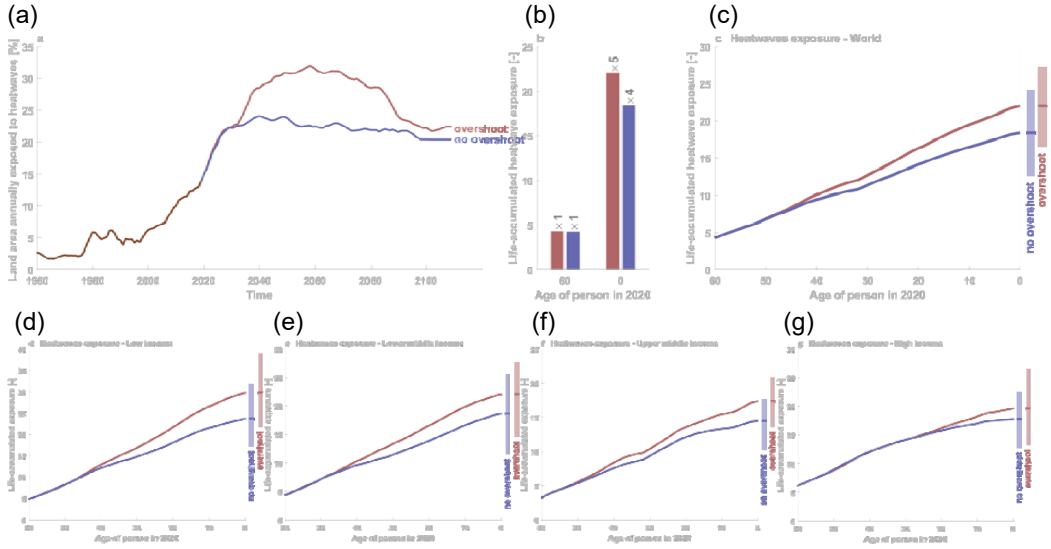

Figure 9: Lifetime exposure to extreme heatwaves under minimal and full overshoot. (a) Total land area annually exposed to extreme heat waves. (b) Lifetime heat wave exposure for different birth cohorts; and associated exposure multiplication factors relative to the 1960 birth cohort. (c) exposure multiplication factors relative to the 1960 birth cohort for all generations born between 1960 and 2020. (d-g) same as (c) but for different regions depending on per-capita income; note the different scaling on the vertical axes.

Discussion and Conclusion

The quest for a temporary overshoot of a long-term climate target in the context of the 1.5°C target needs to consider intertemporal trade-offs and differentiate them regionally. The assessment requires a broad multidisciplinary and comprehensive analysis that maps out various risks and benefits for a set of scenarios. So far, most studies focused on specific issues in separate, disciplinary analysis using scenarios that are not compatible with each other. Such a specialized, yet fragmented approach bears limitations. First, the scenarios are not harmonized and therefore magnitudes of effects are difficult to compare; this includes huge differences (i) the choice of overshooting temperature, CO_2 concentration or cumulative emissions, (ii) the duration and magnitude of the overshoot and (iii) treatment of other climate forcers than only CO_2 as well as land-use change. Second, the systems under investigation and the geographical and temporal boundaries and resolution differ.

In this study we have harmonized the scenarios and included emissions of CO_2, other GHG, other short-lived climate forcers and land-use changes. The resulting overshoot of 700GtCO_2 or 0.35°C is at the upper end of the scenarios assessed by the WG3 of the IPCC, but still smaller than many studies used for assessing additional climate risks. Our analysis is summarized in Table 1, with four major findings.

First, global climate variables show no or only small differences at the end of the 21st century; For instance, by 2100 80% of the peak GMT difference is closed. However, differentiation of the climate system identifies path-dependencies, e.g., the polar amplification remains more persistent than GMT anomalies. Also, CO_2-concentrations in both scenarios are similar in 2100, but additional loss of soil carbon from permafrost thawing is off-set by stronger CO_2 fertilization of the vegetation carbon stock and more ocean carbon up-take. The global temperature overshoot triggers a variety of mostly regional effects, such as sea ice losses, slowing of the meridional overturning and lower coral calcification rates. Global sea level rise is a notable special case. Antarctic ice sheet melting can overtake thermosteric expansion as the major driver after 2100. This is subject to uncertainties about the strength and persistence of polar amplification of global warming and the response of the southern oceans. Thus, a carbon budget overshoot scenario of the magnitude and duration we explored in this study will lead to only small residual relative differences of global climate variables in 2100, like global mean temperature, but there can be more notable and persistent differences in key climatic and environmental sub-systems that vary regionally.

Second, many impacts strongly depend on the global temperature trajectory causing path-dependent processes in socioeconomic systems, particularly in tropical regions with high base year temperatures. Regarding extreme weather event the overshoot can increase life time exposure for young generations substantially with various knock-on effects such as potential reductions of human capital formation. Furthermore, negative impacts on GDP can cumulate and lead to persistent differences. Also here, countries with the disadvantage of high base year temperature are more affected, despite the comparatively smaller temperature increase. Spatial heterogeneity is crucial because countries in the most sensitive regions are developing and emerging economies, typically non-OECD countries, with comparatively lower per-capita incomes.

Third, on the mitigation side non-OECD countries also respond more sensitively to variations of the overshoot. Until 2100 both scenarios lead to similar amounts of cumulative carbon removals but to remarkable differences in land-use, with more afforestation in case with no-overshoot but less removals relying on BECCS. Furthermore, limiting the overshoot requires stronger near-term emission reductions and removals, which causes substantially higher near-term GDP losses with much larger differences in non-OECD countries. The differences turn into a slight benefit of limiting the overshoot after 2050. Thus, the trade-offs between short term mitigation costs and longer-term impacts and damages are stronger in developing and emerging economies than in OECD countries.

Fourth, additional CO_2 emissions in the overshoot scenario act very differently in terrestrial and marine systems. While the terrestrial vegetation is fertilized, marine ecosystems like coral reefs are subject to diminishing natural resilience due to ocean acidification that adds to the additional pressure

of increasing sea surface temperatures. When the impacts of the overshoot propagate into the deeper ocean, they will persist for centuries to millenia (Mathesius et al., 2015), even after the scenarios converge for GMT and CO_2. For the scenarios studied here the major differences in terrestrial vegetation are triggered by human activities like afforestation and reduced deforestation, while marine environments can be strongly affected by the changes in temperatures and CO_2-concentrations. While we can manage and mitigate the terrestrial biosphere to a certain extent we depend on the functioning of the ocean in the short- and long-term.

Future overshoot assessments can benefit from deepening model integration in four areas. First, the mitigation and removal scenarios require improved framing to fully represent the diversity and heterogeneity of socioeconomic systems. The requirement for equitable mitigation burden sharing can lead to very different global scale and regional allocation of CDR (Bauer et al. 2020a). Second, inclusion of additional direct human forcers with spatial resolution help to assess systems under multiple pressures, including nitrogen use, overfishing, water and air pollution, and dam building. Potentially large-scale changes in land use deserve additional analysis, including local climate feedbacks, e.g, UVic results indicate that land-use patterns cause differences in precipitation due to evapotranspiration differences. Furthermore, EMICs can provide useful insights on process interactions in the global terrestrial and marine carbon cycle that allow to study net effects of overshoot scenarios on biogeochemical cycles interacting with climate (e.g., Drüke et al. 2021). Third, overshoot magnitude and duration need to be consistent between IAM scenarios and subsequent ESM evaluation. Fourth, the large and near-term land-use related CDR deployment, particularly in the low-overshoot scenario, requires more in-depth investigation, including biodiversity and socioeconomic consequences.

Models can derive an increasing amount of information. Integrative analysis frameworks are needed to enhance the quantification of trade-offs and uncertainties. Our analysis shows that it is not only important to consider systems' dynamics and lock-ins, but also to represent regional and spatial dimensions to improve the understanding of the various distributional issues and trade-offs. Our analysis suggests that the quest of overshooting the carbon budget implies strong trade-offs between mitigation costs and impacts for developing and emerging economies. Future analysis needs to embed the model analysis into a broader assessment framework that includes aggregate welfare metrics as well as multi-indicator frameworks, e.g., the Sustainable Development Indicators (SDG) as a basis.

515 Table 1: Summary of results regarding temporal and geographical differences between scenarios. Vegetation car

System	Component	Indicator	Minimum Overshoot	Full Overshoot	Persistency in 2100	Regiona
Mitigation	Overshoot	Max. cumulative emissions above carbon budget	50 $GtCO_2$	700 $GtCO_2$	none, by assumption	
	CDR deployment	Cumulative carbon removal 2020-2100	800 $GtCO_2$	950 $GtCO_2$	Storage is assumed permanente; persistent land-use changes	With Low ov in tropical co
	Climate policy	Carbon price in 2030	50 USD/tCO_2	540 USD/tCO_2	Relative difference constant by assumption	Uniform
	Mitigation costs	Reduction in GDP from baseline	1.2%	3.5%	Near- and mid-term losses major effect; reversal after 2050	With low ove 1.2%, but no
Climate system	Carbon cycle	Peak CO_2-concentration	424 ppmv in 2030	474 ppmv in 2050	with full overshoot CO_2 concentration is slightly lower	Uniformly mi
		Change of $GtCO_2$ in pools 2020-2100	Vegetation +174, permafrost -58 soil -183, ocean +336, sum = +269	Vegetation +112, permafrost -80, soil -136, ocean +407, total +303	Vegetation reversible, permafrost persistent, Ocean slowly reversible	Persistent ch pools that ne
	Global mean temperature	GMT in 2065	1.4°C (-0.2; +0.4)	1.8°C (-0.2; +0.4)	20% of peak difference	Polar amplifi portional, pa
	Ocean heat content	Anomaly in 2080	$0.67*10^{24}$ Joule	$0.88*10^{24}$ Joule	>90% of peak difference	Polar amplifi to deeper lay
	Sea ice	Arctic sea ice area	0.4 million km2 drop from 2020	0.61 Million km² further reduction	40% of peak difference remaining	Arctic effect
	Meridional overturning	Reduction compared to 2020	1 Sv in 2100	0.88 Sv in 2100 further reduction	Fully persistent, convergence by 2100	Atlantic ocea
	Sea Level Rise	Increase compared to 2020	39.7 cm in 2100	Additional 3.6 cm in 2100	No convergence between scenarios before 2100	SLR global, affects high a
Eco-system	Maritime ecosystems, coral reefs	Drop of calcification rate in 2065 below 1850 levels	Up to 40%	Up to 50%	Near full reversibility; coral stocks might show different behaviour	Tropical regi Asia, Austral
	Vegetation	Carbon density	Concentrated changes due to land-use change (e.g. affeorestation)	No additional climate induced losses from overshoot	More forest carbon stocks in low-overshoot scenario	largest chang high afforest
Impacts and Damages	Lifetime exposure to climate extremes	Projected lfetime exposure by age cohorts in 2020	Substantial increase of cumulative extreme weather event exposure, particularly heat waves	Significantly stronger heat wave exposure	Cumulative effects can affect socioeconomic developments (human capital) in the long-run	Hot countries affected mor
	GDP reductions	% GDP reduction from baseline	5yr perm.: 2.1% in 2070 15yr perm.: 5.9% in 2100	5yr perm.: 3.4% in 2070 15yr perm.: 8.3% in 2100	5yr perm.: 45% of peak difference 15yr perm.: no convergence	Non-OECD v 2060 and 0.8

516

References

Albright, R., Caldeira, L., Hosfelt, J., Kwiatkowski, L., Maclaren, J.K., Mason, B.M., Nebuchina, Y., Ninokawa, A., Pongratz, J., Ricke, K.L., Rivlin, T., Schneider, K., Sesboüé, M., Shamberger, K., Silverman, J., Wolfe, K., Zhu, K., Caldeira, K., 2016. Reversal of ocean acidification enhances net coral reef calcification. Nature 531, 362–365. https://doi.org/10.1038/nature17155

Aschwanden, A., Bartholomaus, T.C., Brinkerhoff, D.J., Truffer, M., 2021. Brief communication: A roadmap towards credible projections of ice sheet contribution to sea level. The Cryosphere 15, 5705–5715. https://doi.org/10.5194/tc-15-5705-2021

Bauer, N., Rose, S.K., Fujimori, S., van Vuuren, D.P., Weyant, J., Wise, M., Cui, Y., Daioglou, V., Gidden, M.J., Kato, E., Kitous, A., Leblanc, F., Sands, R., Sano, F., Strefler, J., Tsutsui, J., Bibas, R., Fricko, O., Hasegawa, T., Klein, D., Kurosawa, A., Mima, S., Muratori, M., 2018. Global energy sector emission reductions and bioenergy use: overview of the bioenergy demand phase of the EMF-33 model comparison. Climatic Change. https://doi.org/10.1007/s10584-018-2226-y

Bauer, N., Bertram, C., Schultes, A., Klein, D., Luderer, G., Kriegler, E., Popp, A., Edenhofer, O., 2020a. Quantification of an efficiency–sovereignty trade-off in climate policy. Nature 588, 261–266. https://doi.org/10.1038/s41586-020-2982-5

Bauer, N., Klein, D., Humpenöder, F., Kriegler, E., Luderer, G., Popp, A., Strefler, J., 2020b. Bio-energy and CO_2 emission reductions: an integrated land-use and energy sector perspective. Clim. Change. https://doi.org/10.1007/s10584-020-02895-z

Boucher, O., Halloran, P.R., Burke, E.J., Doutriaux-Boucher, M., Jones, C.D., Lowe, J., Ringer, M.A., Robertson, E., Wu, P., 2012. Reversibility in an Earth System model in response to CO_2 concentration changes. Environ. Res. Lett. 7, 024013. https://doi.org/10.1088/1748-9326/7/2/024013

Bueler, E., Brown, J., 2009. Shallow shelf approximation as a "sliding law" in a thermomechanically coupled ice sheet model. J. Geophys. Res. 114, F03008. https://doi.org/10.1029/2008JF001179

Burke, M., Hsiang, S.M., Miguel, E., 2015. Global non-linear effect of temperature on economic production. Nature 527, 235–239. https://doi.org/10.1038/nature15725

Calov, R., Greve, R., 2005. A semi-analytical solution for the positive degree-day model with stochastic temperature variations. J. Glaciol. 51, 173–175. https://doi.org/10.3189/172756505781829601

Dellink, R., Chateau, J., Lanzi, E., Magné, B., 2017. Long-term economic growth projections in the Shared Socioeconomic Pathways. Glob. Environ. Change 42, 200–214. https://doi.org/10.1016/j.gloenvcha.2015.06.004

Drijfhout, S., Bathiany, S., Beaulieu, C., Brovkin, V., Claussen, M., Huntingford, C., Scheffer, M., Sgubin, G., Swingedouw, D., 2015. Catalogue of abrupt shifts in Intergovernmental Panel on Climate Change climate models. Proc Natl Acad Sci USA 112, E5777–E5786. https://doi.org/10.1073/pnas.1511451112

Drüke, M., von Bloh, W., Petri, S., Sakschewski, B., Schaphoff, S., Forkel, M., Huiskamp, W., Feulner, G., Thonicke, K., 2021. CM2Mc-LPJmL v1.0: biophysical coupling of a process-based dynamic vegetation model with managed land to a general circulation model. Geosci. Model Dev. 14, 4117–4141. https://doi.org/10.5194/gmd-14-4117-2021

559 Drouet, L., Bosetti, V., Padoan, S.A., Aleluia Reis, L., Bertram, C., Dalla Longa, F., Després, J.,
560 Emmerling, J., Fosse, F., Fragkiadakis, K., Frank, S., Fricko, O., Fujimori, S., Harmsen, M., Krey,
561 V., Oshiro, K., Nogueira, L.P., Paroussos, L., Piontek, F., Riahi, K., Rochedo, P.R.R., Schaeffer, R.,
562 Takakura, J., van der Wijst, K.-I., van der Zwaan, B., van Vuuren, D., Vrontisi, Z., Weitzel, M.,
563 Zakeri, B., Tavoni, M., 2021. Net zero-emission pathways reduce the physical and economic
564 risks of climate change. Nat. Clim. Chang. 11, 1070–1076. https://doi.org/10.1038/s41558-
565 021-01218-z

566 Friedlingstein, P., Meinshausen, M., Arora, V.K., Jones, C.D., Anav, A., Liddicoat, S.K., Knutti, R., 2014.
567 Uncertainties in CMIP5 Climate Projections due to Carbon Cycle Feedbacks. J. Clim. 27, 511–
568 526. https://doi.org/10.1175/JCLI-D-12-00579.1

569 Friedlingstein, P., Jones, M.W., O'Sullivan, M., Andrew, R.M., Bakker, D.C.E., Hauck, J., Le Quéré, C.,
570 Peters, G.P., Peters, W., Pongratz, J., Sitch, S., Canadell, J.G., Ciais, P., Jackson, R.B., Alin, S.R.,
571 Anthoni, P., Bates, N.R., Becker, M., Bellouin, N., Bopp, L., Chau, T.T.T., Chevallier, F., Chini,
572 L.P., Cronin, M., Currie, K.I., Decharme, B., Djeutchouang, L., Dou, X., Evans, W., Feely, R.A.,
573 Feng, L., Gasser, T., Gilfillan, D., Gkritzalis, T., Grassi, G., Gregor, L., Gruber, N., Gürses, Ö.,
574 Harris, I., Houghton, R.A., Hurtt, G.C., Iida, Y., Ilyina, T., Luijkx, I.T., Jain, A.K., Jones, S.D., Kato,
575 E., Kennedy, D., Klein Goldewijk, K., Knauer, J., Korsbakken, J.I., Körtzinger, A., Landschützer,
576 P., Lauvset, S.K., Lefèvre, N., Lienert, S., Liu, J., Marland, G., McGuire, P.C., Melton, J.R., Munro,
577 D.R., Nabel, J.E.M.S., Nakaoka, S.-I., Niwa, Y., Ono, T., Pierrot, D., Poulter, B., Rehder, G.,
578 Resplandy, L., Robertson, E., Rödenbeck, C., Rosan, T.M., Schwinger, J., Schwingshackl, C.,
579 Séférian, R., Sutton, A.J., Sweeney, C., Tanhua, T., Tans, P.P., Tian, H., Tilbrook, B., Tubiello, F.,
580 van der Werf, G., Vuichard, N., Wada, C., Wanninkhof, R., Watson, A., Willis, D., Wiltshire, A.J.,
581 Yuan, W., Yue, C., Yue, X., Zaehle, S., Zeng, J., 2021. Global Carbon Budget 2021 (preprint).
582 Antroposphere – Energy and Emissions. https://doi.org/10.5194/essd-2021-386

583 Frieler, K., Meinshausen, M., Golly, A., Mengel, M., Lebek, K., Donner, S.D., Hoegh-Guldberg, O., 2013.
584 Limiting global warming to 2 °C is unlikely to save most coral reefs. Nature Clim Change 3,
585 165–170. https://doi.org/10.1038/nclimate1674

586 Frölicher, T.L., Fischer, E.M., Gruber, N., 2018. Marine heatwaves under global warming. Nature 560,
587 360–364. https://doi.org/10.1038/s41586-018-0383-9

588 Garbe, J., Albrecht, T., Levermann, A., Donges, J.F., Winkelmann, R., 2020. The hysteresis of the
589 Antarctic Ice Sheet. Nature 585, 538–544. https://doi.org/10.1038/s41586-020-2727-5

590 Groppo, V., Kraehnert, K., 2017. The impact of extreme weather events on education. J Popul Econ 30,
591 433–472. https://doi.org/10.1007/s00148-016-0628-6

592 Heck, V., Gerten, D., Lucht, W., Popp, A., 2018. Biomass-based negative emissions difficult to reconcile
593 with planetary boundaries. Nature Climate Change 8, 151–155.
594 https://doi.org/10.1038/s41558-017-0064-y

595 Hewitt, A.J., Booth, B.B.B., Jones, C.D., Robertson, E.S., Wiltshire, A.J., Sansom, P.G., Stephenson, D.B.,
596 Yip, S., 2016. Sources of Uncertainty in Future Projections of the Carbon Cycle. J. Clim. 29,
597 7203–7213. https://doi.org/10.1175/JCLI-D-16-0161.1

598 Hofmann, M., Mathesius, S., Kriegler, E., Vuuren, D.P. van, Schellnhuber, H.J., 2019. Strong time
599 dependence of ocean acidification mitigation by atmospheric carbon dioxide removal. Nat
600 Commun 10, 5592. https://doi.org/10.1038/s41467-019-13586-4

601 Hoffman, F.M., Randerson, J.T., Arora, V.K., Bao, Q., Cadule, P., Ji, D., Jones, C.D., Kawamiya, M.,
602 Khatiwala, S., Lindsay, K., Obata, A., Shevliakova, E., Six, K.D., Tjiputra, J.F., Volodin, E.M., Wu,
603 T., 2014. Causes and implications of persistent atmospheric carbon dioxide biases in Earth
604 System Models. J. Geophys. Res. Biogeosciences 119, 141–162.
605 https://doi.org/10.1002/2013JG002381

606 Hsiang, S.M., Jina, A.S., 2014. The Causal Effect of Environmental Catastrophe on Long-Run Economic
607 Growth: Evidence From 6,700 Cyclones (Working Paper No. 20352). National Bureau of
608 Economic Research. https://doi.org/10.3386/w20352

609 Hughes, T.P., Anderson, K.D., Connolly, S.R., Heron, S.F., Kerry, J.T., Lough, J.M., Baird, A.H., Baum,
610 J.K., Berumen, M.L., Bridge, T.C., Claar, D.C., Eakin, C.M., Gilmour, J.P., Graham, N.A.J.,
611 Harrison, H., Hobbs, J.-P.A., Hoey, A.S., Hoogenboom, M., Lowe, R.J., McCulloch, M.T.,
612 Pandolfi, J.M., Pratchett, M., Schoepf, V., Torda, G., Wilson, S.K., 2018. Spatial and temporal
613 patterns of mass bleaching of corals in the Anthropocene. Science 359, 80–83.
614 https://doi.org/10.1126/science.aan8048

615 Johansson, D.J.A., Azar, C., Lehtveer, M., Peters, G.P., 2020. The role of negative carbon emissions in
616 reaching the Paris climate targets: The impact of target formulation in integrated assessment
617 models. Environ. Res. Lett. 15, 124024. https://doi.org/10.1088/1748-9326/abc3f0

618 Jones, C.D., Ciais, P., Davis, S.J., Friedlingstein, P., Gasser, T., Peters, G.P., Rogelj, J., Vuuren, D.P. van,
619 Canadell, J.G., Cowie, A., Jackson, R.B., Jonas, M., Kriegler, E., Littleton, E., Lowe, J.A., Milne, J.,
620 Shrestha, G., Smith, P., A Torvanger, Wiltshire, A., 2016. Simulating the Earth system response
621 to negative emissions. Environ. Res. Lett. 11, 095012. https://doi.org/10.1088/1748-
622 9326/11/9/095012

623 KC, S., Lutz, W., 2017. The human core of the shared socioeconomic pathways: Population scenarios
624 by age, sex and level of education for all countries to 2100. Glob. Environ. Change 42, 181–
625 192. https://doi.org/10.1016/j.gloenvcha.2014.06.004

626 Krichene, H., Geiger, T., Frieler, K., Willner, S.N., Sauer, I., Otto, C., 2021. Long-term impacts of tropical
627 cyclones and fluvial floods on economic growth – Empirical evidence on transmission channels
628 at different levels of development. World Development 144, 105475.
629 https://doi.org/10.1016/j.worlddev.2021.105475

630 Kriegler, E., Weyant, J.P., Blanford, G.J., Krey, V., Clarke, L., Edmonds, J., Fawcett, A., Luderer, G., Riahi,
631 K., Richels, R., Rose, S.K., Tavoni, M., Vuuren, D.P. van, 2014. The role of technology for
632 achieving climate policy objectives: overview of the EMF 27 study on global technology and
633 climate policy strategies. Clim. Change 123, 353–367. https://doi.org/10.1007/s10584-013-
634 0953-7

635 Kriegler, E., Bauer, N., Popp, A., Humpenöder, F., Leimbach, M., Strefler, J., Baumstark, L., Bodirsky,
636 B.L., Hilaire, J., Klein, D., Mouratiadou, I., Weindl, I., Bertram, C., Dietrich, J.-P., Luderer, G., Pehl,
637 M., Pietzcker, R., Piontek, F., Lotze-Campen, H., Biewald, A., Bonsch, M., Giannousakis, A.,
638 Kreidenweis, U., Müller, C., Rolinski, S., Schultes, A., Schwanitz, J., Stevanovic, M., Calvin, K.,
639 Emmerling, J., Fujimori, S., Edenhofer, O., 2017. Fossil-fueled development (SSP5): An energy
640 and resource intensive scenario for the 21st century. Global Environmental Change 42, 297–
641 315. https://doi.org/10.1016/j.gloenvcha.2016.05.015
642
643 Lange, S., Volkholz, J., Geiger, T., Zhao, F., Vega, I., Veldkamp, T., Reyer, C.P.O., Warszawski, L., Huber,
644 V., Jägermeyr, J., Schewe, J., Bresch, D.N., Büchner, M., Chang, J., Ciais, P., Dury, M., Emanuel,
645 K., Folberth, C., Gerten, D., Gosling, S.N., Grillakis, M., Hanasaki, N., Henrot, A., Hickler, T.,
646 Honda, Y., Ito, A., Khabarov, N., Koutroulis, A., Liu, W., Müller, C., Nishina, K., Ostberg, S.,
647 Müller Schmied, H., Seneviratne, S.I., Stacke, T., Steinkamp, J., Thiery, W., Wada, Y., Willner, S.,
648 Yang, H., Yoshikawa, M., Yue, C., Frieler, K., 2020. Projecting Exposure to Extreme Climate
649 Impact Events Across Six Event Categories and Three Spatial Scales. Earths Future 8.
650 https://doi.org/10.1029/2020EF001616

651 MacDougall, A.H., 2013. Reversing climate warming by artificial atmospheric carbon-dioxide removal:
652 Can a Holocene-like climate be restored?: RETURN TO THE HOLOCENE. Geophys. Res. Lett. 40,
653 5480–5485. https://doi.org/10.1002/2013GL057467

Mathesius, S., Hofmann, M., Caldeira, K., Schellnhuber, H.J., 2015. Long-term response of oceans to CO_2 removal from the atmosphere. Nat. Clim. Change 5, 1107–1113. https://doi.org/10.1038/nclimate2729

Matthews, H.D., Gillett, N.P., Stott, P.A., Zickfeld, K., 2009. The proportionality of global warming to cumulative carbon emissions. Nature 459, 829–832. https://doi.org/10.1038/nature08047

Medley, B., Thomas, E.R., 2019. Increased snowfall over the Antarctic Ice Sheet mitigated twentieth-century sea-level rise. Nature Clim Change 9, 34–39. https://doi.org/10.1038/s41558-018-0356-x

Meinshausen, M., Meinshausen, N., Hare, W., Raper, S.C.B., Frieler, K., Knutti, R., Frame, D.J., Allen, M.R., 2009. Greenhouse-gas emission targets for limiting global warming to 2°C. Nature 458, 1158–1162. https://doi.org/10.1038/nature08017

Melnikova, I., Boucher, O., Cadule, P., Ciais, P., Gasser, T., Quilcaille, Y., Shiogama, H., Tachiiri, K., Yokohata, T., Tanaka, K., 2021. Carbon Cycle Response to Temperature Overshoot Beyond 2°C: An Analysis of CMIP6 Models. Earths Future 9. https://doi.org/10.1029/2020EF001967

Mengel, M., Levermann, A., Frieler, K., Robinson, A., Marzeion, B., Winkelmann, R., 2016. Future sea level rise constrained by observations and long-term commitment. Proc. Natl. Acad. Sci. U.S.A. 113, 2597–2602. https://doi.org/10.1073/pnas.1500515113

Mengis, N., Keller, D.P., MacDougall, A.H., Eby, M., Wright, N., Meissner, K.J., Oschlies, A., Schmittner, A., MacIsaac, A.J., Matthews, H.D., Zickfeld, K., 2020. Evaluation of the University of Victoria Earth System Climate Model version 2.10 (UVic ESCM 2.10). Geosci. Model Dev. 13, 4183–4204. https://doi.org/10.5194/gmd-13-4183-2020

Newell, R.G., Prest, B.C., Sexton, S.E., 2021. The GDP-Temperature relationship: Implications for climate change damages. J. Environ. Econ. Manag. 108, 102445. https://doi.org/10.1016/j.jeem.2021.102445

Palter, J.B., Frölicher, T.L., Paynter, D., John, J.G., 2017. Climate, ocean circulation, and sea level changes under stabilizationand overshoot pathways to 1.5 K warming (preprint). Earth system change: climate scenarios. https://doi.org/10.5194/esd-2017-105

Pihl, E., Alfredsson, E., Bengtsson, M., Bowen, K.J., Cástan Broto, V., Chou, K.T., Cleugh, H., Ebi, K., Edwards, C.M., Fisher, E., Friedlingstein, P., Godoy-Faúndez, A., Gupta, M., Harrington, A.R., Hayes, K., Hayward, B.M., Hebden, S.R., Hickmann, T., Hugelius, G., Ilyina, T., Jackson, R.B., Keenan, T.F., Lambino, R.A., Leuzinger, S., Malmaeus, M., McDonald, R.I., McMichael, C., Miller, C.A., Muratori, M., Nagabhatla, N., Nagendra, H., Passarello, C., Penuelas, J., Pongratz, J., Rockström, J., Romero-Lankao, P., Roy, J., Scaife, A.A., Schlosser, P., Schuur, E., Scobie, M., Sherwood, S.C., Sioen, G.B., Skovgaard, J., Sobenes Obregon, E.A., Sonntag, S., Spangenberg, J.H., Spijkers, O., Srivastava, L., Stammer, D.B., Torres, P.H.C., Turetsky, M.R., Ukkola, A.M., van Vuuren, D.P., Voigt, C., Wannous, C., Zelinka, M.D., 2021. Ten new insights in climate science 2020 – a horizon scan. Glob. Sustain. 4, e5. https://doi.org/10.1017/sus.2021.2

Piontek, F., Kalkuhl, M., Kriegler, E., Schultes, A., Leimbach, M., Edenhofer, O., Bauer, N., 2019. Economic Growth Effects of Alternative Climate Change Impact Channels in Economic Modeling. Environ. Resour. Econ. 73, 1357–1385. https://doi.org/10.1007/s10640-018-00306-7

Realmonte, G., Drouet, L., Gambhir, A., Glynn, J., Hawkes, A., Köberle, A.C., Tavoni, M., 2019. An inter-model assessment of the role of direct air capture in deep mitigation pathways. Nat. Commun. 10, 3277. https://doi.org/10.1038/s41467-019-10842-5

Reese, R., Albrecht, T., Mengel, M., Asay-Davis, X., Winkelmann, R., 2018. Antarctic sub-shelf melt rates via PICO. The Cryosphere 12, 1969–1985. https://doi.org/10.5194/tc-12-1969-2018

Riahi, K., Bertram, C., Huppmann, D., Rogelj, J., Bosetti, V., Cabardos, A.-M., Deppermann, A., Drouet, L., Frank, S., Fricko, O., Fujimori, S., Harmsen, M., Hasegawa, T., Krey, V., Luderer, G., Paroussos, L., Schaeffer, R., Weitzel, M., van der Zwaan, B., Vrontisi, Z., Longa, F.D., Després, J., Fosse, F., Fragkiadakis, K., Gusti, M., Humpenöder, F., Keramidas, K., Kishimoto, P., Kriegler, E., Meinshausen, M., Nogueira, L.P., Oshiro, K., Popp, A., Rochedo, P.R.R., Ünlü, G., van Ruijven, B., Takakura, J., Tavoni, M., van Vuuren, D., Zakeri, B., 2021. Cost and attainability of meeting stringent climate targets without overshoot. Nat. Clim. Chang. 11, 1063–1069. https://doi.org/10.1038/s41558-021-01215-2

Rogelj, J., Forster, P.M., Kriegler, E., Smith, C.J., Séférian, R., 2019. Estimating and tracking the remaining carbon budget for stringent climate targets. Nature 571, 335–342. https://doi.org/10.1038/s41586-019-1368-z

Rogelj, J., Shindell, D., Jiang, K., Fifita, S., Forster, P., Ginzburg, V., Handa, C., Kheshgi, H., Kobayashi, S., Kriegler, E., Mundaca, L., Seferian, R., Vilarino, M.V., Calvin, K., Edelenbosch, O., Emmerling, J., Fuss, S., Gasser, T., Gillet, N., He, C., Hertwich, E., Höglund Isaksson, L., Huppmann, D., Luderer, G., Markandya, A., McCollum, D., Millar, R., Meinshausen, M., Popp, A., Pereira, J., Purohit, P., Riahi, K., Ribes, A., Saunders, H., Schadel, C., Smith, C., Smith, P., Trutnevyte, E., Xiu, Y., Zickfeld, K., Zhou, W., 2018. Chapter 2: Mitigation pathways compatible with 1.5°C in the context of sustainable development, in: Global Warming of 1.5 °C an IPCC Special Report on the Impacts of Global Warming of 1.5 °C above Pre-Industrial Levels and Related Global Greenhouse Gas Emission Pathways, in the Context of Strengthening the Global Response to the Threat of Climate Change. Intergovernmental Panel on Climate Change.

Schaphoff, S., von Bloh, W., Rammig, A., Thonicke, K., Biemans, H., Forkel, M., Gerten, D., Heinke, J., Jägermeyr, J., Knauer, J., Langerwisch, F., Lucht, W., Müller, C., Rolinski, S., Waha, K., 2018. LPJmL4 – a dynamic global vegetation model with managed land – Part 1: Model description. Geosci. Model Dev. 11, 1343–1375. https://doi.org/10.5194/gmd-11-1343-2018

Schultes, A., Piontek, F., Soergel, B., Rogelj, J., Baumstark, L., Kriegler, E., Edenhofer, O., Luderer, G., 2021. Economic damages from on-going climate change imply deeper near-term emission cuts. Environ. Res. Lett. 16, 104053. https://doi.org/10.1088/1748-9326/ac27ce

Smith, P., Davis, S.J., Creutzig, F., Fuss, S., Minx, J., Gabrielle, B., Kato, E., Jackson, R.B., Cowie, A., Kriegler, E., van Vuuren, D.P., Rogelj, J., Ciais, P., Milne, J., Canadell, J.G., McCollum, D., Peters, G., Andrew, R., Krey, V., Shrestha, G., Friedlingstein, P., Gasser, T., Grübler, A., Heidug, W.K., Jonas, M., Jones, C.D., Kraxner, F., Littleton, E., Lowe, J., Moreira, J.R., Nakicenovic, N., Obersteiner, M., Patwardhan, A., Rogner, M., Rubin, E., Sharifi, A., Torvanger, A., Yamagata, Y., Edmonds, J., Yongsung, C., 2015. Biophysical and economic limits to negative CO_2 emissions. Nat. Clim. Change 6, 42–50. https://doi.org/10.1038/nclimate2870

Strauss, B.H., Orton, P.M., Bittermann, K., Buchanan, M.K., Gilford, D.M., Kopp, R.E., Kulp, S., Massey, C., Moel, H. de, Vinogradov, S., 2021. Economic damages from Hurricane Sandy attributable to sea level rise caused by anthropogenic climate change. Nat Commun 12, 2720. https://doi.org/10.1038/s41467-021-22838-1

Strefler, J., Kriegler, E., Bauer, N., Luderer, G., Pietzcker, R.C., Giannousakis, A., Edenhofer, O., 2021a. Alternative carbon price trajectories can avoid excessive carbon removal. Nature Communications 12. https://doi.org/10.1038/s41467-021-22211-2

Strefler, J., Bauer, N., Humpenöder, F., Klein, D., Popp, A., Kriegler, E., 2021b. Carbon dioxide removal technologies are not born equal. Environ. Res. Lett. 16, 074021. https://doi.org/10.1088/1748-9326/ac0a11

Sully, S., Burkepile, D.E., Donovan, M.K., Hodgson, G., van Woesik, R., 2019. A global analysis of coral bleaching over the past two decades. Nat Commun 10, 1264. https://doi.org/10.1038/s41467-019-09238-2

Thiery, W., Lange, S., Rogelj, J., Schleussner, C.-F., Gudmundsson, L., Seneviratne, S.I., Andrijevic, M., Frieler, K., Emanuel, K., Geiger, T., Bresch, D.N., Zhao, F., Willner, S.N., Büchner, M., Volkholz, J., Bauer, N., Chang, J., Ciais, P., Dury, M., François, L., Grillakis, M., Gosling, S.N., Hanasaki, N., Hickler, T., Huber, V., Ito, A., Jägermeyr, J., Khabarov, N., Koutroulis, A., Liu, W., Lutz, W., Mengel, M., Müller, C., Ostberg, S., Reyer, C.P.O., Stacke, T., Wada, Y., 2021. Intergenerational inequities in exposure to climate extremes. Science 374, 158–160. https://doi.org/10.1126/science.abi7339

Tokarska, K.B., Zickfeld, K., 2015. The effectiveness of net negative carbon dioxide emissions in reversing anthropogenic climate change. Environ. Res. Lett. 10, 094013. https://doi.org/10.1088/1748-9326/10/9/094013

Trisos, C.H., Merow, C., Pigot, A.L., 2020. The projected timing of abrupt ecological disruption from climate change. Nature 580, 496–501. https://doi.org/10.1038/s41586-020-2189-9

Winkelmann, R., Martin, M.A., Haseloff, M., Albrecht, T., Bueler, E., Khroulev, C., Levermann, A., 2011. The Potsdam Parallel Ice Sheet Model (PISM-PIK) – Part 1: Model description. The Cryosphere 5, 715–726. https://doi.org/10.5194/tc-5-715-2011

Zickfeld, K., Azevedo, D., Mathesius, S., Matthews, H.D., 2021. Asymmetry in the climate–carbon cycle response to positive and negative CO_2 emissions. Nat. Clim. Change 11, 613–617. https://doi.org/10.1038/s41558-021-01061-2

Zickfeld, K., MacDougall, A.H., Matthews, H.D., 2016. On the proportionality between global temperature change and cumulative CO 2 emissions during periods of net negative CO 2 emissions. Environ. Res. Lett. 11, 055006. https://doi.org/10.1088/1748-9326/11/5/055006

Zeitz, M., Reese, R., Beckmann, J., Krebs-Kanzow, U., and Winkelmann, R.: Impact of the melt–albedo feedback on the future evolution of the Greenland Ice Sheet with PISM-dEBM-simple, The Cryosphere, 15, 5739–5764, https://doi.org/10.5194/tc-15-5739-2021, 2021.

Acknowledgements

Development of PISM is supported by NSF grants PLR-1603799 and PLR-1644277 and NASA grant NNX17AG65G. D. P. Keller, Dr. Jessica Strefler and N. Bauer received funding from the German Research Foundation's Priority Program SPP 1689 "Climate Engineering" (CDR-MIA project KE 2149/2-1).

3 Results

In order to asses the dominant drivers of the future sea level contribution from the tipping of the Greenland Ice Sheet, it is central to gain a better understanding of the interplay between ice flow, ice melt and isostatic rebound. The aim of my dissertation is to advance the knowledge of the ice sheet's response to and its resilience against global warming with respect to these processes. An overview of the relevant processes studied in this thesis is given in Figure 1.3. These results can be summarized by considering their contribution to uncertainty as well as by feedback analysis, as done in Section 3.1 and Section 3.2. The implications for future sea level rise are briefly discussed in Section 3.3.

In the following sections, I will discuss the main findings and put them into context.

3.1 Uncertainties associated with ice sheet modeling in Greenland

A major part of this thesis focuses on uncertainties associated with the modeling of the Greenland Ice Sheet. These are particularly important when it comes to future sea level rise projections, since communities and stake holders need to prepare not only for the most probable impacts but also for the full range of uncertainties. In the Ice Sheet Model Intercomparison Project (ISMIP6), Goelzer et al. (2020) find that the projected sea level rise from the Greenland Ice Sheet in the time 2015 - 2100 in an RCP8.5 scenario is 90 ± 50 mm. The major part of the uncertainty (40 mm) can be attributed to differences between ice sheet models, while the spread in the forcing from different climate and ocean models is responsible for 36 mm and 19 mm, respectively. Aschwanden, Fahnestock, Truffer, et al. (2019) also perform a comprehensive uncertainty quantification, showing that up to 53% of the uncertainty are caused by uncertain ice dynamics parameters, in particular related to the basal motion, and uncertainties in the melt may contribute up to 50%.

In this section, I will first explore the effect of uncertainties in flow parameters,

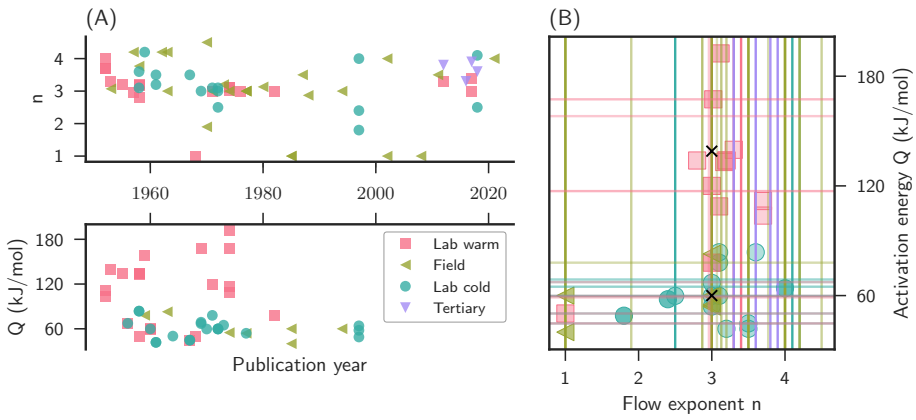

Figure 3.1: (A) Summary of literature values of the flow exponent n and the activation energy Q sorted by the time of the publication. The colors and symbols denote if the value was derived by lab experiments under warm (pink squares) or cold (blue circles) conditions, or in the field (green triangles). Lab experiments, which represent tertiary flow, are represented by violet triangles. (B) The same information summarized in a scatter plot. Data points represent publications, which report both, Q and n, lines represent publications which report only one of these parameters. The standard values used in most ice-sheet models are represented by the two black crosses (distinguishing between cold and warm ice). Colors and symbols are the same as in (A). Note that I did not distinguish between field experiments in regions, where the shallow shelf approximation or the shallow ice approximation can be applied.

then I will focus on uncertainties related to melt models and to the GIA response. The uncertainties addressed in this thesis, however, are not taken from sea level projections directly but from more idealized experiments, and therefore do not compare with the uncertainties mentioned above.

Uncertainties associated with the flow law of ice As described in Section 1.3, the representation of the flow of ice is at the heart of ice-sheet models projecting sea level rise. The first sub-project of my thesis aimed at assessing the uncertainty associated with flow parameters and its impacts.

I performed a major review of the literature over the last six decades on the flow of ice as described by *Glen's flow law* (Equation (1.1)) and its associated parameters (see Section 1.3.1 for the theoretical background). The experimental

measurements of the flow exponent n as well as the activation energies Q_w and Q_c show a substantial spread, which does not converge towards a consensus value over time, as seen in Figure 3.1. On the contrary, newer studies suggest that particularly the widely used flow law exponent of $n = 3$ is likely underestimated (Bons et al. 2018; Millstein et al. 2021).

Despite this uncertainty, most ice sheet modeling studies use the same standard set of flow parameters ($n = 3, Q_w = 139\,\text{kJ/mol}$, and $Q_c = 60\,\text{kJ/mol}$). The impact of the spread in these parameters on ice sheet modeling results had not been systematically studied and therefore the corresponding uncertainties are not represented in most sea level rise projections.

In **Manuscript 1** of my thesis (Chapter 2), I studied the impact of these uncertainties using an idealized, two-dimensional ice sheet sitting on a flat bed. In simulations with the Parallel Ice-Sheet Model (PISM) we varied the values of the flow exponent and the activation energies within the limits of published observations. In order to disentangle the uncertainty associated with flow-driven ice loss from uncertainties due to melt, the climatic mass balance is kept constant in these simulations. However, a warming anomaly applied at the ice surface leads to an increase in ice temperatures through heat transport. As the ice softness is highly temperature dependent, the ice softens and, in consequence, experiences higher deformation rates, and thus higher velocities, at the same applied stress level. Since the velocity of the ice increases, the flow-related ice loss also increases. The relative spread of flow-driven ice loss ΔV, that is $(\Delta V - \Delta V_0)/\Delta V_0$ after 100 years ranges from -50% to +150% compared to the reference simulation (here denoted ΔV_0). The spread is driven mainly by the variation of activation energies, which relate the softness of the ice to the temperature. In the parameterization used in this study, higher activation energies lead to softer ice at temperatures close to the pressure melting point, which in turn has the strongest impact on ice flow velocities. The relative uncertainty decreases over time, as the ice sheet reaches a new steady state in equilibrium with the new boundary condition, i.e., the changed ice-surface temperature. Thus, simulations with high activation energies seem to respond faster to warming, but eventually achieve similar steady states. In this experimental design, where we explicitly study the response of the ice to warming temperatures, the activation energies, relating ice softness to temperature have a stronger influence on the variation of flow-driven ice losses than the flow exponent n.

While uncertainties in the flow parameters could impact other relevant pro-

cesses, e.g. sliding conditions of the Greenland Ice Sheet (Bons et al. 2018), or the stability of grounding lines on retrograde slopes (Schoof 2007), the results of Manuscript 1 are not directly transferable to more realistic simulations of the Greenland Ice Sheet and the limitations of this approach are discussed more thoroughly in Section 4.1.3. In order to assess the full uncertainties in sea level rise projections, variations of the flow parameters should be systematically included in simulations.

Uncertainties associated with surface melt The accurate representation of present and future surface melt of the Greenland Ice Sheet in models is crucial for understanding present mass changes and future sea level rise. However, it is also associated with uncertainties in both, parameters and melt models. In **Manuscript 2** of my thesis, I studied surface melt of the Greenland Ice Sheet and the related uncertainties. To this end I implemented a simplified version of the diurnal Energy Balance Model (dEBM-simple) into the ice sheet model PISM (see Chapter 2). This melt model is as lightweight as the positive degree day (PDD) model, i.e., it only needs near-surface air temperatures as an input to calculate melt rates, however, in contrast to the PDD model it takes the contribution of insolation-driven melt into account (see Section 1.3.2).

The parameters of the melt model are optimized with respect to the output of the regional climate model MAR, however, substantial uncertainties remain. One of the most influential simplifying assumptions, and thus sources of uncertainty, in this model is the direct parameterization of albedo with local melt, neglecting other processes like the grain size evolution of snow. In this parameterization I assume, that the local albedo value can lie between the value of fresh snow (if the melt rate is zero) or bare ice (lower limit at high melt rates), and decreases linearly with increasing melt rates in between.

The uncertainty associated with this parameterization is explored via two variations: Motivated by the observations of dark zones in Greenland (Cook et al. 2020; Ryan, Hubbard, et al. 2018), I first vary the minimal value of the albedo, related to bare ice. Note that I do not explicitly model accumulation of algae or dust here, however a reduced ice albedo might serve as a proxy for those processes. Second, I vary the sensitivity of albedo to the melt rate while keeping the maximal and minimal albedo values fixed. This is motivated by the fact that the sensitivity increases throughout the melt period, as the snow pack diminishes and melt ponds accumulate.

Variations of the minimal albedo value have almost negligible effects in the RCP2.6 scenario, as the melt rates are not high enough to cause minimal albedo values in these experiments. When the bare ice albedo is reduced from 0.47 to 0.4 and 0.3 in the RCP8.5 scenarios, the ice sheet experiences 5.3 cm and 16.0 cm SLE more mass loss until 2300. Thus, in a warmer climate the change in bare ice albedo has a stronger impact on mass losses, compared to the same experiment in moderate climate warming.

In contrast, the effect of the albedo sensitivity parameter is more pronounced in the RCP2.6 experiment. Here, a change in albedo-to-melt sensitivity induces a spread between -34% and +40% with respect to the reference value in projected ice losses until 2300. Even though the variation of the albedo sensitivity has a strong influence on the absolute ice losses in the RCP8.5 scenario , the relative influence is less pronounced compared to the RCP2.6 scenario because of higher overall mass losses. The two warming scenarios differ in the main cause of uncertainty related to the parameterization of albedo changes. While in the moderate warming scenario (RCP2.6) the simulated ice loss is most responsive to variations in the sensitivity of albedo to melt rates, the minimal value for ice albedo is most important in the strong warming scenario (RCP8.5). Uncertainties related to surface melt should therefore always be discussed in the context of the warming scenario as the main driver of uncertainty can change with changing climate conditions and forcing.

Further uncertainties of the future melt rates of the Greenland Ice Sheet are associated with the atmospheric temperature lapse rate, which relates the changes in ice surface elevation to temperature changes. Ice sheet models typically assume the lapse rate to be spatially and temporally constant, however, in reality the lapse rate varies locally and there is a difference for dry and moist air. The free air moist adiabatic lapse rate ranges between 6-7 K/km, but is assumed to be higher if the air is less humid (Gardner, Sharp, et al. 2009). The mean slope lapse rate measured over Greenland, however, tends to be lower and shows seasonal variations (Fausto et al. 2009; Gardner, Sharp, et al. 2009; Hanna, Huybrechts, et al. 2005; Steffen and Box 2001). In order to represent the uncertainty in a model which does not include these seasonal and spatial variations, we vary the lapse rate between 5-7 K/km in **Manuscript 3**, where we explicitly study the impact of the melt-elevation feedback. Changes in the (spatially uniform) lapse rate can lead to qualitatively different responses of the Greenland Ice Sheet to warming, ranging from stabilization at a new equilibrium

to a total and irreversible ice loss under otherwise equal climatic conditions (see Section 3.2).

The uncertainties associated with melt model parameters are also explored in **Manuscript 4**, dealing with the effects of a temperature overshoot, which is still compatible with the Paris Agreement, on different parts of the Earth system and the economic system. We find that for Greenland's contribution to sea level rise the uncertainty of the melt model parameters is almost as important for mass loss as the difference between the two warming scenarios.

Uncertainties associated with GIA response In **Manuscript 3** of my thesis I study the dynamic regimes of the Greenland Ice Sheet arising from the interaction of the melt-elevation feedback and the GIA feedback (see Chapter 2). The GIA feedback is characterized by the lithosphere elasticity and the viscosity of the upper mantle in the solid Earth model. In the scope of this thesis I have focused particularly on the impact of the mantle viscosity. Measurement of bedrock uplift in Greenland suggest mantle viscosity values between $1 \cdot 10^{20} - 5 \cdot 10^{21}$ Pa $\cdot$ s , however, local values might vary even stronger: between $1 \cdot 10^{18}$ and $5 \cdot 10^{23}$ Pa $\cdot$ s (Fleming and Lambeck 2004; Khan et al. 2016; Lambeck et al. 2014; Larour et al. 2019; Lau et al. 2016; Le Meur and Huybrechts 1996; Le Meur and Huybrechts 1998; Lecavalier et al. 2014; Milne et al. 2018; Mordret 2018; Peltier and Drummong 2008; Tosi et al. 2005; Wahr et al. 2001). As the solid Earth model we are using assumes a horizontally and vertically constant viscosity, we chose to explore a slightly narrower range of viscosity values compared to the local observations, namely $1 \cdot 10^{19} - 5 \cdot 10^{21}$ Pa $\cdot$ s. The mantle viscosity mainly influences the time scale of the glacial isostatic adjustment and therefore has a large impact on the qualitative evolution of the Greenland Ice Sheet. In contrast, the lithosphere elasticity did not qualitatively change the response of the ice sheet to warming.

The interactions between the melt-elevation feedback and the GIA feedback lead to qualitatively different responses to warming over the range for upper mantle viscosity values. Therefore, a classical uncertainty analysis did not seem advisable. The results of this study will be discussed more thoroughly in the next Section 3.2 with focus on the feedbacks and their interactions.

3.2 Feedbacks and interactions relevant for the Greenland Ice Sheet

As discussed in Section 1.2, the processes governing the mass balance of the Greenland Ice Sheet interact with each other and sometimes form feedback loops. In my thesis, I specifically studied the following feedback loops: the melt-elevation feedback, the melt-albedo feedback, and the GIA feedback.

In **Manuscript 2** of my thesis, I studied the impact of the melt-albedo feedback (Box, Fettweis, et al. 2012; Box, Wehrlé, et al. 2022) on Greenland Ice Sheet mass loss under two future warming scenarios, RCP2.6 and RCP8.5. The newly implemented PISM-dEBM-simple includes insolation-driven melt and a representation of the melt-albedo feedback through a linear parameterization of the local albedo with melt. To study the effect of this feedback, we established a lower- and an upper-bound scenario. The lower-bound scenario assumes that the albedo does not change in response to increasing melt rates. Instead, it remains fixed at the monthly average values of the 1990s, which breaks the feedback loop. The upper-bound scenario explores the maximal impact of the albedo-driven melt: here we assume that the surface is dark (i.e., at the ice-albedo value) during the whole summer (June, July, and August), irrespective of the actual melt. That breaks the feedback loop again but locks the albedo at the lowest possible value during the entire melt period, defining a reasonable upper bound for albedo-driven mass losses. The feedback loop is closed again in the reference experiments, where the albedo is allowed to evolve in response to increasing warming and melt.

By comparing the reference scenario (closed feedback loop) to the lower-bound scenario (broken feedback loop, high albedo values), we can estimate the contribution of the melt-albedo feedback to mass losses in a warming scenario. Thus we find that the relative contribution of the melt-albedo feedback is higher for the RCP2.6 scenario, where ice losses in the reference scenario almost double compared to the lower-bound scenario. In the warmer RCP8.5 reference scenario, the absolute increase in mass loss due to the melt-albedo feedback is higher. In relative terms, however, the melt-albedo feedback drives only 58% additional mass loss compared to the lower-bound RCP8.5 scenario.

In comparing the upper-bound scenario (broken feedback loop, low albedo values) to the reference scenario (closed feedback loop), we can estimate how much additional ice loss might be possible due to changes in albedo after, e.g., extreme melt events. Note that albedo values might decrease even further than

we assumed in this scenario due to the accumulation of dust or algae growth. In the upper-bound RCP2.6 scenario, mass losses increase more than twofold compared to the reference scenario, while under higher warming (RCP8.5), ice losses in the upper-bound scenario increase by only 12%. The impact of additional decreases in albedo diminished with warmer forcing temperatures, as the melt-albedo feedback is already close to its upper limit even in the reference scenario due to high melt rates.

Note that these scenarios do not explore parametric uncertainty, in contrast to the results discussed in Section 3.1 which refer to the reference experiment with a closed feedback loop, but rather try to establish upper and lower bounds for the possible impact of the melt-albedo feedback in the warming scenarios. However, the ice losses in the upper-bound scenario, in particular, are sensitive to changes in the albedo value applied (here, we used the ice-albedo) and to changes in the duration of the albedo anomaly.

In this study, the melt-elevation feedback seems to have less impact than the melt-albedo feedback on the evolution of the Greenland Ice Sheet under warming: It drives only about 10% of the mass losses until 2300, compared to a simulation where the local temperature does not change with changing ice-surface elevation. However, not only has the melt-albedo feedback an upper bound due to the minimal albedo value, but it is also periodically interrupted by fresh snowfall during the winter months. The melt-elevation feedback, in contrast, does not have an upper bound or seasonal interruptions. It is therefore likely to become more important on longer timescales.

The long-term dynamic regimes and resilience of the Greenland Ice Sheet in response to an instantaneous persistent warming were my focus in **Manuscript 3**. In particular, I studied the interactions between the melt-elevation feedback (Levermann, Albrecht, et al. 2012) and the GIA feedback on timescales of several hundreds of millennia. Here, the influence of the melt-elevation feedback is crucial as it is decisive for the irreversible collapse of the ice sheet even at moderate warming temperatures from 1.5°C. Higher atmospheric temperature lapse rates, corresponding to a stronger melt-elevation feedbacks, also lead to faster ice loss upon warming. We explore the impact of the GIA feedback by varying the value for Earth's upper mantle viscosity: low viscosities lead to faster response times of the solid Earth to perturbations in ice load, and high viscosities correspond to slower response times. At low warming and low temperature-lapse rates, a short response time of the solid Earth can help to

initiate a recovery after an initial ice loss or even stabilize the ice sheet at a high volume. Increasing the upper mantle viscosity (and thereby the response time of the solid Earth) decreases the resilience of the Greenland Ice Sheet on timescales of several millennia, as it increases ice loss rates and the total amount of lost ice. On very long timescales of several hundreds of millennia, however, high viscosity values cause a stronger recovery of the ice volume. In addition, the interaction of the positive melt-elevation feedback and the negative GIA feedback may induce self-sustained oscillations of the Greenland Ice Sheet volume in a constant climate, representing a previously little studied internal mode of variability of the Greenland Ice Sheet which may be relevant for its response to orbital forcing during glacial cycles. These oscillations appear more likely with intermediate warming and lapse rate values and high upper mantle viscosity.

The positive melt-elevation feedback is dominant during the delay time between ice load change and bedrock uplift, reinforcing the initial ice loss. Once the bedrock lifts and the ice sheet starts growing again, the melt-elevation feedback reinforces the ice gains until the bedrock responds to increased ice load and starts sinking. High upper mantle viscosities increase the response time of the bedrock and thus the time period when the melt-elevation feedback is dominant, thereby increasing the amplitude of oscillations. .

3.3 Impacts of realistic forcing onto the mass balance of the Greenland Ice Sheet

While a relevant part of my thesis focused on idealized settings and conceptual understanding of processes, I also explored the response of the Greenland Ice Sheet to more realistic temperature focings. In **Manuscript 2** of my thesis, I explored how changes in albedo impact the melt rates until the year 2300 in the realistic RCP2.6 and RCP8.5 scenarios, clearly within the time frame relevant to present-day human societies (Masson-Delmotte et al. 2021). Note that these simulations, however, should not be read as sea level rise projections, as they neglect the role of ocean forcing and tidewater glacier retreat and likely underestimate the discharge of ice, as the resolution of 4.5 km is not high enough to resolve small outlet glaciers. Further limitations are discussed in Section 4.1.3.

A big difference in climate impacts, such as sea level rise, is not surprising when comparing a worst-case scenario with a moderate climate scenario. With an

ongoing rise in carbon emissions, a trajectory fulfilling the Paris Agreement and keeping global warming below 1.5°C becomes harder to achieve, thus questions of carbon budget flexibility and an overshoot in warming temperatures gain relevance. An integrated view on both, the Earth system and the economic sphere is needed to carve out the difference in impacts from two very similar emission scenarios, which aim to fulfill the Paris Agreement. Therefore, I assessed the sea-level contribution of the Greenland Ice Sheet under two moderate climate warming scenarios, which both reach the same global mean temperature in 2100, while only one of them allows for an overshoot of global warming (Meinshausen et al. 2009). The results are presented in **Manuscript 4**. In the year 2100, the difference in Greenland Ice Sheet mass loss between both scenarios is less than 1 cm, approximately 20 % of the total expected Greenland contribution. To explore the long term consequences of these emission scenarios for the mass evolution of the ice sheets, we fixed the climate forcings at the level of the year 2100 and simulated the sea-level contribution until the end of the millennium. We find that on long timescales, the sea level contributions in both scenarios keep increasing at different rates so that their difference grows. This is caused by persisting differences in air and ocean temperatures in the Arctic region: while the global mean temperature returns to the same level in the year 2100 in both emission scenarios, the high northern latitudes remain warmer than the global average due to Arctic amplification. This difference in temperature causes a difference of 2 cm in Greenland's contribution to sea level rise until 3000.

4 Discussions & Outlook

The Greenland Ice Sheet is an important contributor to sea level rise in a warming world. It is therefore essential to gain a deeper understanding of the processes involved. After presenting the manuscripts in Chapter 2, which lay the foundation of this thesis, and summarizing the results in some detail in Chapter 3, I will here explore in Section 4.1.1 how this work can help answer the questions about the resilience of the Greenland Ice Sheet (raised in Section 1.1.4), with a particular focus on timescales (see Section 4.1.2). Afterwards, I discuss the relevant limitations of my work in Section 4.1.3. Finally, I explore the broader context and implications of this work in Section 4.2 before coming to a conclusion (Chapter 5).

4.1 Discussion

4.1.1 Resilience of the Greenland Ice Sheet

Here, we return to the research question of how resilient the Greenland Ice Sheet is against anthropogenic global warming and what processes might increase or decrease its resilience. The general concept of resilience as well as the specific resilience of the Greenland Ice Sheet were introduced in Section 1.1.4. Some work has been done with regards to mapping the basin of stability of the present day ice volume with regards to changes in the global mean temperature or increased CO_2 concentrations, e.g. by Gregory et al. (2020), Ridley et al. (2010), and Robinson et al. (2012). In particular, Gregory et al. (2020) found that the expected increase in precipitation and a change in precipitation patterns are crucial for maintaining the resilience of the Greenland Ice Sheet volume. In contrast, many processes reduce the resilience of the Greenland Ice Sheet volume. For instance King, Howat, Candela, et al. (2020) showed, that the front retreat of outlet glaciers drives the increase in discharge rates, and even a climatic mass balance corresponding to a preindustrial climate would not sufficiently decrease the mass loss of the Greenland Ice Sheet. Some of the main processes affecting the resilience of the Greenland Ice Sheet are summarized in Table 4.1.

Table 4.1: Summary of processes which increase (↗) or decrease (↘) the resilience of the Greenland Ice Sheet. As defined in Section 1.1.4, when thinking about resilience it is helpful to keep the questions "Resilience regarding what?" and "Resilience against what?" in mind. The numbers in the second column refer to the specific answers to these questions, as listed in Section 1.1.4. Here, Arabic numerals refer to the question "Resilience regarding what?" and Roman numerals refer to the question "Resilience against what?". The entries printed in bold face highlight the processes which were specifically studied in this thesis. The references cited are: 1) Gregory et al. (2020), 2) Levermann and Winkelmann (2016), 3) Zeitz, Haacker, et al. (2022), 4) King, Howat, Candela, et al. (2020), 5) Zeitz, Reese, et al. (2021), 6) Cuffey and Paterson (2010), 7) Zeitz, Levermann, et al. (2020)

Process		Effect	Reference
Atmospheric temperature lapse rate and melt-elevation feedback	1. (i)	↘	2
Melt-albedo feedback	1.-3., 5. (i-iii)	↘	5
Glacial isostatic adjustment	1., 2. (i)	↗	3
Ice softening due to warming	1., 2., 4. (i)	↘	6, 7
Outlet glacier retreat	1., 2., 4. (i)(iv)	↘	4
Increased precipitation and changed patterns of precipitation	1. (i-ii)	↗	1

The first four entries in Table 4.1 address processes which are subject of this thesis, i.e., the melt-elevation feedback, the melt-albedo feedback, the glacial isostatic adjustments, and the softening of ice. I will discuss them briefly in the context of the resilience of the Greenland Ice Sheet. The positive melt-elevation feedback reduces the resilience, as it reinforces initial changes to the ice sheet thickness and thus the loss of ice due to global warming. This feedback is less important on short timescales, as long as changes in topography remain small, however, it becomes more important as topographic changes increase on longer time scales and it has no upper bound (unless the ice is melted completely).

Similarly, the positive melt-albedo feedback reduces the resilience by reinforcing initial changes in melt area. While this particular feedback plays out on a daily to monthly timescale, as soon as melting starts, it is regularly interrupted by fresh snow fall. Moreover, once bare ice is exposed the albedo becomes much less sensitive with respect to additional melt, adding a natural upper bound to this feedback. However, this might not be true locally in the dark zone of the Greenland Ice Sheet, where dust accumulations and algae blooms decrease the albedo even further. In contrast, the glacial isostatic adjustment is increasing the resilience, by stabilizing the ice surface altitude against melt and thickness loss. Finally, the softening of ice due to warming temperatures decreases the resilience, as softer ice flows faster and adds to further ice loss. However, in fast flowing outlet glaciers it is rather sliding than internal ice deformation, which determines the flow velocity.

The latter two processes were not explicitly studied in this thesis, therefore they will be discussed only briefly. Results from King, Howat, Candela, et al. (2020) suggest that the anticipated retreat of outlet glaciers might lead to a permanently negative mass balance of the Greenland Ice Sheet, which would persist even if the negative trend in climatic mass balance could be reversed. Here, the resilience of the volume of the Greenland Ice Sheet against changes in the terminus position of the outlet glaciers is decreased. In contrast, Gregory et al. (2020) have shown, that adaptions in precipitation pattern to the retreat of the Greenland Ice Sheet might be sufficient to prevent total ice loss under global warming. Thus, the change in precipitation increases the resilience of the ice sheet volume against global warming.

4.1.2 Timescales for the relevant processes

All of these processes affecting the resilience of the Greenland Ice Sheet play out on different timescales. Understanding the timescales associated with these processes is not only relevant to understand the impact of the changes of the Greenland Ice Sheet onto human societies, but as e.g. the work in **Manuscript 4** has shown, the interplay of different timescales can also provoke interesting dynamical behavior. Therefore the timescales are an important part of the discussion about the resilience of the Greenland Ice Sheet.

The most relevant timescales are summarized in Table 4.2 and in Figure 4.1 (Colleoni et al. 2018 have a similar overview for the Antarctic Ice Sheet and the Earth System). The timescale on which global climatic change takes place is one

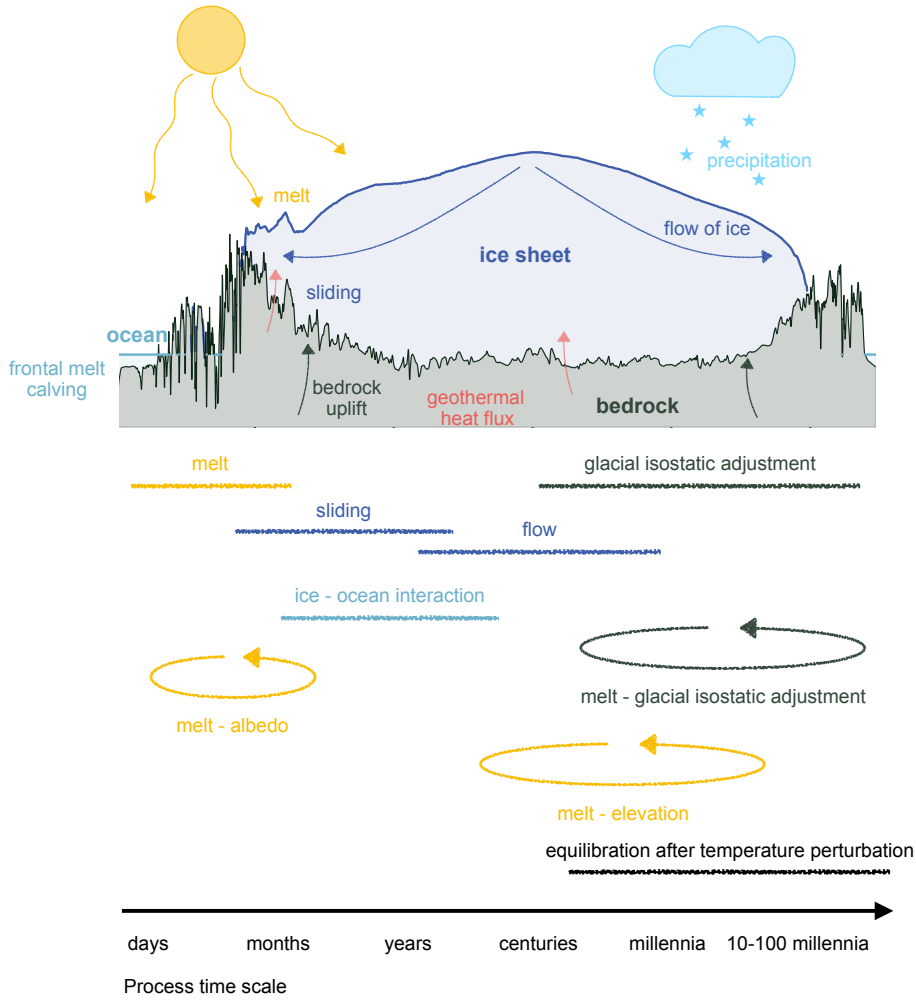

Figure 4.1: Timescales of different processes relevant for the Greenland Ice Sheet. The horizontal bars depict the range of timescales relevant for this particular process. Feedbacks are symbolized by arrow circles, their width depicting the range of timescales. The colors relate the processes to the schematic above; ice-atmosphere interactions depicted in yellow, interactions with the solid Earth depicted in gray, interactions with the ocean depicten in cyan, and internal ice processes depicted in dark blue.

Table 4.2: Summary of processes and timescales relevant for the Greenland Ice Sheet. The references cited are: 1) Masson-Delmotte et al. (2021), 2) Ricke and Caldeira (2014), 3) Le Clec'h et al. (2019), 4) Gregory et al. (2020) 5) Cullather and Nowicki (2018) 6) Tedesco and Fettweis (2020) 7) Cuffey and Paterson (2010), 8) Harrington et al. (2015), 9) King, Howat, Jeong, et al. (2018), 10) Whitehouse (2018), 11) McGrath et al. (2013)

Process	Timescale	Reference
Changes in melt	Days - weeks	5, 6
Acceleration of sliding	Seasonal	9
Upward migration of ELA	Years	11
Atmospheric warming	Decades after emission	1, 2
Increase in precipitation	Several decades	1, 3, 4
Change in emissions	Depends on RCP scenario	1
GIA	Centuries to millennia	10
Warming of deeper ice layers Softening of ice Increase in flow velocities	Several millennia	7 ,8

of the most important ones. While past climatic changes, e.g. the inception or termination of ice ages, have been very slow on human time scales, unfolding over millennia, the current anthropogenic climate change has the highest rates of temperature change at least during the past 2000 years (Masson-Delmotte et al. 2021). As both, the rate and the magnitude of future warming depend on the emission scenario, the timescale of global human activity is the most relevant one for the Greenland Ice Sheet.

The signal of emissions translates into warming via increasing concentrations of greenhouse gases (and aerosols) in the atmosphere. Atmospheric warming unfolds within several decades after the emissions are released into the atmosphere (Ricke and Caldeira 2014). However, not only warming of the atmosphere affects the ice sheet - the access to warmer waters drives sub-shelf melt in Antarctica and glacier retreat in Greenland (Pritchard et al. 2012; Straneo and Heimbach 2013). In contrast to the Antarctic Ice Sheet, which melts mainly at the ice-ocean interface, the impact of warming ocean waters on the Greenland Ice Sheet is

less important relative to surface melt. In addition, the global ocean warming can not necessarily be translated directly into Greenland sub-shelf melting, as many tidewater glaciers are located in narrow fjords and the melt is driven by small-scale processes such as fjord circulation or plume dynamics, which are fed by surface meltwater (D. A. Slater et al. 2020).

The Greenland Ice Sheet itself responds to changes in temperature on several different timescales. Atmospheric warming directly affects the energy balance at the surface of the ice sheet and thereby the melt rates. The melt of the ice sheet responds on a daily timescale to atmospheric conditions. The full climatic mass balance is not only characterized by an increase in melt, but also by an increase in precipitation, since warmer air can hold more moisture (Frieler et al. 2015; I. M. Held and Soden 2006). However, with increasing temperatures only a lower fraction of the precipitation falls as snow and contributes to the accumulation.

The feedbacks between climatic mass balance and the ice take place on different timescales as well. The melt-albedo feedback for instance may set in immediately as melt is happening, since melting snow darkens as it changes its properties. Once the snow is gone, the exposed ice can accumulate meltwater ponds or impurities, further decreasing its albedo. However, this feedback is also interrupted periodically with each fresh snow fall. The melt-elevation feedback only sets in as a consequence of ice sheet topography. 6 K/km is a typical value for the atmospheric temperature lapse rate, that is a surface altitude change of at least hundred meters leads to a significant increase in local air temperature (note that the standard deviation for daily temperatures around the monthly mean is at approx. 5 K). Current rates of thinning amount locally to several meters per year (IMBIE Team 2020), that is the effect of the melt-elevatiion feedback will likely only be measurable within the next decades or centuries. A receding ice sheet may also change atmospheric patterns, allowing for more cloud cover and more precipitation further inland (Gregory et al. 2020).

Warmer temperatures at the surface of the ice also can diffuse or be advected into the ice sheet itself, warming and softening portions of the ice which are not yet temperate and therefore affect the flow of ice. Heat transport through the ice is slow, it takes tens of millennia until the ice sheet is fully equillibrated to a temperature change (Cuffey and Paterson 2010; Greve and Blatter 2009). Processes like cryo-hydrologic warming, which is the warming through latent heat release by refrozen melt water in cracks and crevasses, might contribute to a faster heat transport. However, this process only takes place in regions

where meltwater is available and where it can refreeze in moulins or crevasses. The resulting warming might not penetrate the whole ice sheet. This process is typically not represented in numerical ice sheet models yet (Phillips, Rajaram, William T. Colgan, et al. 2013; Phillips, Rajaram, and Steffen 2010; Poinar et al. 2017).

The response of the solid Earth to changes in ice load, the glacial isostatic adjustment, plays out on several timescales at once. The elastic uplift of the lithosphere is in response to present day ice load chances, which are caused by global warming, and have been shown to contribute up to 25 mm per year to the measured uplift (Wahr et al. 2001; Wake et al. 2016). At the same time, the response to large-scale changes from the last deglaciation and the little ice age are still contributing to the uplift of the solid Earth in Greenland and broader northern latitudes (Adhikari et al. 2021). My results show that the GIA contributes to slowing down ice losses upon global warming within centuries and millenia, and can initiate the recovery of the Greenland Ice Sheet. The recovery, however, takes place on timescales of tens to hundreds of millennia and not on a human timescale, therefore it is not relevant for the resilience of the Greenland Ice Sheet. Nevertheless, the process is relevant for the long-term stability of the Greenland Ice Sheet.

4.1.3 Limitations of this work

This work addresses several important processes of the Greenland Ice Sheet, however, it is important to clearly discuss the limitations, in particular with respect to the resilience of the Greenland Ice Sheet, as outlined in Section 1.1.4.

First of all, regarding the question "Resilience of what? What is the system?" posed in Section 1.1.4, we have to consider that the perspective taken in this thesis is the perspective of an ice sheet modeler. Therefore the system in question is limited to the physical properties of the Greenland Ice Sheet. We cannot answer questions, which go beyond what the ice sheet model can represent. This includes questions that go beyond the physical properties of the ice sheet, e.g. Greenland as a biotope or Greenland as a living space. But even physicals properties and processes are not (and can not be) fully resolved in PISM: As discussed in Section 1.3.1, the ice is assumed to be homogeneous and isotropic, without any impurities which might change the flow properties. Any properties on spatial scales smaller than the resolution cannot be resolved explicitly. While damages and fractures can be represented via a mean damage function (Albrecht

and Levermann 2012), water transport through moulins, cracks and crevasses is, although relevant for the heat transport, not part of the ice sheet model yet. The boundary conditions, in particular at the base of the ice concerning bed topography and geothermal heat fluxes, are difficult to measure and the model can be only as good as the data we use to drive it. Narrow outlet glaciers, which are contributing to the dynamical discharge of the ice, are not well resolved at the horizontal resolutions I chose for the sub-projects of the thesis, moreover I did not put emphasis on the ice-ocean interactions. The ability of the firn to retain meltwater, although important for the resilience of the Greenland Ice Sheet, is not part of the ice sheet model (Noël, Van De Berg, et al. 2017).

Concerning the question "Resilience regarding what? Which property of the system?", this work shows a particular focus on the volume of the Greenland Ice Sheet. One might argue, that the volume itself is not relevant as long as the rate of sea level rise is so slow, that human societies can adapt to it. However, the rate of sea level rise has not been studied here in particular. The same applies to the kinds of perturbations ("Resilience against what?"), as the studies in this thesis mostly focus on the impact of global mean temperature perturbations and surface albedo perturbations, neglecting particular atmospheric patterns and, most importantly, extreme weather events over Greenland.

A further limitation is imposed by the idealized nature of the numerical experiments. Most obviously in **Manuscript 1** I focus on an idealized two-dimensional ice sheet in order to disentangle the effects of the flow parameters from other influences. This ice sheet therefore does not experience lateral backstresses, it is not sitting on a complex bed topography, shaping the dynamics of the ice flow, and it is not subjected to a spatially or temporally varying climatic mass balance and temperature distribution. Moreover, in our idealized experimental setting, the increase in temperature only translates via the ice surface temperature without affecting the climatic mass balance. While we chose this particular experimental setting to clearly emphasize the effect of the flow parameters alone, we are also likely to overestimate their impacts compared to a more realistic setting.

In **Manuscript 2** I presented a simple approach to estimating the upper and lower bounds on Greenland ice loss due to changes in albedo. However, for the sake of a numerically efficient scheme we greatly simplified the processes affecting albedo. While albedo does depend on melt, it does not depend on melt alone: microphysical properties of the snow crystals, the thickness of the snow

or firn layer, and the cloud cover influence, among others, the albedo. In addition, we cannot realistically estimate the spatial extent, intensity, or duration of future darkening due to processes such as ice melt, accumulation of melt water, dust, and other contaminants, or algal growth (see Section 1.1.2 for a brief discussion on this topic). This study can only serve as an initial estimate of the resilience of the Greenland ice sheet against changes in albedo.

The results presented in **Manuscript 3** offer meaningful insights into how the interaction of positive and negative feedbacks may affect the resilience of the overall system. We have made sure to the best of our knowledge that the dynamic regimes emerging in this study are not an artifact created by any particular modeling choice. Nevertheless, all of these dynamical regimes arise in a constant climate. Therefore it remains a challenge to validate in particular the emergence of self-sustained oscillations in a real world setting, simply because Earth does not not experience stable climate condition over the course of hundreds of millennia. Therefore, we can only hypothesize about the implications of these dynamics for the resilience of the Greenland Ice Sheet, i.e. by assuming that they might have interacted with past glaciation-deglaciation cycles.

4.2 Outlook

In my thesis, I approached the question of how resilient the Greenland Ice Sheet is to global warming, with a particular focus on uncertainties and feedbacks. I focussed primarily on feedbacks and on uncertainties of processes, which are well represented within our modeling approach, neglecting other processes.

Uncertainties, both in the flow parameterization and in the albedo driven melt rates, need to be taken into account when projecting future sea level rise. Novel approaches use larger ensembles and Bayesian statistics to constrain the uncertainties in a more informed way, in particular by deducing the posterior probability of modeling parameters (see e.g. Brinkerhoff et al. 2021 with a focus on subglacial processes). It is conceivable to expand a similar approach to other processes as well, and use the inferred parameter uncertainties to inform simulations which assess future sea level rise.

An additional source of uncertainty is the exact impact of a changing climate. The latest ISMIP effort took different climate models into account and addressed the uncertainties linked to these climate models and to different ocean sensitivities (Goelzer et al. 2020). However, the global circulation models used in

those studies are mostly too coarse grained to resolve local climatic events which might lead to extreme conditions over Greenland. Already now the intensity and frequency of heat waves over Greenland has increased (Dobricic et al. 2020). Heat waves and extreme weather patterns are projected to become more likely with ongoing climate change (Rahmstorf and Coumou 2011), and an assessment of their impacts on the resilience of the Greenland Ice Sheet would be a logical next step.

Moreover, in order to assess the resilience of the Greenland Ice Sheet more realistically, not only feedbacks within the ice sheet itself, but also the interactions with the whole Earth system need to be addressed. In particular, feedbacks between the ice sheet topography and the local climatic conditions, concerning both, temperature and precipitation, deserve a lot of attention. Additionally, the interplay between the surface albedo, i.e., snow, ice, or ice free bedrock, and the climatic conditions is likely to have a great influence on the the resilience of the Greenland Ice Sheet. Therefore, process-based ice sheet models are interactively coupled to regional or global climate models. However, simulations which include all relevant processes at a sufficiently high spatial resolution are costly not all research questions can be addressed at once.

5 Conclusion

In my thesis, I analyze the resilience of the Greenland Ice Sheet against future global warming. This is achieved through investigating the impact of relevant feedbacks, in particular the melt-albedo feedback, the melt-elevation feedback and the glacial isostatic adjustment feedback, on various timescales – from several centuries up to half a million years. Furthermore, I analyze the impact of process- and parameter-uncertainties on numerical ice flow simulations.

As one of the key findings, I show that the parametric uncertainty in *Glen's flow law*, which is usually not considered in ice sheet modeling studies, impacts the ice response to warming. The related study highlights the influence of the flow exponent and more importantly also the softness-temperature relation on flow driven ice losses.

Even though the melt-albedo feedback poses a major contribution to the melt rates of the Greenland Ice Sheet at present, it is typically not represented in process-based ice sheet models thus far. I contribute to closing this gap by adapting the diurnal Energy Balance Model to work in a stand-alone mode (dEBM-simple), and implementing it as a surface melt module in the open-source ice sheet model PISM. Therefore, a first-order approximation of the melt-albedo feedback is available to the scientific community, complementing the widely used positive degree day model. Using PISM-dEBM-simple, I have provided a first estimate of Greenland's ice loss under global warming which is driven by the melt-albedo feedback. Here, I focus not only on parametric uncertainties, but also conceptually establish a lower- and an upper-bound of the possible contribution from the feedback itself, advancing our understanding of its relevance for the resilience of the Greenland Ice Sheet.

With my thesis I also contribute to the understanding of how the interaction between a positive and a negative feedback, namely the melt-elevation feedback and the glacial isostatic adjustment (GIA) feedbac, influence the resilience of the Greenland Ice Sheet. In long-term simulations under persistent warming, the GIA increases the resilience of the ice sheet against global warming by mitigating the effects of the melt-elevation feedback. Most importantly, unexpected dynamical

regimes can emerge from the interactions between the positive and the negative feedback. Depending on the warming level, the atmospheric temperature lapse rate and the upper mantle viscosity, my results show the full range of responses, from recovery after initial ice loss to self-sustained oscillations in a constant climate to the complete loss of the ice sheet.

With the ambition of the Paris Agreement of limiting the global warming at well below 2°C and pursuing efforts to limit it at 1.5°C almost out of reach, overshoot scenarios have become of increased interest to the scientific community and the general public. I show that an overshoot of 0.4°C, from a maximal warming of 1.4°C to 1.8°C causes a difference in Greenland's sea level of almost 1 cm by the year 2100, an increase of almost 20 %.

All in all, I show how the interplay of nonlinear feedbacks causes additional ice loss from the Greenland Ice Sheet under ongoing climate change. While the loss of resilience of the Greenland Ice Sheet can in parts be mitigated, for instance by the GIA feedback on the very long term (hundreds of millennia), my work underlines the vulnerability of the Greenland Ice Sheet to global warming on the centennial and millennial scale, impacting the lives of present and future generations.

A Appendix

Supplement of: Sensitivity of ice loss to uncertainty in flow law parameters in an idealized one-dimensional geometry

Supplement of The Cryosphere, 14, 3537–3550, 2020
https://doi.org/10.5194/tc-14-3537-2020-supplement

The Cryosphere Open Access EGU

Supplement of

Sensitivity of ice loss to uncertainty in flow law parameters in an idealized one-dimensional geometry

Maria Zeitz et al.

Correspondence to: Maria Zeitz (maria.zeitz@pik-potsdam.de) and Ricarda Winkelmann (ricarda.winkelmann@pik-potsdam.de)

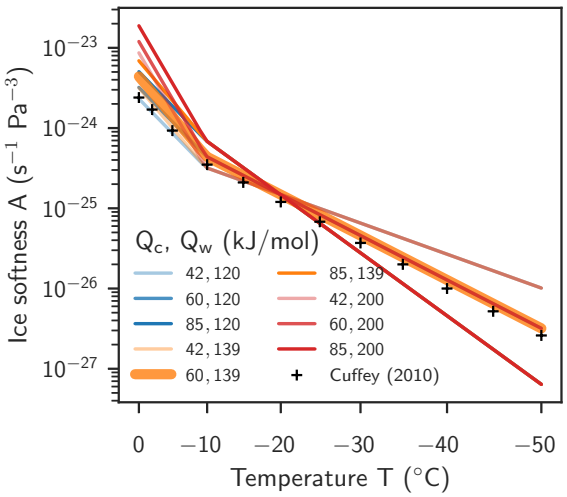

Figure S1. Effect of activation energy parameters on the temperature dependence of the softness A. The temperature dependence of the ice softness A is usually shown in an *Arrhenius plot*, where the softness is shown on a semi-log scale over the inverse temperature. Two parameters for the activation energy Q_c and Q_w for $T \leq -10\,^\circ\mathrm{C}$ and $T > -10\,^\circ\mathrm{C}$ parametrize the relationship of ice softness to pressure adjusted temperature. Here the softness is fixed at a reference temperature of $T = -20\,^\circ\mathrm{C}$. The softness at cold temperatures depends only on the choice of Q_c. Softness at pressure melting point is most sensitive for variations in the Q_w, but varies slightly with Q_c. At pressure melting point the softness increases 8-fold between the limits of parameter combinations, from -47% to + 335% compared to standard parameters. For comparison we show the textbook values of the softness for different temperatures (black crosses) (Cuffey and Paterson, 2010).

References

Cuffey, K. M. and Paterson, W. S. B.: The Physics of glaciers, Elsevier Inc., 4 edn., http://linkinghub.elsevier.com/retrieve/pii/0016718571900868, 2010.

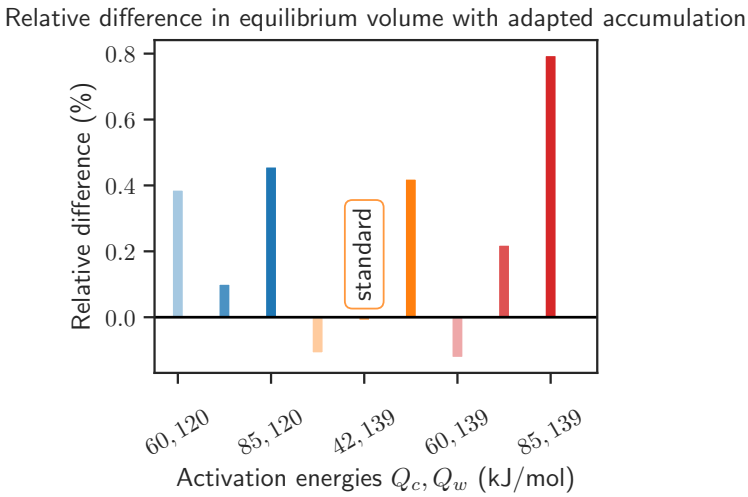

Figure S2. Relative difference in equilibrium volume with adapted accumulation rates compared to the equilibrium state of the simulation with standard parameters and an accumulation rate $a = 0.5\,\mathrm{m/yr}$.

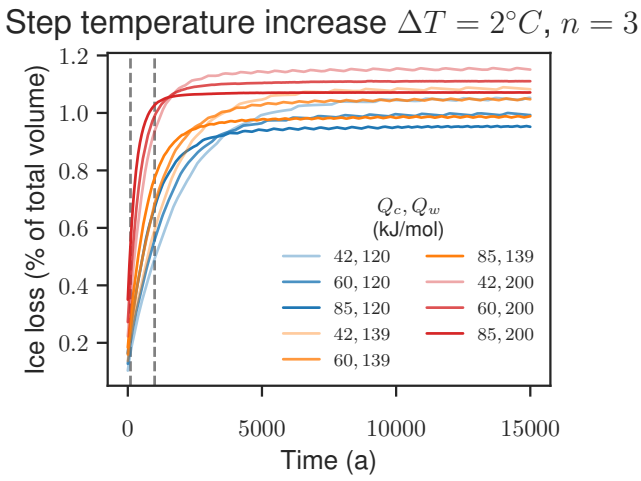

Figure S3. Effect of activation energy and flow exponent on flow-driven ice discharge : Ice loss in a conceptual flowline setup subject to a temperature anomaly forcing of $\Delta T = 2°\mathrm{C}$ and $n = 3$ in percent of the initial volume.

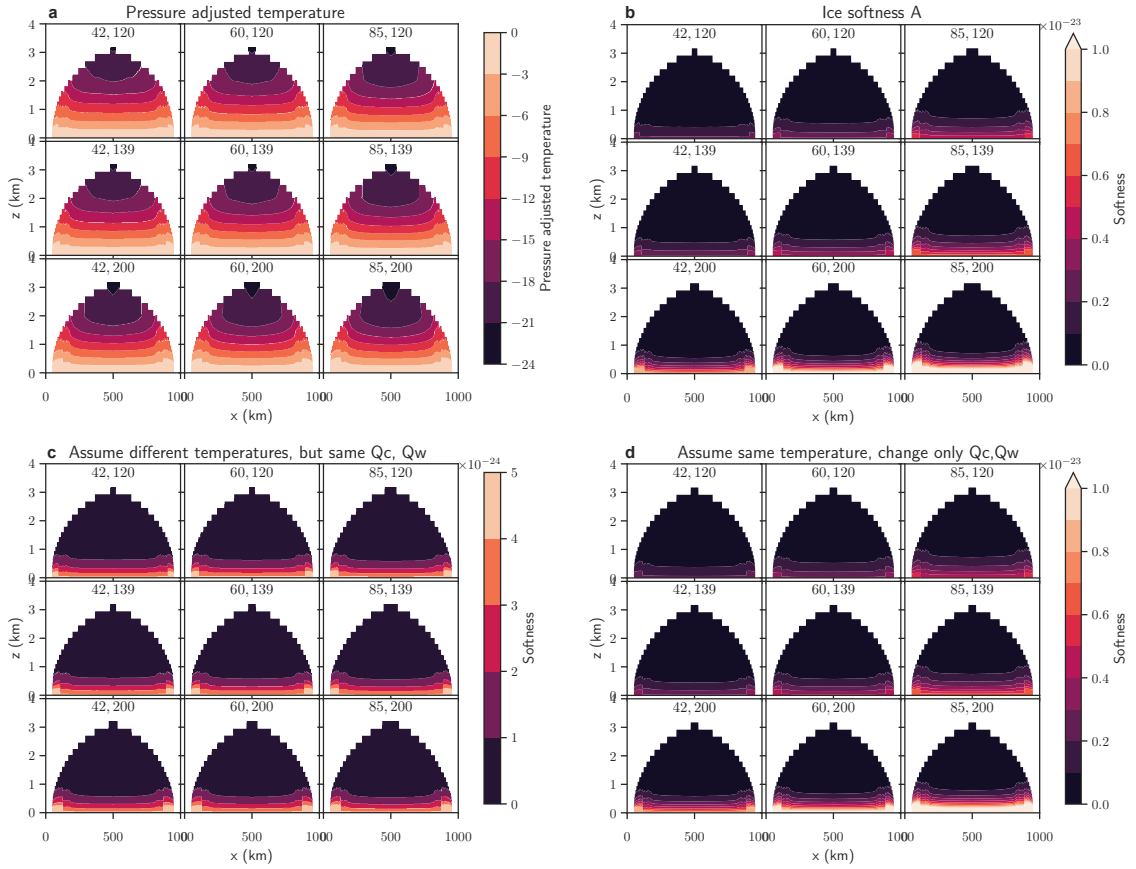

Figure S4. Effect of differences in temperature and different activation energies on ice softness in equilibrium: **(a)** Pressure adjusted temperature of the ice sheet in the equilibrium state for different combinations of activation energies Q_c, Q_w (see title of each tile) with a flow exponent $n = 3$. Note that the accumulation rates are adjusted to keep the equilibrium volume fixed, with decreased accumulation rates for low activation energies and increased accumulation rates for high accumulation energies. The increase in accumulation leads to cooler temperatures at the top of the ice sheet. **(b)** Ice softness A in equilibrium for different combinations of activation energies Q_c and Q_w. A clear increase in softness, in particular at the base of the ice sheet is observed for high activation Q_c and Q_w. **(c)** Ice softness calculated from the pressure adjusted temperatures shown in **(a)** but fixing Q_w and Q_c at the reference values. The changes in temperature distribution alone are not sufficient to reproduce the softness shown in panel **(b)**. **(d)** Ice softness calculated from a fixed pressure adjusted ice temperature and different Q_c and Q_w parameters. The change in activation energies alone can reproduce the softness shown in panel **(b)**. Here we show equilibrium values without a warming anomaly. A very similar behavior is observed for the equilibrium states with increased temperatures.

Supplement of: Impact of the melt–albedo feedback on the future evolution of the Greenland Ice Sheet with PISM-dEBM-simple

Supplement of The Cryosphere, 15, 5739–5764, 2021
https://doi.org/10.5194/tc-15-5739-2021-supplement

The Cryosphere Open Access EGU

Supplement of

Impact of the melt–albedo feedback on the future evolution of the Greenland Ice Sheet with PISM-dEBM-simple

Maria Zeitz et al.

Correspondence to: Maria Zeitz (maria.zeitz@pik-potsdam.de) and Ricarda Winkelmann (ricarda.winkelmann@pik-potsdam.de)

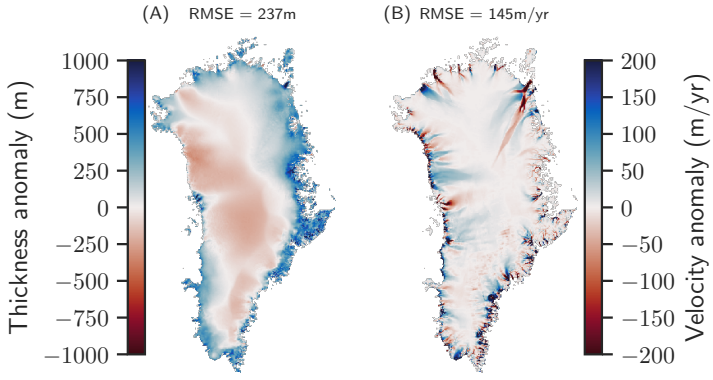

Figure S1. Comparison of simulated thickness and velocity magnitude with observed values. (A) Thickness differences are given between observed data (BedMachine, (Morlighem et al., 2017)) and the initial state for the simulation at the end of the glacial cycle. The root mean square error is at 237m. (B) Differences in the magnitude of surface velocities between observed (Rignot and Mouginot, 2012) and simulated values. The root mean square error is at 145m/yr. The differences are positive (blue), where the simulated values overestimate thicknesses or velocities and negative (red), where the simulated values underestimate thicknesses or velocities.

1 Statistical analysis of the initial state

The initial state was achieved by spinning up the model over 125 ka with a scalar temperature anomaly applied to the climatological mean from 1971-1990 of MAR v3.9 monthly temperature and precipitation fields. The precipitation is scaled with a 7.3% increase for each degree Celsius of warming (Huybrechts, 2002).

References

Huybrechts, P.: Sea-level changes at the LGM from ice-dynamic reconstructions of the Greenland and Antarctic ice sheets during the glacial cycles, Quaternary Science Reviews, 21, 203–231, https://doi.org/10.1016/S0277-3791(01)00082-8, 2002.

Morlighem, M., Williams, C. N., Rignot, E., An, L., Arndt, J. E., Bamber, J. L., Catania, G., Chauché, N., Dowdeswell, J. A., Dorschel, B., Fenty, I. G., Hogan, K., Howat, I., Hubbard, A., Jakobsson, M., Jordan, T. M., Kjeldsen, K. K., Millan, R., Mayer, L., Mouginot, J., Noël, B. P. Y., O'Cofaigh, C., Palmer, S., Rysgaard, S., Seroussi, H., Siegert, M. J., Slabon, P., Straneo, F., Van Den Broeke, M. R., Weinrebe, W., Wood, M., and Zinglersen, K. B.: BedMachine v3: Complete Bed Topography and Ocean Bathymetry Mapping of Greenland From Multibeam Echo Sounding Combined With Mass Conservation, Geophysical Research Letters, 44, 11,051–11,061, https://doi.org/10.1002/2017GL074954, 2017.

Rignot, E. and Mouginot, J.: Ice flow in Greenland for the International Polar Year 2008-2009, Geophysical Research Letters, 39, 1–7, https://doi.org/10.1029/2012GL051634, 2012.

Supplement of: Interaction of melt-elevation and bedrock uplift feedback leads to long term oscillations of Greenland Ice Sheet volume

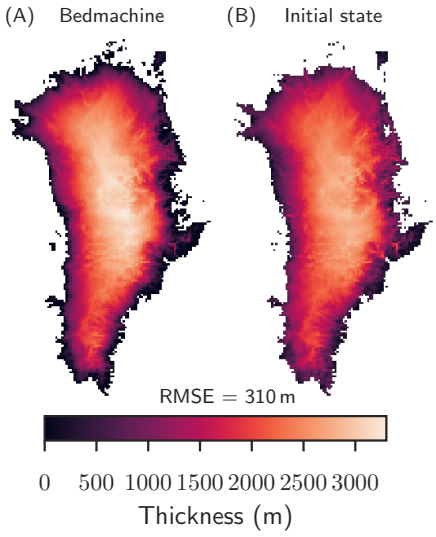

Figure S1. Comparison of the ice thickness of the initial state to BedMachine (Morlighem et al., 2017) (remapped to 15 km resolution to be comparable).

References

Joughin, I., Smith, B. E., and Howat, I.: Greenland Ice Mapping Project: Ice Flow Velocity Variation at sub-monthly to decadal time scales, The Cryosphere Discussions, pp. 1–30, https://doi.org/10.5194/tc-12-2211-2018, 2018.

Morlighem, M., Williams, C. N., Rignot, E., An, L., Arndt, J. E., Bamber, J. L., Catania, G., Chauché, N., Dowdeswell, J. A., Dorschel, B., Fenty, I. G., Hogan, K., Howat, I., Hubbard, A., Jakobsson, M., Jordan, T. M., Kjeldsen, K. K., Millan, R., Mayer, L., Mouginot, J., Noël, B. P. Y., O'Cofaigh, C., Palmer, S., Rysgaard, S., Seroussi, H., Siegert, M. J., Slabon, P., Straneo, F., Van Den Broeke, M. R., Weinrebe, W., Wood, M., and Zinglersen, K. B.: BedMachine v3: Complete Bed Topography and Ocean Bathymetry Mapping of Greenland From Multibeam Echo Sounding Combined With Mass Conservation, Geophysical Research Letters, 44, 11,051–11,061, https://doi.org/10.1002/2017GL074954, 2017.

Noël, B. P. Y., van de Berg, W. J., Lhermitte, S., and van den Broeke, M. R.: Rapid ablation zone expansion amplifies north Greenland mass loss, Science Advances, 5, 2–11, https://doi.org/10.1126/sciadv.aaw0123, 2019.

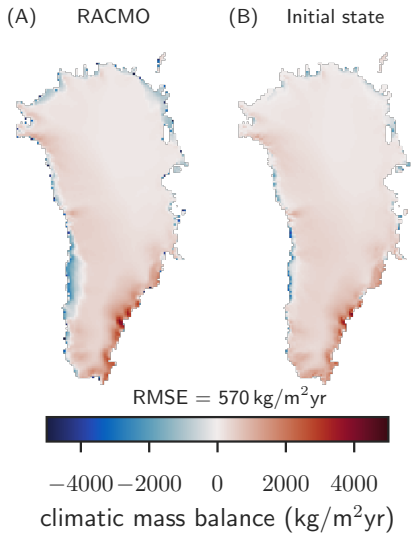

Figure S2. Comparison of the climatic mass balance of the initial state, computed with the positive degree day method and without temperature anomaly, to annually averaged RACMO v2.3 data averaged over 1958 to 1967 (Noël et al., 2019) (remapped to 15 km resolution to be comparable).

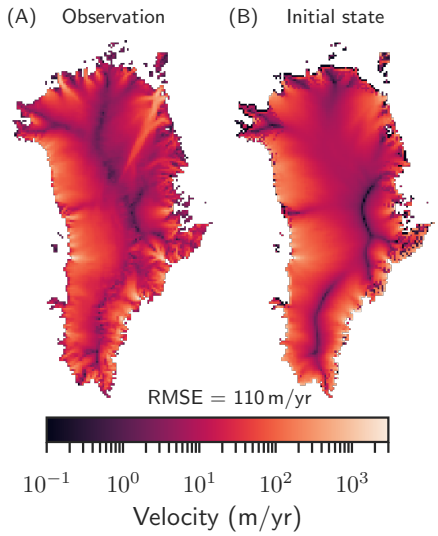

Figure S3. Comparison of the magnitude of the surface velocities of the initial state to observation data (Joughin et al., 2018) (remapped to 15 km resolution to be comparable).

Supplement of: Risks and benefits of overshooting a 1.5°C carbon budget

Methods / Supplementary Material

REMIND-MAgPIE

Methodology

The REMIND and the MAgPIE model are both equilibrium models that apply optimization methods to derive market equilibria. Also both models cover the time horizon up until 2100 and are global in scope differentiating the world into twelve macro regions that form markets for food and energy for which market equilibria are computed. Both models rely on the SSPs for assumptions on socioeconomic drivers for demographic, economic and technological development (Dellink et al., 2017; KC and Lutz, 2017). In this study, both models use the SSP2, a middle-of-the-road narrative, to derive a baseline scenario that is used to assess the impacts of climate policies. Assumptions on technological development, resource potentials, etc. in REMIND and MAgPIE follow the SSP2 narrative and documented in the literature (Kriegler et al., 2017; Riahi et al., 2017). Both models are coupled using a soft-link approach (Bauer et al. 2020b). For REMIND, version 2.0 is applied, which is available open access. For MAgPIE, version 4.1 is used. Both models are open access on GitHub (see Code availability). This version has been previously used in Bauer et al. (2020a).

REMIND is a Ramsey-type general equilibrium model of economic growth with a hard-coupled detailed energy system model that applies optimization methods to find a general market equilibrium (Bauer et al., 2018a, 2012; Luderer et al., 2013). Economic agents are assumed to have perfect foresight on future prices, which implies a rational expectations equilibrium on all markets. The macroeconomic system demands labor, capital and final energy. Final energy use gradually modernizes with growing shares of electricity and gases, whereas shares of liquids and solids decrease. The energy system is a detailed representation of all relevant energy flows from primary to final energy as well as associated GHG emissions. The energy system transformation is consistent with basic energy economic principles of cost competition, but also represents inertia of infrastructures and rigidities to ramp-up new capacities as well as endogenous technological learning. Regions are endowed with fossil fuels, uranium and biomass that are traded internationally subject to transportation costs and infrastructure expansion rigidities as well as balance of payments constraints. Coal, gas and biomass conversion capacities that produce electricity, liquids and hydrogen can be equipped with CCS. An injectivity constraint limits the annual injection of CO_2 into geological formations to 0.5% of the total potential in each region.

MAgPIE 3.0 is a partial equilibrium model of the land-use sector that finds market equilibrium by minimizing the global costs of production given price irresponsive demands for agricultural products (Humpenöder et al., 2018; Popp et al., 2014a). The model assumes adaptative expectations for evaluation of long-term investment decisions implemented by recursive dynamic model structure. The model is driven by demands for agricultural commodities, which are calculated based on population and income projections for the 21st century. For meeting the demand, the model endogenously decides, based on cost-effectiveness, about the level of intensification (yield-increasing technological change), extensification (land-use change), and production relocation (intra-regionally and interregionally through international trade). CO_2 emissions from land-use change are calculated based on differences in carbon stocks for different land types. The calculation of N_2O and CH_4 emissions from agricultural production is based on IPCC 2006 emission guideline factors. The optimization process is subject to various spatially explicit biophysical conditions such as yields, water availability and carbon stocks, which are derived by the global crop growth, vegetation, and hydrology model LPJmL. Due to

computational constraints, spatially explicit input (0.5 degree resolution) is aggregated to 700 simulation units for the optimization process based on a k-means clustering algorithm.

MAgPIE simulates two types of biomass feedstock production: 1st and 2nd generation biomass feedstocks. 1st generation biomass relies on conventional food crops such as maize and sugarcane. Supplies and demands of 1st generation feedstocks are prescribed by exogenous policies. The largest potential is offered by dedicated herbaceous and woody lignocellulosic bioenergy crops (such as Miscanthus, Poplar and Eucalyptus), which feature significantly higher energy specific yields per hectare than 1st generation crops. Lignocellulosic feedstocks can be converted into electricity, hydrogen and liquid fuels also in combination with CCS. Conversion into heat, solid energy carriers and synthetic gases are available, but cannot be combined with CCS. Residues are scaled with production volumes in forestry and agriculture reaching a long-term maximum global potential of 70EJ/yr.

Additional results

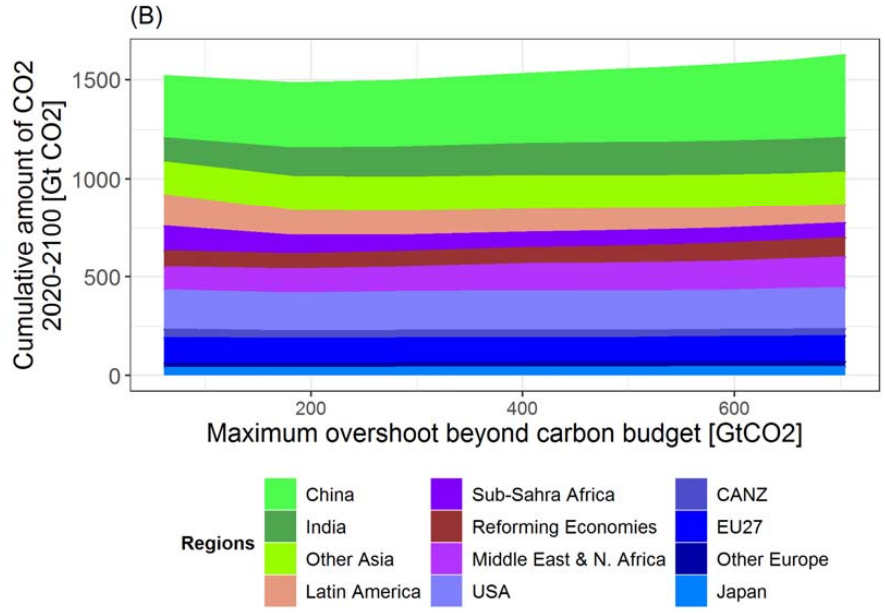

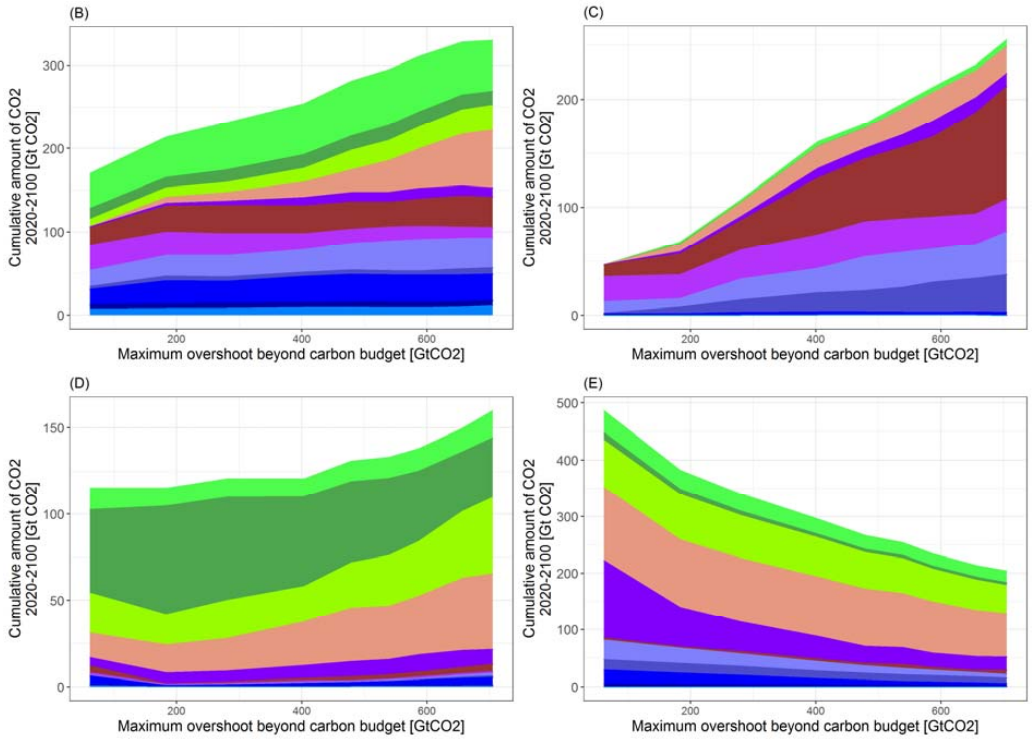

Figure S1: Regional perspective of cumulative anthropogenic carbon fluxes by 2100 for varying degrees of overshoot flexibility. Cumulative gross CO_2 emissions from fossil fuels and industry (A) carbon removal from BECCS (B), DAC (C), Enhanced Weathering (D) and Land-Use Change (E).

Mitigation costs over time

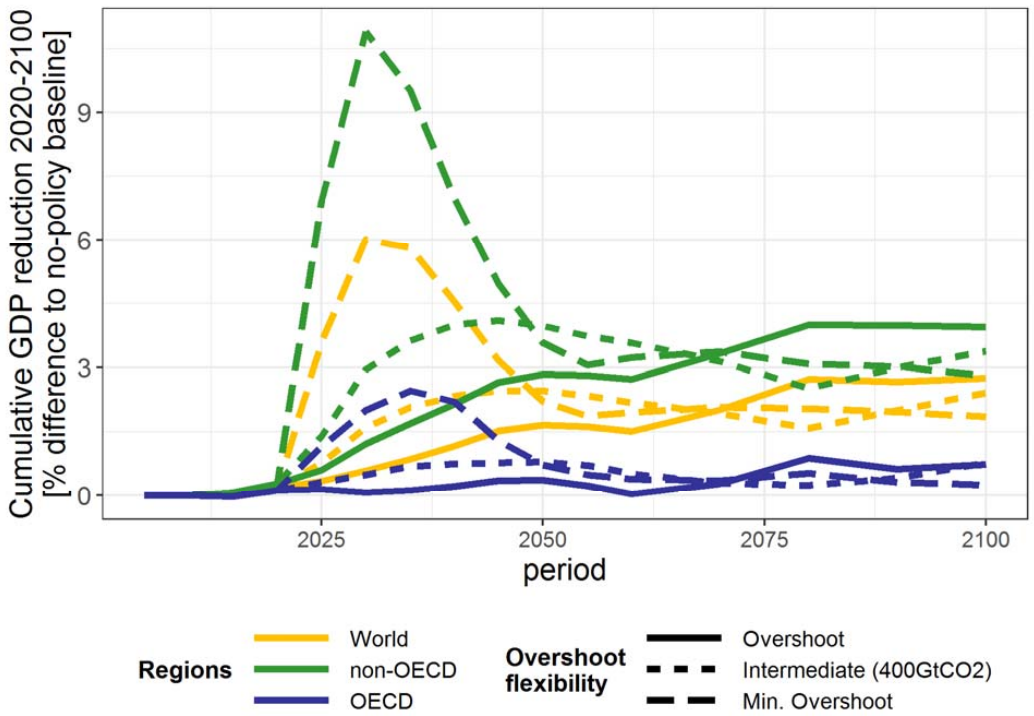

Figure S2: Global GDP reductions over time and differentiated by OECD and non-OECD regions. The Intermediate scenario assume that only 20% of the carbon price for net negative emissions is remunerated.

UVic Simulations

The model (UVic version 2.10; Mengis et al., 2020) consists of three dynamically coupled components: a three-dimensional general circulation model of the ocean that includes an inorganic sediment model and a dynamic-thermodynamic sea ice model, a terrestrial model, and a simple one-layer atmospheric energy-moisture balance model. All components have a common horizontal resolution of 3.6 longitude x 1.8 latitude. The oceanic component has nineteen levels in the vertical with thicknesses ranging from 50 m near the surface to 500 m in the deep ocean. The terrestrial model of vegetation and carbon cycles is based on the Hadley Center model TRIFFID. The soil module includes a 14 layer representation of soil carbon and a representation of soil freeze–thaw processes that includes a permafrost carbon component. The atmospheric energy-moisture balance model interactively calculates heat and water fluxes to the ocean, land, and sea ice. Wind velocities, which are used to calculate the momentum transfer to the ocean and sea ice model, surface heat and water fluxes, and the advection of water vapor in the atmosphere, are determined by adding wind and wind stress anomalies (as determined from surface pressure anomalies that are calculated from deviations in pre-industrial surface air temperature) to prescribed NCAR/NCEP monthly climatological wind data. The model has been extensively used in climate change studies and is well validated under pre-industrial to present day conditions (Mengis et al., 2020).

The model was spun up for 10,000 years under pre-industrial atmospheric and astronomical boundary conditions and then run from 1765 to 2015 using historical fossil-fuel and land-use carbon emissions. From the year 2015 to 2100 the model was forced with CO_2 and other greenhouse gas emissions, as well as land-use change, from REMIND-MAgPIE.

As UVic does not explicitly simulate coral reefs, the presented coral calcification rates relative to the year 1850 were calculated following Hofmann et al., 2019.

To investigate plausible upper and lower bounds of the temperature response in UVic, due to parametric uncertainties, additional simulations are conducted. Only two parameters are varied because earlier studies, where multiple ensembles of parameters were varied, showed that simulated temperatures were very sensitive to their values (Mengis et al., 2018; Tran et al., 2020). Note that results from these simulations were evaluated to ensure that the historical portion of the simulations are within the bounds of historical observational uncertainties for key climate properties (e.g., global mean temperature and CO_2, terrestrial and ocean carbon reservoirs, biogeochemical properties, see Tran et al., 2020).

The overshoot is also expected to bear differences marine environmental impacts such as coral reefs. The UVic model provides information about sea temperature and pH-value to derive gross calcification rates using established methodology (Silverman et al. 2009, Hofmann et al. 2019). Coral reefs are considered the marine ecosystems at high risk to temperature variations and higher CO_2 loadings in the oceans even if global warming remains below 2°C. Observations indicate that marine heat waves become more intense and frequent and that these lead to coral reef bleaching events, which are expected to increase substantially under future warming between 1.5 and 2°C temperature increase (Frieler et al. 2013). At the same time the environmental conditions for growth and regeneration of

892 coral reefs worsen with increasing ocean temperatures and ocean acidification due to decreasing
893 calcification rates.

894

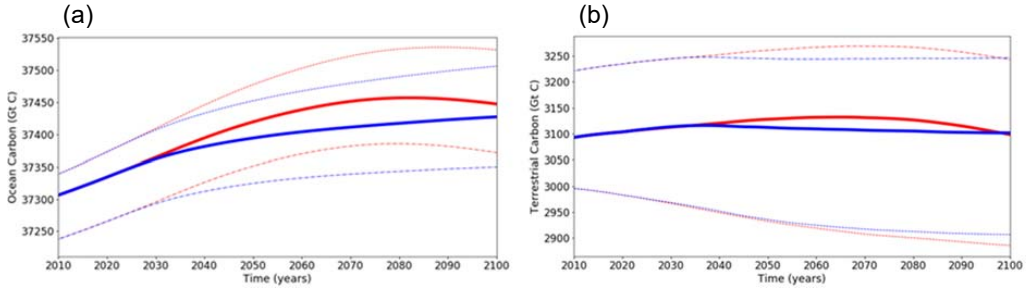

Figure S3: Carbon content of oceans and terrestrial systems.

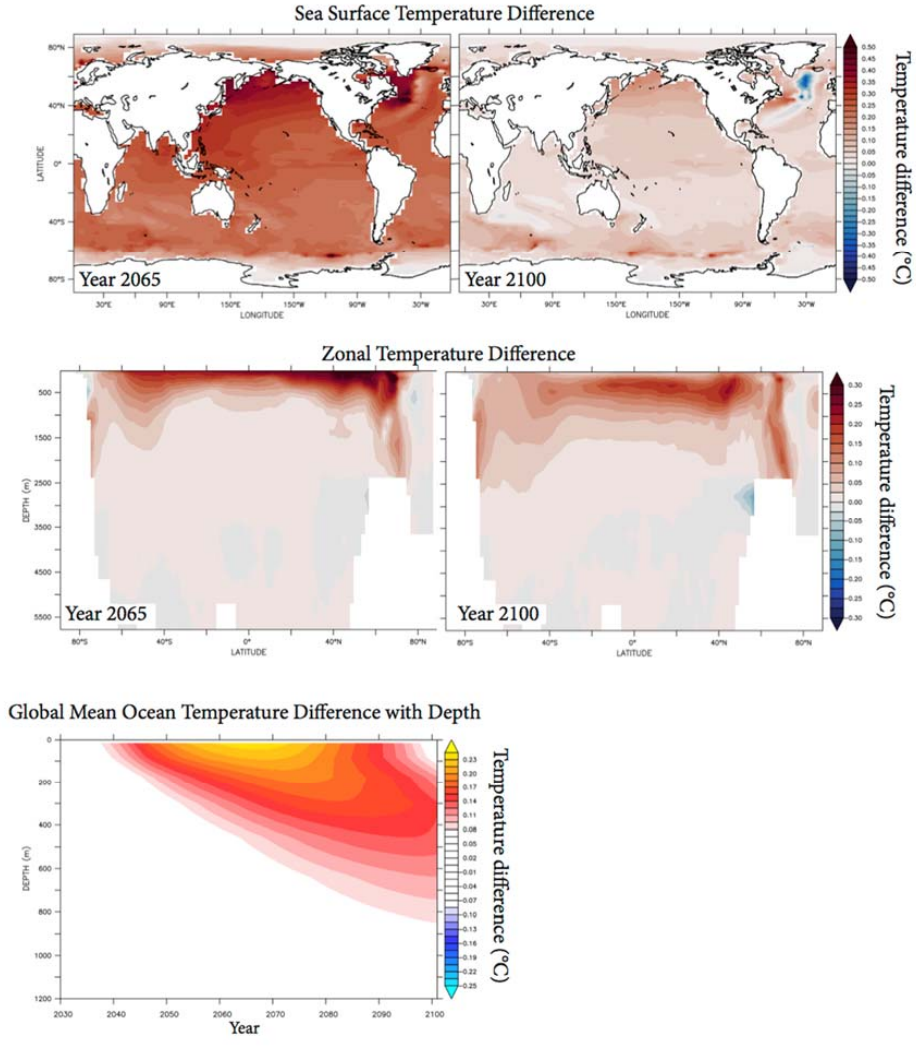

Figure S4. Ocean temperature differences.

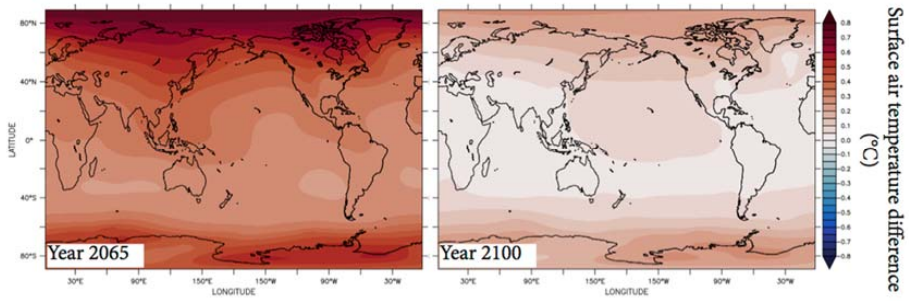

900

901 Figure S5. Near surface air temperature differences of full minus minimal overshoot scenario.

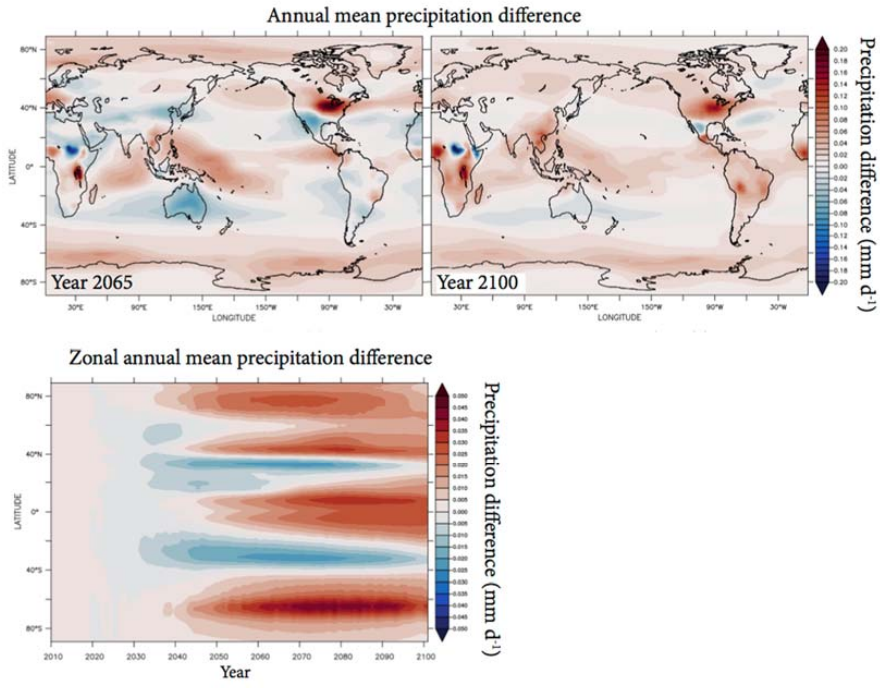

902

903 Figure S6. Annual mean precipitation differences of full minus minimal overshoot scenario.

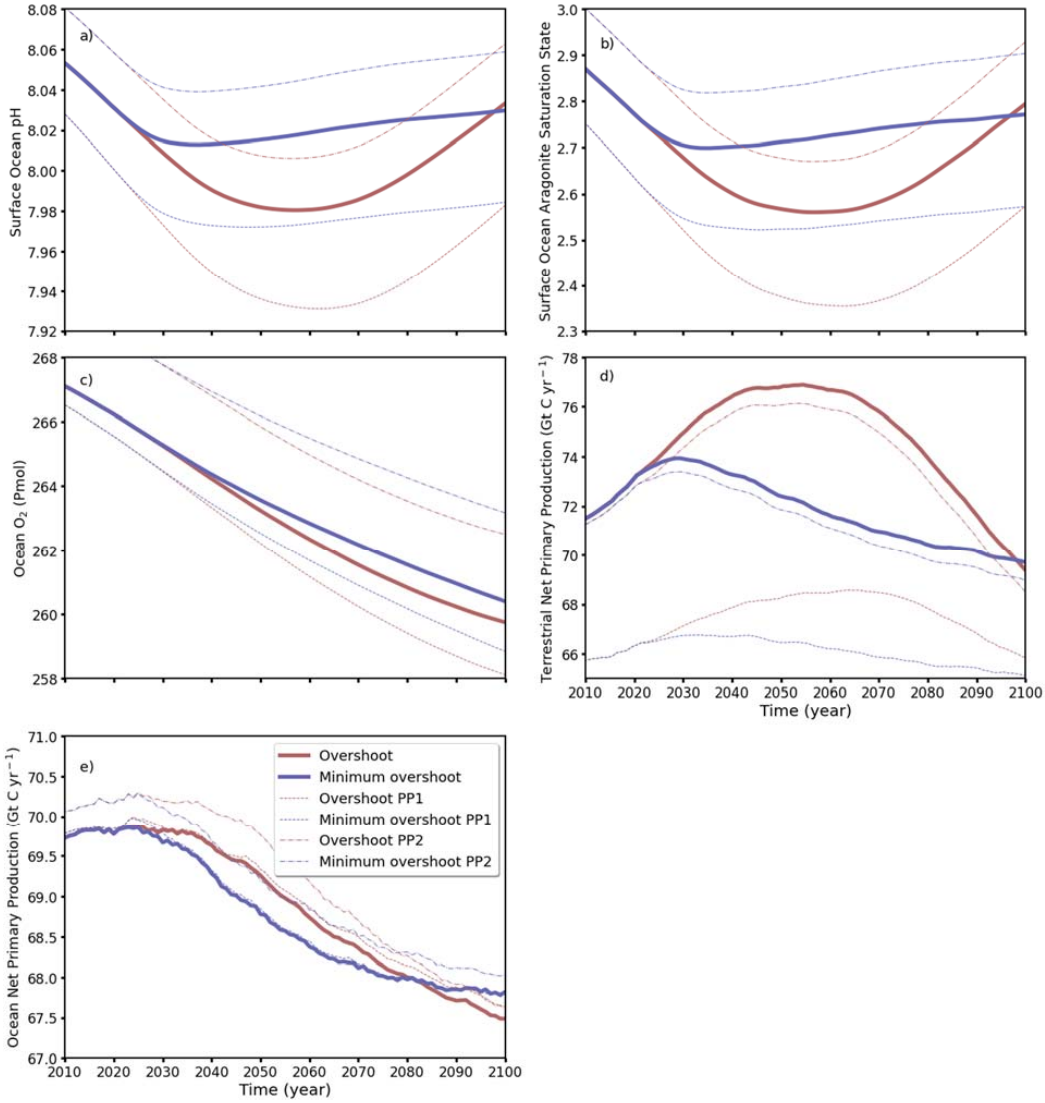

Figure S7. Comparison of UVic simulated global annual mean changes in (a) surface ocean pH, (b) surface ocean aragonite saturation state, (c) total ocean oxygen, (d) terrestrial net primary production, and (e) ocean net primary production. The dotted and dashed-dot lines are from perturbed parameter simulations that were chosen to investigate potential upper (dotted; PP1) and lower (dashed-dot; PP2) temperature responses to the forcing in these scenarios.

Ice-sheet simulations with PISM

The Parallel Ice Sheet Model (PISM v1.1; Winkelmann et al., 2011) is a thermo-mechanically coupled (polythermal) ice-sheet/ice-shelf model. It uses a hybrid of the shallow-ice approximation (SIA) and the shallow-shelf approximation (SSA) to calculate ice velocities over the entire domain. PISM is discretized on a regular rectangular grid using finite differences. The grounding-line position is determined using hydrostatic equilibrium, with sub-grid interpolation of the friction (Feldmann et al., 2014). The calving front position is determined by the "eigencalving" parameterization (Levermann et al., 2012) and a terminal thickness threshold of 50 m.

Basal sliding of the ice over the bedrock is calculated using a "pseudo-plastic" power law with sliding exponents 0.75 for Antarctica and 0.6 for Greenland, respectively. Subglacial meltwater is stored in the till. The yield stress is determined via the Mohr-Coulomb criterion, which parametrizes till material properties, and the effective pressure on the saturated till which depends on the amount of subglacial meltwater stored. (Bueler and van Pelt, 2015).

The melt rate underneath the ice shelves is calculated with the Potsdam Ice-shelf Cavity mOdel (PICO; Reese et al., 2018).

For the Antarctic ice sheet simulations, the model is initialized from Bedmap2 geometry (Fretwell et al., 2013), regridded to a horizontal resolution of 8 km. PICO is initialized using an ocean data compilation from Locarnini et al. (2018) and Schmidtko et al. (2014). Temperatures in the Amundsen Sea had to be reduced to cold conditions (−1.25°C) to prevent collapse of the region irrespective of basal sliding parameters. The near-surface climate, surface mass balance, and ice surface temperature are initialized from RACMO2.3p2 (van Wessem et al., 2018). The UVic ocean temperature, air temperature, and precipitation fields are then applied as anomalies to the climatic boundary conditions.

For the Greenland ice sheet simulations the initialization of the model is analogous to Zeitz et al. 2021. The model runs are performed at a horizontal resolution of 4.5km, which is high enough to capture the dynamic contribution of the ice sheet, but underestimates the role of small outlet glaciers which are not fully resolved. The UVic overshoot and small overshoot scenarios are averaged over the Greenland simulation domain and are used as a scalar anomaly forcing, which changes the RACMO temperature and precipitation field uniformly. In addition a temperature lapse rate of 6 K/km and a precipitation correction are applied.

The climatic mass balance is determined through dEBM-simple model (Zeitz et al. 2021).An ensemble of 100 simulations is performed. The dEBM-simple model parameters are varies as described in Zeitz et al. (2021), Appendix E. In addition we vary the refreeze rate r and the atmospheric lapse rate Γ as truncated normal distributions with the mean of 0.5 and 6°C/km and the standard deviation of 0.2 and 0.5°C/km respectively.

LPJmL

Anomalies from UVic are used and added to the observation-based climate data from the Climate Research Unit (CRU TS version 3.23, University of East Anglia Climatic Research Unit, 2015; Harris et al., 2014) and precipitation provided by the Global Precipitation Climatology Centre (GPCC Full Data Reanalysis version 7.0; Becker et al., 2013). Shortwave downward radiation and net downward longwave radiation reanalysis data from ERAInterim (Dee et al., 2011) are used to fill this gap.

Figure S8 shows the change of carbon stocks, if the land-use patterns are kept constant at the year 2005. The model runs only vary climate variables as delivered by the UVic model. The figure depicts changes in carbon density in each cell as the difference between carbon densities in 2090-2100 as compared with 2010-2020 in units of gC per m^2. Both figures are very similar, which supports the argument that land-use change, which has been set constant for these figures, is more important than differences in climate variables.

(a) (b)

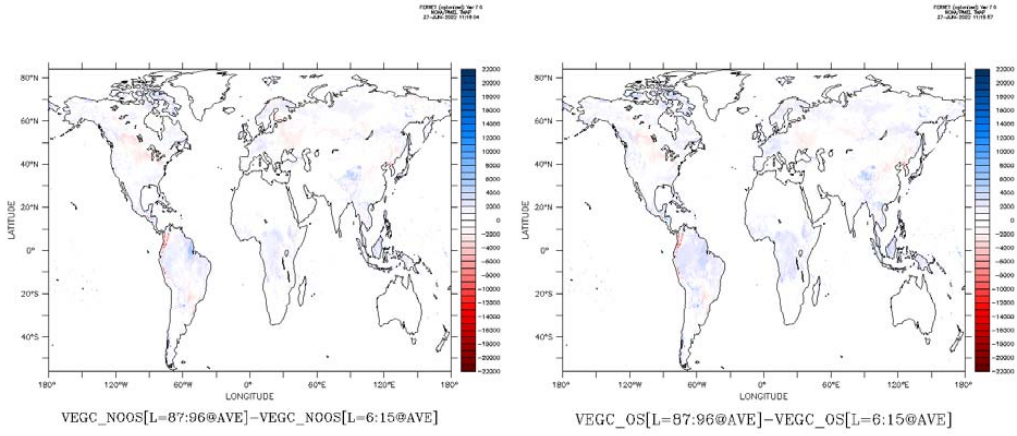

Figure S8: Changes in carbon stocks for the scenarios with low-overshoot (a) and high overshoot (b). Same as in Figure 7, but constant land use.

Figure S9 shows the development of annual net biomass production for the two scenarios. While Panel (a) shows the results for the cases including land-use changes such as afforestation, Panel (b) shows the results for the two scenarios with constant land-use. The results show that accounting only for changes in climate variables the vegetation carbon stock is first higher in the scenario with the full overshoot but falls below and even turns into a net source of carbon after 2080. If also land-use change is included in both scenarios the vegetation carbon stock increases more substantially and the scenario with low overshoot is consistently above the full overshoot scenario.

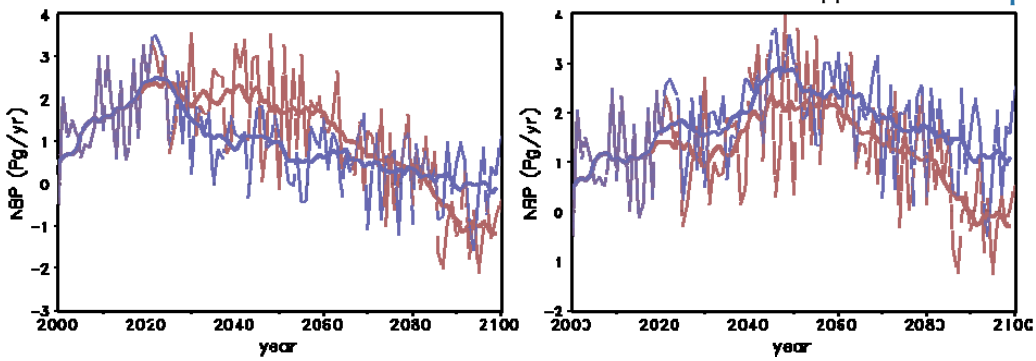

Figure S9: Net biomass production in scenarios with low (blue) and with full overshoot (red). The thin lines depict annual values, whereas thick lines are the corresponding 5-year moving averages. Panel (a) only considers climate variables of temperature, CO_2-concentration and precipitation, whereas Panel (b) also includes the information about land-use change, incl. afforestation.

Extreme event exposure

The estimation of the extreme events frequency at the grid level is based on 273 global-scale impact projections available through phase 2b of the Inter-Sectoral Impact Model Intercomparison Project (ISIMIP2b, Frieler et al. 2017), which uses a broad set of climate and impact models under three Representative Concentration Pathways (RCPs: RCP2.6, 6.0 and 8.5).Here, we drive the estimates using the global mean temperatures trajectories from the UVic model and assess two different metrics. First, we compare projected frequencies of extreme events over time. Second, we compare the cumulative frequency distribution of extreme events over time and weigh it with the population distribution to yield lifetime exposure of an average representative person of an age cohort in a specific country. The country-level estimates are subsequently aggregated to the regional and global scale accounting for total population and cohort size. Note that the method relies on transferring simulated extreme events from the RCP scenarios to the UVic overshoot/minimal-overshoot trajectories using global mean temperature anomalies relative to the pre-industrial period, thereby assuming the occurrence of extreme weather events to scale with global warming levels. This assumption can be considered reasonably valid for the considered extreme event categories (Lange et al., 2020). The method focuses on exposure rather than risk, that is, it does not relate to a welfare analysis.

997 References for SI

998 Noël, B., van de Berg, W. J., van Wessem, J. M., van Meijgaard, E., van As, D., Lenaerts, J. T. M.,
999 Lhermitte, S., Kuipers Munneke, P., Smeets, C. J. P. P., van Ulft, L. H., van de Wal, R. S. W., and
1000 van den Broeke, M. R.: Modelling the climate and surface mass balance of polar ice sheets
1001 using RACMO2 – Part 1: Greenland (1958–2016), The Cryosphere, 12, 811–831,
1002 https://doi.org/10.5194/tc-12-811-2018, 2018.

1003 Tran, G.T., Oschlies, A., Keller, D.P., 2020. Comparative Assessment of Climate Engineering Scenarios in
1004 the Presence of Parametric Uncertainty. J. Adv. Model. Earth Syst. 12.
1005 https://doi.org/10.1029/2019MS001787

1006 Zeitz, M., Reese, R., Beckmann, J., Krebs-Kanzow, U., and Winkelmann, R.: Impact of the melt–albedo
1007 feedback on the future evolution of the Greenland Ice Sheet with PISM-dEBM-simple, The
1008 Cryosphere, 15, 5739–5764, https://doi.org/10.5194/tc-15-5739-2021, 2021.

1009

1010

Bibliography

Adhikari, Surendra, Glenn A. Milne, Lambert Caron, Shfaqat Abbas Khan, K. K. Kjeldsen, J. Nilsson, Eric Y. Larour, and Erik R. Ivins (2021). **Decadal to Centennial Timescale Mantle Viscosity Inferred From Modern Crustal Uplift Rates in Greenland**. *Geophysical Research Letters* 48:19, 1–11. ISSN: 0094-8276. DOI: 10.1029/2021gl094040 (see page 139).

Albrecht, Torsten and Anders Levermann (2012). **Fracture field for large-scale ice dynamics**. *Journal of Glaciology* 58:207, 165–176 (see page 139).

Armstrong McKay, David I., Arie Staal, Jesse F Abrams, Ricarda Winkelmann, Boris Sakschewski, Sina Loriani, Ingo Fetzer, Sarah E Cornell, Johan Rockström, and Timothy M. Lenton (2021). **Updated assessment suggests > 1 . 5 ° C global warming could trigger multiple climate tipping points**, 1–80. DOI: 10.1002/essoar.10509769.1 (see pages 2, 8).

Aschwanden, Andy, Mark A. Fahnestock, and Martin Truffer (2016). **Complex Greenland outlet glacier flow captured**. *Nature Communications* 7:May 2015, 10524. ISSN: 2041-1723. DOI: 10.1038/ncomms10524. URL: http://dx.doi.org/10.1038/ncomms10524 (see page 14).

Aschwanden, Andy, Mark A. Fahnestock, Martin Truffer, Douglas J. Brinkerhoff, Regine Hock, Constantine Khroulev, Ruth H. Mottram, and Shfaqat Abbas Khan (2019). **Contribution of the Greenland Ice Sheet to sea level over the next millennium**. *Science Advances* 5:6, eaav9396. ISSN: 2375-2548. DOI: 10.1126/sciadv.aav9396. URL: http://advances.sciencemag.org/lookup/doi/10.1126/sciadv.aav9396 (see pages 3, 4, 12, 18, 123).

Beckmann, Johanna, Mahé Perrette, Sebastian Beyer, Reinhard Calov, Matteo Willeit, and Andrey Ganopolski (2018). **Modeling the response of Greenland outlet glaciers to global warming using a coupled flowline-plume model**. *The Cryosphere*: 880 mm, 1–32. ISSN: 1994-0424. DOI: 10.5194/tc-2018-89 (see page 4).

Bevis, Michael, Christopher Harig, Shfaqat Abbas Khan, Abel Brown, Frederik J. Simons, Michael Willis, Xavier Fettweis, Michiel R. Van Den Broeke, Finn Bo Madsen, Eric Kendrick, Dana J. Caccamise, Tonie Van Dam, Per Knudsen, and Thomas Nylen (2019). **Accelerating changes in ice mass within Greenland, and the ice sheet's sensitivity to atmospheric forcing**. *Proceedings of the National Academy of Sciences of the United States of America* 116:6, 1934–1939. ISSN: 10916490. DOI: 10.1073/pnas.1806562116 (see page 6).

Boers, Niklas and Martin Rypdal (2021). **Critical slowing down suggests that the western Greenland Ice Sheet is close to a tipping point**. *Proceedings of the National*

Academy of Sciences of the United States of America 118:21, 1–7. ISSN: 10916490. DOI: 10.1073/pnas.2024192118 (see pages 4, 10).

Bons, Paul D., Thomas Kleiner, Maria Gema Llorens, David J. Prior, T Sachau, Ilka Weikusat, and Daniela Jansen (July 2018). **Greenland Ice Sheet: Higher Nonlinearity of Ice Flow Significantly Reduces Estimated Basal Motion**. *Geophysical Research Letters* 45:13, 6542–6548. ISSN: 00948276. DOI: 10.1029/2018GL078356. URL: http://doi.wiley.com/10.1029/2018GL078356 (see pages 125, 126).

Box, Jason E. (2013). **Greenland ice sheet mass balance reconstruction. Part II: Surface mass balance (1840-2010)**. *Journal of Climate* 26:18, 6974–6989. ISSN: 08948755. DOI: 10.1175/JCLI-D-12-00518.1 (see page 11).

Box, Jason E., Xavier Fettweis, Julienne C. Stroeve, Marco Tedesco, Dorothy K. Hall, and Konrad Steffen (Aug. 2012). **Greenland ice sheet albedo feedback: thermodynamics and atmospheric drivers**. *The Cryosphere* 6:4, 821–839. ISSN: 1994-0424. DOI: 10.5194/tc-6-821-2012. URL: www.the-cryosphere.net/6/821/2012/%20https://tc.copernicus.org/articles/6/821/2012/ (see pages 11, 17, 129).

Box, Jason E., Dirk van As, Konrad Steffen, Robert Schjøtt Fausto, Andreas P. Ahlstrøm, Michele Citterio, and Signe B. Andersen (2017). **Greenland, Canadian and Icelandic land-ice albedo grids (2000–2016)**. *Geological Survey of Denmark and Greenland Bulletin* 38:July 2016, 53–56. ISSN: 16048156 (see page 11).

Box, Jason E., Adrien Wehrlé, Dirk van As, Robert S Fausto, Kristian K Kjeldsen, Amrin Dachauer, Andreas P Ahlstrøm, and Ghislain Picard (2022). **Greenland Ice Sheet Rainfall, Heat and Albedo Feedback Impacts From the Mid-August 2021 Atmospheric River**. *Geophysical Research Letters* 49:11, e2021GL097356. DOI: 10.1029/2021GL097356. URL: https://agupubs.onlinelibrary.wiley.com/doi/full/10.1029/2021GL097356 (see pages 10, 129).

Brinkerhoff, Douglas J., Andy Aschwanden, and Mark A. Fahnestock (2021). **Constraining subglacial processes from surface velocity observations using surrogate-based Bayesian inference**. *Journal of Glaciology* 67:263, 385–403. ISSN: 00221430. DOI: 10.1017/jog.2020.112. arXiv: 2006.12422 (see page 141).

Bueler, Ed and Jed Brown (2009). **Shallow shelf approximation as a "sliding law" in a thermomechanically coupled ice sheet model**. *Journal of Geophysical Research: Solid Earth* 114:3, 1–21. ISSN: 21699356. DOI: 10.1029/2008JF001179. arXiv: 0810.3449 (see page 15).

Bueler, Ed, Craig S. Lingle, and Jed Brown (2007). **Fast computation of a viscoelastic deformable Earth model for ice-sheet simulations**. *Annals of Glaciology* 46:May 2021, 97–105. ISSN: 02603055. DOI: 10.3189/172756407782871567 (see page 20).

Caesar, L., S. Rahmstorf, A. Robinson, G. Feulner, and V. Saba (2018). **Observed fingerprint of a weakening Atlantic Ocean overturning circulation**. *Nature* 556:7700, 191–196. ISSN: 14764687. DOI: 10.1038/s41586-018-0006-5 (see page 7).

Carroll, Dustin, D. A. Sutherland, B. Hudson, Twila Alexandra Moon, Ginny A. Catania, E. L. Shroyer, J. D. Nash, Timothy C. Bartholomaus, Denis Felikson, Leigh A. Stearns,

Brice P. Y. Noël, and Michiel R. van den Broeke (Sept. 2016). **The impact of glacier geometry on meltwater plume structure and submarine melt in Greenland fjords**. *Geophysical Research Letters* 43:18, 9739–9748. ISSN: 00948276. DOI: 10.1002/2016GL070170. URL: http://doi.wiley.com/10.1002/2016GL070170 (see page 12).

Climate Analytics and NewClimate (2021). **Warming Projections Global Update**. Tech. rep. November, 1–31. URL: https://climateactiontracker.org/publications/glasgows-2030-credibility-gap-net-zeros-lip-service-to-climate-action/ (see page 2).

Colleoni, Florence, Laura De Santis, Christine S Siddoway, Andrea Bergamasco, Nicholas R. Golledge, Gerrit Lohmann, Sandra Passchier, and Martin J Siegert (Dec. 2018). **Spatio-temporal variability of processes across Antarctic ice-bed–ocean interfaces**. *Nature Communications* 9:1, 2289. ISSN: 2041-1723. DOI: 10.1038/s41467-018-04583-0. URL: https://doi.org/10.1038/s41467-018-04583-0%20http://www.nature.com/articles/s41467-018-04583-0 (see page 135).

Cook, Joseph M., Andrew J. Tedstone, Christopher J. Williamson, Jenine McCutcheon, Andrew J. Hodson, Archana Dayal, McKenzie Skiles, Stefan Hofer, Robert Bryant, Owen McAree, Andrew McGonigle, Jonathan C. Ryan, Alexandre M. Anesio, Tristram D. L. Irvine-Fynn, Alun Hubbard, Edward Hanna, Mark Flanner, Sathish Mayanna, Liane G. Benning, Dirk van As, Marian Yallop, James B. McQuaid, Thomas Gribbin, and Martyn Tranter (Jan. 2020). **Glacier algae accelerate melt rates on the south-western Greenland Ice Sheet**. *The Cryosphere* 14:1, 309–330. ISSN: 1994-0424. DOI: 10.5194/tc-14-309-2020. URL: https://tc.copernicus.org/articles/14/309/2020/ (see pages 3, 11, 17, 126).

Cuffey, Kurt M. and William Stanley Bryce Paterson (2010). **The Physics of glaciers**. 4th ed. Elsevier Inc., 90–. ISBN: 9780123694614. URL: http://linkinghub.elsevier.com/retrieve/pii/0016718571900868 (see pages 15, 16, 134, 137, 138).

Cullather, Richard I. and Sophie M. J. Nowicki (2018). **Greenland Ice Sheet surface melt and its relation to daily atmospheric conditions**. *Journal of Climate* 31:5, 1897–1919. ISSN: 08948755. DOI: 10.1175/JCLI-D-17-0447.1 (see page 137).

De Boer, B., P. Stocchi, and R. S.W. Van De Wal (2014). **A fully coupled 3-D ice-sheet-sea-level model: Algorithm and applications**. *Geoscientific Model Development* 7:5, 2141–2156. ISSN: 19919603. DOI: 10.5194/gmd-7-2141-2014 (see page 19).

DeConto, Robert M. and David Pollard (2016). **Contribution of Antarctica to past and future sea-level rise**. *Nature* 531:7596, 591–597. ISSN: 14764687. DOI: 10.1038/nature17145. URL: http://dx.doi.org/10.1038/nature17145 (see page 8).

Di Mauro, B, R Garzonio, G Baccolo, A Franzetti, F Pittino, B Leoni, and D Remias (2020). **Glacier algae foster ice-albedo feedback in the European Alps**. *Scientific Reports* 10:1, 1–9. ISSN: 2045-2322. DOI: 10.1038/s41598-020-61762-0. URL: http://dx.doi.org/10.1038/s41598-020-61762-0 (see page 17).

Dobricic, Srdjan, Simone Russo, Luca Pozzoli, Julian Wilson, and Elisabetta Vignati (Feb. 2020). **Increasing occurrence of heat waves in the terrestrial Arctic**. *Environ-*

mental Research Letters 15:2, 024022. ISSN: 1748-9326. DOI: 10.1088/1748-9326/ab6398. URL: https://iopscience.iop.org/article/10.1088/1748-9326/ab6398 (see page 142).

Donges, Jonathan F., J. Heitzig, W. Barfuss, M. Wiedermann, J. A. Kassel, T. Kittel, J. J. Kolb, T. Kolster, F. Müller-Hansen, I. M. Otto, K. B. Zimmerer, and W. Lucht (2020). **Earth system modeling with endogenous and dynamic human societies: the copan:CORE open World–Earth modeling framework**. *Earth System Dynamics* 11:2, 395–413. DOI: 10.5194/esd-11-395-2020. URL: https://esd.copernicus.org/articles/11/395/2020/ (see page 8).

Donges, Jonathan F., W. Lucht, S. E. Cornell, J. Heitzig, W. Barfuss, S. J. Lade, and M. Schlüter (2021). **Taxonomies for structuring models for World–Earth systems analysis of the Anthropocene: subsystems, their interactions and social–ecological feedback loops**. *Earth System Dynamics* 12:4, 1115–1137. DOI: 10.5194/esd-12-1115-2021. URL: https://esd.copernicus.org/articles/12/1115/2021/ (see page 8).

Donges, Jonathan F., Ricarda Winkelmann, Wolfgang Lucht, Sarah E Cornell, James G Dyke, Johan Rockström, Jobst Heitzig, and Hans Joachim Schellnhuber (2017). **Closing the loop: Reconnecting human dynamics to Earth System science**. *The Anthropocene Review* 4:2, 151–157. DOI: 10.1177/2053019617725537. eprint: https://doi.org/10.1177/2053019617725537. URL: https://doi.org/10.1177/2053019617725537 (see page 8).

Edwards, Tamsin L., Mark A. Brandon, Gael Durand, Neil R. Edwards, Nicholas R. Golledge, Philip B. Holden, Isabel J. Nias, Antony J. Payne, Catherine Ritz, and Andreas Wernecke (Feb. 2019). **Revisiting Antarctic ice loss due to marine ice-cliff instability**. *Nature* 566:7742, 58–64. ISSN: 0028-0836. DOI: 10.1038/s41586-019-0901-4. URL: http://dx.doi.org/10.1038/s41586-019-0901-4%20http://www.nature.com/articles/s41586-019-0901-4 (see page 8).

Fausto, Robert Schjøtt, Andreas P. Ahlstrøm, Dirk Van As, Carl E. Bøggild, and Sigfus J. Johnsen (Sept. 2009). **A new present-day temperature parameterization for Greenland**. *Journal of Glaciology* 55:189, 95–105. ISSN: 0022-1430. DOI: 10.3189/002214309788608985. URL: https://www.cambridge.org/core/product/identifier/S0022143000200099/type/journal%7B%5C_%7Darticle (see page 127).

Fettweis, Xavier, Jason E. Box, Cécile Agosta, Charles Amory, Christoph Kittel, Charlotte Lang, Dirk van As, Horst Machguth, and Hubert Gallée (Apr. 2017). **Reconstructions of the 1900–2015 Greenland ice sheet surface mass balance using the regional climate MAR model**. *The Cryosphere* 11:2, 1015–1033. ISSN: 1994-0424. DOI: 10.5194/tc-11-1015-2017. URL: https://tc.copernicus.org/articles/11/1015/2017/ (see pages 17, 18).

Fettweis, Xavier, B. Franco, Marco Tedesco, J. H. van Angelen, Jan T.M. Lenaerts, Michiel R. Van Den Broeke, and Hubert Gallée (Mar. 2013). **Estimating the Greenland ice sheet surface mass balance contribution to future sea level rise using the regional atmospheric climate model MAR**. *The Cryosphere* 7:2, 469–489. ISSN:

1994-0424. DOI: 10.5194/tc-7-469-2013. URL: https://tc.copernicus.org/articles/7/469/2013/ (see page 17).

Fettweis, Xavier, Stefan Hofer, Uta Krebs-Kanzow, Charles Amory, Teruo Aoki, Constantijn J. Berends, Andreas Born, Jason E. Box, Alison Delhasse, Koji Fujita, Paul Gierz, Heiko Goelzer, Edward Hanna, Akihiro Hashimoto, Philippe Huybrechts, Marie-luise Kapsch, Michalea D. King, Christoph Kittel, Charlotte Lang, Peter L. Langen, Jan T.M. Lenaerts, Glen E. Liston, Gerrit Lohmann, Sebastian H. Mernild, Uwe Mikolajewicz, Kameswarrao Modali, Ruth H. Mottram, Masashi Niwano, Brice P. Y. Noël, Jonathan C. Ryan, Amy Smith, Jan Streffing, Marco Tedesco, Willem Jan van de Berg, Michiel R. Van Den Broeke, Roderik S. W. van de Wal, Leo van Kampenhout, David J. Wilton, Bert Wouters, Florian A. Ziemen, and Tobias Zolles (Nov. 2020). **GrSMBMIP: intercomparison of the modelled 1980–2012 surface mass balance over the Greenland Ice Sheet**. *The Cryosphere* 14:11, 3935–3958. ISSN: 1994-0424. DOI: 10.5194/tc-14-3935-2020. URL: https://tc.copernicus.org/articles/14/3935/2020/ (see page 18).

Fleming, Kevin and Kurt Lambeck (2004). **Constraints on the Greenland Ice Sheet since the Last Glacial Maximum from sea-level observations and glacial-rebound models**. *Quaternary Science Reviews* 23:9-10, 1053–1077. ISSN: 02773791. DOI: 10.1016/j.quascirev.2003.11.001 (see pages 19, 128).

Folke, Carl, Stephen R. Carpenter, Brian Walker, Marten Scheffer, Terry Chapin, and Johan Rockström (2010). **Resilience thinking: Integrating resilience, adaptability and transformability**. *Ecology and Society* 15:4. ISSN: 17083087. DOI: 10.5751/ES-03610-150420 (see page 5).

Frieler, Katja, Peter U. Clark, Feng He, Christo Buizert, Ronja Reese, Stefan R.M. Ligtenberg, Michiel R. Van Den Broeke, Ricarda Winkelmann, and Anders Levermann (2015). **Consistent evidence of increasing Antarctic accumulation with warming**. *Nature Climate Change* 5:4, 348–352. ISSN: 17586798. DOI: 10.1038/nclimate2574 (see page 138).

Fürst, J. J., Heiko Goelzer, and Philippe Huybrechts (2015). **Ice-dynamic projections of the Greenland ice sheet in response to atmospheric and oceanic warming**. *The Cryosphere* 9:3, 1039–1062. ISSN: 1994-0440. DOI: 10.5194/tcd-8-3851-2014. URL: http://www.the-cryosphere-discuss.net/8/3851/2014/ (see page 3).

Fyke, Jeremy G., Olga V. Sergienko, Marcus Löfverström, Stephen Price, and Jan T.M. Lenaerts (2018). **An Overview of Interactions and Feedbacks Between Ice Sheets and the Earth System**. *Reviews of Geophysics* 56:2, 361–408. ISSN: 19449208. DOI: 10.1029/2018RG000600 (see pages 6, 12).

Gardner, Alex S. and Martin J. Sharp (2010). **A review of snow and ice albedo and the development of a new physically based broadband albedo parameterization**. *Journal of Geophysical Research: Earth Surface* 115:1, 1–15. ISSN: 21699011. DOI: 10.1029/2009JF001444 (see page 11).

Gardner, Alex S., Martin J. Sharp, Roy M. Koerner, Claude Labine, Sarah Boon, Shawn J. Marshall, David O. Burgess, and David Lewis (2009). **Near-surface temperature lapse rates over arctic glaciers and their implications for temperature downscaling**. *Journal of Climate* 22:16, 4281–4298. ISSN: 08948755. DOI: 10.1175/2009JCLI2845.1 (see page 127).

Gaucherel, Cedric and Vincent Moron (Jan. 2016). **Potential stabilizing points to mitigate tipping point interactions in Earth's climate**. *International Journal of Climatology* 37:1, 399–408. ISSN: 08998418. DOI: 10.1002/joc.4712. URL: https://onlinelibrary.wiley.com/doi/10.1002/joc.4712 (see page 7).

Goelzer, Heiko, Sophie M. J. Nowicki, Antony J. Payne, Eric Y. Larour, Hélène Seroussi, William H. Lipscomb, Jonathan M. Gregory, Ayako Abe-Ouchi, Andrew Shepherd, Erika Simon, Cécile Agosta, Patrick Alexander, Andy Aschwanden, Alice Barthel, Reinhard Calov, Christopher Chambers, Youngmin Choi, Joshua K. Cuzzone, Christophe Dumas, Tamsin Edwards, Denis Felikson, Xavier Fettweis, Nicholas R. Golledge, Ralf Greve, Angelika Humbert, Philippe Huybrechts, Sébastien Le Clec'h, Victoria Lee, Gunter R. Leguy, Chris Little, Daniel P. Lowry, Mathieu Morlighem, Isabel Nias, Aurélien Quiquet, Martin Rückamp, Nicole-Jeanne Schlegel, Donald A. Slater, Robin S. Smith, Fiammetta Straneo, Lev Tarasov, Roderik S. W. van de Wal, and Michiel R. Van Den Broeke (Sept. 2020). **The future sea-level contribution of the Greenland ice sheet: a multi-model ensemble study of ISMIP6**. *The Cryosphere* 14:9, 3071–3096. ISSN: 1994-0424. DOI: 10.5194/tc-14-3071-2020. URL: https://tc.copernicus.org/articles/14/3071/2020/ (see pages 3, 123, 141).

Goldsby, David L. and D. L. Kohlstedt (2001). **Superplastic deformation of ice: Experimental observations**. *Journal of Geophysical Research* 106:B6, 11017–11030. ISSN: 0148-0227. DOI: 10.1029/2000JB900336. URL: http://doi.wiley.com/10.1029/2000JB900336 (see page 16).

Gomez, Natalya, Konstantin Latychev, and David Pollard (2018). **A coupled ice sheet-sea level model incorporating 3D earth structure: Variations in Antarctica during the Last Deglacial Retreat**. *Journal of Climate* 31:10, 4041–4054. ISSN: 08948755. DOI: 10.1175/JCLI-D-17-0352.1 (see page 19).

Gomez, Natalya, David Pollard, and Jerry X. Mitrovica (2013). **A 3-D coupled ice sheet - sea level model applied to Antarctica through the last 40 ky**. *Earth and Planetary Science Letters* 384, 88–99. ISSN: 0012821X. DOI: 10.1016/j.epsl.2013.09.042. URL: http://dx.doi.org/10.1016/j.epsl.2013.09.042 (see page 19).

Gomez, Natalya, Michael E. Weber, Peter U. Clark, Jerry X. Mitrovica, and Holly Kyeore Han (2020). **Antarctic ice dynamics amplified by Northern Hemisphere sea-level forcing**. *Nature* 587:7835, 600–604. ISSN: 14764687. DOI: 10.1038/s41586-020-2916-2. URL: http://dx.doi.org/10.1038/s41586-020-2916-2 (see page 19).

Gregory, Jonathan M., Steven E. George, and Robin S. Smith (Dec. 2020). **Large and irreversible future decline of the Greenland ice sheet**. *The Cryosphere* 14:12,

4299–4322. ISSN: 1994-0424. DOI: 10.5194/tc-14-4299-2020. URL: https://tc.copernicus.org/articles/14/4299/2020/ (see pages 4, 7, 11, 133–135, 137, 138).

Greve, Ralf and Heinz Blatter (2009). **Dynamics of Ice Sheets and Glaciers**. Ed. by K Hutter. Advances in Geophysical and Environmental Mechanics and Mathematics. Berlin, Heidelberg: Springer Berlin Heidelberg. ISBN: 978-3-642-03414-5. DOI: 10.1007/978-3-642-03415-2. URL: http://link.springer.com/10.1007/978-3-642-03415-2 (see pages 14–16, 138).

Haeger, C., Mikhail K. Kaban, M. Tesauro, Alexey G. Petrunin, and W. D. Mooney (2019). **3-D Density, Thermal, and Compositional Model of the Antarctic Lithosphere and Implications for Its Evolution**. *Geochemistry, Geophysics, Geosystems* 20:2, 688–707. ISSN: 15252027. DOI: 10.1029/2018GC008033 (see page 19).

Hall, Alex (2004). **The role of surface albedo feedback in climate**. *Journal of Climate* 17:7, 1550–1568. ISSN: 08948755. DOI: 10.1175/1520-0442(2004)017<1550:TROSAF>2.0.CO;2 (see page 6).

Hanna, Edward, Philippe Huybrechts, Ives Janssens, John Cappelen, Konrad Steffen, and Ag Stenhens (2005). **Runoff and mass balance of the Greenland ice sheet: 1958-2003**. *Journal of Geophysical Research Atmospheres* 110:13, 1–16. ISSN: 01480227. DOI: 10.1029/2004JD005641 (see page 127).

Hanna, Edward, Sebastian H. Mernild, John Cappelen, and Konrad Steffen (2012). **Recent warming in Greenland in a long-term instrumental (1881-2012) climatic context: I. Evaluation of surface air temperature records**. *Environmental Research Letters* 7:4. ISSN: 17489326. DOI: 10.1088/1748-9326/7/4/045404 (see page 2).

Hanna, Edward, Frank Pattyn, Francisco Navarro, Vincent Favier, Heiko Goelzer, Michiel R. van den Broeke, Miren Vizcaíno, Pippa L. Whitehouse, Catherine Ritz, Kevin Bulthuis, and Ben Smith (2020). **Mass balance of the ice sheets and glaciers – progress since AR5 and challenges**. *Earth-Science Reviews* 201:June 2019, 102976. ISSN: 0012-8252. DOI: 10.1016/j.earscirev.2019.102976. URL: https://www.sciencedirect.com/science/article/pii/S0012825219303848?dgcid=rss%7B%5C_%7Dsd%7B%5C_%7Dall%7B%5C&%7Dutm%7B%5C_%7Dsource=researcher%7B%5C_%7Dapp%7B%5C&%7Dutm%7B%5C_%7Dmedium=referral%7B%5C&%7Dutm%7B%5C_%7Dcampaign=RESR%7B%5C_%7DMRKT%7B%5C_%7DResearcher%7B%5C_%7Dinbound (see page 2).

Harrington, Joel A., Neil F. Humphrey, and Joel T. Harper (2015). **Temperature distribution and thermal anomalies along a flowline of the Greenland ice sheet**. *Annals of Glaciology* 56:70, 98–104. ISSN: 02603055. DOI: 10.3189/2015AoG70A945 (see page 137).

Held, Isaac M. and Brian J. Soden (Nov. 2006). **Robust Responses of the Hydrological Cycle to Global Warming**. *Journal of Climate* 19:21, 5686–5699. ISSN: 1520-0442. DOI: 10.1175/JCLI3990.1. URL: http://journals.ametsoc.org/doi/10.1175/JCLI3990.1 (see page 138).

Hock, Regine (1999). **A distributed temperature-index ice- and snowmelt model including potential direct solar radiation**. *Journal of Glaciology*: 149 (see page 18).

Hu, Aixue, Gerald A. Meehl, Weiqing Han, Jianjun Yin, Bingyi Wu, and Masahide Kimoto (2013). **Influence of continental ice retreat on future global climate**. *Journal of Climate* 26:10, 3087–3111. ISSN: 08948755. DOI: 10.1175/JCLI-D-12-00102.1 (see page 7).

IMBIE Team (Mar. 2020). **Mass balance of the Greenland Ice Sheet from 1992 to 2018.** *Nature* 579:7798, 233–239. ISSN: 1476-4687. DOI: 10.1038/s41586-019-1855-2. URL: http://www.nature.com/articles/s41586-019-1855-2%20http://www.ncbi.nlm.nih.gov/pubmed/31822019 (see pages 2, 12, 138).

Karlsson, Nanna B, Anne M Solgaard, Kenneth D Mankoff, Fabien Gillet-Chaulet, Joseph A MacGregor, Jason E. Box, Michele Citterio, William T Colgan, Signe H Larsen, Kristian K Kjeldsen, et al. (2021). **A first constraint on basal melt-water production of the Greenland ice sheet**. *Nature Communications* 12:1, 1–10. DOI: 10.1038/s41467-021-23739-z. URL: https://doi.org/10.1038/s41467-021-23739-z (see page 12).

Khan, Shfaqat Abbas, Ingo Sasgen, Michael Bevis, Tonie van Dam, Jonathan L. Bamber, John Wahr, Michael Willis, Kurt H. Kjær, Bert Wouters, Veit Helm, Beata Csatho, Kevin Fleming, Anders Anker Bjørk, Andy Aschwanden, Per Knudsen, and Peter Kuipers Munneke (2016). **Geodetic measurements reveal similarities between post–Last Glacial Maximum and present-day mass loss from the Greenland ice sheet**. *Science Advances* 2:9, e1600931. ISSN: 2375-2548. DOI: 10.1126/sciadv.1600931. URL: http://advances.sciencemag.org.biblioplanets.gate.inist.fr/content/2/9/e1600931 (see pages 19, 128).

King, Michalea D., Ian M. Howat, Salvatore G. Candela, Myoung J. Noh, Seongsu Jeong, Brice P. Y. Noël, Michiel R. van den Broeke, Bert Wouters, and Adelaide Negrete (2020). **Dynamic ice loss from the Greenland Ice Sheet driven by sustained glacier retreat**. *Communications Earth & Environment* 1:1, 1–7. ISSN: 2662-4435. DOI: 10.1038/s43247-020-0001-2. URL: http://dx.doi.org/10.1038/s43247-020-0001-2 (see pages 2, 133–135).

King, Michalea D., Ian M. Howat, Seongsu Jeong, Myoung J. Noh, Bert Wouters, Brice P. Y. Noël, and Michiel R. van den Broeke (Dec. 2018). **Seasonal to decadal variability in ice discharge from the Greenland Ice Sheet**. *The Cryosphere* 12:12, 3813–3825. ISSN: 1994-0424. DOI: 10.5194/tc-12-3813-2018. URL: https://tc.copernicus.org/articles/12/3813/2018/ (see page 137).

Krapp, Mario, Alexander Robinson, and Andrey Ganopolski (July 2017). **SEMIC: an efficient surface energy and mass balance model applied to the Greenland ice sheet**. *The Cryosphere* 11:4, 1519–1535. ISSN: 1994-0424. DOI: 10.5194/tc-11-1519-2017. URL: http://www.the-cryosphere-discuss.net/tc-2016-252/%20https://www.the-cryosphere.net/11/1519/2017/ (see pages 17, 18).

Krebs-Kanzow, Uta, Paul Gierz, and Gerrit Lohmann (Dec. 2018). **Brief communication: An ice surface melt scheme including the diurnal cycle of solar radiation**. *The*

Cryosphere 12:12, 3923–3930. ISSN: 1994-0424. DOI: 10.5194/tc-12-3923-2018. URL: https://www.the-cryosphere.net/12/3923/2018/ (see page 18).

Krebs-Kanzow, Uta, Paul Gierz, Christian B. Rodehacke, Shan Xu, Hu Yang, and Gerrit Lohmann (May 2021). **The diurnal Energy Balance Model (dEBM): a convenient surface mass balance solution for ice sheets in Earth system modeling**. *The Cryosphere* 15:5, 2295–2313. ISSN: 1994-0424. DOI: 10.5194/tc-15-2295-2021. URL: https://tc.copernicus.org/articles/15/2295/2021/ (see page 18).

Kriegler, Elmar, Jim W. Hall, Hermann Held, Richard Dawson, and Hans Joachim Schellnhuber (2009). **Imprecise probability assessment of tipping points in the climate system**. *Proceedings of the National Academy of Sciences of the United States of America* 106:13, 5041–5046. ISSN: 00278424. DOI: 10.1073/pnas.0809117106 (see page 7).

Kuiper, Ernst-Jan N., Ilka Weikusat, Johannes H. P. de Bresser, Daniela Jansen, Gill M. Pennock, and Martyn R. Drury (July 2020). **Using a composite flow law to model deformation in the NEEM deep ice core, Greenland – Part 1: The role of grain size and grain size distribution on deformation of the upper 2207 m**. *The Cryosphere* 14:7, 2429–2448. ISSN: 1994-0424. DOI: 10.5194/tc-14-2429-2020. URL: https://tc.copernicus.org/articles/14/2429/2020/ (see page 16).

Lambeck, Kurt, Hélène Rouby, Anthony Purcell, Yiying Sun, and Malcolm Sambridge (2014). **Sea level and global ice volumes from the Last Glacial Maximum to the Holocene**. *Proceedings of the National Academy of Sciences of the United States of America* 111:43, 15296–15303. ISSN: 10916490. DOI: 10.1073/pnas.1411762111 (see pages 19, 128).

Langen, Peter L., Ruth H. Mottram, J. H. Christensen, F. Boberg, Christian B. Rodehacke, M. Stendel, Dirk van As, Andreas P. Ahlstrøm, J. Mortensen, S. Rysgaard, D. Petersen, K. H. Svendsen, G. Aðalgeirsdóttir, and John Cappelen (May 2015). **Quantifying Energy and Mass Fluxes Controlling Godthåbsfjord Freshwater Input in a 5-km Simulation (1991–2012)*,+**. *Journal of Climate* 28:9, 3694–3713. ISSN: 0894-8755. DOI: 10.1175/JCLI-D-14-00271.1. URL: http://journals.ametsoc.org/doi/10.1175/JCLI-D-14-00271.1 (see page 17).

Larour, Eric Y., Hélène Seroussi, Surendra Adhikari, Erik R. Ivins, Lambert Caron, Mathieu Morlighem, and N. Schlegel (June 2019). **Slowdown in Antarctic mass loss from solid Earth and sea-level feedbacks**. *Science* 364:6444, eaav7908. ISSN: 0036-8075. DOI: 10.1126/science.aav7908. URL: https://www.sciencemag.org/lookup/doi/10.1126/science.aav7908 (see page 128).

Lau, Harriet C.P., Jerry X. Mitrovica, Jacqueline Austermann, Ophelia Crawford, David Al-Attar, and Konstantin Latychev (2016). **Inferences of mantle viscosity based on ice age data sets: Radial structure**. *Journal of Geophysical Research: Solid Earth* 121:10, 6991–7012. ISSN: 21699356. DOI: 10.1002/2016JB013043 (see page 128).

Le Clec'h, Sébastien, Sylvie Charbit, Aurélien Quiquet, Xavier Fettweis, Christophe Dumas, Masa Kageyama, Coraline Wyard, and Catherine Ritz (Feb. 2019). **Assessment**

of the Greenland ice sheet–atmosphere feedbacks for the next century with a regional atmospheric model coupled to an ice sheet model. *The Cryosphere* 13:1, 373–395. ISSN: 1994-0424. DOI: 10.5194/tc-13-373-2019. URL: https://www.the-cryosphere.net/13/373/2019/ (see pages 7, 18, 137).

Le Meur, Emmanuel and Philippe Huybrechts (Jan. 1996). **A comparison of different ways of dealing with isostasy: examples from modelling the Antarctic ice sheet during the last glacial cycle**. *Annals of Glaciology* 23, 309–317. ISSN: 0260-3055. DOI: 10.1017/S0260305500013586. URL: https://www.cambridge.org/core/product/identifier/S0260305500013586/type/journal%7B%5C_%7Darticle (see pages 20, 128).

– (1998). **Present-day uplift patterns over Greenland from a coupled ice-sheet/visco-elastic bedrock model**. *Geophysical Research Letters* 25:21, 3951–3954. ISSN: 00948276. DOI: 10.1029/1998GL900052 (see page 128).

Lecavalier, Benoit S., Glenn A. Milne, Matthew J.R. Simpson, Leanne M. Wake, Philippe Huybrechts, Lev Tarasov, Kristian K. Kjeldsen, Svend Funder, Antony J. Long, Sarah Woodroffe, Arthur S. Dyke, and Nicolaj K. Larsen (2014). **A model of Greenland ice sheet deglaciation constrained by observations of relative sea level and ice extent**. *Quaternary Science Reviews* 102, 54–84. ISSN: 02773791. DOI: 10.1016/j.quascirev.2014.07.018. URL: http://dx.doi.org/10.1016/j.quascirev.2014.07.018 (see page 128).

Lenton, Timothy M., H. Held, E. Kriegler, Jim W. Hall, W. Lucht, S. Rahmstorf, and Hans Joachim Schellnhuber (Feb. 2008). **Tipping elements in the Earth's climate system**. *Proceedings of the National Academy of Sciences* 105:6, 1786–1793. ISSN: 0027-8424. DOI: 10.1073/pnas.0705414105. URL: http://www.pnas.org/cgi/doi/10.1073/pnas.0705414105 (see pages 2, 4, 7).

Lenton, Timothy M., Johan Rockström, Owen Gaffney, Stefan Rahmstorf, Katherine Richardson, Will Steffen, and Hans Joachim Shellnhuber (2019). **Climate tipping points - too risky to bet against**. *Nature* 575, 592–595 (see page 2).

Levermann, Anders, Torsten Albrecht, Ricarda Winkelmann, Maria A. Martin, Marianne Haseloff, and I. Joughin (Mar. 2012). **Kinematic first-order calving law implies potential for abrupt ice-shelf retreat**. *The Cryosphere* 6:2, 273–286. ISSN: 1994-0424. DOI: 10.5194/tc-6-273-2012. URL: https://tc.copernicus.org/articles/6/273/2012/ (see page 130).

Levermann, Anders, Peter U. Clark, Ben Marzeion, Glenn A. Milne, David Pollard, Valentina Radic, and Alexander Robinson (2013). **The multimillennial sea-level commitment of global warming.** *Proceedings of the National Academy of Sciences* 110:34, 13745–13750. ISSN: 1091-6490. DOI: 10.1073/pnas.1219414110. URL: http://www.ncbi.nlm.nih.gov/pubmed/23858443 (see page 8).

Levermann, Anders and Ricarda Winkelmann (Aug. 2016). **A simple equation for the melt elevation feedback of ice sheets**. *The Cryosphere* 10:4, 1799–1807. ISSN: 1994-0424. DOI: 10.5194/tc-10-1799-2016. URL: https://tc.copernicus.org/articles/10/1799/2016/ (see pages 4, 10, 134).

Lingle, Craig S. and J. A. Clark (1985). **A numerical model of interactions between a marine ice sheet and the solid Earth: application to a West Antarctic ice stream.** *Journal of Geophysical Research* 90:C1, 1100–1114. ISSN: 01480227. DOI: 10.1029/JC090iC01p01100 (see page 20).

Ma, Ying, Olivier Gagliardini, Catherine Ritz, Fabien Gillet-Chaulet, Gaël Durand, and Maurine Montagnat (Sept. 2010). **Enhancement factors for grounded ice and ice shelves inferred from an anisotropic ice-flow model**. *Journal of Glaciology* 56:199, 805–812. ISSN: 0022-1430. DOI: 10.3189/002214310794457209. URL: http://www.agu.org/pubs/crossref/2011/2011GL048892.shtml%20https://www.cambridge.org/core/product/identifier/S0022143000214068/type/journal%7B%5C_%7Darticle (see page 17).

Martin, Maria A., Olga Alcaraz Sendra, Ana Bastos, Nico Bauer, Christoph Bertram, Thorsten Blenckner, Kathryn Bowen, Paulo M Brando, Tanya Brodie Rudolph, Milena Büchs, Mercedes Bustamante, Deliang Chen, Helen Cleugh, Purnamita Dasgupta, Fatima Denton, Jonathan F. Donges, Felix Kwabena Donkor, Hongbo Duan, Carlos M. Duarte, Kristie L. Ebi, Clea M. Edwards, Anja Engel, Eleanor Fisher, Sabine Fuss, Juliana Gaertner, Andrew Gettelman, Cécile A.J. Girardin, Nicholas R. Golledge, Jessica F. Green, Michael R. Grose, Masahiro Hashizume, Sophie Hebden, Helmke Hepach, Marina Hirota, Huang-Hsiung Hsu, Satoshi Kojima, Sharachchandra Lele, Sylvia Lorek, Heike K. Lotze, H. Damon Matthews, Darren McCauley, Desta Mebratu, Nadine Mengis, Rachael H. Nolan, Erik Pihl, Stefan Rahmstorf, Aaron Redman, Colleen E. Reid, Johan Rockström, Joeri Rogelj, Marielle Saunois, Lizzie Sayer, Peter Schlosser, Giles B. Sioen, Joachim H. Spangenberg, Detlef Stammer, Thomas N.S. Sterner, Nicola Stevens, Kirsten Thonicke, Hanqin Tian, Ricarda Winkelmann, and James Woodcock (Oct. 2021). **Ten new insights in climate science 2021: a horizon scan**. *Global Sustainability* 4, e25. ISSN: 2059-4798. DOI: 10.1017/sus.2021.25. URL: https://www.cambridge.org/core/product/identifier/S2059479821000259/type/journal%7B%5C_%7Darticle (see page 8).

Martinec, Zdenèk (2000). **Spectral-finite element approach to three-dimensional viscoelastic relaxation in a spherical earth**. *Geophysical Journal International* 142:1, 117–141. ISSN: 0956540X. DOI: 10.1046/j.1365-246X.2000.00138.x (see page 19).

Masson-Delmotte, V., P. Zhai, A. Pirani, S.L. Connors, C. Péan, S. Berger, N. Caud, Y. Chen, L. Goldfarb, M.I. Gomis, M. Huang, K. Leitzell, E. Lonnoy, J.B.R. Matthews, T.K. Maycock, T. Waterfield, O. Yelekçi, R. Yu, and B. Zhou, eds. (2021). **Climate Change 2021: The Physical Science Basis. Contribution of Working Group I to the Sixth Assessment Report of the Intergovernmental Panel on Climate Change**. Cambridge University Press. URL: https://www.ipcc.ch/report/ar6/wg1/downloads/report (see pages 1–3, 8, 14, 131, 137).

McCutcheon, Jenine, Stefanie Lutz, Christopher J. Williamson, Joseph M. Cook, Andrew J. Tedstone, Aubry Vanderstraeten, Siobhan A Wilson, Anthony Stockdale, Steeve Bonneville, Alexandre M. Anesio, Marian L Yallop, James B. McQuaid, Martyn Tranter,

and Liane G. Benning (Dec. 2021). **Mineral phosphorus drives glacier algal blooms on the Greenland Ice Sheet**. *Nature Communications* 12:1, 570. ISSN: 2041-1723. DOI: 10.1038/s41467-020-20627-w. URL: http://dx.doi.org/10.1038/s41467-020-20627-w%20http://www.nature.com/articles/s41467-020-20627-w (see pages 3, 17).

McGrath, Daniel, William Colgan, Nicolas Bayou, Atsuhiro Muto, and Konrad Steffen (2013). **Recent warming at Summit, Greenland: Global context and implications**. *Geophysical Research Letters* 40:10, 2091–2096. DOI: https://doi.org/10.1002/grl.50456. eprint: https://agupubs.onlinelibrary.wiley.com/doi/pdf/10.1002/grl.50456. URL: https://agupubs.onlinelibrary.wiley.com/doi/abs/10.1002/grl.50456 (see page 137).

Meinshausen, Malte, Nicolai Meinshausen, William Hare, Sarah CB Raper, Katja Frieler, Reto Knutti, David J Frame, and Myles R Allen (2009). **Greenhouse-gas emission targets for limiting global warming to 2 C**. *Nature* 458:7242, 1158–1162. DOI: 10.1038/nature08017. URL: https://doi.org/10.1038/nature08017 (see page 132).

Millstein, Joanna D, Brent M. Minchew, Samuel S Pegler, and Planetary Sciences (2021). **Reassessing the flow law of glacier oce using satellite observations**. *(preprint) Communications Earth & Environment*, 1–7 (see page 125).

Milne, Glenn A., Konstantin Latychev, Andrew Schaeffer, John W. Crowley, Benoit S. Lecavalier, and Alexandre Audette (2018). **The influence of lateral Earth structure on glacial isostatic adjustment in Greenland**. *Geophysical Journal International* 214:2, 1252–1266. ISSN: 1365246X. DOI: 10.1093/GJI/GGY189 (see page 128).

Montagnat, Maurine and Paul Duval (2000). **Rate controlling processes in the creep of polar ice, influence of grain boundary migration associated with recrystallization**. *Earth and Planetary Science Letters* 183:1-2, 179–186. ISSN: 0012821X. DOI: 10.1016/S0012-821X(00)00262-4 (see page 16).

Moon, Twila Alexandra, Ian Joughin, B. Smith, and Ian M. Howat (2012). **21st-Century Evolution of Greenland Outlet Glacier Velocities**. *Science* 336:May, 576–578. ISSN: 0036-8075. DOI: 10.1126/science.1219985 (see page 2).

Moon, Twila Alexandra, Ian Joughin, Ben Smith, Michiel R. van den Broeke, Willem Jan van de Berg, Brice P. Y. Noël, and Mika Usher (2014). **Distinct patterns of seasonal Greenland glacier velocity**. *Geophysical Research Letters* 41:20, 7209–7216. DOI: https://doi.org/10.1002/2014GL061836. eprint: https://agupubs.onlinelibrary.wiley.com/doi/pdf/10.1002/2014GL061836. URL: https://agupubs.onlinelibrary.wiley.com/doi/abs/10.1002/2014GL061836 (see page 2).

Mordret, Aurélien (2018). **Uncovering the Iceland Hot Spot Track Beneath Greenland**. *Journal of Geophysical Research: Solid Earth* 123:6, 4922–4941. ISSN: 21699356. DOI: 10.1029/2017JB015104 (see page 128).

Morlighem, Mathieu, C. N. Williams, Eric Rignot, Lu An, Jan Erik Arndt, Jonathan L. Bamber, G. Catania, N. Chauché, J. A. Dowdeswell, B. Dorschel, Ian G. Fenty, K. Hogan, Ian M. Howat, A. Hubbard, Martin Jakobsson, T. M. Jordan, Kristian K. Kjeldsen, Romain Millan, L. Mayer, Jérémie Mouginot, Brice P. Y. Noël, C. O'Cofaigh, S. Palmer, S. Rysgaard, Hélène Seroussi, Martin J Siegert, P. Slabon, Fiammetta Straneo,

Michiel R. van den Broeke, W. Weinrebe, Michael Wood, and K. B. Zinglersen (2017). **BedMachine v3: Complete Bed Topography and Ocean Bathymetry Mapping of Greenland From Multibeam Echo Sounding Combined With Mass Conservation**. *Geophysical Research Letters* 44:21, 11, 051–11, 061. ISSN: 19448007. DOI: 10.1002/2017GL074954 (see pages 2, 13).

Mouginot, Jérémie, Eric Rignot, Anders Anker Bjørk, Michiel R. Van Den Broeke, Romain Millan, Mathieu Morlighem, Brice P. Y. Noël, Bernd Scheuchl, and Michael Wood (Apr. 2019). **Forty-six years of Greenland Ice Sheet mass balance from 1972 to 2018**. *Proceedings of the National Academy of Sciences* 116:19, 201904242. ISSN: 0027-8424. DOI: 10.1073/pnas.1904242116. URL: http://www.pnas.org/lookup/doi/10.1073/pnas.1904242116 (see pages 2, 3, 12).

Mouginot, Jérémie, Eric Rignot, Bernd Scheuchl, and Romain Millan (2017). **Comprehensive annual ice sheet velocity mapping using Landsat-8, Sentinel-1, and RADARSAT-2 data**. *Remote Sensing* 9:4, 1–20. ISSN: 20724292. DOI: 10.3390/rs9040364 (see page 3).

Müller-Hansen, F., M. Schlüter, M. Mäs, Jonathan F. Donges, J. J. Kolb, K. Thonicke, and J. Heitzig (2017). **Towards representing human behavior and decision making in Earth system models – an overview of techniques and approaches**. *Earth System Dynamics* 8:4, 977–1007. DOI: 10.5194/esd-8-977-2017. URL: https://esd.copernicus.org/articles/8/977/2017/ (see page 8).

Nghiem, S. V., Dorothy K. Hall, T. L. Mote, Marco Tedesco, M. R. Albert, K. Keegan, Christopher A. Shuman, N. E. DiGirolamo, and G. Neumann (2012). **The extreme melt across the Greenland ice sheet in 2012**. *Geophysical Research Letters* 39:20, 6–11. ISSN: 00948276. DOI: 10.1029/2012GL053611 (see page 2).

Niwano, Masashi, Teruo Aoki, Akihiro Hashimoto, Sumito Matoba, Satoru Yamaguchi, Tomonori Tanikawa, Koji Fujita, Akane Tsushima, Yoshinori Iizuka, Rigen Shimada, and Masahiro Hori (Feb. 2018). **NHM–SMAP: spatially and temporally high-resolution nonhydrostatic atmospheric model coupled with detailed snow process model for Greenland Ice Sheet**. *The Cryosphere* 12:2, 635–655. ISSN: 1994-0424. DOI: 10.5194/tc-12-635-2018. URL: https://tc.copernicus.org/articles/12/635/2018/ (see page 17).

Noël, Brice P. Y., Willem Jan Van De Berg, Stef Lhermitte, Bert Wouters, H. Machguth, Ian M. Howat, Michele Citterio, G. Moholdt, Jan T.M. Lenaerts, and Michiel R. Van Den Broeke (Mar. 2017). **A tipping point in refreezing accelerates mass loss of Greenland's glaciers and ice caps**. *Nature Communications* 8:9296, 14730. ISSN: 2041-1723. DOI: 10.1038/ncomms14730. URL: http://www.nature.com/articles/ncomms14730%20http://www.nature.com/doifinder/10.1038/ncomms14730 (see page 140).

Noël, Brice P. Y., Willem Jan van de Berg, Erik van Meijgaard, Peter Kuipers Munneke, Roderik S. W. van de Wal, and Michiel R. Van Den Broeke (Sept. 2015). **Evaluation of the updated regional climate model RACMO2.3: summer snowfall impact**

on the Greenland Ice Sheet. *The Cryosphere* 9:5, 1831–1844. ISSN: 1994-0424. DOI: 10.5194/tc-9-1831-2015. URL: https://tc.copernicus.org/articles/9/1831/2015/ (see pages 11, 17).

Noël, Brice P. Y., Willem Jan van de Berg, Jan Melchior van Wessem, Erik van Meijgaard, Dirk van As, Jan T.M. Lenaerts, Stef Lhermitte, Peter Kuipers Munneke, C. J. P. Paul Smeets, Lambertus H. van Ulft, Roderik S. W. van de Wal, and Michiel R. van den Broeke (Mar. 2018). **Modelling the climate and surface mass balance of polar ice sheets using RACMO2 – Part 1: Greenland (1958–2016)**. *The Cryosphere* 12:3, 811–831. ISSN: 1994-0424. DOI: 10.5194/tc-12-811-2018. URL: https://tc.copernicus.org/articles/12/811/2018/ (see page 18).

Peltier, W. Richard and Rosemarie Drummong (2008). **Rheological stratification of the lithosphere: A direct inference based upon the geodetically observed pattern of the glacial isostatic adjustment of the North American continent**. *Geophysical Research Letters* 35:16, 1–5. ISSN: 00948276. DOI: 10.1029/2008GL034586 (see page 128).

Phillips, Thomas, Harihar Rajaram, William T. Colgan, Konrad Steffen, and Waleed Abdalati (2013). **Evaluation of cryo-hydrologic warming as an explanation for increased ice velocities in the wet snow zone, Sermeq Avannarleq, West Greenland**. *Journal of Geophysical Research: Earth Surface* 118:3, 1241–1256. ISSN: 21699011. DOI: 10.1002/jgrf.20079 (see page 139).

Phillips, Thomas, Harihar Rajaram, and Konrad Steffen (2010). **Cryo-hydrologic warming: A potential mechanism for rapid thermal response of ice sheets**. *Geophysical Research Letters* 37:20, 1–5. ISSN: 00948276. DOI: 10.1029/2010GL044397 (see page 139).

Poinar, Kristin, Ian Joughin, Jan T.M. Lenaerts, and Michiel R. Van Den Broeke (2017). **Englacial latent-heat transfer has limited influence on seaward ice flux in western Greenland**. *Journal of Glaciology* 63:237, 1–16. ISSN: 00221430. DOI: 10.1017/jog.2016.103 (see page 139).

Pörtner, H.-O., D.C. Roberts, V. Masson-Delmotte, P. Zhai, M. Tignor, E. Poloczanska, K. Mintenbeck, M. Nicolai, A. Okem, J. Petzold, B. Rama, and N. Weyer (2019). **IPCC Special Report on the Ocean and Cryosphere in a Changing Climate**. Tech. rep. (see pages 2, 8, 14).

Pritchard, Hamish, Stefan R.M. Ligtenberg, Helen Amanda Fricker, David G. Vaughan, Michiel R. Van Den Broeke, and Laurie Padman (2012). **Antarctic ice-sheet loss driven by basal melting of ice shelves**. *Nature* 484:7395, 502–505. ISSN: 00280836. DOI: 10.1038/nature10968 (see page 137).

Rahmstorf, Stefan and Dim Coumou (2011). **Increase of extreme events in a warming world**. *Proceedings of the National Academy of Sciences* 108:44, 17905–17909 (see page 142).

Reeh, Niels (1991). **Parameterization of melt rate and surface temperature on the Greenland ice sheet**. *Polarforschung* 59:3, 113–128. URL: http://epic.awi.de/2522/

1/Ree1989c.pdf%7B%5C%%7D0Apapers3://publication/uuid/EE2F413B-59F1-4D0B-A26F-7D6EB53624F8 (see pages 10, 17, 18).

Ricke, Katharine L. and Ken Caldeira (2014). **Maximum warming occurs about one decade after a carbon dioxide emission**. *Environmental Research Letters* 9:12. ISSN: 17489326. DOI: 10.1088/1748-9326/9/12/124002 (see page 137).

Ridley, Jeff, Jonathan M. Gregory, Philippe Huybrechts, and Jason Lowe (2010). **Thresholds for irreversible decline of the Greenland ice sheet**. *Climate Dynamics* 35:6, 1065–1073. ISSN: 09307575. DOI: 10.1007/s00382-009-0646-0 (see page 133).

Rignot, Eric, Michele Koppes, and Isabella Velicogna (2010). **Rapid submarine melting of the calving faces of West Greenland glaciers**. *Nature Geoscience* 3:3, 187–191. ISSN: 1752-0894. DOI: 10.1038/ngeo765. URL: http://www.nature.com/doifinder/10.1038/ngeo765 (see page 12).

Robinson, Alexander, Reinhard Calov, and Andrey Ganopolski (Apr. 2010). **An efficient regional energy-moisture balance model for simulation of the Greenland Ice Sheet response to climate change**. *The Cryosphere* 4:2, 129–144. ISSN: 1994-0424. DOI: 10.5194/tc-4-129-2010. URL: https://tc.copernicus.org/articles/4/129/2010/ (see page 18).

– (2012). **Multistability and critical thresholds of the Greenland ice sheet**. *Nature Climate Change* 2:6, 429–432. ISSN: 1758-678X. DOI: 10.1038/nclimate1449. URL: http://dx.doi.org/10.1038/nclimate1449 (see pages 2, 4, 133).

Rockström, Johan, Will Steffen, Kevin Noone, Åsa Persson, F. Stuart Chapin, Eric Lambin, Timothy M. Lenton, Marten Scheffer, Carl Folke, Hans Joachim Schellnhuber, Björn Nykvist, Cynthia A. de Wit, Terry Hughes, Sander van der Leeuw, Henning Rodhe, Sverker Sörlin, Peter K. Snyder, Robert Costanza, Uno Svedin, Malin Falkenmark, Louise Karlberg, Robert W. Corell, Victoria J. Fabry, James Hansen, Brian Walker, Diana Liverman, Katherine Richardson, Paul Crutzen, and Jonathan Foley (2009). **Planetary boundaries: Exploring the safe operating space for humanity**. *Ecology and Society* 14:2. ISSN: 17083087. DOI: 10.5751/ES-03180-140232 (see page 5).

Rückamp, Martin, Ralf Greve, and Angelika Humbert (Sept. 2019). **Comparative simulations of the evolution of the Greenland ice sheet under simplified Paris Agreement scenarios with the models SICOPOLIS and ISSM**. *Polar Science* 21:July, 14–25. ISSN: 18739652. DOI: 10.1016/j.polar.2018.12.003. URL: https://doi.org/10.1016/j.polar.2018.12.003%20https://linkinghub.elsevier.com/retrieve/pii/S1873965218301403 (see page 18).

Ryan, Jonathan C., Alun Hubbard, Marek Stibal, Tristram D. L. Irvine-Fynn, Joseph M. Cook, Laurence C. Smith, Karen A. Cameron, and Jason E. Box (2018). **Dark zone of the Greenland Ice Sheet controlled by distributed biologically-active impurities**. *Nature Communications* 9:1, 1–10. ISSN: 20411723. DOI: 10.1038/s41467-018-03353-2. URL: http://dx.doi.org/10.1038/s41467-018-03353-2 (see pages 3, 126).

Ryan, Jonathan C., Laurence C. Smith, Dirk van As, S. W. Cooley, Matthew G Cooper, Lincoln H Pitcher, and A Hubbard (Mar. 2019). **Greenland Ice Sheet surface melt**

amplified by snowline migration and bare ice exposure. *Science Advances* 5:3, eaav3738. ISSN: 2375-2548. DOI: 10.1126/sciadv.aav3738. URL: http://advances.sciencemag.org/lookup/doi/10.1126/sciadv.aav3738 (see page 11).

Saruya, Tomotaka, Koki Nakajima, Morimasa Takata, Tomoyuki Homma, Nobuhiko Azuma, and Kumiko Goto-Azuma (2019). **Effects of microparticles on deformation and microstructural evolution of fine-grained ice**. *Journal of Glaciology* 65:252, 531–541. ISSN: 00221430. DOI: 10.1017/jog.2019.29 (see page 16).

Schellnhuber, Hans Joachim, Stefan Rahmstorf, and Ricarda Winkelmann (2016). **Why the right climate target was agreed in Paris**. *Nature Climate Change* 6 (see pages 2, 8).

Schoof, Christian (2007). **Ice sheet grounding line dynamics: Steady states, stability, and hysteresis**. *Journal of Geophysical Research: Earth Surface* 112:3, 1–19. ISSN: 21699011. DOI: 10.1029/2006JF000664 (see pages 8, 126).

Simpson, Matthew J.R., Glenn A. Milne, Philippe Huybrechts, and Antony J. Long (2009). **Calibrating a glaciological model of the Greenland ice sheet from the Last Glacial Maximum to present-day using field observations of relative sea level and ice extent**. *Quaternary Science Reviews* 28:17-18, 1631–1657. ISSN: 02773791. DOI: 10.1016/j.quascirev.2009.03.004. URL: http://dx.doi.org/10.1016/j.quascirev.2009.03.004 (see page 20).

Slater, Donald A., Denis Felikson, Fiammetta Straneo, Heiko Goelzer, Christopher M. Little, Mathieu Morlighem, Xavier Fettweis, and Sophie M. J. Nowicki (Mar. 2020). **Twenty-first century ocean forcing of the Greenland ice sheet for modelling of sea level contribution**. *The Cryosphere* 14:3, 985–1008. ISSN: 1994-0424. DOI: 10.5194/tc-14-985-2020. URL: https://tc.copernicus.org/articles/14/985/2020/ (see page 138).

Slater, Thomas, Isobel R. Lawrence, Inès N. Otosaka, Andrew Shepherd, Noel Gourmelen, Livia Jakob, Paul Tepes, Lin Gilbert, and Peter Nienow (Jan. 2021). **Review article: Earth's ice imbalance**. *The Cryosphere* 15:1, 233–246. ISSN: 1994-0424. DOI: 10.5194/tc-15-233-2021. URL: https://tc.copernicus.org/articles/15/233/2021/ (see pages 2, 4).

Smith, E. Keith, Marc Wiedermann, Jonathan F. Donges, Jobst Heitzig, and Ricarda Winkelmann (2022). **Concern and anticipation of sea-level rise provide grounds for social tipping towards climate action**. DOI: 10.31219/osf.io/nyquv (see page 8).

Solgaard, Anne M. and Peter L. Langen (2012). **Multistability of the Greenland ice sheet and the effects of an adaptive mass balance formulation**. *Climate Dynamics* 39:7-8, 1599–1612. ISSN: 09307575. DOI: 10.1007/s00382-012-1305-4 (see page 4).

Steffen, Konrad and Jason E. Box (Dec. 2001). **Surface climatology of the Greenland Ice Sheet: Greenland Climate Network 1995-1999**. *Journal of Geophysical Research: Atmospheres* 106:D24, 33951–33964. ISSN: 01480227. DOI: 10.1029/2001JD900161. URL: http://doi.wiley.com/10.1029/2001JD900161 (see page 127).

Stibal, Marek, Jason E. Box, Karen A. Cameron, Peter L. Langen, Marian L. Yallop, Ruth H. Mottram, Alia L. Khan, Noah P. Molotch, Nathan A. M. Chrismas, Filippo Calì Quaglia, Daniel Remias, C. J. P. Paul Smeets, Michiel R. van den Broeke, Jonathan C. Ryan, Alun Hubbard, Martyn Tranter, Dirk As, and Andreas P. Ahlstrøm (Nov. 2017). **Algae Drive Enhanced Darkening of Bare Ice on the Greenland Ice Sheet**. *Geophysical Research Letters* 44:22, 11, 463–11, 471. ISSN: 0094-8276. DOI: 10.1002/2017GL075958. URL: https://onlinelibrary.wiley.com/doi/abs/10.1002/2017GL075958 (see page 3).

Straneo, Fiammetta and Patrick Heimbach (Dec. 2013). **North Atlantic warming and the retreat of Greenland's outlet glaciers**. *Nature* 504:7478, 36–43. ISSN: 0028-0836. DOI: 10.1038/nature12854. URL: http://www.nature.com/doifinder/10.1038/nature12854 (see pages 6, 137).

Stroeve, Julienne (2001). **Assessment of Greenland albedo variability from the advanced very high resolution radiometer Polar Pathfinder data set**. *Journal of Geophysical Research: Atmospheres* 106:D24, 33989–34006. DOI: 10.1029/2001JD900072 (see page 10).

Tamberg, Lea A., Jobst Heitzig, and Jonathan F. Donges (2022). **A modeler's guide to studying the resilience of social-technical-environmental systems**. *Environmental Research Letters* 17:5, 055005 (see pages 4, 5).

Tedesco, Marco and Xavier Fettweis (Apr. 2020). **Unprecedented atmospheric conditions (1948–2019) drive the 2019 exceptional melting season over the Greenland ice sheet**. *The Cryosphere* 14:4, 1209–1223. ISSN: 1994-0424. DOI: 10.5194/tc-14-1209-2020. URL: https://tc.copernicus.org/articles/14/1209/2020/ (see pages 2, 137).

Tedesco, Marco, Xavier Fettweis, Michiel R. Van Den Broeke, Roderik S. W. van de Wal, C. J. P. Paul Smeets, Willem Jan van de Berg, M. C. Serreze, and Jason E. Box (Jan. 2011). **The role of albedo and accumulation in the 2010 melting record in Greenland**. *Environmental Research Letters* 6:1, 014005. ISSN: 1748-9326. DOI: 10.1088/1748-9326/6/1/014005. URL: https://iopscience.iop.org/article/10.1088/1748-9326/6/1/014005 (see page 2).

Tedstone, Andrew J., Jonathan L. Bamber, Joseph M. Cook, Christopher J. Williamson, Xavier Fettweis, Andrew J. Hodson, and Martyn Tranter (Nov. 2017). **Dark ice dynamics of the south-west Greenland Ice Sheet**. *The Cryosphere* 11:6, 2491–2506. ISSN: 1994-0424. DOI: 10.5194/tc-11-2491-2017. URL: https://tc.copernicus.org/articles/11/2491/2017/ (see pages 3, 11, 17).

Tedstone, Andrew J., Joseph M. Cook, Christopher J. Williamson, Stefan Hofer, Jenine McCutcheon, Tristram D. L. Irvine-Fynn, Thomas Gribbin, and Martyn Tranter (Feb. 2020). **Algal growth and weathering crust state drive variability in western Greenland Ice Sheet ice albedo**. *The Cryosphere* 14:2, 521–538. ISSN: 1994-0424. DOI: 10.5194/tc-14-521-2020. URL: https://tc.copernicus.org/articles/14/521/2020/ (see pages 11, 17).

The PISM authors (2018). *PISM, a Parallel Ice Sheet Model*. URL: http://www.pism-docs.org (see pages 15, 17).

Tosi, N., Roberto Sabadini, A. M. Marotta, and L. L.A. Vermeersen (2005). **Simultaneous inversion for the Earth's mantle viscosity and ice mass imbalance in Antarctica and Greenland**. *Journal of Geophysical Research: Solid Earth* 110:7, 1–14. ISSN: 21699356. DOI: 10.1029/2004JB003236 (see pages 20, 128).

Trusel, Luke D., Sarah B. Das, Matthew B. Osman, Matthew J. Evans, Benjamin E. Smith, Xavier Fettweis, Joseph R. McConnell, Brice P. Y. Noël, and Michiel R. van den Broeke (2018). **Nonlinear rise in Greenland runoff in response to post-industrial Arctic warming**. *Nature* 564:7734, 104–108. ISSN: 0028-0836. DOI: 10.1038/s41586-018-0752-4. URL: http://www.nature.com/articles/s41586-018-0752-4 (see page 2).

Van den Berg, Jojanneke, Roderik S. W. van de Wal, and Hans Oerlemans (2008). **A mass balance model for the Eurasian Ice Sheet for the last 120,000 years**. *Global and Planetary Change* 61:3-4, 194–208. ISSN: 09218181. DOI: 10.1016/j.gloplacha.2007.08.015 (see page 18).

Vizcaíno, Miren, Uwe Mikolajewicz, Florian A. Ziemen, Christian B. Rodehacke, Ralf Greve, and Michiel R. Van Den Broeke (2015). **Coupled simulations of Greenland Ice Sheet and climate change up to A.D. 2300**. *Geophysical Research Letters* 42:10, 3927–3935. ISSN: 19448007. DOI: 10.1002/2014GL061142 (see page 7).

Wahr, John, Tonie van Dam, Kristine M. Larson, and Olivier Francis (Aug. 2001). **Geodetic measurements in Greenland and their implications**. *Journal of Geophysical Research: Solid Earth* 106:B8, 16567–16581. ISSN: 01480227. DOI: 10.1029/2001JB000211. URL: http://doi.wiley.com/10.1029/2001JB000211 (see pages 128, 139).

Wake, Leanne M., Benoit S. Lecavalier, and Michael Bevis (2016). **Glacial Isostatic Adjustment (GIA) in Greenland: a Review**. *Current Climate Change Reports* 2:3, 101–111. ISSN: 21986061. DOI: 10.1007/s40641-016-0040-z. URL: http://dx.doi.org/10.1007/s40641-016-0040-z (see page 139).

Weertman, Johannes (1961). **Stability of ice-age ice sheets**. *Journal of Geophysical Research* 66:11, 3783–3792. DOI: 10.1029/jz066i011p03783 (see page 4).

– (1974). **Stability of the Junction of an Ice Sheet and an Ice Shelf**. *Journal of Glaciology* 13:67, 3–11. ISSN: 0022-1430. DOI: 10.3189/s0022143000023327 (see page 8).

Whitehouse, Pippa L. (2018). **Glacial isostatic adjustment modelling: Historical perspectives, recent advances, and future directions**. *Earth Surface Dynamics* 6:2, 401–429. ISSN: 2196632X. DOI: 10.5194/esurf-6-401-2018 (see pages 20, 137).

Whitehouse, Pippa L., Natalya Gomez, Matt A. King, and Douglas A. Wiens (2019). **Solid Earth change and the evolution of the Antarctic Ice Sheet**. *Nature Communications* 10:1, 1–14. ISSN: 20411723. DOI: 10.1038/s41467-018-08068-y. URL: http://dx.doi.org/10.1038/s41467-018-08068-y (see page 20).

Whitehouse, Pippa L., Konstantin Latychev, Glenn A. Milne, Jerry X. Mitrovica, and Roblyn Kendall (2006). **Impact of 3-D Earth structure on Fennoscandian glacial isostatic adjustment: Implications for space-geodetic estimates of present-day crustal deformations**. *Geophysical Research Letters* 33:13, 3–7. ISSN: 00948276. DOI: 10.1029/2006GL026568 (see page 20).

Williamson, Christopher J., Joseph M. Cook, Andrew J. Tedstone, Marian Yallop, Jenine McCutcheon, Ewa Poniecka, Douglas Campbell, Tristram D. L. Irvine-Fynn, James B. McQuaid, Martyn Tranter, Rupert Perkins, and Alexandre M. Anesio (2020). **Algal photophysiology drives darkening and melt of the Greenland Ice Sheet**. *Proceedings of the National Academy of Sciences of the United States of America* 117:11, 5694–5705. ISSN: 10916490. DOI: 10.1073/pnas.1918412117 (see pages 3, 11, 17).

Wilton, David J., Amy Jowett, Edward Hanna, Grant R. Bigg, Michiel R. Van Den Broeke, Xavier Fettweis, and Philippe Huybrechts (2017). **High resolution (1 km) positive degree-day modelling of Greenland ice sheet surface mass balance, 1870-2012 using reanalysis data**. *Journal of Glaciology* 63:237, 176–193. ISSN: 00221430. DOI: 10.1017/jog.2016.133 (see page 18).

Winkelmann, Ricarda, Maria A. Martin, Marianne Haseloff, Torsten Albrecht, Ed Bueler, Constantine Khroulev, and Anders Levermann (Sept. 2011). **The Potsdam Parallel Ice Sheet Model (PISM-PIK) – Part 1: Model description**. *The Cryosphere* 5:3, 715–726. ISSN: 1994-0424. DOI: 10.5194/tc-5-715-2011. URL: https://www.the-cryosphere.net/5/715/2011/ (see pages 15, 17).

Wunderling, Nico, Jonathan F. Donges, Ju¨rgen Kurths, and Ricarda Winkelmann (2021). **Interacting tipping elements increase risk of climate domino effects under global warming**. *Earth System Dynamics* 12:2, 601–619. ISSN: 21904987. DOI: 10.5194/esd-12-601-2021 (see page 8).

Wunderling, Nico, Maximilian Gelbrecht, Ricarda Winkelmann, Jürgen Kurths, and Jonathan F. Donges (2020). **Basin stability and limit cycles in a conceptual model for climate tipping cascades**. *New Journal of Physics* 22:12. ISSN: 13672630. DOI: 10.1088/1367-2630/abc98a. arXiv: 2009.09902 (see page 8).

Wunderling, Nico, Matteo Willeit, Jonathan F. Donges, and Ricarda Winkelmann (2020). **Global warming due to loss of large ice masses and Arctic summer sea ice**. *Nature Communications* 11:1, 1–8. ISSN: 20411723. DOI: 10.1038/s41467-020-18934-3. URL: http://dx.doi.org/10.1038/s41467-020-18934-3 (see page 6).

Zeitz, Maria, Jan M Haacker, Jonathan F Donges, Torsten Albrecht, and Ricarda Winkelmann (2022). **Dynamic regimes of the Greenland Ice Sheet emerging from interacting melt-elevation and glacial isostatic adjustment feedbacks**. *Earth System Dynamics*: December, 1–25. DOI: 10.5194/esd-13-1077-2022. URL: https://esd.copernicus.org/articles/13/1077/2022/ (see page 134).

Zeitz, Maria, Anders Levermann, and Ricarda Winkelmann (2020). **Sensitivity of ice loss to uncertainty in flow law parameters in an idealized one-dimensional geometry**. *The Cryosphere* 14:10, 3537–3550. ISSN: 1994-0424. DOI: 10.5194/tc-14-3537-2020. URL: https://tc.copernicus.org/articles/14/3537/2020/ (see page 134).

Zeitz, Maria, Ronja Reese, Johanna Beckmann, Uta Krebs-Kanzow, and Ricarda Winkelmann (2021). **Impact of the melt–albedo feedback on the future evolution of the Greenland Ice Sheet with PISM-dEBM-simple**. *The Cryosphere* 15:12, 5739–

5764. ISSN: 1994-0424. DOI: 10.5194/tc-15-5739-2021. URL: https://tc.copernicus.org/articles/15/5739/2021/ (see page 134).

Zweck, Chris and Philippe Huybrechts (2005). **Modeling of the northern hemisphere ice sheets during the last glacial cycle and glaciological sensitivity**. *Journal of Geophysical Research Atmospheres* 110:7, 1–24. ISSN: 01480227. DOI: 10.1029/2004JD005489 (see page 20).

List of Publications

Articles in Refereed Journals relevant for this thesis

1 Zeitz, Maria, Jan M Haacker, Jonathan F Donges, Torsten Albrecht, and Ricarda Winkelmann (2022). **Dynamic regimes of the Greenland Ice Sheet emerging from interacting melt-elevation and glacial isostatic adjustment feedbacks**. *Earth System Dynamics*: December, 1–25. DOI: 10.5194/esd-13-1077-2022. URL: https://esd.copernicus.org/articles/13/1077/2022/.

2 Zeitz, Maria, Anders Levermann, and Ricarda Winkelmann (2020). **Sensitivity of ice loss to uncertainty in flow law parameters in an idealized one-dimensional geometry**. *The Cryosphere* 14:10, 3537–3550. ISSN: 1994-0424. DOI: 10.5194/tc-14-3537-2020. URL: https://tc.copernicus.org/articles/14/3537/2020/.

3 Zeitz, Maria, Ronja Reese, Johanna Beckmann, Uta Krebs-Kanzow, and Ricarda Winkelmann (2021). **Impact of the melt–albedo feedback on the future evolution of the Greenland Ice Sheet with PISM-dEBM-simple**. *The Cryosphere* 15:12, 5739–5764. ISSN: 1994-0424. DOI: 10.5194/tc-15-5739-2021. URL: https://tc.copernicus.org/articles/15/5739/2021/.

Other Articles in Refereed Journals

4 Zeitz, Maria, Pavel Gurevich, and Holger Stark (2015). **Feedback control of flow vorticity at low Reynolds numbers**. *The European Physical Journal E* 38:3, 1–8. DOI: 10.1140/epje/i2015-15022-7. URL: https://link.springer.com/article/10.1140/epje/i2015-15022-7.

5 Zeitz, Maria and Jan Kierfeld (2014). **Feedback mechanism for microtubule length regulation by stathmin gradients**. *Biophysical journal* 107:12, 2860–2871. DOI: 10.1016/j.bpj.2014.10.056. URL: https://www.sciencedirect.com/science/article/pii/S000634951401145X.

6 Zeitz, Maria and Pierre Sens (2012). **Reversibility of red blood cell deformation**. *Physical Review E* 85:5, 051904. DOI: 10.1103/PhysRevE.85.051904. URL: https://journals.aps.org/pre/abstract/10.1103/PhysRevE.85.051904.

7 Zeitz, Maria, Katrin Wolff, and Holger Stark (2017). **Active Brownian particles moving in a random Lorentz gas**. *The European Physical Journal E* 40:2, 1–10. DOI: 10.1140/epje/i2017-11510-0. URL: https://link.springer.com/article/10.1140/epje/i2017-11510-0.

Selbstständigkeitserklärung

Diese Arbeit ist bisher an keiner anderen Hochschule eingereicht worden. Sie wurde selbständig und ausschließlich mit den angegebenen Mitteln angefertigt. Dies versichere ich hiermit an Eides statt.

Berlin, den 29. November 2022

Maria Zeitz